Title

THEORETICAL STUDY OF INDIRECT PHOTO-DISSOCIATION: ELECTRONIC STRUCTURE AND PRODUCT ROVIBRATIONAL DISTRIBUTIONS OF C2N2 (C1 -nu)

Author

Dateo, C.E.

Publication Date

1987-06-01

Lawrence Berkeley Laboratory
UNIVERSITY OF CALIFORNIA

Materials & Chemical Sciences Division

Theoretical Study of Indirect Photodissociation: Electronic Structure and Product Rovibrational Distributions of $C_2N_2(\tilde{C}\ ^1\Pi_u)$

C.E. Dateo
(Ph.D. Thesis)

June 1987

Prepared for the U.S. Department of Energy under Contract DE-AC03-76SF00098

DISCLAIMER

LBL-23944

Theoretical Study of Indirect Photodissociation: Electronic Structure and Product Rovibrational Distributions of $C_2N_2(\tilde{C}\ ^1\Pi_u)$

Ph.D Thesis

Christopher Edward Dateo

Materials and Chemical Sciences Division
Lawrence Berkeley Laboratory
Berkeley, California 94720
and
Department of Chemistry
University of California
Berkeley, California 94720

June 1987

Theoretical Study of Indirect Photodissociation: Electronic Structure and Product Rovibrational Distributions of $C_2N_2(\tilde{C}\ ^1\Pi_u)$

Christopher Edward Dateo

Abstract

Polyatomic indirect photodissociation is treated as a quantum transition between quasidiscrete and dissociative (photofragment) states within a diabatic representation of the electronic Hamiltonian following a formalism developed by Kresin and Lester (KL). Relative product energy distributions are obtained from the evaluation of a multidimensional Franck-Condon overlap integral. The KL adiabatic method is followed to describe the nuclear dynamics of the dissociative state. The theory is applied to single-photon dissociation of $C_2N_2(\tilde{C}\ ^1\Pi_u)$ at 164, 158.7, and 153.6 nm to form $CN(X\ ^2\Sigma^+)$ + $CN(A\ ^2\Pi)$. Ab initio multiconfiguration Hartree-Fock (MCHF) excited state calculations are carried out to provide essential potential energy surface properties for the heavy-particle dynamics treatment. Product vibrational distributions are obtained in a collinear model and theoretical predictions are found to be in good agreement with recent experiments. An extension of the theory to 3-dimensions is described. Product rovibrational distributions and rotational temperatures are reported which take into account bending-vibrational modes and rotations employing only the adiabatic sudden limit of the general formalism of KL.

Acknowledgements

My experience as a graduate student at Berkeley for the most part has been a rewarding one.

I would like to thank my advisor Professor William A. Lester, Jr. for his support and guidance. I have also had the opportunity to work closely with two exceptional persons, Dr. Vladimir Z. Kresin and Dr. Michel Dupuis, and am indebted to each of them for his help over these past years. I would also like to express my gratitude to all the members in the Lester group: Rob Barnett, Dr. Bernard Bernu, Brian Hammond, Sheng-Yu Huang, Randy Grimes, Maudie Noyd, Kent Owen, and Dr. Peter Reynolds. All have been extremely helpful to me in many ways.

Special thanks go to Phil Wilmarth and Janis Shampay, and Bob and Adrienne Thieke for their friendship, support, and making the years here in Berkeley so much more enjoyable. I would also like to thank Beth Altman, Jamie Kelly, Paul Levy, Chuck Rubin, and Gail Tenore, all of whom, though miles away have helped me through some of the rough times.

This research was supported by the Director, Office of Basic Energy Sciences, Chemical Sciences Division of the U.S. Department of Energy under Contract No. DE-AC03-76SF00098.

Dedication

To George and Shirley,

whom I love, respect, and am very proud to be their son.

Table of Contents

CHAPTER 1

Introduction

Photodissociation is initiated by the interaction of radiation with a molecule, which subsequently undergoes fragmentation. This process is often the initial process in photochemical reaction chains important to problems studied in many fields of interest including atmospheric chemistry, astrophysics, and biology. In the past, experimental studies of primary photodissociative processes were only able to give information concerning reactions of secondary or tertiary by-products from the initial photofragmentation. However, in the past decade and a half, primarily made possible by the development of the laser, major technological advances have enabled experimentalists to prepare many systems in well-defined initial electronic rovibrational states and to probe accurately the final quantum state distributions of the nascent photofragments.[1–3] These detailed, state selected experiments are now capable of accurately measuring energy partitioning in the photofragments (electronic, rotational, vibrational, and translational distributions), angular distributions (orientation and alignment), and the effect of initial photon energy on these distributions. This progress has stimulated considerable interest in obtaining a better theoretical understanding of state-to-state polyatomic photodissociation dynamics.

The study of photodissociation processes offers certain advantages over the

study of bimolecular reactions. The observables for each case are similar; i.e., one measures the disposal of available energy into translational, vibrational, and rotational degrees of freedom, and the angular distributions of the product fragments. However, in a photodissociation experiment it is easier to obtain a well-defined initial state with known initial conditions than in a bimolecular reaction because one need not consider a range of relative energies, impact parameters and initial angular momentum. For photodissociation, there is no initial relative orbital angular momentum. The internal angular momentum of the initial molecule can be made small by cooling in a supersonic jet expansion and at most one quantum of angular momentum is added by the photon.

The dynamics of diatomic photodissociation is fairly well understood when only a single excited repulsive electronic potential energy surface (PES) is involved.[4–6] The receding atoms depart along the repulsive PES with kinetic energy determined by constraints of energy conservation. The angular distributions of the atoms will depend primarily on the initial rotation of the diatom and on the lifetime of the excited state. When more than one repulsive electronic PES is involved, there exists the possibility of transitions between them, leading to curve crossing problems which have been of interest in the theory of collision dynamics.[7–9] In these cases one must consider the complications arising from the breakdown of the Born-Oppenheimer (BO) approximation.

Whereas diatomics are describable by a single nuclear coordinate (one

vibrational degree of freedom), polyatomic systems are inherently more complex needing a minimum of 3N-6 (3N-5 for linear molecules, N being the number of atoms comprising the molecule) coordinates for a proper description of the nuclear dynamics. Consequently, the molecular fragments can be internally (vibrationally and rotationally) as well as electronically excitated.

A qualitative description of polyatomic photodissociation might separate the process into three steps:

1. Initial state preparation by photon excitation

$$AB(E_{int}^{AB}) + h\nu \rightarrow AB^{*}(E_{int}^{AB^{*}}) \tag{1.1}$$

2. Energy redistribution within modes of the excited molecule (intramolecular dynamics)

$$AB^{*}(E_{int}^{AB^{*}}) \rightarrow AB^{\dagger}(E_{int}^{AB^{\dagger}}) \tag{1.2}$$

3. Dissociation, enough energy exists in the dissociative coordinate to break a chemical bond.

$$AB^{\dagger}(E_{int}^{AB^{\dagger}}, \mathbf{p}) \rightarrow A(E_{int}^{A}, \mathbf{p}_A) + B(E_{int}^{B}, \mathbf{p}_B) \tag{1.3}$$

Here, A and B are product fragments which may, in general, be atoms, molecules, or ions. Energy disposal in the products will be subject to conservation of energy and momentum constraints:

$$\begin{aligned} \mathbf{p} = \mathbf{p}_A &= -\mathbf{p}_B \\ \mathbf{J}_{AB^{*}} = \mathbf{J}_{AB^{\dagger}} &= \mathbf{J}_A + \mathbf{J}_B + \mathbf{L} \\ E_{int}^{AB} + h\nu &= E_{int}^{A} + E_{int}^{B} + \frac{\mathbf{p}^2}{2\mu_{AB}} + D_o \end{aligned} \tag{1.4}$$

The terms E_{int}^{i}, $\mathbf{p}_i$, $\mathbf{J}_i$ refer to the internal energy (rotation and vibration), linear momentum, and total angular momentum of each species; $\mathbf{L}$ is the rela-

tive orbital angular momentum of the fragments; μ_{AB} is the reduced mass of the system; and D_o is the dissociation energy.

Clearly, for many cases, the separation into three distinct steps as described above will be inadequate. For example, consider photon excitation above the dissociation energy directly into the dissociative coordinate . The excited molecule may not have time for energy redistribution and could proceed directly from 1 to 3. There also exists the possibility of contributions from excitations to virtual states which need not conserve energy. As the photofragments recede along the repulsive PES, transitions between the different product rovibrational channels (i.e., the so called final state interactions) may occur.

In photodissociation theory, the specific details of the dynamics must be intimately related to the shapes and relative positions of the ground and excited state PES's. Accurate information concerning these states is generally unavailable from experiment and ab initio PES's are often difficult and time consuming to compute, thus not many exist. However, a complete PES is not always required for adequate treatment of the dynamics. In some cases, the reaction dynamics can be understood from consideration of regions near the transition state[10,11] or perhaps along some intrinsic reaction coordinate or reaction path.[12,13]

A detailed theory of single-photon photodissociation should be able to answer fundamental questions such as what are the branching ratios for

different product channels, what are the translational, vibrational, and rotational energy distributions of the fragments, what are the angular distributions, and what are the effects of initial conditions (e.g., photon energy or polarization, initial population of states, etc.) and the constraints imposed by energy and angular momentum conservation on these distributions. Most calculations in this rapidly growing area of chemical dynamics have been restricted to diatomic molecules, and models which make approximations to reduce the dimensionality of polyatomics (e.g., quasidiatomic models, or collinear models neglecting rotational and bending motions). It was only recently that full 3-D quantum mechanical treatments of triatomic systems were presented.[14,15] These "exact" treatments are well formulated,[14–20] however, in practice, they quickly become intractable as the number of exit channels becomes prohibitively large for most systems. The details concerning the relevant PES's for only a few small systems are available.

Due to the limitations of exact treatments, significant effort is presently involved in developing more approximate theories which do not become impractical for larger systems, but still possess the necessary physical content for a reliable description of polyatomic photodissociation. The present work was undertaken in this spirit. Here, polyatomic photodissociation is treated employing the quantum theory of transitions, as described in a typical quantum text book.[21] The polyatomic molecule in an initial bound (quasibound) state undergoes a quantum transition to a final dissociative fragment state.

An adiabatic description of the nuclear dynamics of the dissociative state explicitly treats the final state interactions. The theory is applied to the indirect photodissociation of $C_2N_2(\tilde{C}\ ^1\Pi_u)$.

The rest of this introductory chapter describes the different types of photodissociation and concludes with a brief summary of some simplified models and theories that treat photodissociation as a half-collision. In chapter 2, the electronic structure analysis of several low-lying electronic states of C_2N_2 is discussed. These calculations were performed to obtain relevant details of the PES's involved in the indirect photodissociation of $C_2N_2(\tilde{C}\ ^1\Pi_u)$. In Chapter 3, the theory of Kresin and Lester (KL) is presented and applied to the indirect dissociation of $C_2N_2(\tilde{C}\ ^1\Pi_u)$ to obtain product vibrational distributions which are then compared to experimental data. Chapter 4 presents the extension of the theory to three-dimensions and preliminary results of product rotational-vibrational distributions.

I. Types of Photodissociation

Photodissociation is the result of the interaction of incident radiation with a molecule. One can distinguish between two main types of photodissociation. The first type, direct photodissociation, corresponds to the absorption of light from a bound rovibrational state of the electronic ground state PES that results in a direct transition to a continuum state of the photofragments on the repulsive excited PES.

The second type, indirect photodissociation, consists of two steps. The first

step is a radiation-induced transition, similar to that for direct photodissociation, but to an intermediate predissociative state characterized by a finite lifetime τ. This metastable state then undergoes a radiationless transition to a final dissociative state of the fragments. The broadening of the energy levels, $\delta\epsilon \approx \hbar/\tau$, should be considerably smaller than the spacing between energy levels of the predissociating state. As the broadening becomes larger, τ gets shorter and one reaches the limiting case of direct photodissociation.

The concepts of direct and indirect photodissociation are just limiting cases, and the actual experimental situation may correspond to some intermediate condition. The question then arises: how does one distinguish experimentally between these two types of photodissociation? The answer can often be found by analysis of the absorption spectrum. The predissociative state is quasibound, and therefore, is characterized by a set of discrete levels with some broadening. The indirect channel implies the appearance of resonant structure in the photodissociation cross section as a function of incident radiation frequency. On the other hand, direct photodissociation is characterized by a broad smooth absorption spectrum. As an example, analysis of the absorption spectrum for C_2N_2[22] indicates discrete levels and suggests that the process $C_2N_2(\tilde{C}\ ^1\Pi_u) + h\nu \rightarrow CN(X\ ^2\Sigma^+) + CN(A\ ^2\Pi)$ at $\nu = 164$ nm is an indirect photodissociation process.

Another possibility for distinguishing between direct and indirect channels arises from analysis of the angular distributions of the fragments. In direct

photodissociation, there is generally a correlation between the direction of incident radiation and the angular distribution. For indirect photodissociation, the intermediate state exists for a finite lifetime during which the molecule can lose all memory of the photon during nuclear rearrangement (except of course for total energy), and such correlations are not possible.

Indirect photodissociation of polyatomic molecules can be further subdivided into three classifications,[23] electronic (type I), vibrational (type II), and rotational (type III) predissociation. Electronic predissociation occurs when the radiationless transition from the intermediate state to the final dissociative state is accompanied by a change of electronic PES's. Vibrational predissociation actually occurs on the same adiabatic electronic PES as a result of redistribution of vibrational energy from bound modes to the dissociative coordinate. Note, that this mechanism for photodissociaton is not possible for diatomics which only possess one vibrational degree of freedom. Finally, rotational predissociation is the result of quasibound states existing above the dissociation limit due to the centrifugal barrier.

II. Simple Models, Franck-Condon, and Half-Collision Approaches

As to be expected in such a rapidly growing field as photochemistry, there have been quite a few excellent review papers presented on polyatomic photodissociation.[24–30] This section is by no means an attempt to be a comprehensive review of the field, but rather an introduction to some of the basic concepts necessary for a general theory of polyatomic photodissociation.

As noted previously, the photodissociation dynamics of diatoms is fairly well understood. The multidimensional aspect of polyatomic molecules renders the understanding of these systems more difficult. The initial nuclear degrees of freedom for vibrational motion must correlate not only to the considerably different vibrations in the photofragments, but also to unbound degrees of freedom coresponding to fragment relative motion and rotations. Several earlier models were aimed at simplifying the multidimensionality associated with polyatomic photodissociation. The hope of such models is to obtain a qualitative description of the phenomenom and some of the important aspects.

One such model is the quasidiatomic model,[31–33] which is based on the assumption that the normal modes of the dissociative fragment state are the same as those of the precursor molecular state. For example, in the photodissociation of a linear triatomic, ABC + $h\nu \rightarrow$ A + BC, the BC oscillator is assumed to be a normal mode vibration of ABC. This implies (ignoring the bending vibration) that the potential can be written as

$$V(r,R) = V_1 \cdot r^2 + V_2 \cdot R^2 \tag{1.5}$$

Here r is the BC distance and R is the distance from atom A to the center of mass of diatom BC. In general, there will be a coupling term $V_3 \cdot r \cdot R$, but this term is neglected. Since the modes of both states are identical, the only mechanism for vibrational excitation comes from the repulsive interaction between the atom and diatom on the dissociative PES.

The quasidiatomic model deals primarily with the "half-collision" aspect of

photodissociation, i.e., the dynamics associated with the separation of the fragments on the repulsive electronic PES. Though the final state interactions (i.e., the interfragment coupling that is a result of the nonseparability of fragment internal and relative motions in the dissociative state potential) do play an important role in determining the photofragment energy distributions, this model neglects important features about the relevant PES's. In general, the normal modes of each PES are different; in many systems the dissociative coordinate on the upper PES is not a normal mode of the precursor system. Possible geometry and frequency shifts of the passive oscillator(s) which do not undergo dissociation can also be important.[34]

Berry[35] proposed a Golden rule model to obtain the initial energy distributions on the repulsive PES. In his development, polyatomic photodissociation is treated as a nonstationary phenomenon where the probability of a transition $i \rightarrow f$ is given from first-order perturbation theory by

$$W_{i \rightarrow f} = \frac{2\pi}{\hbar} \mid \langle f \mid V \mid i \rangle \mid^2 \rho_f(E) \tag{1.6}$$

where ρ_f is the final density of states. The operator V describing the transition was not specified. In the sudden limit the problem is reduced to the evaluation of a Franck-Condon (FC) factor:

$$\mid \langle f \mid V \mid i \rangle \mid^2 \approx \mid \langle f \mid i \rangle \mid^2 \tag{1.7}$$

This model completely neglects the effects of final state interactions. The probability distribution is obtained from a bound-bound FC overlap integral between the nuclear wave functions describing the vibrational modes of the

inital (ground) state and the particular vibrational modes of the dissociative state fragments which are of interest. In order to simplify the integrals, Berry uses the dressed oscillator model, the essence of which is similar to the quasidiatomic model. The contributions from the other vibrational modes as well as the wave function describing fragment relative motion are neglected except for their effect on the final density of states through conservation of energy requirements.

The quasidiatomic and Golden rule models described above both make a series of approximations about the dissociation process aimed at reducing the difficulty of multidimensionality present in the description of polyatomic photodissociation. Though each approach is restrictive, they contain some of the basic elements that must be included in a more general theory.

A number of theories have been developed to incorporate the fundamental features discussed above. Many such approaches are based on expressing the cross section for the photodissociative transition from the initial bound state to a dissociative fragment state as[25,36–40]

$$\sigma_{f\,i} = \left| \sum_{\bar{f}} S_{f\,\bar{f}}\, A_{\bar{f}\,i} \right|^2 \tag{1.8}$$

where $A_{\bar{f}\,i}$ gives the relative probability amplitude for the transition from initial (ground or intermediate) state to a state $\bar{f}$ of the fragments. $S_{f\,\bar{f}}$ is the scattering matrix for the half-collision which allows for transitions from the state $\bar{f}$ to final states f as the fragments separate on the repulsive PES during dissociation. The main difference between these theories lies in the method of

calculating the scattering matrix. If $S_{f\bar{f}}$ is taken to be unity (i.e., the neglect of final state interactions), Eq. (1.8) reduces to a Franck-Condon matrix element, which in principle is a multidimensional nonseparable bound-continuum overlap integral between the initial and final dissociative state wave functions.

In a series of papers, Band and Freed[25,37,41] have developed a fully quantum treatment of the FC rearrangement process that incorporates the normal modes of the polyatomic bound (quasibound) system and those of the dissociating fragments. They introduce the concept of natural collision coordinates for the description of the dissociative fragment state. One of the conditions governing the choice of coordinates is that they be able to describe properly the dissociative state in the Franck-Condon region as well as the asymptotic region. In order to evaluate the integrals the normal coordinates of the initial state are expressed as functions of the dissociative state coordinates. Integration over the bound coordinates results in a one-dimensional bound-continuum integral between an effective oscillator and the wave function describing the relative motion of the fragments receding on the repulsive PES.

The effects incorporated in the half-collision dynamics include the coupling or distortions of the normal modes orthogonal to the reaction (dissociative) coordinate during the separation of the fragments. Band and Freed have suggested that including these dynamical effects into the basis functions would give a more natural representation of the wave function of the dissociative state on the repulsive PES. This requires detailed information about the

repulsive PES, which is generally not available. In principle, however, this information is obtainable through present ab initio quantum mechanical electronic structure methods.

There have also been a variety of exact quantum treatments[14–20] which are derived from formal scattering theory. These methods avoid the separation of the dissociation process into the FC rearrangement followed by half-collision (as suggested by eq. (1.8)). This is accomplished by solving a set of coupled differential (or integral) equations involving both repulsive and bound state nuclear basis functions. As noted previously, these methods readily become impractical since the number of product channels increases rapidly with energy or system size.

The present study is based on the KL theory of photodissociation,[28,42–44] which will be described in more detail in chapters 3 and 4. Polyatomic photodissociation is treated as a quantum transition between initial bound (quasi-bound) and final dissociative states. Final state interactions are treated explicitly within a FC-like formalism by using a specific adiabatic method to describe the nuclear dynamics. Ab initio quantum chemistry techniques are employed to obtain the necessary data of the involved electronic PES's.

CHAPTER 2

Ab initio Study of Low-Lying Electronic States of Cyanogen: The $\tilde{X}\ ^1\Sigma_g^+$, $\tilde{a}\ ^3\Sigma_u^+$, $\tilde{B}\ ^1\Delta_u$, and $\tilde{C}\ ^1\Pi_u$ States

I. Introduction

As emphasized in chapter 1, a correct description of polyatomic photodissociation must be intimately related to the PES's of the relevant electronic states. Accurate PES's are available for a relatively small number of ground state systems, and even fewer for excited state systems. Recent photodissociation studies[45,46] of C_2N_2 ($\tilde{B}\ ^1\Delta_u$) have shown that this state predissociates via a radiationless transition to ground state CN ($X\ ^2\Sigma^+$) fragments and have described the energy distribution of the fragments. Other studies of the photodissociation of C_2N_2 ($\tilde{C}\ ^1\Pi_u$) have found that this state predissociates to CN ($X\ ^2\Sigma^+$) and CN ($A\ ^2\Pi$).[22,47-50] The present work is a study of the latter process. The photodissociation theory of Kresin and Lester[28,42-44] requires vibrational frequencies of the excited state to predict internal energies of photofragments. We have carried out ab initio studies to obtain this information which, in addition to its importance for photodissociation theory, also extends knowledge of electronically excited states of polyatomic molecules. In this chapter, we present the results of an ab initio multiconfiguration Hartree-Fock (MCHF) study of the $\tilde{X}\ ^1\Sigma_g^+$, $\tilde{a}\ ^3\Sigma_u^+$, $\tilde{B}\ ^1\Delta_u$, and $\tilde{C}\ ^1\Pi_u$ states of C_2N_2.

Cyanogen shows four weak electronic transitions in the near ultraviolet region. They have been assigned to absorptions from the ground state C_2N_2 ($\tilde{X}\ ^1\Sigma_g^+$) to C_2N_2 ($\tilde{a}\ ^3\Sigma_u^+$)[51] at 3000Å, to C_2N_2 ($\tilde{b}\ ^3\Delta_u$)[52] at 2500Å, to C_2N_2 ($\tilde{A}\ ^1\Sigma_u^-$)[53] at 2200Å, and to C_2N_2 ($\tilde{B}\ ^1\Delta_u$)[54] at 2070Å. These states are believed to be derived from a $\pi^3\pi$ electronic configuration. Cyanogen also has a strong electronic transition in the vacuum ultraviolet with origin near 1700 Å (7.3 ev, 58900 cm^{-1}). The upper state of the absorption has been assigned $^1\Pi_u$ symmetry.[54] A vibrational progression of 2100 cm^{-1} has been observed and assigned to the symmetric CN stretching mode,[55] although the Renner-Teller character of C_2N_2 ($\tilde{C}\ ^1\Pi_u$) is expected to produce a complicated absorption pattern.

Two theoretical studies of the electronic structure of electronically excited C_2N_2 have been reported.[55,56] Connors et al.[55] used the CNDO/CI method to characterize the valence shell transitions of cyanogen. They obtained qualitative agreement between the observed and calculated excitation energies, and described the structure of C_2N_2 ($\tilde{C}\ ^1\Pi_u$) as resulting from an $n\rightarrow\pi^*$ excitation where a nitrogen lone-pair electron n is excited into an antibonding π^* orbital. Bell[56] used the Hartree-Fock (HF) method to describe many excited states of C_2N_2. His calculated excitation energies were in qualitative agreement with experiment for C_2N_2 ($\tilde{a}\ ^3\Sigma_u^+$) and C_2N_2 ($\tilde{B}\ ^1\Delta_u$) but in poor agreement for the $\tilde{C}\ ^1\Pi_u$ state where he represented the latter as a $\pi\rightarrow\sigma^*$ excitation.

In the present study excitation and dissociation energies, equilibrium structures, and harmonic vibrational frequencies are determined for the subject states. In addition, we analyze the discrepancy between the two previous theoretical studies of the $\tilde{C}\ ^1\Pi_u$ state and characterize the Renner-Teller interaction in this state. In the next section we discuss some features of C_2N_2 pertinent to the study of the excited states mentioned above, especially the $n\rightarrow\pi^*$ character of C_2N_2 ($\tilde{C}\ ^1\Pi_u$), and present the Walsh diagram of cyanogen orbital energies to interpret the Renner-Teller character of this state. In the final section we report the results of the MCHF calculations.

II. Theoretical Considerations

A. Energy correlation diagram

The energy correlation diagram of C_2N_2 is shown in Fig. 2.1. Adiabatically C_2N_2 ($\tilde{X}\ ^1\Sigma_g^+$) correlates to two ground state CN ($X\ ^2\Sigma^+$) fragments. The C_2N_2 ($\tilde{a}\ ^3\Sigma_u^+$) state also correlates to the same dissociation limit. Both C_2N_2 ($\tilde{b}\ ^3\Delta_u$) and C_2N_2 ($\tilde{A}\ ^1\Sigma_u^-$) dissociate to two excited state CN ($A\ ^2\Pi$) fragments. The C_2N_2 ($\tilde{B}\ ^1\Delta_u$) state correlates to two nonidentical CN ($^2\Pi$) radicals. The C_2N_2 ($\tilde{C}\ ^1\Pi_u$) state dissociates to CN ($X\ ^2\Sigma^+$) and CN ($A\ ^2\Pi$).

The electronic states of the CN radical have been fully characterized by Schaefer and Heil.[57] Ground state CN ($X\ ^2\Sigma^+$) has a triple bond between the carbon and nitrogen atoms, and an unpaired electron localized on the carbon atom. Collinear approach of two CN ($X\ ^2\Sigma^+$) singlet-coupled radicals leads to

the ground C_2N_2 ($\tilde{X}\ ^1\Sigma_g^+$) state. If the two radicals are triplet coupled, then the interaction is repulsive. The C_2N_2 ($\tilde{a}\ ^3\Sigma_u^+$) state, which arises from a $\pi \rightarrow \pi^*$ excitation, correlates diabatically to two excited CN (A $^2\Pi$) fragments. Thus the dissociation of C_2N_2 ($\tilde{a}\ ^3\Sigma_u^+$) correlates to two ground state fragments via an avoided curve crossing as depicted in Fig. 2.2. The excited CN (A $^2\Pi$) state is best described as a $\pi \rightarrow \sigma$ excitation. A π electron of the CN triple bond is excited into the half-filled orbital of the CN radical. The interaction of two CN (A $^2\Pi$) radicals in the first excited state is therefore repulsive because of the electrostatic interaction of two lone pairs. Thus the C_2N_2 ($\tilde{b}\ ^3\Delta_u$) and C_2N_2 ($\tilde{A}\ ^1\Sigma_u^-$) states both have a barrier to dissociation resulting from an avoided curve crossing.

B. Predissociation of C_2N_2 ($\tilde{C}\ ^1\Pi_u$)

Similar to the approach of two CN (A $^2\Pi$) radicals, for collinear approach of CN ($X\ ^2\Sigma^+$) to CN (A $^2\Pi$), the interaction of the unpaired electron of the ground state fragment with the lone pair of the excited state fragment is repulsive. On the other hand, the HF calculation of C_2N_2 ($\tilde{X}\ ^1\Sigma_g^+$) by McLean and Yoshimine[58] indicates that the $4\sigma_u$ and $5\sigma_g$ orbitals (antisymmetric and symmetric combinations of nitrogen lone pairs) are nearly degenerate in energy with the π orbitals. Thus an $n \rightarrow \pi^*$ excitation requires less energy than a $\pi \rightarrow \sigma^*$ excitation. Also, C_2N_2 ($\tilde{C}\ ^1\Pi_u$, $n \rightarrow \pi^*$) would dissociate diabatically to an $n \rightarrow \pi^*$ fragment of high energy were it not for the avoided curve crossing

depicted in Fig. 2.2, in accord with the observed predissociation of that state.

C. Broken symmetry structure

As indicated earlier the excited states of C_2N_2 near their equilibrium structures are best represented by $\pi \rightarrow \pi^*$ or $n \rightarrow \pi^*$ excitations. The occupied π orbitals ($1\pi_u$ and $1\pi_g$) in the HF configuration of the ground-state correspond to symmetric and antisymmetric combinations of bonding CN π orbitals. The low-lying unoccupied $2\pi_u$ and $2\pi_g$ orbitals correspond to symmetric and antisymmetric combinations of antibonding CN π^* orbitals. The nodal features of the π orbitals of C_2N_2 are shown in Fig. 2.3. The occupied $4\sigma_u$ and $5\sigma_g$ orbitals correspond to antisymmetric and symmetric combinations of nitrogen lone-pair electrons.

As observed in many theoretical studies of symmetric radicals,[59] a HF wave function describing $\pi \rightarrow \pi^*$ excited states preferentially localizes the hole on one moiety leading to a broken symmetry structure of the states with unequal bond lengths for the minimum energy structure. Similarly for the $n \rightarrow \pi^*$ C_2N_2 ($\tilde{C}\ ^1\Pi_u$) state, the lone-pair electron to be excited can originate from the left or the right nitrogen atom. Here too, a HF wave function localizes the hole on one of the symmetric atoms (here N) preferentially leading to a broken symmetry structure. This behavior is depicted in Fig. 2.4.

Using a minimal basis set,[60] the lowest HF energy structure belonging to the $D_{\infty h}$ molecular symmetry point group has R(CC) = 1.345 Å, R(CN) = 1.203 Å, and E = -181.839444 a.u. This is the point labeled "HF (symmetric

mo's)" in Fig. 2.4. The lowest energy structure for $C_{\infty v}$ symmetry obtained with a HF wave function with $C_{\infty v}$ orbitals has R(CN) = 1.214 Å, R(CC) = 1.304 Å, R(CN) = 1.196 Å, and E = -181.914262 a.u. This is the minimum on the curve labeled HF in Fig. 2.4. For this structure the n and π^* orbitals are strongly localized. If we use these orbitals as an initial guess for a HF energy calculation at the $D_{\infty h}$ structure given above, the energy is -181.912467 a.u. This is the point labeled "HF (localized mo's)" in Fig. 2.4.

Mixing of equivalent classical valence-bond structures is needed to obtain a qualitatively correct description of the broken-symmetry state. The multiconfiguration Hartree-Fock (MCHF) method provides a means to accomplish this end. A "correct" potential curve labeled "MCHF" is shown in Fig. 2.4. A MCHF wave function which displays the correct behavior includes all configurations obtained by distributing 12 electrons among all of the lone pairs ($4\sigma_u$, $5\sigma_g$) and π orbitals ($1\pi_u$, $1\pi_g$, $2\pi_u$, and $2\pi_g$) in all possible ways consistent with $^1\Pi_u$ symmetry. MCHF wave functions of comparable quality for C_2N_2 ($\tilde{a}$ $^3\Sigma_u^+$) and C_2N_2 ($\tilde{B}$ $^1\Delta_u$) involve π electrons and π orbitals only. For these MCHF wave functions an optimization of the molecular geometry starting from the HF $C_{\infty v}$ structure yielded a structure with $D_{\infty h}$ symmetry. Finally, no symmetry breaking difficulties were encounted for the closed shell C_2N_2 ($\tilde{X}$ $^1\Sigma_g^+$), although an MCHF wave function involving the π electrons must be used for meaningful comparisons with the excited states.

D. Walsh Diagram

For C_2N_2 ($\tilde{C}\ ^1\Pi_u$) there are two degenerate bending vibrations, a cis-bending mode leading to a C_{2v} structure and a trans-bending mode leading to a C_{2h} structure. The Renner-Teller interaction of the electronic state with these bending modes can be analyzed by considering the nodal surfaces of the various molecular orbitals, or equivalently by considering the change in molecular orbital energies as shown in the Walsh diagram of C_2N_2 in Fig. 2.5. Considering the trans-bending mode first, it appears that the energies of the lone-pair orbitals $4\sigma_u$ and $5\sigma_g$ stay nearly constant upon bending up to 20 degrees. The $1\pi_u$ orbital splits into two components, a_u and b_u, which have very slowly varying energies. The splitting of the $1\pi_g$ orbital into b_g and a_g components is more pronounced with the a_g orbital becoming less bonding. The $2\pi_u^*$ orbital splits into b_u and a_u components with the b_u orbital strongly stabilized and the a_u orbital nearly constant in energy. The splitting is even more pronounced for the $2\pi_g^*$ orbital. The $n\rightarrow\pi^*$ excitation ($5\sigma_g \rightarrow 2\pi_u^*$) becomes ($a_g \rightarrow b_u$) and is stabilized as the bending angle increases. We note that the $1\pi_g$ electrons concomitantly become less bonding upon bending, so that a slightly trans-bent structure is expected to be most favorable. For the cis-bending mode we note that the lone-pair orbital energies are nearly constant as found for the trans-bending mode. Both the bonding $1\pi_u$ and $1\pi_g$ orbitals split into two orbitals, one with slowly varying orbital energy and the other with increasing orbital energy. The $2\pi_u^*$ orbital also splits into two orbitals, one of

which becomes increasingly antibonding. Finally, one of the components of the $2\pi_g^*$ orbital becomes rapidly more strongly bonding. The linear conformation is expected to be the minimum energy structure for the cis-bending mode of the $n \rightarrow \pi^*$ state.

III. Computational Results

A. Ground State C_2N_2 ($\tilde{X}\ ^1\Sigma_g^+$)

The geometry of the ground state was determined using HF and MCHF wave functions. Three basis sets were used: i) a minimal basis set (MB) STO-3G;[60] ii) a double zeta quality (DZ) basis set (9S,5P)/[3S,2p] of Dunning and Hay;[61] and iii) a basis set (DZP) obtained by adding a set of d polarization functions to the DZ set ($\sigma_d^C = 0.75$, $\sigma_d^N = 0.80$).

The HF optimized structures for all three basis sets are given in the first three rows of Table 2.1. The agreement with the experimentally determined structure is good overall. The HF (DZ) structure is fortuitously excellent. The CN bond length for the HF(DZP) structure is shorter than the experimental value while the CC bond length is longer. The calculated harmonic frequencies for the HF(DZP) wave function are also given. The bending frequencies reproduce well the observed fundamentals. For the stretching frequencies, we note that the two highest ones can be assigned to the symmetric and antisymmetric combinations of CN stretches. They are $\sim$ 20 cm^{-1} larger than the observed frequencies. In general we expect the error to be $\sim$6-10% at this level of theory. However, in the present case the CN bonds have triple-bond

character and therefore it is not surprising that electron correlation effects ought to be more important. The CC stretching frequency is close (60 cm^{-1}) to the observed fundamental frequency.

In Section II we justified the need for describing electron correlation effects in the π orbitals of C_2N_2. In the HF wave function the $1\pi_u$ and $1\pi_g$ orbitals are filled with eight electrons. The $2\pi_u^*$ and $2\pi_g^*$ orbitals are empty. The MCHF wave function is constructed by allowing the eight π electrons to be distributed among the four π orbitals in all possible ways consistent with $^1\Sigma_g^+$ symmetry. We denote this wave function MC8. The structures of C_2N_2 ($\tilde{X}$ $^1\Sigma_g^+$) obtained with MC8 and the three basis sets are given in Table 2.1. Compared to the HF structures we note that the MCHF structures have longer CN bond lengths and nearly identical CC bond lengths. This is understandable if one considers the nodal shapes of the four π orbitals depicted in Fig. 2.3. The $1\pi_u$ and $1\pi_g$ orbitals correspond to the symmetric and antisymmetric combinations of the bonding orbitals of the CN triple bonds. The $2\pi_u^*$ and $2\pi_g^*$ orbitals are the corresponding antibonding orbitals. Excitation of the electrons in these antibonding orbitals results in weaker CN bonds and longer bond lengths. Calculated bond lengths are a few hundredths of an angstrom longer than experimental values. This finding is typical for MCHF wave functions of the above description which overemphasize left-right correlation effects in bonds.

The harmonic frequencies calculated with the MCHF wave functions are in

good agreement with the observed fundamentals. Most notable is the effect of electron correlation on the two CN stretching frequencies, which are now less than 7% above the observed frequencies. The lowering of the frequencies is in accord with the lengthening of the CN bonds. The CC stretching mode and the bending modes are also in good agreement with experiment.

The force constants calculated with the MC8(MB) wave function are given in Table 2.2 along with the experimentally derived force constants, and the measured force constants with anharmonicity removed. The agreement between the calculated and the experimental values is good, especially for the interaction force constants. In particular the calculations reproduce the negative sign of $f_{CN/CN}$ found from experiment. Typical force constants[62] for a CC single bond are 4.5-5.5 mdynes/Å; for a CN triple bond 16-18 mdynes/Å; for a CC double bond 9.5-9.9 mdynes/Å; and for a CN double bond 10-11 mdynes/Å. The calculated force constants given in Table 2.2 lie in the appropriate ranges.

Finally, we provide the occupation numbers of the orbitals in the MC8(DZP) wave function: $occ(1\pi_u) = 1.942\times2$; $occ(1\pi_g) = 1.917\times2$; $occ(2\pi_u^*) = 0.092\times2$; $occ(2\pi_g^*) = 0.049\times2$.

To allow for proper dissociation of C_2N_2 ($\tilde{X}\ ^1\Sigma_g^+$) and C_2N_2 ($\tilde{a}\ ^3\Sigma_u^+$) to two CN ($X\ ^2\Sigma^+$) fragments, configuration mixing in the CC bond electron pair must be described in addition to the configuration mixing provided by the MC8 wave function involving the eight π electrons. This can be done by

promoting the CC bond electrons from the bonding σ orbital to the antibonding σ^* orbital. Thus we also calculated MCHF wave functions constructed by distributing the eight π electrons and the two CC (σ) electrons among the four π orbitals and the two σ and σ^* orbitals in all possible ways consistent with spin and symmetry of the states. This wave function is denoted MC10. The MC8(MB) and MC10(MB) geometries are nearly identical although the CC bond is slightly longer in the MC10 structure. The dissociation energy D_e calculated from the MC10(MB) energies is 6.10 eV (D_e(exp.) = 5.58 eV).[1]

B. Excited States C_2N_2 ($\tilde{a}\ ^3\Sigma_u^+$) and C_2N_2 ($\tilde{B}\ ^1\Delta_u$)

The equilibrium structure of C_2N_2 ($\tilde{a}\ ^3\Sigma_u^+$) was calculated with the MC10(MB) wave function which dissociates correctly for this state. The MC8(MB) wave function was used for C_2N_2 ($\tilde{B}\ ^1\Delta_u$). The results are given in Table 2.3.

As indicated above, MCHF wave functions of the type used in this study typically yield bond lengths slightly longer than experimental values. For C_2N_2 ($\tilde{a}\ ^3\Sigma_u^+$), however, the calculated CC bond length is smaller than the experimental value, while the calculated CN bond length is much longer by $\sim$0.086Å. The most important configurations contributing to the MCHF wave functions are given in Table 2.4. In accord with the nodal features of the π orbitals as depicted in Fig. 2.2, the lowest unoccupied $2\pi_u^*$ orbital in C_2N_2 has bonding character between the carbon atoms, and antibonding char-

acter between the carbon and nitrogen atoms. Excitation of a π electron from the $1\pi_g$ orbital to the $2\pi_u^*$ orbital results in weakened CN bonds and a stronger CC bond, and therefore longer CN bond lengths and a shorter CC bond length than the ground state. The calculated structures of C_2N_2 ($\tilde{a}\ ^3\Sigma_u^+$) and C_2N_2 ($\tilde{B}\ ^1\Delta_u$) are in accord with these comments.

We note that a triply excited configuration has the second largest contribution to the C_2N_2 ($\tilde{a}\ ^3\Sigma_u^+$) wave function. No comparable configuration contributes to the C_2N_2 ($\tilde{B}\ ^1\Delta_u$) wave function. This configuration is responsible for the CC and CN bond lengths in C_2N_2 ($\tilde{a}\ ^3\Sigma_u^+$) being shorter and longer, respectively, than in C_2N_2 ($\tilde{B}\ ^1\Delta_u$). We also expect the CN bond in the triplet state to be a weak double bond, and in the singlet state to be a normal double bond. These expectations are borne out by the calculated force constants, as discussed below.

The dissociation energy and excitation energy of C_2N_2 ($\tilde{a}\ ^3\Sigma_u^+$) are in good agreement with experiment. The calculated excitation energy for C_2N_2 ($\tilde{B}\ ^1\Delta_u$) is somewhat larger than the experimental value, but the ordering of the states is qualitatively correct. We note that the calculated excitation energy of C_2N_2 ($\tilde{C}\ ^1\Pi_u$) is $\sim$8.3 eV using similar computational methods (see below). Thus C_2N_2 ($\tilde{a}\ ^3\Sigma_u^+$), and C_2N_2 ($\tilde{B}\ ^1\Delta_u$) are calculated to lie below C_2N_2 ($\tilde{C}\ ^1\Pi_u$) in accord with the observed absorption spectrum.

The harmonic force constants and vibrational frequencies for the $\tilde{X}\ ^1\Sigma_g^+$, $\tilde{a}$

$^3\Sigma_u^+$, $\tilde{B}\ ^1\Delta_u$, and $\tilde{C}\ ^1\Pi_u$ states of C_2N_2 are given in Tables 2.2 and 2.5, respectively. Earlier we noted that our calculated force constants for C_2N_2 ($\tilde{X}\ ^1\Sigma_g^+$) were in agreement with experimentally derived force constants with values typical for triple-bonded CN and single-bonded CC. Comparison of the calculated force constants with typical experimental values indicates that C_2N_2 ($\tilde{a}\ ^3\Sigma_u^+$) has weak CN double-bonds and a weak CC double-bond. The weakness of the CN double-bond was anticipated in the previous section from an analysis of the MCHF wave function. The C_2N_2 ($\tilde{B}\ ^1\Delta_u$) state, however, has typical f_{CN} and f_{CC} values for CN and CC double-bonds. Of special note is the magnitude of the through-bond interaction force constant $f_{CN/CN}$ which is large for both C_2N_2 ($\tilde{a}\ ^3\Sigma_u^+$) and C_2N_2 ($\tilde{B}\ ^1\Delta_u$). In order to explain the magnitude of these interactions, we provide a classical picture of the dominating configurations in these states.

To this end we consider the configurations given in Table 2.4, and substitute the following expressions:

$$\begin{aligned} 1\pi_u &= p_N + p_C + p_C + p_N \\ 1\pi_g &= p_N + p_C - p_C - p_N \\ 2\pi_u &= p_N - p_C - p_C - p_N \\ 2\pi_g &= p_N - p_C + p_C - p_N \end{aligned} \tag{2.1}$$

where p_N and p_C represent the atomic $p\pi$ functions on the nitrogen and carbon atoms, and the left-to-right order corresponds to the left-to-right order of the atoms. After algebraic manipulation, the $1\pi_u^4 1\pi_g^3 2\pi_u^1$ configuration, which

dominates the description of both the $\tilde{a}\ ^3\Sigma_u^+$ and the $\tilde{B}\ ^1\Delta_u$ states, is found to correspond to the classical structures $^+NCCN^-$ and $^-NCCN^+$, i.e., to charge-transfer configurations. The electrostatic interaction arising from the transferred charge is responsible for the large through-bond interaction.

We note also that the C_2N_2 ($\tilde{B}\ ^1\Delta_u$) state is doubly degenerate, and therefore undergoes Renner-Teller splitting due to the interaction of the Δ electronic state with the bending vibrations. A symmetry state correlation diagram for this electronic state is presented in Table 2.6. However, it is known for Δ states that bending leads to higher energy and that the splitting between the A′ and A″ components is small.[63] Indeed, through quadratic terms in the potential, we could not differentiate between the two components.

The calculated harmonic frequencies are in qualitative agreement with the observed fundamental frequencies. The only exception occurs with the ν_4 trans-bend frequency of C_2N_2 ($\tilde{B}\ ^1\Delta_u$) for which the experimental value (274 cm^{-1}) is in better accord with our calculated cis-bend frequency (261 cm^{-1}) than the calculated ν_4 (464 cm^{-1}). Earlier we noted that the calculated ν_1 frequencies for C_2N_2 ($\tilde{X}\ ^1\Sigma_g^+$) were within 5% the observed fundamentals. For C_2N_2 ($\tilde{a}\ ^3\Sigma_u^+$), ν_1 is 8% smaller than the experimental value, and for C_2N_2 ($\tilde{B}\ ^1\Delta_u$) ν_1 is 11% larger. The small size of the basis set used in this study precludes further comment on the accuracy of these calculated frequencies.

C. Excited state C_2N_2 ($\tilde{C}\ ^1\Pi_u$)

The wave function for C_2N_2 ($\tilde{C}\ ^1\Pi_u$) was described in Section II. It is a MCHF wave function which is necessary for a qualitatively correct representation of the state. In addition to the four π orbitals of the C_2N_2 ($\tilde{X}\ ^1\Sigma_g^+$) wave function, the nitrogen lone-pair electrons and orbitals are included in the MCHF wave function. Thus 12 electrons are distributed among two σ and four π orbitals to form a wave function of $^1\Pi_u$ symmetry. We label this wave function MC12.

As discussed in Section II we need to consider the description of the two components of the C_2N_2 ($\tilde{C}\ ^1\Pi_u$) state: i) the A'' state (C_s symmetry) which is expected to have a linear minimum energy structure. It is the third lowest-lying C_2N_2 ($^1\Pi_u$) state in C_{2h} symmetry, or the lowest C_2N_2 ($^1B_1$) state in C_{2v} symmetry; ii) A' state (C_s symmetry) which is expected to have a nonlinear minimum energy structure. It is the trans-bent second lowest-lying C_2N_2 ($^1\Pi_u$) state in C_{2h} symmetry. A state correlation diagram for the $^1\Pi_u$ state is given in Table 2.7.

1. Linear C_2N_2 ($\tilde{C}\ ^1\Pi_u$, $^1A''$)

The structure of the C_2N_2 ($\tilde{C}\ ^1\Pi_u$, $^1A''$) state obtained with the MC12 wave function, and the three basis sets is given in Table 2.8. Because of the quality of the basis set the MC12(DZP) results ought to be the most reliable. The most notable change from the ground state structure is the lengthening of

the CN bonds and the shortening of the CC bond. The CN bond lengths in C_2N_2 ($^1\Pi_u$, $^1A''$) are 0.05Å longer than in C_2N_2 ($\tilde{X}\ ^1\Sigma_g^+$), and the CC bond length is 0.08Å shorter. The nodal shape of the $2\pi_u^*$ orbital is responsible for the direction of the change. The origin of these bond length changes for the $\tilde{C}$ $^1\Pi_u$ state is the same as that presented above for the $\tilde{a}\ ^3\Sigma_u^+$ and $\tilde{B}\ ^1\Delta_u$ states.

The term energy given in the last column of Table 2.8 was calculated by taking the difference in energy between the MC8 energy of the ground state and the MC12 energy of the excited state for the given basis set. The value of 8.2 eV. from the DZP basis set is in semiquantitative agreement with the origin of the absorption at 7.3 eV. The present results confirm the findings of Connors et al.[55] and are quite different from Bell's.[56] The occupation numbers of the MC12(DZP) orbitals are: occ($4\sigma_u$) = 1.805; occ($5\sigma_g$) = 1.188; occ($1\pi_u$) = 0.062×2; occ($1\pi_g$) = 1.854×2; occ($2\pi_u^*$) = 0.640×2; occ($2\pi_g^*$) = 0.062×2. A comparison of these numbers with the ground state occupation numbers clearly shows the importance of configuration mixing in this state. Excitation from the $4\sigma_u$ nitrogen lone-pair orbital is very important as expected from the near degeneracy of the $4\sigma_u$ and $5\sigma_g$ orbitals.

The harmonic frequencies calculated with the MC12(MB) wave function for linear C_2N_2 ($\tilde{C}\ ^1\Pi_u$, $^1A''$) are given in Table 2.5, and were derived from the force constants given in Table 2.2. We note first that the ν_3 frequency of the asymmetric combination of CN stretches is a real positive frequency clearly

indicating that the molecule has a symmetric structure with a center of inversion. With more limited MCHF wave functions, the symmetry-breaking problem discussed in Section II would have manifested itself here: the MC12 wave function is the smallest MCHF wave function which predicts a stable symmetric minimum. Turning to the symmetric stretch frequencies we note that the ν_1 mode is 2145 cm^{-1} and that a vibrational progression of 2100 cm^{-1} is observed experimentally and is assigned to the symmetric combination of CN stretches. The calculated and experimental values are fortuitously in excellent agreement. By comparison with the frequencies calculated for the lower states we expect ν_1, ν_2, and ν_3 for C_2N_2 ($\tilde{C}$ $^1\Pi_u$, $^1A''$) to lie within $\sim$10% of the experimental frequencies.

The force constants given in Table 2.2 show the strong double-bond character of the CC bond in C_2N_2 ($\tilde{C}$ $^1\Pi_u$) and the double-bond character of the CN bonds in this excited state. This finding agrees with the qualitative description obtained from the nodal shape of the $2\pi_u^*$ orbital.

To summarize we find that the $^1A''$ component of C_2N_2 ($\tilde{C}$ $^1\Pi_u$) has a linear equilibrium structure as indicated by the two positive frequencies for the trans-bend and the cis-bend vibrational modes.

2. Trans-Bent C_2N_2 ($\tilde{C}$ $^1\Pi_u$, $^1A'$)

With the MC12(MB) and MC12(DZ) wave functions we located a minimum energy structure for the C_2N_2 ($\tilde{C}$ $^1\Pi_u$, $^1A'$) state with a trans-bent

conformation. The geometrical parameters are given in Table 2.9. The structure is only slightly bent (10° and 6° from linearity for the MB and DZ basis sets, respectively). In addition, the CN and CC bond lengths are nearly identical to their values for C_2N_2 ($\tilde{C}$ $^1\Pi_u$, $^1A''$); c.f. Table 2.7. The energy differences between the linear and trans-bent structures are very small. Although we did not fully optimize the structure using the MC12(DZP) wave function, we carried out a single calculation of the energy and energy gradients for a geometry only slightly trans-bent from linearity. The energy of this conformation was lower than the energy of the linear structure, a clear indication that this distortion leads to a minimum with a trans-bent conformation. As discussed in Section II a trans-bent structure of C_2N_2 ($\tilde{C}$ $^1\Pi_u$, $^1A'$) is in accord with the conclusion drawn from the Walsh diagram. A qualitative picture of the bending potential of C_2N_2($\tilde{C}$ $^1\Pi_u$) is shown in Fig. 2.6. However the bending angle depends on the basis set and on the electron correlation treatment, although it is likely that this angle remains small. Consideration of the small change in bond length between the $^1A'$ and $^1A''$ components of C_2N_2 ($\tilde{C}$ $^1\Pi_u$) suggests that the vibrational stretching frequencies of the C_{2h} minimum energy structure should be very close to values for the linear state. For this reason we did not calculate the harmonic frequencies for the trans-bent structure of C_2N_2 ($\tilde{C}$ $^1\Pi_u$, $^1A'$). We attempted to calculate the cis-bending mode frequency for the linear conformation of C_2N_2 ($\tilde{C}$ $^1\Pi_u$, $^1A'$). However, we failed to obtain

convergence of the SCF process for the C_2N_2 ($\tilde{C}\ ^1\Pi_u$, $^1A_1$) in C_{2v} due to the presence of a nearly degenerate $^1A_1$ state.

IV. Conclusions

We have presented an ab initio MCHF study of the $\tilde{X}\ ^1\Sigma_g^+$, $\tilde{a}\ ^3\Sigma_u^+$, $\tilde{B}\ ^1\Delta_u$, and $\tilde{C}\ ^1\Pi_u$ states of C_2N_2. We have shown that configuration mixing among the π and n electrons is needed to obtain a qualitatively correct description of the excited states. The computed excitation energies are in semiquantitative agreement with experiment.

The results of this study are in accord with the description of the $\tilde{a}\ ^3\Sigma_u^+$ and $\tilde{B}\ ^1\Delta_u$ states near their equilibrium structure as $\pi \rightarrow \pi^*$ excitations. The C_2N_2 ($\tilde{C}\ ^1\Pi_u$) state is best described as a $n \rightarrow \pi^*$ state with a nitrogen lone-pair electron excited into the lowest empty π^* orbital.

The C_2N_2 ($\tilde{B}\ ^1\Delta_u$) and C_2N_2 ($\tilde{C}\ ^1\Pi_u$) states are Renner-Teller states. No splitting is observed between the A′ and A″ components of the B state in the harmonic approximation. However, the Renner-Teller interaction in C_2N_2 ($\tilde{C}\ ^1\Pi_u$) leads to a lower state with $^1A'$ symmetry which most likely has a slightly trans-bent minimum energy structure, and an upper state with $^1A''$ symmetry which has a linear structure.

Computed harmonic force constants indicate a strong through-bond interaction for C_2N_2 ($\tilde{a}\ ^3\Sigma_u^+$) and C_2N_2 ($\tilde{B}\ ^1\Delta_u$) which is due to the dominance of the charge transfer configuration $^+NCCN^-$. The calculated harmonic

frequencies confirm that C_2N_2 ($\tilde{C}\ ^1\Pi_u$) has a symmetric structure. The frequency corresponding to the symmetric combination of CN stretches (2145 cm^{-1}) is in agreement with the observed vibrational progression of 2100 cm^{-1}. The frequency of the asymmetric combination of CN stretches is calculated to be 1789 cm^{-1}. Finally, the Renner-Teller interaction in C_2N_2 ($\tilde{C}\ ^1\Pi_u$) gives rise to a complicated structure due to the bending vibrations.

Table 2.1. Calculated properties of $C_2N_2(\tilde{X}^1\Sigma_g^+)$.

WFN	E (hartrees)	R(CN) (Å)	R(CC) (Å)	ν_1 (cm^{-1}) sym. CN	ν_2 (cm^{-1}) CC	ν_3 (cm^{-1}) asym. CN	ν_4 (cm^{-1}) trans-bend degenerate	ν_5 (cm^{-1}) cis-bend degenerate
HF(MB)	-182.219458	1.160	1.411					
HF(DZ)	-184.515989	1.150	1.387					
HF(DZP)	-184.613676	1.137	1.403	2720	905	2522	599	275
MC8(MB)	-182.421963	1.199	1.412	2463	890	2251	437	206
MC8(DZ)	-184.700565	1.179	1.387	2453	901	2201	477	232
MC8(DZP)	-184.781534	1.164	1.398	2482	895	2283	416	213
MC10(MB)	-184.429340	1.201	1.429					
Expt.		1.154[a]	1.389[a]	2330[b] (2355)	854[b] (877)	2158[b] (2192)	507[b] (513)	233[b] (234)

[a]A.G. Maki, J. Chem. Phys. **43**, 3193 (1965).

[b]Experimental harmonic frequencies in parentheses. See L.H. Jones, J. Mol. Spect. **45**, 55 (1973).

Table 2.2. Force constants[a] of $C_2N_2(\tilde{X}^1\Sigma_g^+)$, $C_2N_2(\tilde{a}^3\Sigma_u^+)$, $C_2N_2(\tilde{B}^1\Delta_u)$, and linear $C_2N_2(\tilde{C}^1\Pi_u)$.

	$\tilde{X}^1\Sigma_g^+$			$\tilde{a}^3\Sigma_u^+$	$\tilde{B}^1\Delta_u$	$\tilde{C}^1\Pi_u$
	Calc.[b]	Obs.[e]	Harm.[e]	Calc.[c]	Calc.[b]	Calc.[d]
f_{CN}	18.99	18.03	17.98	6.78	10.31	12.51
f_{CC}	7.52	6.90	7.08	9.56	11.87	10.52
$f_{CC/CN}$	0.31	0.42	0.58	1.41	0.42	1.35
$f_{CN/CN'}$	-0.31	-0.26	-0.32	2.58	2.74	0.32
$f_<$	0.24	0.29	0.30	0.19	0.34[f]	0.31
$f_{</<'}$	-0.003	-0.013	-0.02	0.11	0.34	-0.27

[a]In mdynes/Å.

[b]Determined with MC8(MB) wavefunction.

[c]Determined with MC10(MB) wavefunction.

[d]Determined with MC12(MB) wavefunction.

[e]L. H. Jones, J. Mol. Spectrosc. **49**, 82 (1974), where "Harm." indicates the harmonic contribution from experiment.

[f]The A′ and A″ components of the bending modes have the same harmonic force constants (see text).

Table 2.3. Energies and structures of $C_2N_2(\tilde{X}^1\Sigma_g^+, \tilde{a}^3\Sigma_u^+, \tilde{B}^1\Delta_u)$[a].

	$\tilde{X}^1\Sigma_g^+$		$\tilde{a}^3\Sigma_u^+$		$\tilde{B}^1\Delta_u$	
	Calc.[b]	(Obs.)[d]	Calc.[b]	(Obs.)[e]	Calc.[c]	(Obs.)[f]
R(CC)	1.429	(1.389)	1.309	(1.323)	1.303	
R(CN)	1.201	(1.154)	1.310	(1.224)	1.279	
E	-182.42934		-182.30771		-182.13695	
T_e		3.85	(4.1)		7.75	(6.0)
D_e	6.10	(5.58)[g]	2.25	(2.16)		

[a]Bond lengths in Å; term energies T_e, and dissociation energies D_e, in eV; total energies E in hartrees.

[b]Calculated from MC10(MB) wavefunction.

[c]Calculated from MC8(MB) wavefunction.

[d]Experimental structure from A. G. Maki, J. Chem. Phys. **43**, 3193 (1965).

[e]Experimental values from J. A. Meyer, D. H. Siedman, D. W. Setser, J. Mol. Spectrosc. **44**, 206 (1972).

[f]Ref. 54.

[g]Ref. 1.

Table 2.4. Characteristics of the MC10 wavefunctions.

$\tilde{X}^1\Sigma_g^+$		$\tilde{a}^3\Sigma_u^+$		$\tilde{B}^1\Delta_u$	
Configuration (configuration coefficient)					
$1\pi_u^4 1\pi_g^4$	(0.91)[a]	$1\pi_u^4 1\pi_g^3 2\pi_u$	(0.60)	$1\pi_u^4 1\pi_g^3 2\pi_u$	(0.63)
$1\pi_u^3 1\pi_g^3 2\pi_u 2\pi_g$	(0.14)	$1\pi_u^4 1\pi_g 2\pi_u^3$	(0.20)	$1\pi_u^3 1\pi_g^3 2\pi_u^2$	(0.14)
$1\pi_g^4 1\pi_g^2 2\pi_u^2$	(0.13)	$1\pi_u^3 1\pi_g^4 2\pi_g$	(0.14)	$1\pi_u^4 1\pi_g^2 2\pi_u 2\pi_g$	(0.11)
$1\pi_u^4 1\pi_g^2 2\pi_u^2$	(0.11)	$1\pi_u^3 1\pi_g^2 2\pi_u^3$	(0.13)		
Occupation					
CC(σ)	1.977	1.977		1.981	
$1\pi_g$	2.924×2	1.884×2		1.916×2	
$1\pi_g$	1.883×2	1.387×2		1.460×2	
$2\pi_u$	0.123×2	0.619×2		0.557×2	
$2\pi_g$	0.069×2	0.109×2		0.066×2	
CC(σ^*)	0.022	0.024		0.020	

[a]These configuration coefficients were determined from the MC8(MB) wavefunction.

Table 2.5. Harmonic vibrational frequencies (in cm^{-1}).

	$\tilde{X}^1\Sigma_g^+$		$\tilde{a}^3\Sigma_u^+$		$\tilde{B}^1\Delta_u$		$\tilde{C}^1\Pi_u$	
	Calc.[a]	(Obs.)[d]	Calc.[b]	(Obs.)[e]	Calc.[a]	(Obs.)[f]	Calc.[c]	(Obs.)[g]
ν_1 (sym. CN str.)	2463	(2330)	1881	(2050)	2366	(2140)	2145	(2100)
ν_2 (CC str.)	890	(854)	911	(899)	973		989	
ν_3 (asym. CN str.)	2252	(2158)	1052		1410		1789	
ν_4 (trans-bend)	438	(507)	253	(264)	464	(274)	698	
ν_5 (cis-bend)	206	(233)	214	(211)	261	85		

[a]Determined from the MC8 wavefunction.
[b]Determined from the MC10 wavefunction.
[c]Determined from the MC12 wavefunction.
[d]L. H. Jones, J. Mol. Spectrosc. **45**, 55 (1973).
[e]J. A. Meyer, D. M. Stedman, D. W. Setser, J. Mol. Spectrosc. **44**, 206 (1972).
[f]S. C. Woo and R. M. Badger, Phys. Rev. **39**, 932 (1932).
[g]Ref. 55.

Table 2.6. State correlation diagram for bent $C_2N_2(\tilde{B}\,^1\Delta_u)$

$D_{\infty h}$ linear	C_s bent	C_{2h} trans-bent	C_{2v} cis-bent
$^1\Delta_u$	$^1A'$	^1A_u	$^1A_2$
	$^1A''$	^1B_u	$^1B_2$

Table 2.7. State correlation diagram for bent $C_2N_2(\tilde{C}\,^1\Pi_u)$

$D_{\infty h}$ linear	C_s bent	C_{2h} trans-bent	C_{2v} cis-bent
$^1\Pi_u$	$^1A'$	^1B_u	$^1A_1$
	$^1A''$	^1A_u	$^1B_1$

Table 2.8. Structure of $C_2N_2(\tilde{C}\,^1\Pi_u, {}^1A'')$.

WFN	Energy (a.u.)	R(CN) (Å)	R(CC) (Å)	T_e (eV)
MC12(MB)	-182.115609	1.25236	1.30787	8.3
MC12(DZ)	-184.404646	1.23205	1.31318	8.1
MC12(DZP)	-184.475805	1.21307	1.31755	8.2

Table 2.9. Structure of $C_2N_2(\tilde{C}\,^1\Pi_u, {}^1A')$ (C_{2h} symmetry).

WFN	Energy (a.u.)	R(CN) (Å)	R(CC) (Å)	< (CCN) (deg)
MC12(MB)	-184.115833	1.25291	1.31692	169.9
MC12(DZ)	-184.404655	1.23201	1.31565	174.0

Figure Captions

Fig. 2.1 Correlation diagram for $C_2N_2 \rightarrow 2CN$

Fig. 2.2 Schematic representation of the interaction of CN ($X\ ^2\Sigma^+$) with CN ($X\ ^2\Sigma^+$) and CN ($X\ ^2\Sigma^+$) with CN ($A\ ^2\Pi$).

Fig. 2.3 Nodal character of the π orbitals of C_2N_2.

Fig. 2.4 Energy diagram for symmetry breaking behavior in electronically excited C_2N_2.

Fig. 2.5 Walsh diagram of NCCN.

Fig. 2.6 Qualitative bending potential of C_2N_2 ($\tilde{C}\ ^1\Pi_u$).

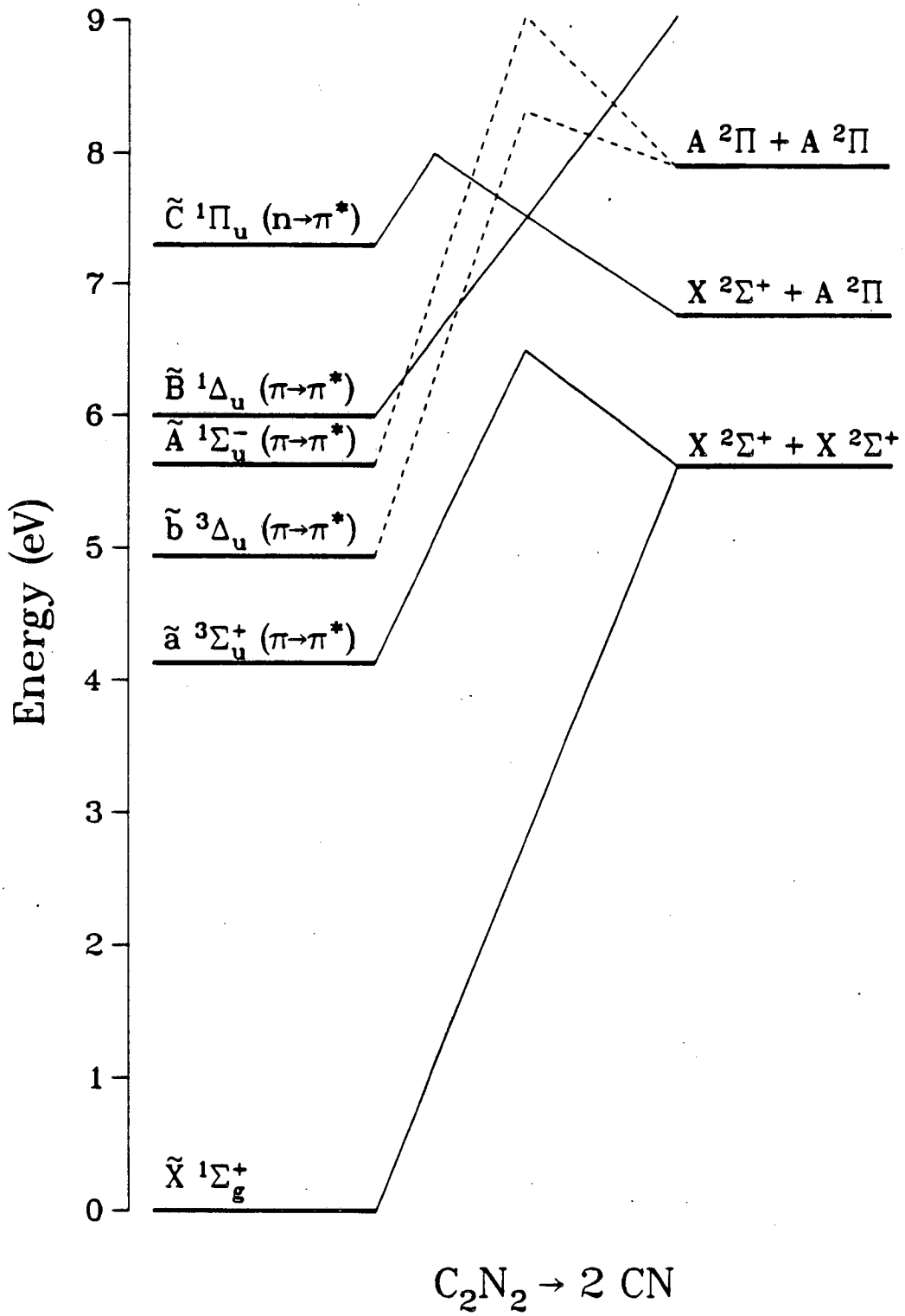
Energy (eV)
9
8
7
6
5
4
3
2
1
0
$\tilde{C}\ ^1\Pi_u$ (n→π*)
$\tilde{B}\ ^1\Delta_u$ (π→π*)
$\tilde{A}\ ^1\Sigma_u^-$ (π→π*)
$\tilde{b}\ ^3\Delta_u$ (π→π*)
$\tilde{a}\ ^3\Sigma_u^+$ (π→π*)
$\tilde{X}\ ^1\Sigma_g^+$
A $^2\Pi$ + A $^2\Pi$
X $^2\Sigma^+$ + A $^2\Pi$
X $^2\Sigma^+$ + X $^2\Sigma^+$
$C_2N_2 \rightarrow 2\ CN$

Figure 2.1

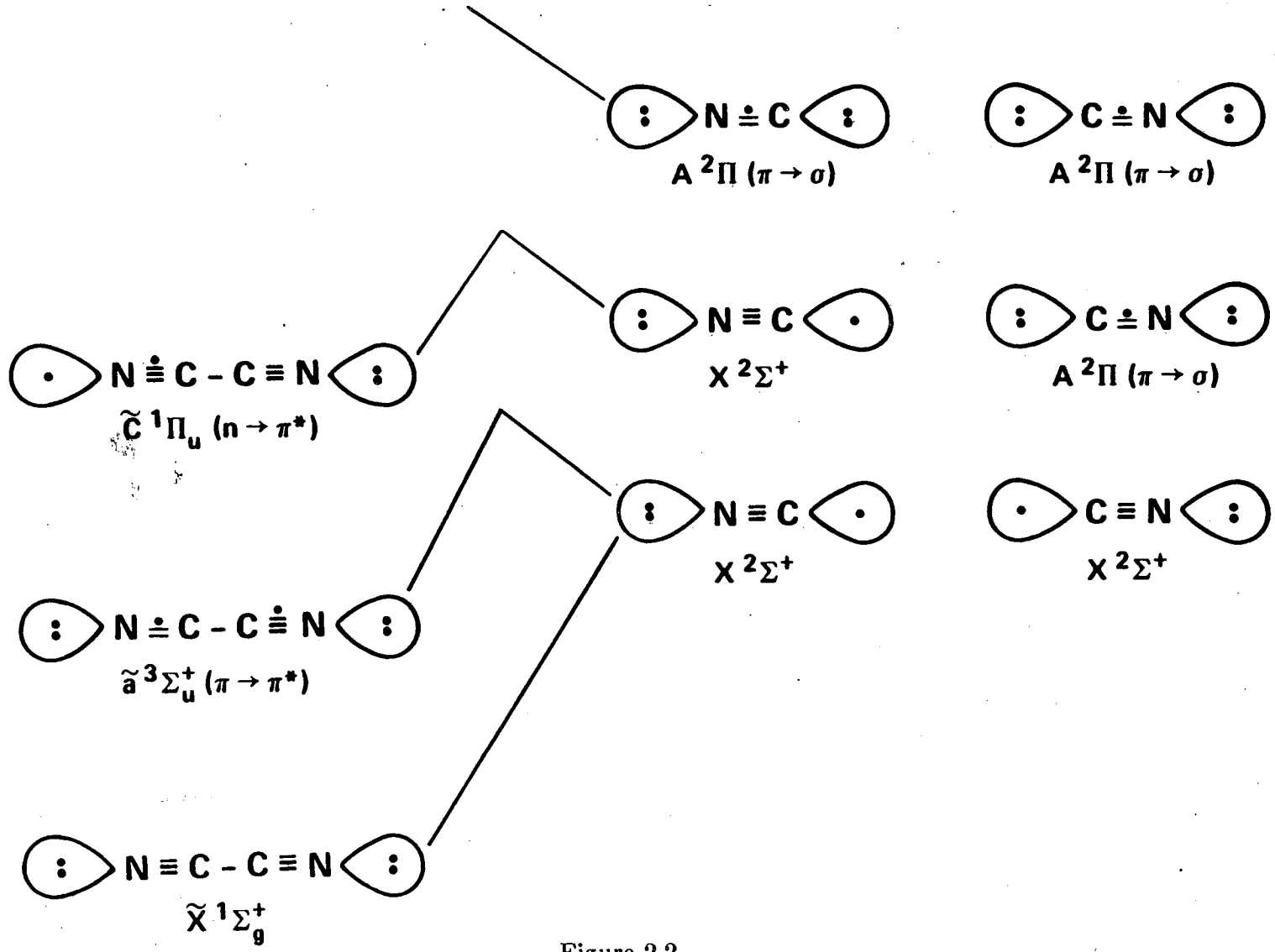
N ≐ C
A ²Π (π → σ)
C ≐ N
A ²Π (π → σ)
N ≡ C
X ²Σ⁺
C ≐ N
A ²Π (π → σ)
N ≐ C – C ≡ N
c̃ ¹Π_u (n → π*)
N ≡ C
X ²Σ⁺
C ≡ N
X ²Σ⁺
N ≐ C – C ≐ N
ã ³Σ⁺_u (π → π*)
N ≡ C – C ≡ N
X̃ ¹Σ⁺_g

Figure 2.2

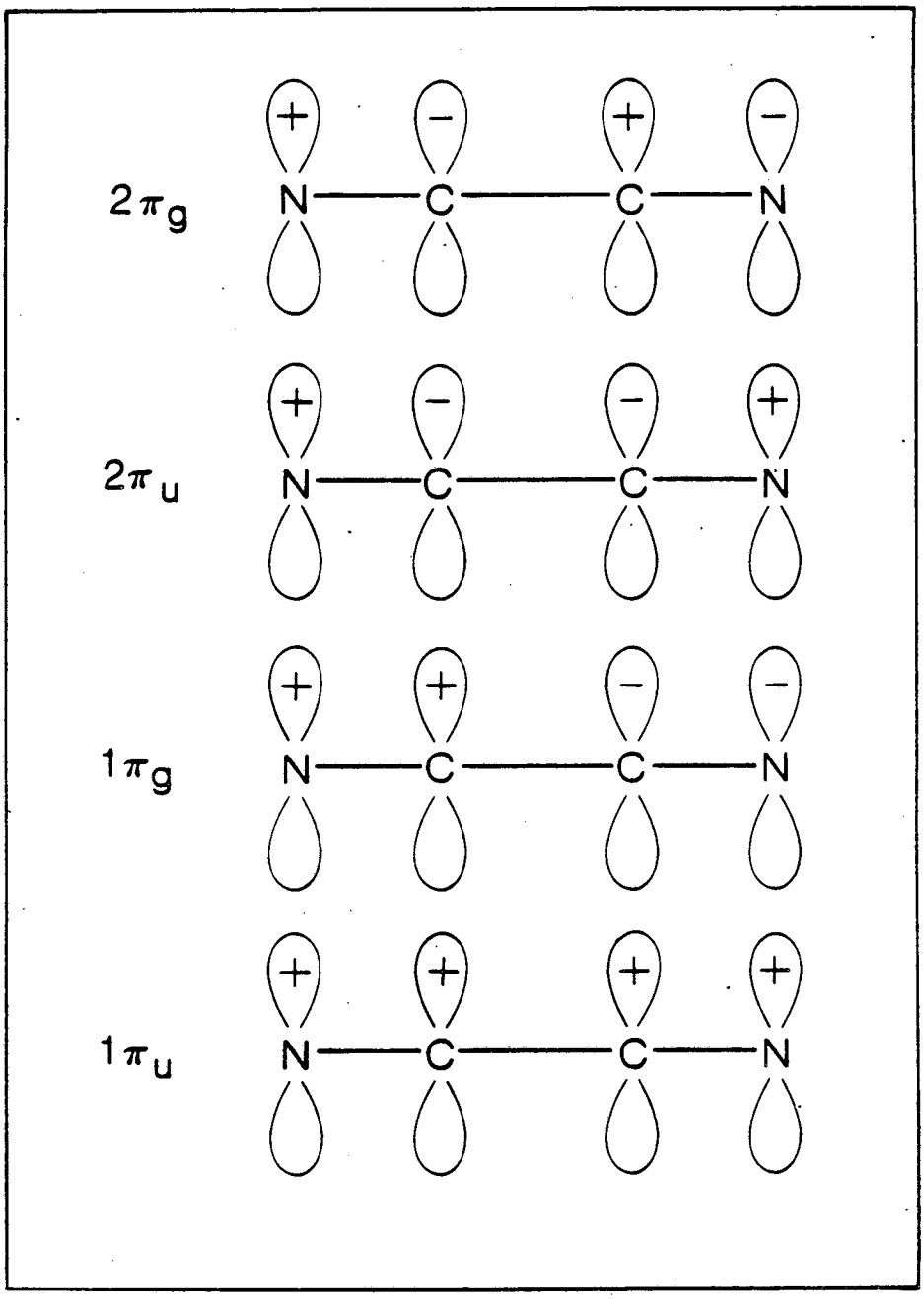

Figure 2.3

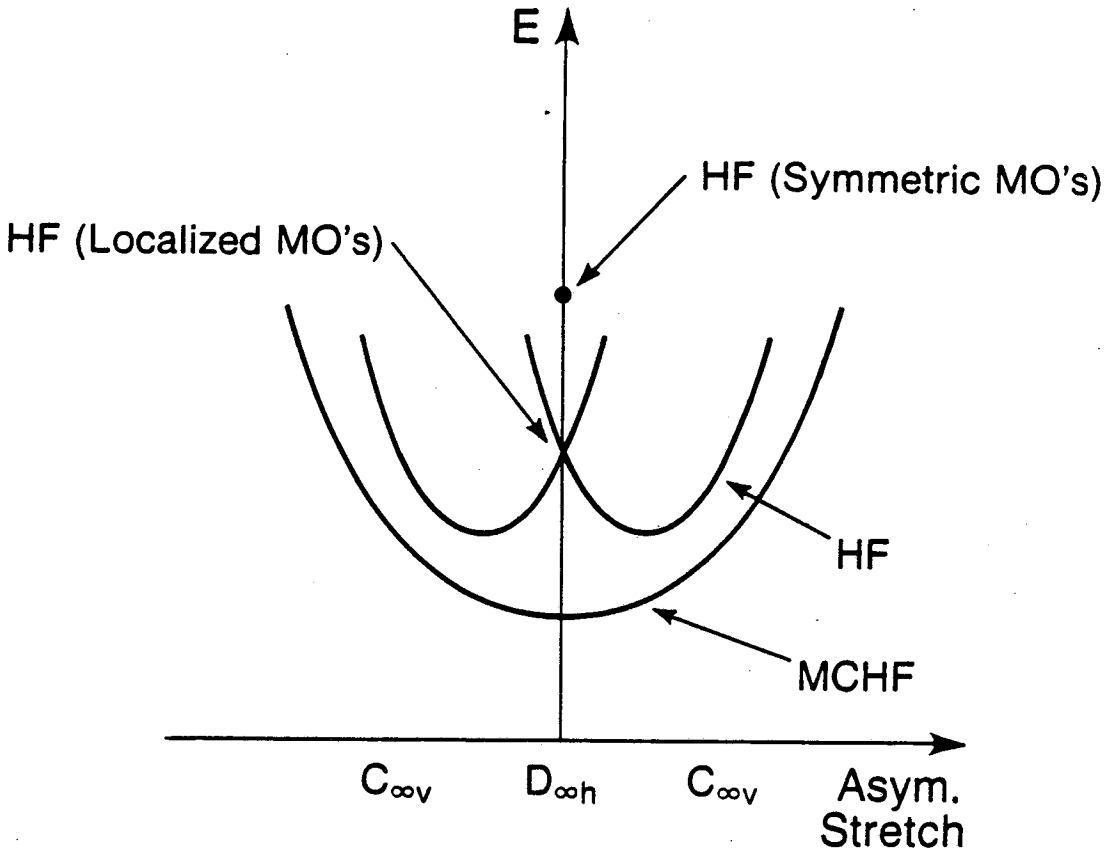
E
HF (Symmetric MO's)
HF (Localized MO's)
HF
MCHF
C∞v
D∞h
C∞v
Asym.
Stretch

Figure 2.4

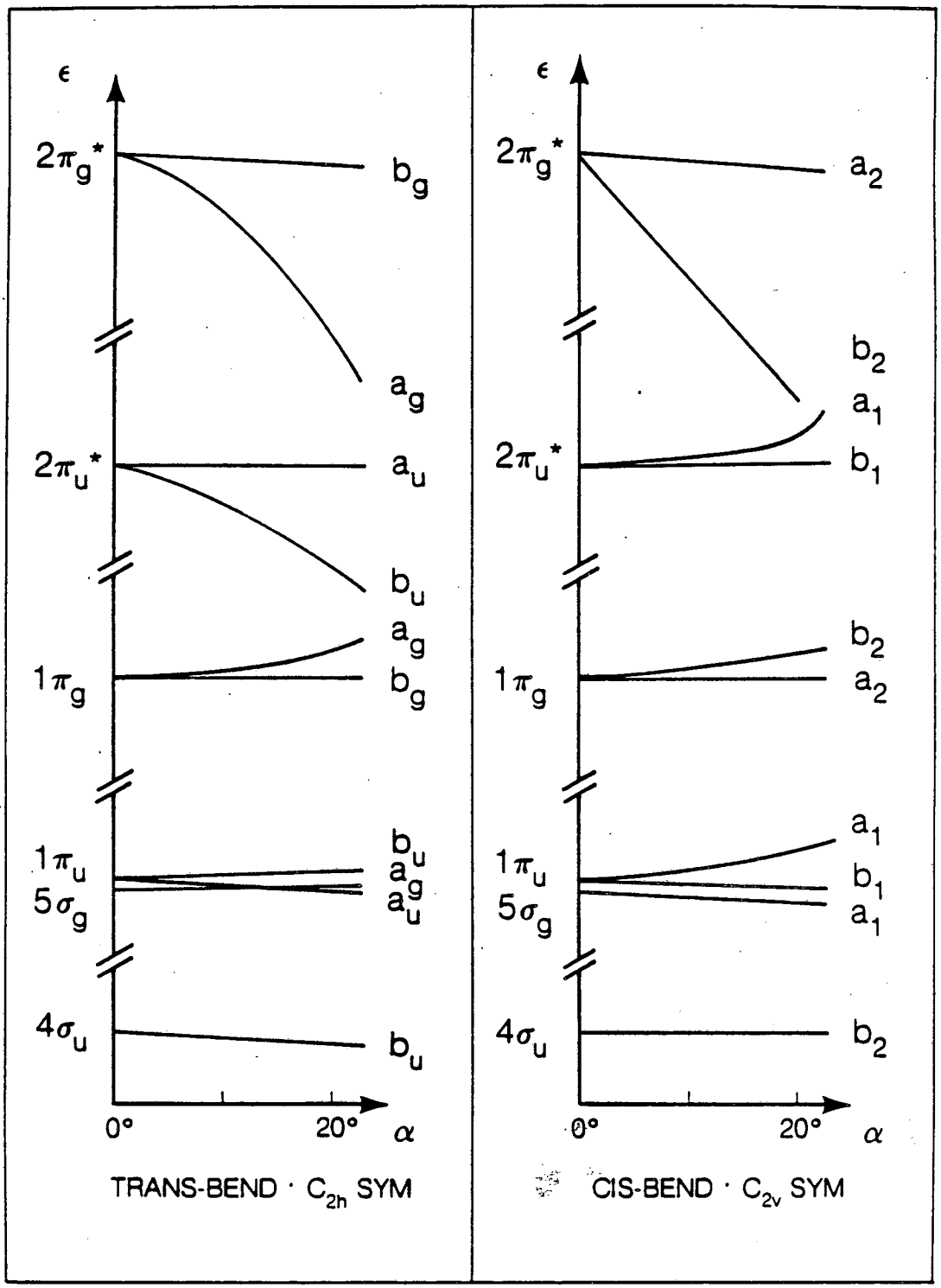
ϵ
2π_g*
b_g
a_g
2π_u*
a_u
b_u
a_g
1π_g
b_g
b_u
1π_u
a_g
5σ_g
a_u
4σ_u
b_u
0°
20°
α
TRANS-BEND · C_2h SYM
ϵ
2π_g*
a_2
b_2
a_1
2π_u*
b_1
b_2
1π_g
a_2
a_1
1π_u
b_1
5σ_g
a_1
4σ_u
b_2
0°
20°
α
CIS-BEND · C_2v SYM

Figure 2.5

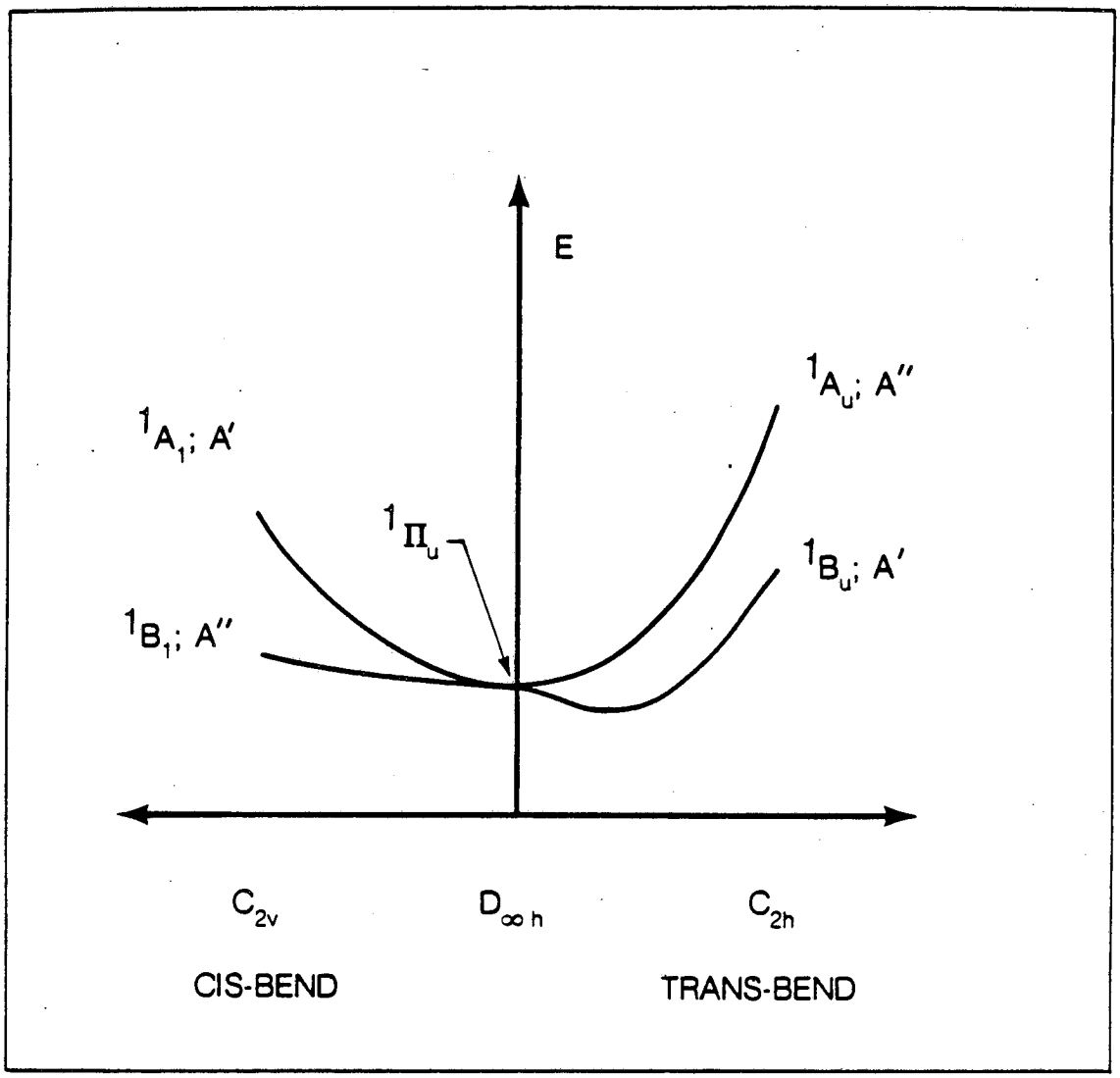
E
^1A_u; A″
$^1A_1$; A′
$^1\Pi_u$
^1B_u; A′
$^1B_1$; A″
C_{2v}
$D_{\infty h}$
C_{2h}
CIS-BEND
TRANS-BEND

Figure 2.6

CHAPTER 3

Photodissociation As A Quantum Transition: Photofragment Vibrational Distributions Of $C_2N_2(\tilde{C}\ ^1\Pi_u)$ Predissociation

I. Introduction

Most theoretical treatments of polyatomic photodissociation have been limited to triatomic systems.[24–30] Some are based on the formal theory of scattering and lead to the necessity of solving sets of coupled differential or integral equations.[14–20] Such methods present well-known computational difficulties and become prohibitively difficult with the size of the polyatomic system. Approximations in formal scattering approaches can lead to simpler expressions requiring evaluation of a Franck-Condon (FC) matrix element.[41,64,65] Other FC approaches arise from perturbation theory.[35,41–43] Various FC methods have been found to yield reliable relative product energy distributions for direct single-photon photodissociation,[36,37,66–69] but present difficulties in obtaining accurate absolute distributions. In this chapter consideration is directed to indirect photodissociation which presents even more fundamental complications.[28]

Recent experimental studies[22,47–50] of cyanogen (C_2N_2) photodissociation have shown that the $\tilde{C}\ ^1\Pi_u$ state predissociates via a radiationless transition to ground state $CN(X\ ^2\Sigma^+)$ and electronically excited $CN(A\ ^2\Pi)$ fragments and

have reported product vibrational distributions (PVD's) at several photon energies. An adiabatic correlation analysis identifies the predissociation as type II (vibrational), see below, which occurs on a single adiabatic electronic potential energy surface (PES). Although indirect photodissociation has been discussed in the theoretical literature,[65,70,71] most computational studies have treated triatomic systems.

In this chapter we focus on the evaluation of photofragment PVD's using an adiabatic theory of polyatomic photodissociation developed by Kresin and Lester[28,42–44] (KL). The theory treats indirect photodissociation as a quantum transition between quasiadiabatic (diabatic) states[72–76] and leads to a localized description of the excited electronic adiabatic PES. Obtaining PVD's in this approach requires the evaluation of a FC-type factor. The method includes important contributions from final state interactions,[44] i.e., the translational-vibrational coupling in the dissociative channel. This contrasts with other FC approaches which neglect final state interactions in the zeroeth-order approximation and include this coupling via a second step distorting the zeroeth-order solution.

This chapter is organized as follows. In section II we summarize the theory, which has been presented in detail elsewhere.[42–44] Section III outlines the application of the approach to predissociation of $C_2N_2(\tilde{C}\ ^1\Pi_u)$ and compares computed and measured fragment PVD's. A summary and concluding remarks comprise section IV.

II. Theory

A. Photodissociation as a Quantum Transition

Indirect photodissociation occurs when absorption of radiation leaves the molecule in an excited electronic state of finite lifetime that subsequently undergoes a radiationless transition (predissociation) to a final dissociative state. Herzberg distinguishes three types of predissociation:[23,63] electronic (type I), vibrational (type II), and rotational (type III). Type I is accompanied by a change of PES, whereas types II and III occur on the same adiabatic electronic PES. For the latter cases, dissociation is caused by redistribution of vibrational or rotational energy of the molecule to translational and internal degrees of freedom of the fragments. Because of the finite lifetime of the excited state, it is a good approximation to neglect any dependence on the electronic ground state and photon energy other than the specification of the transition.

The general theory of quantum transitions is well-known and appears in several quantum texts.[21] We summarize here the first-order perturbation theory analysis for the present application and note that the method is valid to any order (see Appendix A). The probability of a radiationless transition from a quasidiscrete state (Q) to a dissociative state (D) is given by the golden rule expression

$$dW_{D\leftarrow Q} = \frac{2\pi}{\hbar} \left| H'_{D\leftarrow Q} \right|^2 \delta(E'-E)\, \rho_E\, dE, \tag{3.1}$$

where

$$H'_{D\leftarrow Q} = \int \Psi_D^*(\vec{r}, \vec{R})\ \hat{H}'\ \Psi_Q(\vec{r}, \vec{R})\, d\vec{R}\, d\vec{r}. \tag{3.2}$$

Here $\hat{H}'$ is the perturbation operator which governs the transition, ρ_E is the

density of states, Ψ_D and Ψ_Q are the total wave functions for the D and Q states, and $\vec{r}$ and $\vec{R}$ refer to the electronic and nuclear coordinates. To calculate the probability of a D←Q transition it is necessary to obtain expressions for $\hat{H}'$, Ψ_D, and Ψ_Q.

The applicability of the quantum theory of transitions arises from the capability of identifying that part of the total Hamiltonian, $\hat{H}'$, which causes the transition. For direct photodissociation it is the matter-radiation interaction which is the pertinent term of the Hamiltonian.[21] For type I indirect photodissociation, $\hat{H}'$ is the deviation from the Born-Oppenheimer (BO) approximation resulting from the neglect of nuclear motion (or spin-orbit coupling if the states are of different spin).[21] For type II (vibrational) and type III (rotational) predissociation, the transition from the initial Q state to the final D photofragment state takes place on a single adiabatic PES. In the former case we employ our method developed to treat chemical reaction as a quantum transition.[77,78] Type III predissociation could be treated similarly. Transformation to a diabatic representation yields a localized description of the quantum transition between two diabatic PES's. In this representation there are direct coupling terms which cause the transition between the diabatic states.

B. Diabatic Representation

The total Schrödinger equation can be written

$$\hat{H}\,\Psi(\vec{r},\vec{R}) = (\hat{H}_e + \hat{T}_{\vec{R}})\,\Psi(\vec{r},\vec{R}) = E\,\Psi(\vec{r},\vec{R}), \tag{3.3}$$

where $\hat{T}_{\vec{R}}$ is the nuclear kinetic energy operator and $\hat{H}_e$ is the electronic Hamil-

tonian

$$\hat{H}_e = \hat{T}_r + V(\vec{r}, \vec{R}). \tag{3.4}$$

Here $\hat{T}_r$ is the electronic kinetic energy operator and $V(\vec{r}, \vec{R})$ is the total potential energy. In accord with the BO approximation, the electronic wave function is defined by

$$\hat{H}_e \, \psi_n(\vec{r}; \vec{R}) = \epsilon_n(\vec{R}) \, \psi_n(\vec{r}; \vec{R}). \tag{3.5}$$

The term $\epsilon_n(\vec{R})$ represents the nth adiabatic electronic PES and labels both the excited C_2N_2 molecule (Q state) and the photofragments (D state). We introduce a new potential $\tilde{V}(\vec{r}, \vec{R})$, constructed so that the D←Q process is a surface crossing in the diabatic representation, i.e., the effect of substituting $\tilde{V}(\vec{r}, \vec{R})$ for $V(\vec{r}, \vec{R})$ in the electronic Schrödinger equation (3.5) is to change the adiabatic PES's $\epsilon_n(\vec{R})$ and $\epsilon_{n+1}(\vec{R})$ to diabatic PES's $\tilde{\epsilon}_Q(\vec{R})$ and $\tilde{\epsilon}_D(\vec{R})$ that are solutions to

$$\begin{aligned} \left[\hat{T}_r + \tilde{V}(\vec{r}, \vec{R})\right] \tilde{\psi}_Q(\vec{r}; \vec{R}) &= \tilde{\epsilon}_Q(\vec{R}) \, \tilde{\psi}_Q(\vec{r}; \vec{R}) \\ \left[\hat{T}_r + \tilde{V}(\vec{r}, \vec{R})\right] \tilde{\psi}_D(\vec{r}; \vec{R}) &= \tilde{\epsilon}_D(\vec{R}) \, \tilde{\psi}_D(\vec{r}; \vec{R}). \end{aligned} \tag{3.6}$$

More specifically, we choose the potential $\tilde{V}(\vec{r}, \vec{R})$ such that the term $\tilde{\epsilon}_Q(\vec{R})$ corresponds to the Q (predissociative) channel and is equivalent to $\epsilon_n(\vec{R})$ for small interfragment distances, ρ, and becomes $\epsilon_{n+1}(\vec{R})$ in the asymptotic region $\rho \to \infty$; similarly, $\tilde{\epsilon}_D(\vec{R})$ is equivalent to $\epsilon_n(\vec{R})$ for large ρ as shown in Fig. 3.1.

Formally, one can introduce the total wave functions $\tilde{\Psi}_Q(\vec{r}, \vec{R}) = \tilde{\psi}_Q(\vec{r}; \vec{R}) \, \tilde{\phi}_Q(\vec{R})$ and $\tilde{\Psi}_D(\vec{r}, \vec{R}) = \tilde{\psi}_D(\vec{r}; \vec{R}) \, \tilde{\phi}_D(\vec{R})$, that are eigenfunctions of the total Hamiltonian

$$\tilde{H} = \hat{T}_{\vec{R}} + \hat{T}_{\vec{r}} + \tilde{V}(\vec{r}, \vec{R}) = \hat{T}_{\vec{R}} + \tilde{H}_e \tag{3.7}$$

in a diabatic representation and lead to a PES crossing between the Q and D diabatic states. In the BO approximation, the diabatic nuclear wave functions are solutions of

$$\begin{bmatrix} \hat{T}_{\vec{R}} + \tilde{\epsilon}_Q(\vec{R}) \end{bmatrix} \tilde{\phi}_Q(\vec{R}) = E\, \tilde{\phi}_Q(\vec{R}) \\ \begin{bmatrix} \hat{T}_{\vec{R}} + \tilde{\epsilon}_D(\vec{R}) \end{bmatrix} \tilde{\phi}_D(\vec{R}) = E\, \tilde{\phi}_D(\vec{R}). \tag{3.8}$$

This choice of diabatic representation yields a localized description of PES's. The function $\tilde{\phi}_Q(\vec{R})$ (and, hence, $\tilde{\Psi}_Q(\vec{r}, \vec{R})$) is exponentially small in the D channel, and $\tilde{\phi}_D(\vec{R})$ (and $\tilde{\Psi}_D(\vec{r}, \vec{R})$) is exponentially small in the Q channel.

Note that the total Schrödinger equation (3.3) can be rewritten in the form

$$\hat{H}\, \Psi(\vec{r}, \vec{R}) = (\tilde{H} + \Delta H)\, \Psi(\vec{r}, \vec{R}) = E\, \Psi(\vec{r}, \vec{R}), \tag{3.9}$$

where $\tilde{H}$ is defined by Eq. (3.7), and

$$\Delta H = V(\vec{r}, \vec{R}) - \tilde{V}(\vec{r}, \vec{R}) = \hat{H}_e - \tilde{H}_e. \tag{3.10}$$

The operator, ΔH governs the D$\leftarrow$Q transition given by Eq. (3.1). Note that ΔH does not depend on time and thus can only cause transitions between states of the same energy.[21]

Using Eq. (3.6) and the orthogonality of $\tilde{\psi}_Q$ to $\tilde{\psi}_D$ the transition matrix element of Eq. (3.2) can be reduced to the form

$$H'_{D\leftarrow Q} = \int \tilde{\phi}^*_D(\vec{R})\, \tilde{\phi}_Q(\vec{R})\, L(\vec{R})\, d\vec{R}, \tag{3.11}$$

where

$$L(\vec{R}) = \int \tilde{\psi}^*_D(\vec{r}; \vec{R})\, \hat{H}_e\, \tilde{\psi}_Q(\vec{r}; \vec{R})\, d\vec{r}. \tag{3.12}$$

The function $L(\vec{R})$ contains relatively slowly varying functions of $\vec{R}$. The major contribution to the matrix element will come from the region of overlap

of the nuclear wave functions. This region will encompass the crossing point, $\vec{R}_o$, of the diabatic PES's (which, in general, will include the transition state of the adiabatic PES). Thus we can approximate Eq. (3.11) by

$$H'_{D\leftarrow Q} = L(\vec{R}_o) \int \tilde{\phi}^*_D(\vec{R})\, \tilde{\phi}_Q(\vec{R})\, d\vec{R}. \tag{3.13}$$

Hence, determination of absolute photofragment energy distributions requires the evaluation of a multidimensional FC-type integral and an electronic factor, $L(\vec{R}_o)$. Evaluation of $L(\vec{R}_o)$ is not trivial; however, relative energy distributions can be obtained from just the FC-type integrals reducing the determination of product energy distributions to a problem involving only nuclear degrees of freedom.

Equation (3.13) is similar to expressions derived from scattering theory for chemical reactions.[79–81] However, the present approach is based on the theory of quantum transitions and is similar in spirit to Bardeen's treatment of tunneling.[82] Since the golden rule given by Eq. (3.1) results from first-order time-dependent perturbation theory, all virtual transitions are neglected.[83] If higher-order corrections are important, the probability is given by an expression similar to Eq. (3.1) but with the matrix element $H'_{D\leftarrow Q}$ replaced by the T-matrix element connecting the Q and D states. These higher-order corrections correspond to virtual transitions to electronic states lying above the diabatic states. These terms contain products of FC factors resulting in additional orders of smallness, in a perturbative sense, and thus serve as a check of the applicability of Eq. (3.1). It is important to note here that the validity of the

Eq. (3.1) depends on the product of the coupling matrix element and the characteristic time of the perturbation being small. Hence, Eq. (3.1) is valid even if $H'_{D\leftarrow Q}$ is large for sufficiently short characteristic times. Our treatment differs from those based on scattering theory which lead to a single FC factor.[79,81]

C. Adiabatic Approach to Nuclear Dynamics

In order to evaluate the FC integral it is necessary to obtain expressions for the nuclear wave functions $\tilde{\phi}_Q$ and $\tilde{\phi}_D$, that are solutions to Eq. (3.8). In general, rotational motion is slower than translational and vibrational motion. In a consistent adiabatic development one can therefore neglect rotational motion initially. In chapter 4, we take appropriate account of rotational motion as an additional step in an adiabatic development. The Q state can often be described in the harmonic approximation as a product of normal modes. If the absorption spectrum consists of a set of equidistant bands, the harmonic approximation should be accurate, otherwise it is necessary to include anharmonicity corrections.

One of the most difficult aspects in treating polyatomic photodissociation is the proper description of the D state wave function, $\tilde{\phi}_D(\rho, q_i^A, q_l^B)$, where q_i^A and q_l^B are internal coordinates of fragments A and B. The complication arises because $\tilde{\phi}_D$ contains factors describing both discrete spectra corresponding to the internal motion of the individual photofragments, and continuous spectra associated with their relative motion. In general, there is strong

coupling between these two types of motion and, unlike the Q state, the potential energy $U(\rho, q_i^A, q_l^B)$ for the D state cannot be expanded in a series of deviations of all variables from equilibrium. The reason is that ρ, the distance between the centers of mass of the two fragments, represents unbounded translational motion. The major contribution to the transition matrix element will come from the region of overlap of the nuclear wave functions, where it is necessary to take explicit account of the interfragment interaction.

Following the adiabatic method of reference,[28,44] the D state of a linear tetra-atomic molecule may be described by the wave function

$$\tilde{\phi}_D(\rho, q_i^A, q_l^B) = \phi_{rel}(\rho, q^A, q^B)\, \phi_{int}(\rho, q^A, q^B). \tag{3.14}$$

where ϕ_{rel} is the wave function for translational motion, and ϕ_{int} in the wave function for internal motion. This result was obtained following an adiabatic approach. A general expression is constructed from rigorous solutions in two adiabatic limits: (i) $\alpha_v \equiv \dfrac{\epsilon_{rel}}{\epsilon_{vib}} >> 1$, relative motion fast compared to internal motion, and (ii) $\alpha_v << 1$, the opposite condition.

For case (i) ($\alpha_v >> 1$), one can use the clamped translational function approximation, for which it has been shown[44] that the fragment frequencies and bond lengths are constants and well approximated by isolated fragment or asymptotic (asy) values, i.e.,

$$\begin{aligned} \omega^i &\approx \omega_{asy} \\ q_o^i &\approx q_{asy}. \end{aligned} \tag{3.15}$$

Conceptually, case (ii) can be described as the slow formation of photofrag-

ments along the repulsive surface with adiabatic adjustment of frequencies and bond lengths. The wave function describing the internal motion depends parametrically on the interfragment distance ρ. This limit implies a minimum energy (reaction) path for the dissociative coordinate which can be defined mathematically as simultaneously satisfying the conditions,

$$\left.\frac{\partial U(\rho, q^A, q^B)}{\partial q^A}\right|_{q^A = q_o^{A'}(\rho)} = \left.\frac{\partial U(\rho, q^A, q^B)}{\partial q^B}\right|_{q^B = q_o^{B'}(\rho)} = 0$$
$$\text{and} \qquad \frac{\partial U(\rho, q^A, q^B)}{\partial \rho} \neq 0. \tag{3.16}$$

The relative motion part of $\tilde{\phi}_D$ (Eq. (3.14)) is the solution to

$$\left[-\frac{\hbar^2}{2\mu}\frac{\partial^2}{\partial \rho^2} + U_{eff}(\rho, q^A, q^B) \right] \phi_{rel}(\rho, q^A, q^B) = E\, \phi_{rel}(\rho, q^A, q^B), \tag{3.17}$$

where μ is the reduced mass of the system,

$$\begin{aligned} U_{eff}(\rho, q^A, q^B) &= U(\rho, q_o^A(\rho), q_o^B(\rho)) + \epsilon_{vib}(\rho) \\ \epsilon_{vib}(\rho) &= (n_A + 1/2)\,\hbar\,\Omega^A(\rho) + (n_B + 1/2)\,\hbar\,\Omega^B(\rho), \end{aligned} \tag{3.18}$$

and $q_o^A(\rho)$ and $q_o^B(\rho)$ are determined by the conditions

$$\left(\frac{\partial U(\rho, q^A, q^B)}{\partial q^{A(B)}} \right) \Big|_{q^{A(B)} = q_o^{A(B)}(\rho)} = 0. \tag{3.19}$$

The internal motion wave function, ϕ_{int} of Eq. (3.14) is given by

$$\phi_{int}(\rho, q^A, q^B) = \phi^A(Q_A(q^A, q^B, \rho))\, \phi^B(Q_B(q^A, q^B, \rho)), \tag{3.20}$$

where (in the harmonic approximation)

$$\phi^{A(B)} = \left(\frac{\Omega^{A(B)}(\rho)}{\pi \hbar} \right)^{1/4} \frac{1}{\sqrt{2^{n_{A(B)}}\, n_{A(B)}!}} \exp\left(- \frac{\Omega^{A(B)}(\rho)\, Q^2_{A(B)}(q^A, q^B, \rho)}{2\hbar} \right) \cdot H_{n_{A(B)}}\left(Q_{A(B)}(qa, qb, \rho) \sqrt{\frac{\Omega^{A(B)}(\rho)}{\hbar}} \right). \tag{3.21}$$

Here $Q_{A(B)}(q^A, q^B, \rho)$ are normal coordinates for internal motion of the D state, which asymptotically become individual bond stretches of each product fragment, and $H_{n_{A(B)}}$ is an $n_{A(B)}$-order Hermite polynomial. The explicit form of $Q_{A(B)}(q^A, q^B, \rho)$ is discussed in Sec. III. The frequencies $\Omega(\rho)$ and the bond lengths $q_o(\rho)$ depend on the interfragment distance and are in general different from their asymptotic values ω_{asy} and q_{asy}. Specifically, we have[44]

$$\Omega(\rho) = \omega^i \left(\frac{\omega^{ii}(\rho)}{\omega^i} \right)^{\beta}; \quad \beta \equiv (\alpha_v + 1)^{-1}$$
$$q_o(\rho) = q_o^{\,i} \left(\frac{q_o^{\,ii}(\rho)}{q^i} \right)^{\beta} \tag{3.22}$$

where the superscripts refer to the limiting cases (i) and (ii) above.

The form of the general solution for the D state nuclear wave function (c.f. Eqs.(3.14,3.17-3.22)) can be inferred by the comparison of each solution in the two adiabatic limits. In both limits the wave function $\tilde{\phi}_D$ is expressed as a product of two functions describing relative and internal motion of the fragments; moreover, the corresponding functions possess similar structure. The limiting cases differ only in the behavior of the vibrational frequencies and equilibrium bond lengths. For $\alpha_v \ll 1$, the frequencies and equilibrium bond lengths are functions of ρ; whereas, the opposite limit is characterized by constant values

of these parameters. The similar structure for the solutions of the two limiting cases suggests it is reasonable to conclude that a continuous transition occurs in proceeding from the case $\alpha_v << 1$ to $\alpha_v >> 1$ that is accompanied by a change of the dependence of $\omega^{ii}(\rho)$ and $q_o^{ii}(\rho)$ to $\omega^i \approx \omega_{asy}$ and $q_o^i \approx q_{asy}$; see Eq. (3.15). This change may be described by the interpolation scheme of Eq. (3.22). The explicit solutions for the two adiabatic limits for a linear tetra-atomic system are given in Appendix B.

We emphasize that the interaction between the fragments is taken into account in two ways. First, the vibrational frequencies and reaction path bond lengths depend on the interfragment distance ρ. Second, the effective potential energy U_{eff}, describing the relative motion, contains the vibrational energy.

III. Application and Results for $C_2N_2(\tilde{C}\ ^1\Pi_u)$

A. Experiment

Recent experimental studies[22,47–50] have indicated that $C_2N_2(\tilde{C}\ ^1\Pi_u)$ undergoes predissociation at wavelengths between 164 nm and 154 nm resulting in $CN(X\ ^2\Sigma^+)$ and $CN(A\ ^2\Pi)$. From Fig. 2.1, the three lowest-energy channels for dissociation and their thresholds are

$$\begin{aligned} C_2N_2 &\rightarrow CN(X\ ^2\Sigma^+) + CN(X\ ^2\Sigma^+) \quad 222.2\text{nm} \quad \text{I} \\ &\rightarrow CN(X\ ^2\Sigma^+) + CN(A\ ^2\Pi) \quad 184.7\text{nm} \quad \text{II} \\ &\rightarrow CN(A\ ^2\Pi) + CN(A\ ^2\Pi) \quad 157.9\text{nm} \quad \text{III.} \end{aligned} \tag{3.23}$$

For wavelengths between 164 and 184.7 nm earlier studies[22,48] have shown the

ratio of CN(A $^2\Pi$) to CN(X $^2\Sigma^+$) to be nearly unity indicating that only channel II occurs. At shorter wavelengths this ratio was found to be greater than unity implying that channel III must contribute. From Fig. 2.1 it is seen that channel II adiabatically correlates to $C_2N_2(\tilde{C}\ ^1\Pi_u)$ and as such is an example of type II (vibrational) predissociation. Dissociation via channel III involves different electronic PES's and thus is type I (electronic) predissociation.

Miller et al.[22] photolyzed C_2N_2 under collisionless conditions at 164, 158.7, and 153.6 nm and measured nascent CN(X $^2\Sigma^+$) vibrational populations using laser induced fluorescence (LIF). They reported the vibrational population ratios (β) of $\nu = 1$ to $\nu = 0$, and at all wavelengths found $\beta<1$, but increasing with photon energy. Taherian et al.[50] measured the CN(A $^2\Pi$) vibrational distribution resulting from F_2 laser excitation of C_2N_2 at 157.6 nm. They reported a CN(A $^2\Pi$) vibrational population detected by CN(X←A) emission spectra and observed vibrational levels up to the thermodynamic limit of $\nu = 5$ in a bimodal distribution with peaks at $\nu = 0$ and $\nu = 2$.

B. Diabatic States for $C_2N_2(\tilde{C}\ ^1\Pi_u) \rightarrow CN(X\ ^2\Sigma^+) + CN(A\ ^2\Pi)$

As described in Sec. II, the Q and D state wave functions, $\tilde{\psi}_Q$, and $\tilde{\psi}_D$, are not eigenstates of the electronic Hamiltonian, $\hat{H}_e$, of the system but of a diabatic Hamiltonian $\tilde{H}_e$ consistent with the transformation $V(\vec{r}, \vec{R}) \rightarrow \tilde{V}(\vec{r}, \vec{R})$. In general, diabatic states result from a nondiagonal representation of $\hat{H}_e$, of which there may be several of physical interest. The adiabatic states are

unique, however, resulting from the diagonalization of $\hat{H}_e$. Hence, diabatic and adiabatic representations are rigorously equivalent, and the problem lies in specifying the representation that provides the most useful physical description of the system.[72,76]

As discussed in chapter 2, electronic structure studies of $C_2N_2(\tilde{C}\ ^1\Pi_u)$ indicate it is best described as an $n \rightarrow \pi^*$ excitation from the ground state $n^3\pi^8\pi^{*1}$ electronic configuration. Here n represents a nitrogen atom lone-pair electron and π^* is the lowest-lying unoccupied orbital.[84] The $CN(A\ ^2\Pi)$ radical results from the excitation of a π electron into a half-filled σ orbital localized on carbon. The $CN(X\ ^2\Sigma^+) + CN(A\ ^2\Pi)$ supermolecule has an $n^4\pi^7\sigma^{*1}$ electronic configuration. The adiabatic electronic PES reflects this change in character for increasing ρ. In the diabatic representation, however, $C_2N_2(\tilde{C}\ ^1\Pi_u)$ dissociates to $CN(X\ ^2\Sigma^+)$ and a higher energy $CN(^2\Pi)$ state. Collinear approach of $CN(X\ ^2\Sigma^+)$ to $CN(A\ ^2\Pi)$ results in a repulsive diabatic surface because of the interaction of the two lone-pair electrons of carbon in the $A^2\Pi$ radical with the single lone-pair electron of carbon in the ground state fragment (see Figure 2.2). It is the interaction between these two diabatic PES's (i.e., the off-diagonal terms in the diabatic representation of $\hat{H}_e$) that leads to the predissociative nature of the adiabatic surface.

The diabatic surfaces for the quasidiscrete and dissociative states can be constructed using the ab initio multiconfiguration Hartree-Fock (MCHF) method. The $n \rightarrow \pi^*$ character of the $C_2N_2(\tilde{C}\ ^1\Pi_u)$ state and the $\pi \rightarrow \sigma^*$

character of the CN(X $^2\Sigma^+$) + CN(A $^2\Pi$) supermolecule can be obtained by restricting the orbital occupations in the respective MCHF wave functions. To construct an MCHF wave function that correctly describes the adiabatic surface, it is necessary to include all configurations obtained by distributing 14 electrons among both the lone-pair orbitals (n_u, n_g), the π orbitals (π_u, π_g, π_u^*, π_g^*), and the CC bonding and antibonding orbitals (σ_g, σ_u^*) in all possible ways consistent with $^1\Pi_u$ symmetry. We denote this wave function as MC[σ_g, n_u, n_g, π_u, π_g, π_u^*, π_g^*, σ_u^*]^{14} (or just simply MC14). The diabatic Q state is obtained by omitting those configurations which include excitations out of the CC(σ_g) or into the CC(σ_u^*) orbitals. This restricts the σ_g orbital to remain fully occupied and the σ_u^* orbital to be empty. By this specification, the Q state wave function, MC[n_u, n_g, π_u, π_g, π_u^*, π_g^*]^{12} (MC12), will not dissociate to adiabatic products but will retain its n $\rightarrow \pi^*$ character. Similarly, if the configurations which include excitations from the lone pair orbitals are neglected, forcing them to remain fully occupied, the D state wave function, MC[σ_g, π_u, π_g, π_u^*, π_g^*, σ_u^*]^{10} (MC10) with $\pi \rightarrow \sigma^*$ character is obtained.

Following these ideas, the optimized molecular geometry, force constants, and harmonic frequencies have been obtained[84] for $C_2N_2(\tilde{C}\ ^1\Pi_u)$ in excellent agreement with experimental data. The absorption spectrum consists of an equidistant set of bands,[22] and thus the quasidiscrete state nuclear wave function is expected to be well approximated by a product of harmonic oscillator functions of the normal modes. Frequencies and normal coordinates were

determined from force constants obtained from a minimum basis set (STO-3G) MC12 wave function. The results of these calculations are summarized in Table 3.1.

Because it is not possible experimentally to obtain geometries and force constants of fragments along the reaction path, we also employ ab initio MCHF methods to determine these data needed to describe the D state in the FC overlap region. A simple relationship can be derived for specifying the minimum energy path of a tetra-atomic system using the method of Lagrange multipliers (see Appendix C).

Figure 3.2 and Table 3.2 display the results of the D state MCHF calculations. We note a strong ρ-dependence for both photofragment equilibrium bond lengths and frequencies along the repulsive PES. For small ρ the system resembles the symmetric C_2N_2 supermolecule rather than distinct CN($X\ ^2\Sigma^+$) and CN($A\ ^2\Pi$) radicals. A normal mode analysis yields normal coordinates expressible as symmetric and asymmetric linear combinations of the localized fragment bond stretches similar to those of quasidiscrete $C_2N_2(\tilde{C}\ ^1\Pi_u)$. The CN photofragments remain indistinguishable until an abrupt symmetry breaking at $\rho = 3.2$ Å. There the fragments are distinct, the bond lengths differ, and by $\rho = 3.6$ Å the fragments have almost reached the equilibrium bond lengths and frequencies of isolated CN($X\ ^2\Sigma^+$) and CN($A\ ^2\Pi$). For larger ρ a normal mode analysis gives normal coordinates primarily composed of the individual localized bond stretches. For small ρ the normal mode corresponding to

the symmetric CN stretch is found to correlate asymptotically to the ground state CN(X $^2\Sigma^+$) stretch; and that for the asymmetric CN stretch, which has the lower frequency, correlates to the excited state CN(A $^2\Pi$) stretch.

The quasidiscrete state nuclear wave function will be nonzero for a region near its equilibrium geometry (ρ_o, q_o^A, q_o^B). Therefore the main contributions to the FC overlap will also come from this region. For $C_2N_2(\tilde{C}\ ^1\Pi_u)$ $\rho_o = 2.656$ Å. As shown in Figure 3.2, the frequencies and bond lengths in this region are clearly not the same as those for the isolated fragments.

C. Evaluation of the Franck-Condon Overlap Integral

Obtaining relative product energy distributions requires evaluation of the multidimensional overlap integral of the quasidiscrete and dissociative state nuclear wave functions,

$$H'_{D\leftarrow Q} \sim \int \tilde{\phi}^*_D(\vec{R})\, \tilde{\phi}_Q(\vec{R})\, d\vec{R}. \tag{3.24}$$

In this chapter we are primarily concerned with vibrational distributions of the CN(X $^2\Sigma^+$) and CN(A $^2\Pi$) fragments resulting from predissociation of $C_2N_2(\tilde{C}\ ^1\Pi_u)$. Both the ground ($\tilde{X}\ ^1\Sigma_g^+$) and excited ($\tilde{C}\ ^1\Pi_u$) molecular states are linear; and, as a further adiabatic approximation, we may neglect bending vibrations and rotations and limit the analysis to the collinear arrangement. The general theory is applicable to nonlinear polyatomics and is presented in detail in reference 42. Evaluation of the fragment rotational distributions would, of course, require inclusion of the corresponding degrees of freedom.

This treatment is discussed in chapter 4.

In the harmonic approximation, the nuclear wave function describing the internal motion of the quasidiscrete $C_2N_2(\tilde{C}\ ^1\Pi_u)$ state is given by a product of three oscillator functions,

$$\tilde{\phi}_Q(\vec{R}) = \prod_{i=1}^{3} \phi_{n_i}(Q_i), \tag{3.25}$$

where Q_i are normal mode stretches and n_i are the vibrational quantum numbers of the harmonic oscillators with frequencies ω_i, given in Table 3.1.

To describe the internal motion of the dissociative state, we use harmonic oscillator functions with ρ-dependent frequencies and bond lengths given by Eqs. (3.20-3.22). The translational wave function describing relative motion is the solution of Eq. (3.17), which contains the coupling between internal and relative motions in the effective potential of Eq. (3.18). This approach for the D state surface differs from the usual procedures of approximating this region of the PES by a linear or exponential function,[36,37] and neglecting the ρ-dependence of the vibrational energy contributions to U_{eff}. The latter approaches result in analytical forms (Airy or Bessel functions) for the translational wave function. In the present method both terms of $U_{eff}(\rho, q^A, q^B)$ can be obtained from MCHF calculations. As will be discussed below, the ab initio MCHF data points are used to obtain an exponential fit for the dissociative state electronic PES in the crossing point region. The calculated vibrational energy is added to the electronic potential resulting in $U_{eff}(\rho, q^A, q^B)$, from

which the translational wave function, $\phi_{rel}(\rho, q^A, q^B)$, is calculated using standard numerical methods.[85]

The nuclear wave functions of the quasidiscrete and dissociative states are conveniently expressed in terms of their respective sets of normal coordinates. However, evaluation of the FC integral of Eq. (3.24) is computationally simpler if the nuclear wave functions are expressed in a single coordinate system. For this purpose, we choose the internal coordinates (ρ, q^A, q^B). The normal modes of the quasidiscrete state can be expressed as

$$Q_i = a_i \tau_A + b_i \tau_B + c_i \rho' \qquad i = \{1,2,3\}, \tag{3.26}$$

where

$$\begin{aligned} \tau_A &= q^A - q_o^A \\ \tau_B &= q^B - q_o^B \\ \rho' &= \rho - \rho_o \end{aligned} \tag{3.27}$$

represent the deviations from the equilibrium geometry. Similarly, the normal mode functions of the dissociative state can be written

$$\begin{gathered} Q_Z = a_Z(\rho)\,[\tau_A - \delta q^A(\rho)] + b_Z(\rho)\,[\tau_B - \delta q^B(\rho)] + c_Z(\rho)\,\rho' \\ Z \equiv \{A,B\}, \end{gathered} \tag{3.28}$$

where the difference between the equilibrium bond lengths of the quasidiscrete and dissociative states are given by

$$\begin{aligned} \delta q^A(\rho) &= q_o^A - q_{oD}^A(\rho) \\ \delta q^B(\rho) &= q_o^B - q_{oD}^B(\rho). \end{aligned} \tag{3.29}$$

In this coordinate system the multidimensional FC overlap of Eq. (3.24) can be written

$$H'_{D\leftarrow Q} \sim \int \Big[\int \phi_{n_1}(\tau_A, \tau_B, \rho')\, \phi_{n_2}(\tau_A, \tau_B, \rho')\, \phi_{n_3}(\tau_A, \tau_B, \rho') \phi_{n_A}(\tau_A, \tau_B, \rho')\, \phi_{n_B}(\tau_A, \tau_B, \rho')\, d\tau_A\, d\tau_B \Big] \phi_{rel}(\rho')\, d\rho'. \tag{3.30}$$

Integrations over τ_A and τ_B can be done analytically resulting in a one-dimensional integral of the form

$$H'_{D\leftarrow Q} \sim \int \phi_{vib}(\rho')\, \phi_{rel}(\rho')\, d\rho', \tag{3.31}$$

where $\phi_{vib}(\rho')$ is an effective vibrational wave function of the form

$$\phi_{vib}(\rho') \sim F(\rho') \exp[-(\rho' - \delta\rho)^2/c^2]. \tag{3.32}$$

Here F is a complicated function of the vibrational frequencies, the coordinate transformation coefficients, the vibrational quantum numbers, the changes in the equilibrium bond lengths, and ρ'. The explicit form of ϕ_{vib} is given in Appendix D. The gaussian factor is centered at $\rho_o + \delta\rho$ and has width c. The shift $\delta\rho$ results from the difference in magnitude of the equilibrium bond lengths of the CN fragments in the D state from the CN bond lengths in the molecular Q state. Because we do not have an analytical form of $\phi_{rel}(\rho')$ (see Eqs. (3.17-3.18), the final integration of Eq. (3.31) is performed numerically. The transition probability in Eq. (3.1) is obtained from the product of the square of the transition matrix element, $H_{D\leftarrow Q}$, multiplied by the final density of states, ρ_E. The one-dimensional final density of states is proportional to the inverse of the asymptotic momentum,[21]

$$\rho_E \sim (\epsilon_{avl} - \epsilon_{vib})^{-1/2}, \tag{3.33}$$

where ϵ_{avl} is the amount of energy available to go into translation and vibration of the product fragments.

Because $H'_{D\leftarrow Q}$ is explicitly a function of the vibrational quantum numbers, it yields state-to-state transition probabilities and thus final state vibrational energy distributions. It has been shown previously[43] that Eqs. (3.31) and (3.32) can lead to inverted vibrational distributions. The possibility of an inverted distribution arises from the fact that for low vibrational levels and hence large relative kinetic energy the translational wave function is a highly oscillatory function which can lead to small nuclear overlap and transition probabilities. However, transition probabilities to high vibrational states can also be reduced because of a larger effective potential which displaces the classical turning point further from the center of the effective vibrational wave function. The latter favors a noninverted distribution. In general, the PVD's will depend on these competing factors which ultimately are determined by the PES's and the ρ-dependence of the vibrational energy.

D. Vibrational Distributions

Figure 3.3 shows a section of the diabatic potential energy surfaces from the ab initio STO-3G MCHF calculations of the Q and D states. The points of the D state curve define the minimum energy path that satisfies the conditions of Eqs. (3.16) and (C3). The corresponding points of the Q surface were calculated at the same nuclear geometries. The crossing point of the two curves occurs near $\rho = 2.95$ Å corresponding to 8.9 eV. The main contributions to the FC overlap will come from the region near the crossing point. It is reasonable to approximate the repulsive electronic PES by an exponential of

the form

$$U(\rho, q_o^A(\rho), q_o^B(\rho)) = U_\infty + A \exp(-\gamma \rho'). \quad (3.34)$$

Others[36,69,70] have employed similar exponential forms for a D state PES, where the parameters A and γ were determined from experimental data or electronic structure calculations. This results in a Bessel function for the translational wave function simplifying the $H'_{D\leftarrow Q}$ integral. The present ab initio calculations for the $C_2N_2(\tilde{C}\ ^1\Pi_u)$ D state PES yield $A = 2.4 \cdot 10^9$ cm^{-1} and $\gamma = 3.95$ Å^{-1} in Eq. (3.34).

The magnitudes of the transition probabilities and PVD's will be sensitive to the classical turning points of the D state PES. The effective vibrational wave function is centered near the Q state minimum, ρ_o. The translational wave function will not have appreciable amplitude until the classical turning point, ρ_{tp}. Inspection of Figure 3.3 indicates that $\rho_o = 2.66$Å and $\rho_{tp} = 3.15$Å at 164 nm. The STO-3G PES's yield very small transition probability with overlap resulting mainly from the exponentially decreasing tails of the nuclear wave functions in the classically forbidden region.

The computed transition probabilities (and ρ_{tp}) are found to be considerably more sensitive to the PES parameter γ than to the preexponential factor A of Eq. (3.34). Variations in A displace the D state curve without changing its shape; whereas, changes in γ affect the curvature. For example, at 164 nm, a 20% decrease in A from $2.4 \cdot 10^9$ to $1.82 \cdot 10^9$ cm^{-1} decreases ρ_{tp} by 0.06 Å (2% change); however, a 20% increase in γ from 3.95 to 4.74 Å^{-1} decreases ρ_{tp}

by 0.54 Å (17% change) which significantly alters the computed PVD.s

The 164 nm photon energy is only 0.26 eV above the ground vibrational level of $C_2N_2(\tilde{C}\ ^1\Pi_u)$. Because predissociation is experimentally observed at this energy, we expect the crossing point to occur actually at lower energy and a smaller interfragment distance than depicted by the calculated STO-3G MCHF PES's. Given the sensitivity of computed PVD's to the D state electronic PES parameters, we have carried out the analysis using the ab initio STO-3G value for the less sensitive pre-exponential factor A leaving the exponential constant γ to be determined from a fit to the experimental data.

Extended basis set calculations (DZP level) have been carried out for a number of points along the D state minimum energy path and for the Q state at the same geometries. Fig. 3.3 indicates the results of these calculations. As expected, the crossing point region is moving towards more favorable nuclear overlap lowering the crossing point energy to 8.5 eV. However, the DZP crossing point is still an eV above the available energy at 164 nm. From a similar fit to Eq. (3.34), we obtain $A=2.15\cdot10^9$ cm$^-$ and $\gamma = 4.05$ Å^{-1}. These changes are in the expected directions but not significant enough to change the analysis at the minimum basis set level. It appears that a much larger basis set calculation is needed to determine accurately the relevent PES's for $C_2N_2(\tilde{C}\ ^1\Pi_u)$. The results that follow were obtained from the minimum basis set STO-3G PES's.

1. CN(X $^2\Sigma^+$) PVD's.

The experiments of Miller et al. and Jackson[22,48,49] were done at three photon wavelengths separated by $\sim$ 2100 cm^{-1}, the vibrational frequency of the symmetric CN stretch. The lowest wavelength, 164 nm, is also about 2100 cm^{-1} above the ground vibrational level of $C_2N_2(\tilde{C}\ ^1\Pi_u)$. Thus, it is reasonable to assume that the initial state reached at 164 nm is (1,0,0) corresponding to one vibrational quantum in the symmetric CN stretch. Here we label the initial Q state by (ν_1, ν_2, ν_3) where ν_1 refers to the vibrational quantum number of the symmetric CN stretch, ν_2 identifies the CC stretch, and ν_3 corresponds to the asymmetric CN stretch. On this basis the symmetric CN stretch is excited at 158.7nm with one additional quantum (2,0,0), and two more quanta (3,0,0) at 153.6nm. Because Miller et al. report only the CN(X $^2\Sigma^+$) vibrational populations at these wavelengths, our computed results, which only consider the single surface predissociation of channel II, can be directly compared to experiment.

Figure 3.4 compares computed CN(X $^2\Sigma^+$) PVD's to the measurements of Miller et al. Good qualitative agreement is obtained for A = 2.4 $\cdot$ 10^9 cm^{-1} and $\gamma \approx$ 4.64–4.88 Å^{-1} of Eq. (3.34). These values indicate a more repulsive surface in the FC region to obtain increased nuclear overlap than that obtained from the minimum basis set MCHF calculations. The effective potential curves (Eq. (3.18)) for transitions at 164 nm to several final states are shown in Figure 3.5. The dips in the effective potential at 3.2 Å reflect the ρ-

dependence of the frequencies in the vibrational energy contribution (see Fig. 3.2). We had sought a single γ to satisfy the experimental data, but found instead a small range of values that provided agreement with the CN(X $^2\Sigma^+$) data. These findings support our expectation of a crossing point lower in energy and at a smaller interfragment separation as shown in Fig. 3.5.

In a recent study, Eros et. al.,[46] reported 133 kcal for the dissociation energy of ground state $C_2N_2(\tilde{X}\ ^1\Sigma_g^+)$ - 5 kcal larger than the previously accepted value. This difference ($\sim$ 1750 cm^{-1}) changes the number of energeticially accessible fragment vibrational channels and hence the calculated distributions. The effect of increased binding is to raise the effective potential, resulting in less nuclear overlap and smaller transition probabilties. Similar qualitative agreement between calculated and experimental CN(X $^2\Sigma^+$) vibrational distributions is obtained with this magnitude of increased dissociation energy, but it requires a slightly larger γ, i.e., $4.72 < \gamma < 5.02$ Å^{-1} to compensate for the larger binding.

2. CN(A $^2\Pi$) PVD's.

At 157.6 nm laser energy used in the experiments of Taherian et al., channel III becomes accessible with the possibility of forming two CN(A $^2\Pi$, $\nu = 0$) fragments. We have not calculated contributions from this channel and therefore cannot make a direct comparison with experiment. Because channel III can only contribute CN(A $^2\Pi$) fragments in $\nu = 0$, the vibrational distribution solely from channel II should be peaked at $\nu = 2$ in order that the total

distribution from both channels have the bimodal character with major peak at ν=2 observed by Taherian et al.[50] (c.f. section III.A).

At 157.6 nm it is not clear which initial vibrational level of $C_2N_2(\tilde{C}\ ^1\Pi_u)$ is reached. A 157.6 nm photon lies 440 cm^{-1} above the (2,0,0) vibrational state, and it is possible that this excess energy goes into the bending and rotational modes not considered here. With the assumption that the initial state is (2,0,0) we have estimated the contribution from channel II. We found no values of the exponential parameters of Eq. (3.34) that resulted in a vibrational distribution peaked at $\nu = 2$. At all wavelengths for which the initial state contained only excitation into the symmetric CN stretch of $C_2N_2(\tilde{C}\ ^1\Pi_u)$, all PVD's had greater than 99% of the CN(A $^2\Pi$) fragments formed in $\nu = 0$. Inclusion of contributions from channel III would only lead to poorer agreement with experiment.

The behavior of the CN(A $^2\Pi$) vibrational distributions can be explained with symmetry arguments. As discussed above, the photofragments have a supermolecule appearance in the FC region. The normal modes of the dissociative state in this region are symmetric (Σ_g^+) and asymmetric (Σ_u^+) linear combinations of localized CN bond stretches similar to those of $C_2N_2(\tilde{C}\ ^1\Pi_u)$. Orthogonality of the Hermite functions describing these normal modes yields a propensity rule for the sum of the vibrational quantum numbers of the asymmetric stretches. Their sum must be even for a nonzero transition probability. Since we assume that the quasidiscrete initial states are excitations of the

symmetric CN stretch with the asymmetric CN stretch in its zero-point level, by symmetry the transition probabilty to fragment states with odd quanta in the asymmetric CN stretching mode (which asymptotically becomes the CN(A $^2\Pi$) stretch) will be small.

Okabe and Jackson[49] note that if the $C_2N_2(\tilde{X}\ ^1\Sigma_g^+)$ dissociation energy is 133 kcal, then the thermodynamic limit for the CN(A $^2\Pi$) fragment at 157.6 nm would be $\nu = 4$. According to these authors, for Taherian et al. to observe $\nu = 5$, coupled with the possibility of multiphoton effects, casts doubt on the latter's analysis. Okabe and Jackson[49] state that the two experiments (Taherian et al. and Miller et al.) are in direct contradiction unless the predissociative dynamics are highly sensitive to the exact point within the absorption band excited by the laser.

3. Mode Specificity.

Photodissociation dynamics offer a unique possibility for the study of internal energy redistribution in a molecule. A predissociating molecule can be prepared in different initial levels of nearly the same energy from which one can observe whether mode-specific behavior occurs. Figure 3.6 compares theoretical vibrational distributions obtained for different initial states at 164 nm. Our computations yield characteristically different PVD's depending on the quantum number of the Q state asymmetric CN stretch, ν_3. The propensity rule described in the previous section, namely that the sum of the quantum numbers of the asymmetric stretches of the Q and D states, $\nu_3 + \nu_A$, be

even for nonzero probability for the transition $(\nu_X, \nu_A) \leftarrow (\nu_1, \nu_2, \nu_3)$, accounts for this behavior. This propensity rule can be expressed

$$W_{D\leftarrow Q} = \begin{cases} W_{(\nu_X, \nu_A)\leftarrow(\nu_1, \nu_2, \nu_3)} & , \nu_3 + \nu_A \text{ even} \\ \sim 0 & , \nu_3 + \nu_A \text{ odd} \end{cases} \tag{3.35}$$

Here the probability of a specific D←Q transition is given by $W_{D\leftarrow Q}$ and we denote final states by (ν_X, ν_A) where the subscripts refer to the vibrational quantum numbers of the CN(X $^2\Sigma^+$) and CN(A $^2\Pi$) stretches. The population of X-state or A-state fragments with vibrational quantum number, ν_X or ν_A can be written

$$\begin{aligned} P^X_{\nu_X\leftarrow(\nu_1, \nu_2, \nu_3)} &\sim \sum_{\nu_A} W_{(\nu_X, \nu_A)\leftarrow(\nu_1, \nu_2, \nu_3)} \\ P^A_{\nu_A\leftarrow(\nu_1, \nu_2, \nu_3)} &\sim \sum_{\nu_X} W_{(\nu_X, \nu_A)\leftarrow(\nu_1, \nu_2, \nu_3)} \quad . \end{aligned} \tag{3.36}$$

At 164 nm there is enough energy to reach final states for which $\nu_T \equiv \nu_X + \nu_A \leq 3$. Following the propensity rule Eq. (3.35), for Q state (1,0,0) transitions occur to D state channels with ν_A even. On the other hand, for Q state (0,0,1) transitions occur to product channels with ν_A odd. Our results for 164 nm indicate that the transition probabilities to states with $\nu_T \geq 2$ are negligible. Table 3.4 gives the dominant terms that contribute to the fragment populations in Eq. (3.36).

From Figure 3.6, we see that for (1,0,0), both fragments are primarily populated in their ground vibrational level. Nearly 100% of the CN(A $^2\Pi$) fragments are in $\nu_A = 0$ due to the propensity rule which does not allow transitions to product channels with $\nu_A = 1$. We can explain the PVD for the

ground state CN(X $^2\Sigma^+$) fragments from the dominant terms contributing to the populations (see Table 3.4). For product channels with larger ν_T the effective potential increases. The classical turning point will be shifted to a larger interfragment distance and, in general, away from the effective oscillator. In many cases, we would expect this shift to result in less nuclear overlap and smaller transition probabilities. From this reasoning, $W_{(0,0)\leftarrow(1,0,0)}$ would be larger than $W_{(1,0)\leftarrow(1,0,0)}$; and hence, $P^X_{0\leftarrow(1,0,0)} > P^X_{1\leftarrow(1,0,0)}$.

The effect of the propensity rule is seen much more strongly in the CN(A $^2\Pi$) PVD's. The behavior of the PVD's changes dramatically between Q (1,0,0) and Q (0,0,1). For (1,0,0), the CN(A $^2\Pi$) fragments are predominantly populated in $\nu_A = 0$, as transitions to product channels with $\nu_A = 1$ are not allowed. The opposite is true for (0,0,1), as product channels with $\nu_A = 0$ are nearly zero and A-state fragments are mostly $\nu_A = 1$, resulting in an inverted vibrational distribution. We emphasize that the propensity rule, Eq. (3.35), arises from the symmetry of the system in the FC region at small interfragment separations

IV. Conclusions

In this chapter we have applied the KL adiabatic theory of polyatomic photodissociation to $C_2N_2(\tilde{C}\ ^1\Pi_u)$ to obtain product vibrational distributions for CN(X $^2\Sigma^+$) and CN(A $^2\Pi$) photofragments. The theory treats type II (vibrational) predissociation as a quantum transition in a diabatic representation. Relative product vibrational distributions are obtained from the

evaluation of multidimensional Franck-Condon overlap integrals. The adiabatic description of the nuclear dynamics explicitly treats final state interactions, i.e, the coupling between the relative motion of the fragments with their internal degrees of freedom, as an integral part of the theory.

Ab initio MCHF calculations using a minimum basis set (STO-3G) were used to construct the diabatic electronic potential energy surfaces and to compute the geometries and force constants necessary to determine nuclear wave functions. We found a strong dependence of the dissociative state fragment bond lengths and frequencies on the interfragment distance, ρ. As depicted in Figure 3.2, our calculations show that the CN(X $^2\Sigma^+$) + CN(A $^2\Pi$) dissociative state has a supermolecule appearance for small interfragment separations, where the CN fragments are indistinguishable. There exists a large variation of CN vibrational frequencies that correlates with symmetry breaking of the CN fragments as they separate and become recognizable as CN(X $^2\Sigma^+$) and CN(A $^2\Pi$) radicals.

Qualitative agreement with experiment is obtained for relative vibrational distributions for CN(X $^2\Sigma^+$) at 164, 158.7, and 153.6 nm. These results were obtained assuming the initial state of the precursor $C_2N_2(\tilde{C}\ ^1\Pi_u)$ system to include only excitation of the symmetric CN stretching mode. At 157.6 nm the initial $C_2N_2(\tilde{C}\ ^1\Pi_u)$ vibrational state could not be ascertained from the present study. Direct comparison with experiment would entail inclusion of the product channel corresponding to two CN(A $^2\Pi$) fragments. However, at

this photon energy, the experimental bimodal distribution obtained for CN(A $^2\Pi$) could not be reproduced. As the distributions are sensitive to shapes and relative positions of the PES's, inclusion of anharmonicities with the use of Morse functions or other similar functions could result in modification of the distributions. It is possible that bending vibrations or rotations are important which must await full three-dimensional studies. Preliminary studies will be reported in chapter 4.

Another result of our analysis is the occurrence of mode specificity. Computed product vibrational distributions for $C_2N_2(\tilde{C}\ ^1\Pi_u)$ prepared with quanta solely in the symmetric CN stretching mode ν_1 differ from those with the same number of quanta solely in the asymmetric mode ν_3. A propensity rule is found for $\sigma \equiv \nu_3 + \nu_{A\ ^2\Pi}$: for σ odd, the transition probabilty will be small or nearly zero. This propensity rule results from symmetry restrictions arising from the parity of normal modes functions for the Franck-Condon-type integrals.

Table 3.1. Computed Properties of C_2N_2 and CN

State	Property	Calculated	Experimental
$C_2N_2(\tilde{C}\ ^1\Pi_u)$	R(CC)	1.308 Å	--
	R(CN)	1.252 Å	--
	ν_1 (sym CN)	2082 cm^{-1}	2100 cm^{-1}[a]
	ν_2 (CC)	896 cm^{-1}	--
	ν_3 (asym CN)	1726 cm^{-1}	--
	$T_e(\tilde{C}\ ^1\Pi_u \leftarrow \tilde{X}\ ^1\Sigma_g^+)$	8.64 eV	7.30 eV[a]
CN($A\ ^2\Pi$)	r(CN)	1.2983 Å	1.2327 Å[b]
	ν_A	1716 cm^{-1}	1814 cm^{-1}[b]
	$T_e(A^2\Pi \leftarrow X^2\Sigma^+)$	1.53 eV	1.146 eV[b]
CN($X\ ^2\Sigma^+$)	r(CN)	1.2087 Å	1.1718 Å[b]
	ν_X	2101 cm^{-1}	2069 cm^{-1}[b]

[a]Reference 55
[b]Reference 63

Table 3.2. Computed MC10 STO-3G C_2N_2 Dissociative State PES Fragment Geometries and Vibrational Frequencies Along Reaction Path.

ρ (Å)	R(CC) (Å)	R(NC) (Å)	R(CN) (Å)	T_e^a (eV)	ω_1^b (cm^{-1})	ω_2^b (cm^{-1})
2.700	1.42106	1.1878	1.1878	13.56	2345.9	1801.7
2.888	1.58278	1.2126	1.2126	10.75	2196.9	1539.8
2.956	1.64270	1.2198	1.2198	10.08	2150.9	1409.0
3.065	1.74066	1.2299	1.2299	9.29	2086.7	1121.4
3.159	1.82745	1.2366	1.2366	8.83	2038.5	638.3
3.200	1.86594	1.2342	1.2437	8.67	2022.2	153.7i
3.250	1.91425	1.2118	1.2694	8.51	1986.1	1074.0
3.300	1.96296	1.2040	1.2795	8.37	1978.4	1578.3
3.653	2.30809	1.2036	1.2941	7.79	2142.6	1738.7
4.000	2.65208	1.2071	1.2967	7.62	2117.9	1727.2
4.750	3.40064	1.2087	1.2978	7.60	2103.3	1722.6
5.349	4.00000	1.2085	1.2977	7.61	2103.9	1722.9
∞	∞	1.2087	1.2983	7.63	2101.4	1716.5

[a] T_e values refer to electronic energy above MC10 $C_2N_2(\tilde{X}\ ^1\Sigma_g^+)$ minimum.

[b] Harmonic frequencies of normal modes orthogonal to reaction path. Values obtained have been adjusted by taking 0.9 times diagonal force constant elements.

Table 3.3. Adjusted[a] C_2N_2 Dissociative State PES Fragment Geometries and Vibrational Frequencies Along Reaction Path.

ρ (Å)	R(NC) (Å)	R(CN) (Å)	T_e^b (eV)	ω_1 (cm^{-1})	ω_2 (cm^{-1})
2.700	1.1397	1.1397	12.70	2309.4	1904.
2.888	1.1635	1.1635	9.89	2162.7	1627.
2.956	1.1704	1.1704	9.22	2117.4	1489.
3.065	1.1801	1.1801	8.43	2054.2	1185.
3.159	1.1865	1.1865	7.97	2006.8	674.
3.200	1.1842	1.1933	7.81	1990.7	162.0i
3.250	1.1748	1.2052	7.65	1955.2	1135.
3.300	1.1672	1.2148	7.51	1947.6	1668.
3.653	1.1669	1.2287	6.93	2109.3	1836.
4.000	1.1702	1.2312	6.76	2084.9	1825.1
4.750	1.1717	1.2322	6.74	2070.6	1819.8
5.349	1.1716	1.2321	6.75	2070.6	1819.0
∞	1.1718	1.2327	6.77	2068.7	1814.

[a] Adusted values = (expt./theory) $\Big|_{\rho=\infty}$ *theory(ρ)

Symmetry is forced for $\rho < 3.20$Å; R(NC) = R(CN).

[b] Relative energies shifted by -0.86 eV to agree with experimental value of separated fragments.

Table 3.4. Dominant Terms for the CN(X $^2\Sigma^+$) and CN(A $^2\Pi$) Populations at 164 nm

	Q (1,0,0)	Q (0,0,1)
$P^X_{0\leftarrow Q}$	$W_{(0,0)\leftarrow(1,0,0)}$	$W_{(0,1)\leftarrow(0,0,1)}$
$P^X_{1\leftarrow Q}$	$W_{(1,0)\leftarrow(1,0,0)}$	~ 0
$P^X_{2\leftarrow Q}$	~ 0	~ 0
$P^A_{0\leftarrow Q}$	$W_{(0,0)\leftarrow(1,0,0)} + W_{(1,0)\leftarrow(1,0,0)}$	~ 0
$P^A_{1\leftarrow Q}$	~ 0	$W_{(0,1)\leftarrow(0,0,1)}$
$P^A_{2\leftarrow Q}$	~ 0	~ 0

Figure Captions

Figure 3.1. Adiabatic potential energy surfaces $\epsilon_n(\vec{R})$ and $\epsilon_{n+1}(\vec{R})$ from diagonalization of the electronic Hamiltonian, $\hat{H}_e$ (·····). Diabatic potential energy surfaces $\tilde{\epsilon}_Q(\vec{R})$ and $\tilde{\epsilon}_D(\vec{R})$, which cross, from a nondiagonal representation of $\hat{H}_e$ (——).

Figure 3.2. Bond lengths and frequencies versus ρ for CN(X $^2\Sigma^+$) and CN(A $^2\Pi$) states from ab initio MCHF minimal basis set (STO-3G) calculations for the minimum energy path for collinear dissociation of $C_2N_2(\tilde{C}\ ^1\Pi_u)$.

Figure 3.3. Section of calculated diabatic electronic potential energy surfaces. The solid line indicates energy of 164 nm photon. Crossing point of STO-3G PES's occurs at 8.9 eV which is 1.4 ev above 164 nm photon energy. Crossing point of DZP PES's occurs at 8.5 eV which is 1.0 ev above 164 nm photon energy.

Figure 3.4. CN(X $^2\Sigma^+$) Vibrational Distributions. Calculated O and experimental ◇ relative PVDs for CN(X $^2\Sigma^+$) at wavelengths studied by Jackson et al. STO-3G computed results obtained for $A = 2.4 \cdot 10^9$ cm^{-1} at all energies, and $\gamma = 4.88$ Å^{-1} at 164 nm, $\gamma = 4.81$ Å^{-1} at 158.7 nm, and $\gamma = 4.64$ Å^{-1} at 153.6 nm; see Eq. (33).

Figure 3.5. Effective Potentials for Transitions at 164 nm. Calculated electronic potential (STO-3G) for minimum energy path (——). Labeled curves indicate effective potentials for transitions to fragment states (ν_X, ν_A) for $A = 2.4\ 10^9$ cm^{-1} and $\gamma = 4.88$ Å^{-1}; see Eq. (33).

Figure 3.6. Computed CN(X $^2\Sigma^+$) and CN(A $^2\Pi$) PVDs at 164 nm. O - initial quasidiscrete state with one quantum in the symmetric CN stretch. ◇ -initial state with one quantum in the asymmetric CN stretch.

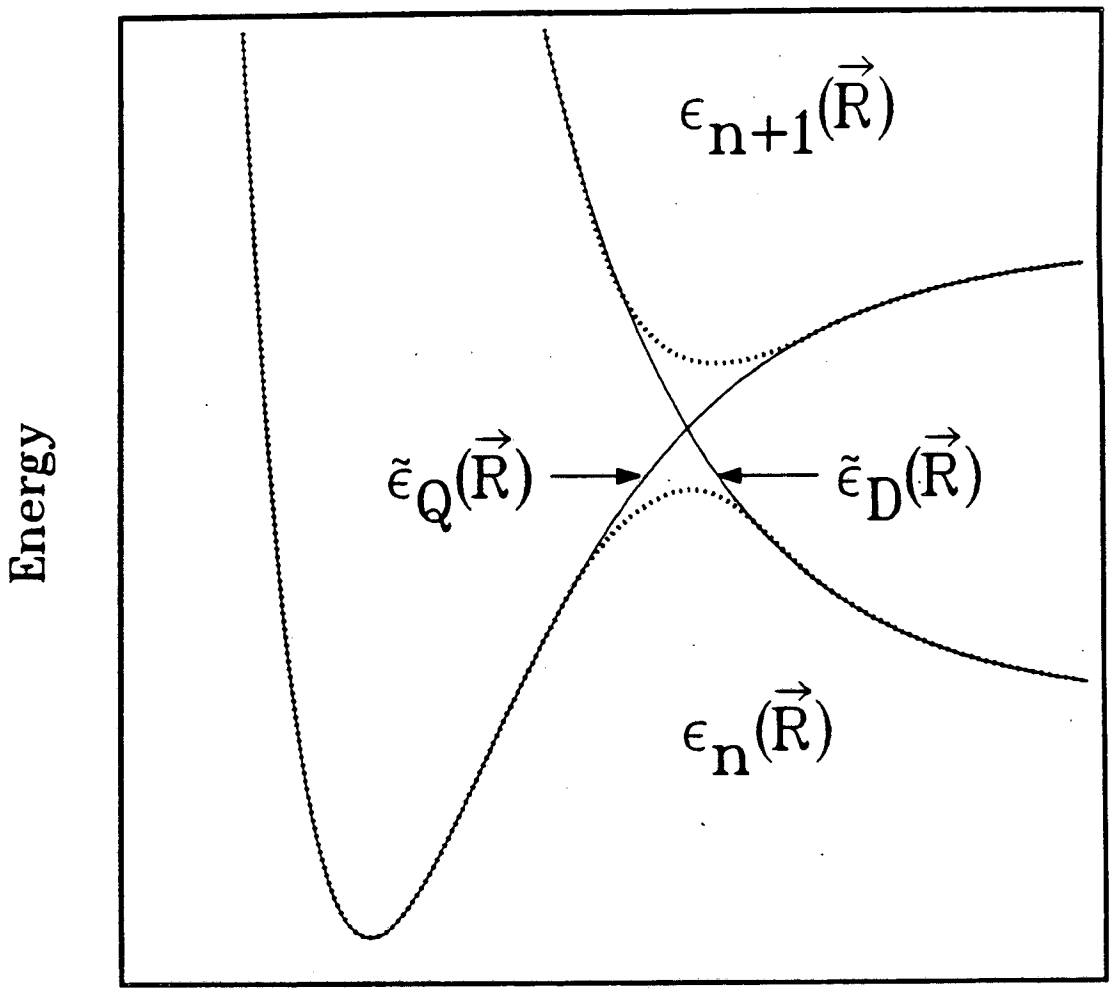
Energy
$\epsilon_{n+1}(\vec{R})$
$\tilde{\epsilon}_Q(\vec{R})$
$\tilde{\epsilon}_D(\vec{R})$
$\epsilon_n(\vec{R})$
Dissociative Coordinate

Figure 3.1

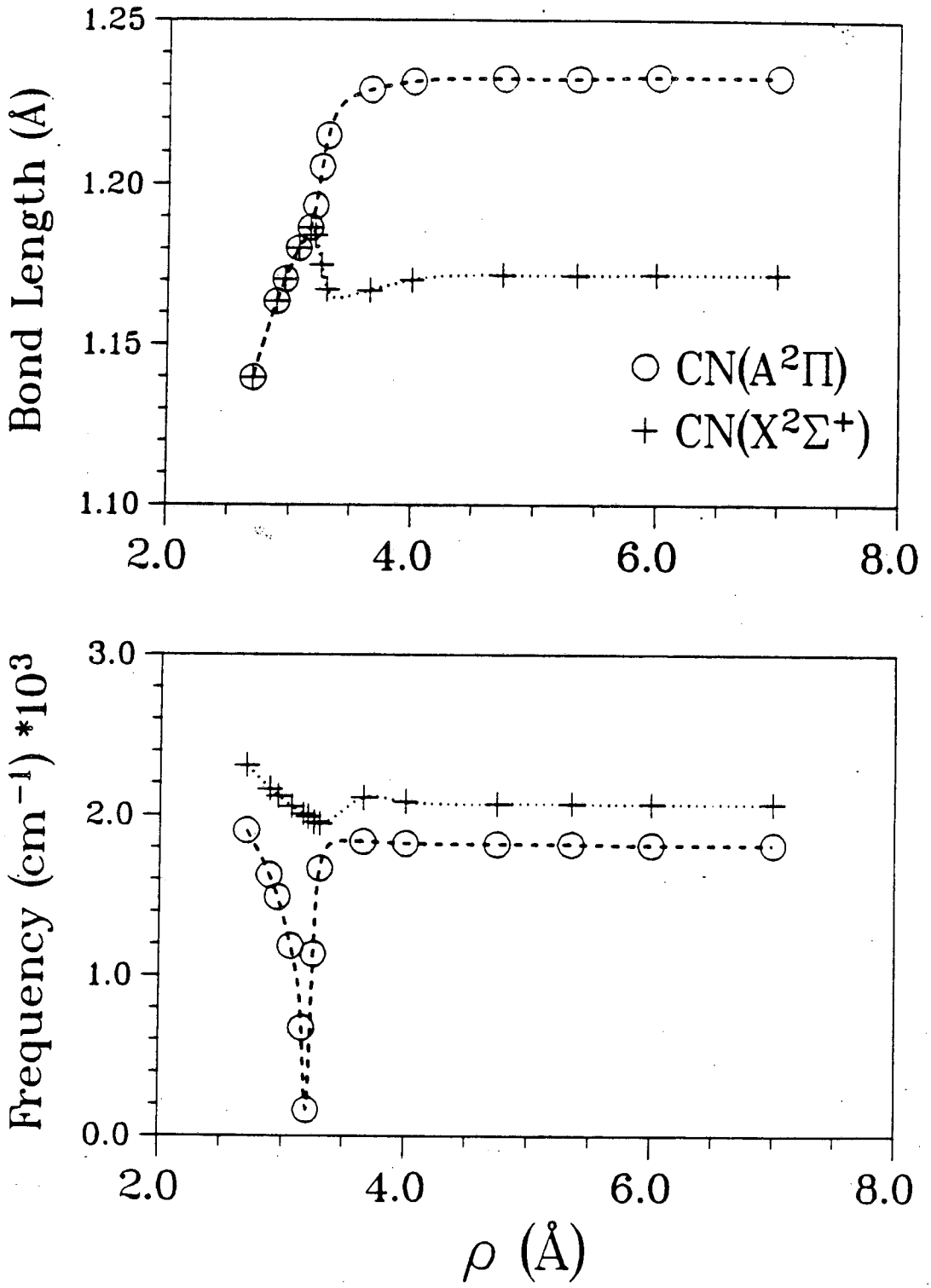
Bond Length (Å)
1.25
1.20
1.15
1.10
2.0
4.0
6.0
8.0
○ CN(A²Π)
+ CN(X²Σ⁺)
Frequency (cm⁻¹) *10³
3.0
2.0
1.0
0.0
2.0
4.0
6.0
8.0
ρ (Å)

Figure 3.2

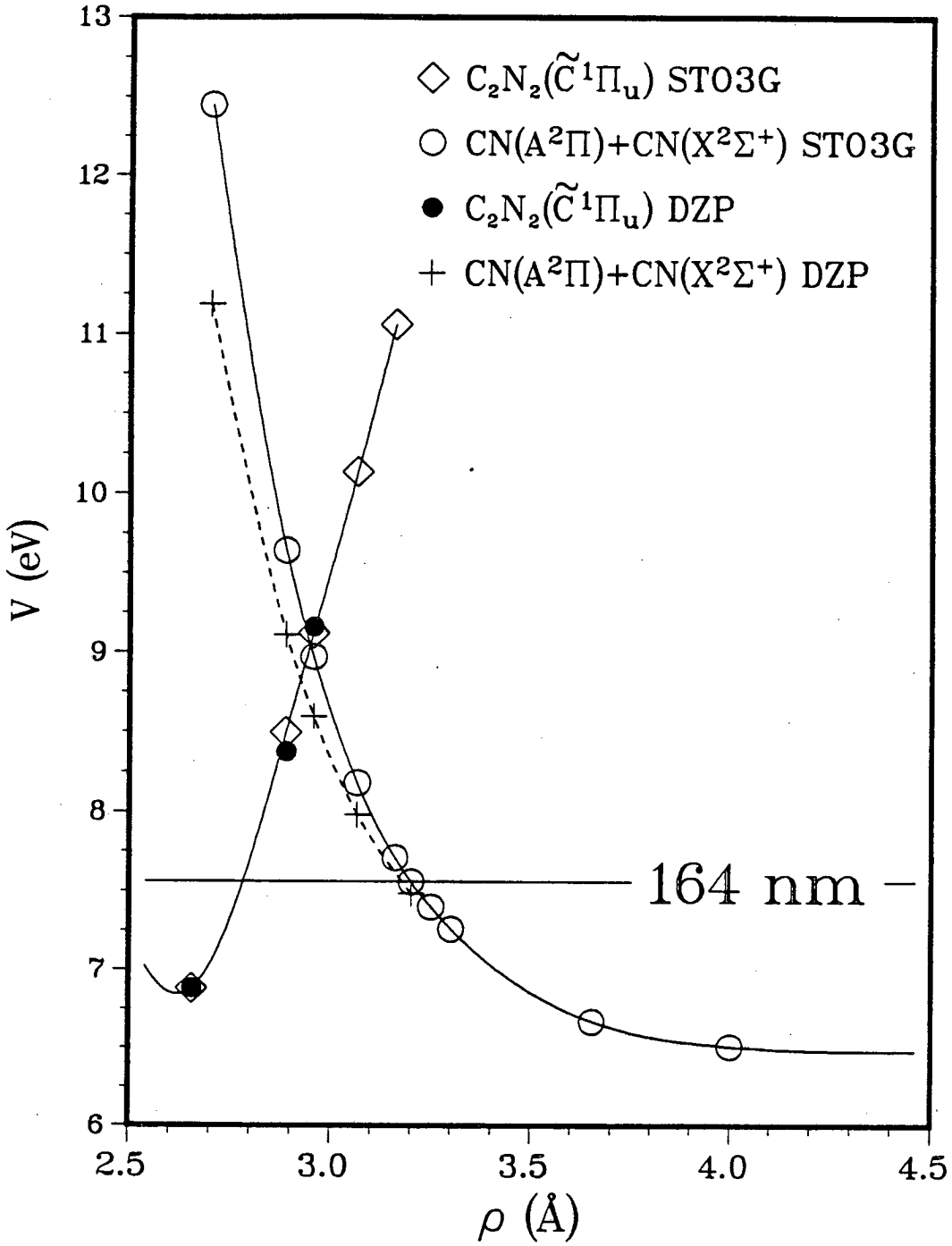
$C_2N_2(\tilde{C}^1\Pi_u)$ STO3G
$CN(A^2\Pi)+CN(X^2\Sigma^+)$ STO3G
$C_2N_2(\tilde{C}^1\Pi_u)$ DZP
$CN(A^2\Pi)+CN(X^2\Sigma^+)$ DZP
164 nm
V (eV)
ρ (Å)
13
12
11
10
9
8
7
6
2.5
3.0
3.5
4.0
4.5

Figure 3.3

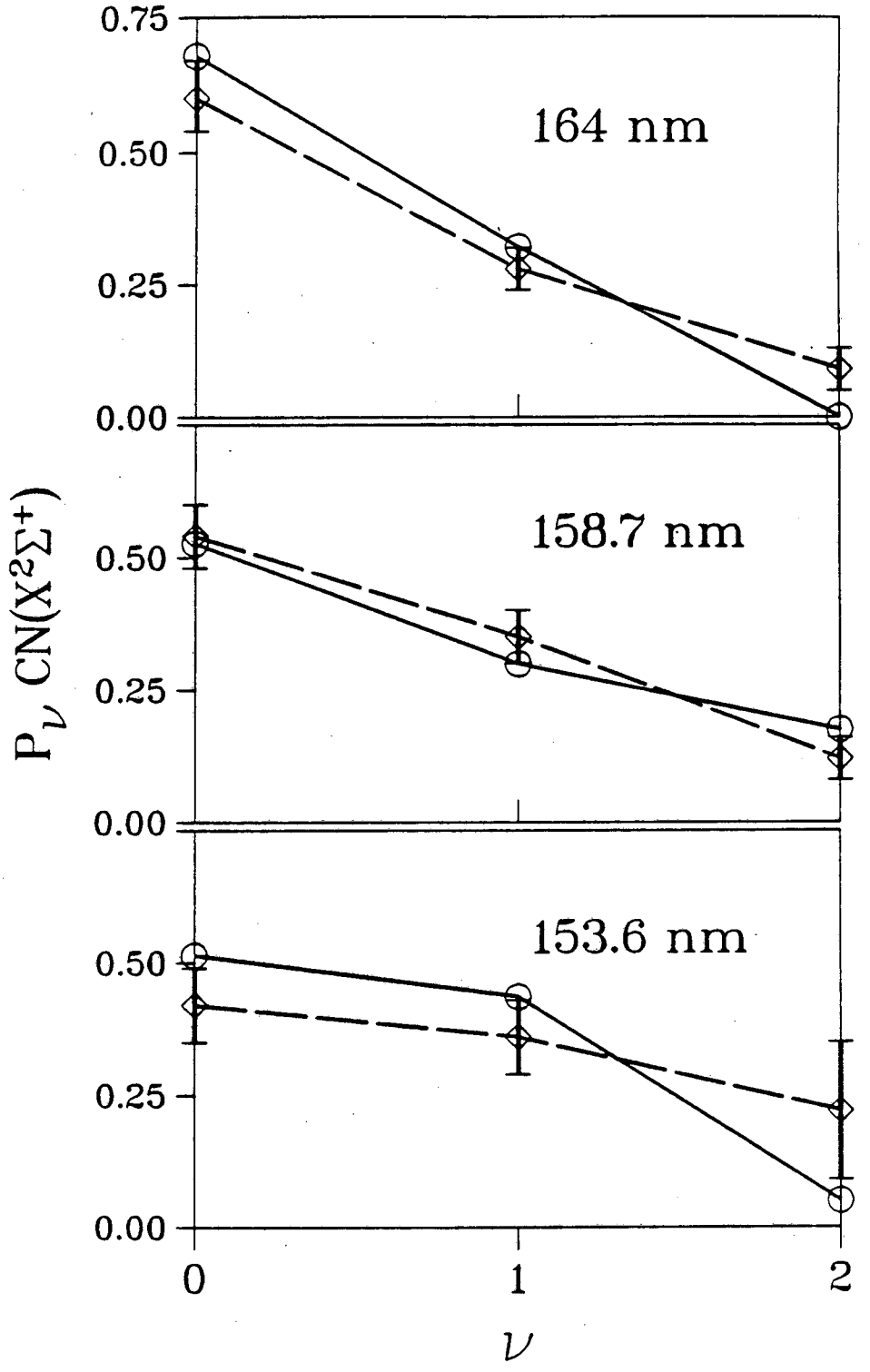

Figure 3.4

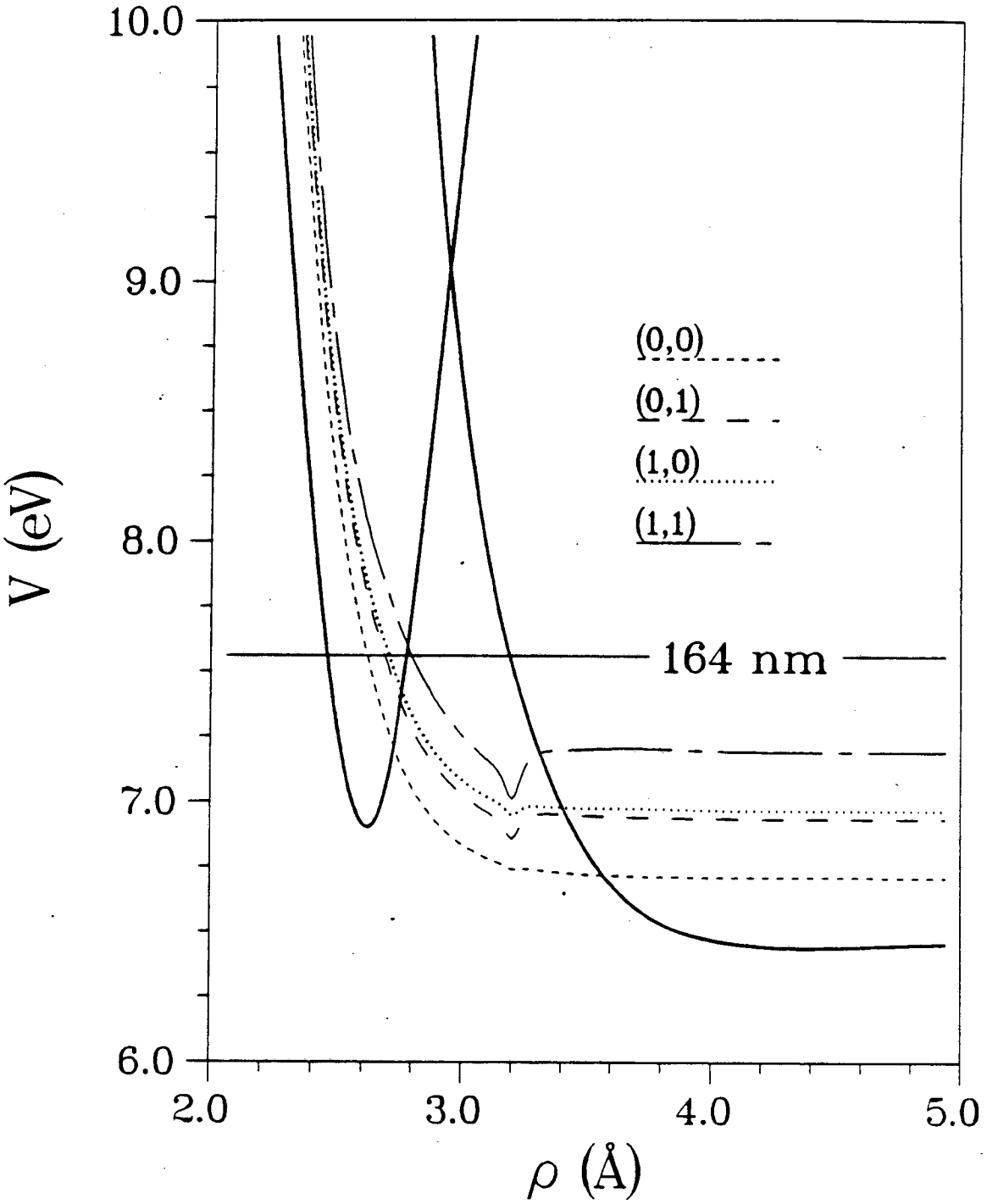

Figure 3.5

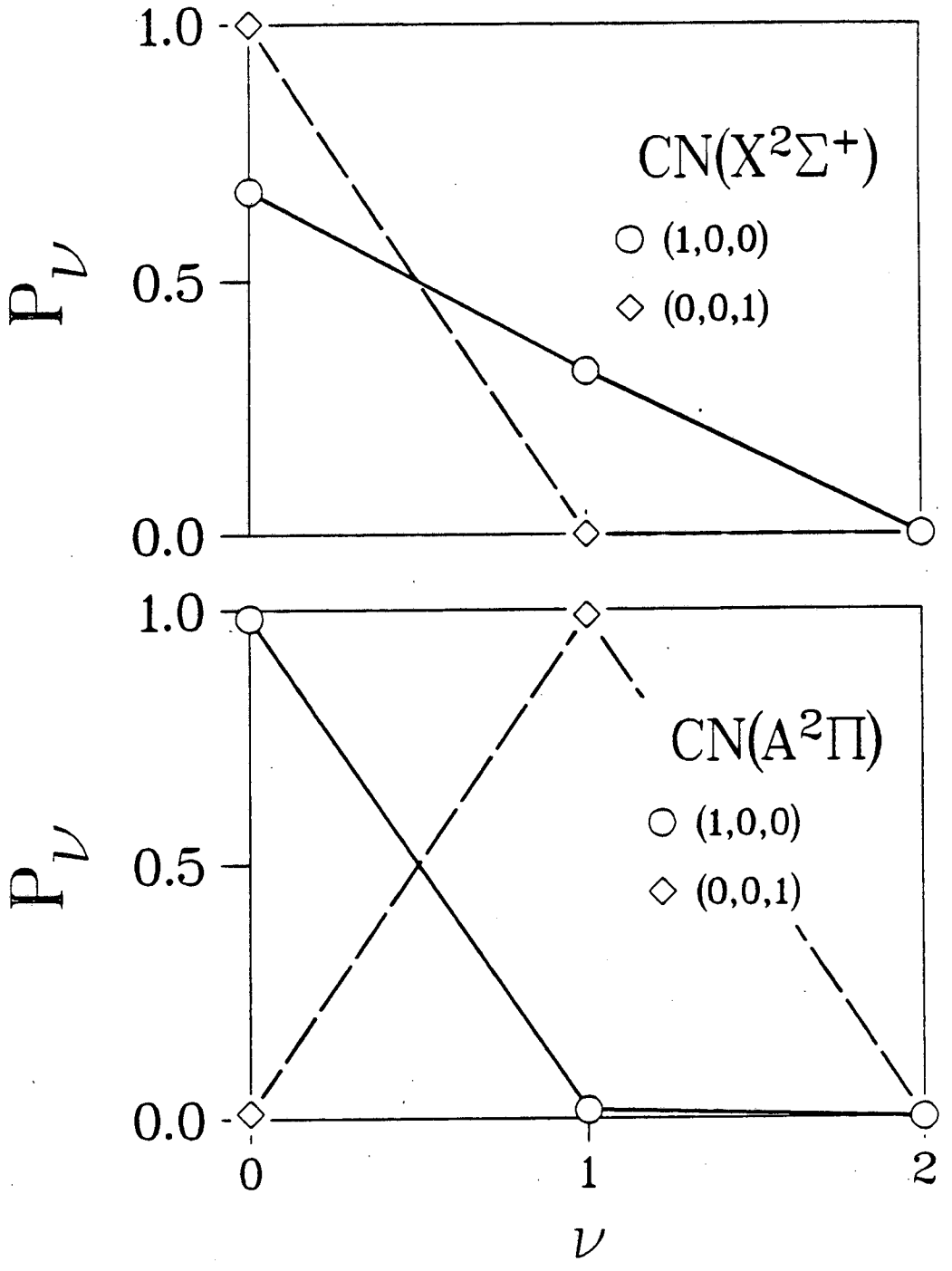
1.0
0.5
0.0
P_ν
$CN(X^2\Sigma^+)$
(1,0,0)
(0,0,1)
1.0
0.5
0.0
P_ν
$CN(A^2\Pi)$
(1,0,0)
(0,0,1)
0
1
2
ν

Figure 3.6

CHAPTER 4

Photofragment Rovibrational Distributions of $C_2N_2(\tilde{C}\ ^1\Pi_u)$ Predissociation

I. Introduction

This chapter deals with the extension of the KL theory of indirect photodissociation to obtain rovibrational distributions which necessitates the inclusion of bending vibrational and rotational motion in the anaylsis. Inclusion of bending vibrations and rotations introduces additional complexities which need to be considered. Conservation of total angular momentum becomes an important aspect in the analysis. In addition to molecular rotations, there may exist contributions to vibrational angular momentum from certain bending modes. Electronic angular momentum can also play a vital role.

Further complications arise in the choice of a proper set of coordinates to describe the nuclear dynamics. In the collinear photodissociation of C_2N_2 the three stretching modes become the two fragment diatom stretches and the dissociative coordinate describing the relative motion of the receding fragments. A set of normal modes which are dependent on the interfragment separation are employed which display the proper character for both the supermolecule in the FC region and the separated fragments asymptotically (see Eqs. (3.28,3.29)). Consideration of the two doubly-degenerate bending vibrations

indicates that they must asymptotically correlate to rotational motion in the fragments (the rotation of each diatom and the relative rotation of one with respect to the other).

In the FC region, these motions have an entirely different appearance from the asymptotic free rotations. They behave more like bending modes of a $CN(X\ ^2\Sigma^+) + CN(A\ ^2\Pi)$ supermolecule. Initially these bending modes become hindered rotors as the fragments begin to separate. Finally, at larger interfragment distances the fragments become uncoupled and can rotate freely. A choice of normal coordinates to describe the bending motions seems more appropriate at small interfragment separations. However, this implies the existence of restoring forces to some pseudo-equilibrium geometry of lower energy. These forces must diminish rapidly as the fragments separate. Ambiguity results as to the proper choice of coordinates to describe how these bending modes in the FC region correlate to the final fragment rotational motions.

This chapter is organized as follows. The theory is presented in section II. In section III, we present application to the predissociation of $C_2N_2(\tilde{C}\ ^1\Pi_u)$ and report preliminary results for product rovibrational distributions (PRVD's). A summary and conluding remarks comprise section IV.

II. Theory

The framework to obtain PRVD's is the same as that introduced in chapter 3. The indirect photodissociation is treated as a quantum transition between diabatic quasidiscrete and dissociative states.[28] Relative product

energy distributions are obtained from the evaluation of a multidimensional nonseparable FC-type integral (c.f. Eq. (3.24)). The main difficulty is obtaining nuclear wave functions which give a proper description of the nuclear dynamics and include the effects of final state interactions.

A. Quasidiscrete (Q) State

As discussed in chapter 3, the motion of a molecule can be characterized by several steps of adiabaticity. Just as fast electronic motion can be separated from the slow vibrational motion of the nuclei, the latter can be separated from the much slower rotational motion. For the present study, we neglect vibrational-rotational coupling which enables the quasidiscrete nuclear wave function to be expressed as

$$\phi_Q(\vec{R}) = \phi_Q^{vib}(Q_i)\ \phi_Q^{rot}(\Theta'), \tag{4.1}$$

where Θ' refers to the set of Euler angles specifying the orientation of the molecule. Throughout this chapter we drop the tildes, and references to wave functions imply those of the diabatic states introduced in chapter 3. In the harmonic approximation for C_2N_2, ϕ_Q^{vib} can be expressed as a product of seven oscillator functions (3 stretches and two pairs of degenerate bends)

$$\phi_Q^{vib}(Q_i) = \prod_{i=1}^{7} \phi_{n_i}(Q_i). \tag{4.2}$$

where i=1,2,3 denote the symmetric CN, CC, and asymmetric CN stretching modes, i=4,6 the degenerate trans-bending modes, and i=5,7 refer to the degenerate cis-bending modes (see vibrational analysis in chapter 2).

In a space-fixed (SF) frame the molecular axis is specified by the Euler angles (α,β,γ), and the rotational wave function for a rigid linear molecule can be written[21]

$$\phi_Q^{rot}(\Theta') = \sqrt{\frac{2J+1}{8\pi^2}}\ D^J_{M\ k+\Lambda}(\alpha,\beta,\gamma). \tag{4.3}$$

Here $D^J_{M\,M'}(\Theta)$ are the well-known rotational matrices,[86,87] where J is the total angular momentum with projection M along the SF z-axis and projection $M'=k+\Lambda$ along the body-fixed (BF) z-axis (in this case the molecular axis). For a linear molecule, the contributions to angular momentum along the BF z-axis come from the electronic angular momentum Λ and vibrational angular momentum k. C_2N_2 has two doubly-degenerate bends, designated as trans- and cis-bending modes. The vibrational angular momentum is given by $k \equiv l_{trans} + l_{cis}$, where l_{trans} and l_{cis} can take on possible values given by[21]

$$\begin{aligned} l_{trans} &= \pm\, n_{trans},\ \pm n_{trans}-2,\ \cdots,\ \pm 1(0) \\ l_{cis} &= \pm\, n_{cis},\ \pm n_{cis}-2,\ \cdots,\ \pm 1(0), \end{aligned} \tag{4.4}$$

and $n_{trans} \equiv n_4 + n_6$ and $n_{cis} \equiv n_5 + n_7$ are the total vibrational quantum numbers for the respective bending modes. For linear molecules, the value of J is also restricted to be greater than or equal to $k+\Lambda$,[23,63] e.g. for Π electronic states $J \geq 1$.

B. Dissociative (D) State

We reemphasize here, that the main difficulty in obtaining the nuclear wavefunctions describing the D state lies in the potential which is a nonseparable function dependent on both the dissociative coordinate and internal

coordinates of the product fragments. It is not until the product fragments are well apart that the potential becomes independent of ρ. Because of the FC principle, the main contribution to the transition matrix element $H'_{D\leftarrow Q}$ is not connected with this asymptotic region, but rather from the region ρ_o, that encompasses the crossing point of the diabatic electronic PES's. As results in chapter 3 indicate, there is in general a strong interfragment interaction in the FC region due to the ρ-dependence of the potential.

In the present analysis, we neglect rotational-vibrational couplings which is an appropriate approximation for most systems due to the relative characteristic time scales of the two types of motion.[28] The D state nuclear wave function can be expressed as

$$\phi_D(\vec{R}) = \phi_D^{vib}(q_i^A, q_j^B; \rho)\ \phi_D^{rot}(\Theta; \rho)\ \phi_D^{rel}(\rho; q_i^A, q_j^B), \tag{4.5}$$

where q_i^A, q_j^B, and Θ refer to the set of internal coordinates and the collective set of angles of the product fragments. In chapter 3, we treated the vibrational-translational coupling via an adiabatic method. A general solution for $\phi_D(\vec{R})$ was obtained from the rigorous solutions for two limiting cases, $\alpha_v \equiv \epsilon_{rel}/\epsilon_{vib} >> 1$ and $\alpha_v << 1$, which imply fast or slow translational motion relative to the vibrational motion of the D state fragments. In this chapter we will treat the rotational-translational coupling in an analogous fashion, in which a general solution of the form given by Eq. (4.5) can be obtained.

We define the quantity $\alpha_r \equiv \dfrac{\epsilon_{rel}}{\epsilon_{rot}}$ which is similar to α_v and will be used

to characterize two limiting cases where the translational motion is either much faster ($\alpha_r >> 1$) or slower ($\alpha_r << 1$) than the rotational motion of the D state fragments. Note that $\epsilon_{rel} = \epsilon_{avl} - \epsilon_{vib} - \epsilon_{rot}$, where ϵ_{avl} is the total available energy that can go into translational, vibrational, or rotational degrees of freedom of the fragments. In general ϵ_{vib} is greater than ϵ_{rot}, hence, α_v will be smaller than α_r. The solution of ϕ_D^{vib} was described in chapter 3, and in this chapter we concern ourselves with the solution of the rotational wave function ϕ_D^{rot}. For clarity of presentation, we initially derive the general expressions for a tetra-atomic molecule that following photodissociation results in two Σ state diatomic fragments. The inclusion of electronic angular momentum for the $C_2N_2(\tilde{C}\ ^1\Pi_u)$ predissociation will be discussed in section III.

1. Case (i): Fast Translational Motion, $\alpha_r >> 1$

This limit is equivalent to a "sudden" approximation[88–89] and generally corresponds to a mapping of the initial Q state onto the asymptotic rotational states of the product fragments. For two diatomic molecules, the asymptotic rotational states can be written with respect to a SF reference frame,[90–93]

$$\phi_\gamma^{JM}(\Theta) = \sum_{\substack{m_A m_B \\ m_{AB} m_l}} <j_A m_A j_B m_B \mid j_{AB} m_{AB}> <j_{AB} m_{AB} l m_l \mid JM> \\ Y_{j_A m_A}(\theta_A,\phi_A)\, Y_{j_B m_B}(\theta_B,\phi_B)\, Y_{l\, m_l}(\theta,\phi). \tag{4.6}$$

Here, $Y_{j\,m}$ are spherical harmonics,[86–87] γ is the set of quantum numbers j_A, j_B, j_{AB}, l, and $< \cdots \mid \cdots >$ are Clebsch-Gordan coupling coefficients.[86–87] The rotational quantum numbers of each diatom j_A and j_B

couple to give j_{AB}, which is coupled with l,the relative angular momentum, resulting in a state of total angular momentum J. The angles specify orientation within the SF frame. The coordinates of the system are illustrated in figure 4.1.

Note that $\alpha_r >> 1$ generally places no restrictions on the value of α_v. Either limiting case of α_v presented in chapter 3 is possible. We also point out that despite the neglect of rotational-vibrational coupling, there exists indirect coupling of these two types of motion. This can be seen in the evaluation of the final density of states and through conservation of energy and angular momentum constraints.

In the sudden limit, details of the dynamics come primarily from the initial Q state. It completely neglects the repulsive electronic PES of the D state and as such does not include final state interactions. However, several approaches to photodissociation[36c,63a,94,95] have been successful employing more rigorous treatments of vibrational motion and using the sudden limit to describe rotational motion.

2. Case (ii): Slow Translational Motion, $\alpha_r << 1$

Conceptually this limit can be described as the slow formation of photofragments receding along the repulsive D state PES via a minimum energy path. As the fragments separate, the modes orthogonal to the dissociative coordinate adiabatically relax to a equilibrium configuration dependent on the interfragment separation. Note that in general $\alpha_r << 1$ will imply $\alpha_v << 1$.

Again the solutions to the vibrational problem are the same as those given in chapter 3, and we concentrate on the solution of the rotational wave function.

In the FC region, the normal modes of the CN(X $^2\Sigma^+$) + CN(A $^2\Pi$) supermolecule which are orthogonal to the dissociative coordinate will have an appearance similar to the bending vibrational modes in the Q state. In general, the potential for a 4-atom molecule will depend on 6 internal coordinates (7 for a linear molecule). One such set $\{q^A, \chi_A, q^B, \chi_B, \rho, \chi\}$ is defined in Figure 4.1. However, at larger interfragment distance the potential will only depend on q^A and q^B, the two diatom bond lengths, and only kinetic energy and centrifugal terms of the Hamiltonian will asymptotically depend on ρ and the angular variables. A choice of normal coordinate oscillator wave functions, though perhaps most appropriate in the FC region, does not satisfy the criteria of correlating to the proper asymptotic form given by Eq. (4.6).

One possible choice of wave function which will satisfy the above criteria is an expansion employing the asymptotic free rotor states of Eq. (4.6) as a basis set. The rotational wave function of total angular momentum J can be expressed in all regions as

$$\phi^{JM}(\Theta,\rho) = \sum_{\gamma} B^{D}_{\gamma;JM}(q_o^A(\rho),\, q_o^B(\rho),\, \rho)\, \phi_\gamma^{JM}(\Theta) \qquad (4.7)$$

We note that the coupling of the rotational motion with the relative motion of the fragments is explicitly included by the ρ-dependence of the expansion coefficients $B^{D}_{\gamma;JM}$.

The Hamiltonian for a two diatom system in center of mass coordinates

can be written as[90]

$$H = -\frac{\hbar}{2\mu}\nabla_\rho^2 + H_A(q^A) + H_B(q^B) + V(q^A,q^B,\rho) \tag{4.8}$$

where the first term is the kinetic energy operator for the relative motion of the system with reduced mass μ. The terms $H_{A(B)}$ are the Hamiltonians for the free diatoms. The last term in Eq. (4.8) is the interfragment potential, which goes to zero in the limit $\rho\rightarrow\infty$. If rotational-vibrational coupling is neglected, the rotational Hamiltonian for two diatoms can be written

$$H_{rot} = \frac{\mathbf{l}^2}{2\mu\rho^2} + \frac{\mathbf{j}_A^2}{2\mu_A q_o^A(\rho)^2} + \frac{\mathbf{j}_B^2}{2\mu_B q_o^B(\rho)^2} + V(q_o^A(\rho),q_o^B(\rho),\rho,\Theta). \tag{4.9}$$

Here μ_A and μ_B are the reduced masses of the diatom fragments. The use of equilibrium fragment geometries (given by Eqs. (3.22)) results from neglecting rotational-vibrational couplings.[96] This is equivalent to a modified rigid rotor approximation, where the nonvibrating rotors adiabatically adjust to their equilibrium lengths for a given value of ρ on the minimum energy path.

It is convenient to expand the intermolecular potential (which goes to zero in the limit $\rho \rightarrow \infty$) in a complete set of SF spherical harmonics.[90-93]

$$\begin{aligned} V(q_o^A(\rho),q_o^B(\rho),\rho,\Theta) = \sum_{\lambda_1\lambda_2\lambda}\sum_{\mu_1\mu_2\mu} & A_{\lambda_1\lambda_2\lambda}(q_o^A(\rho),q_o^B(\rho),\rho) \\ & < \lambda_1\,\mu_1\,\lambda_2\,\mu_2 \mid \lambda\,\mu > Y_{\lambda_1\mu_1}(\theta_A,\phi_A)\,Y_{\lambda_2\mu_2}(\theta_B,\phi_B)\,Y^*_{\lambda\mu}(\theta,\phi) \end{aligned} \tag{4.10}$$

The Schrödinger equation for the rotational motion is

$$H_{rot}\,\phi^{JM}(\Theta,\rho) = E^J(\rho)\,\phi^{JM}(\Theta,\rho). \tag{4.11}$$

Substituting Eqs. (4.7) and (4.9) into Eq. (4.11), multiplying by $\phi_\gamma^{JM*}(\Theta)$, and integrating over the angular variables Θ yields a set of coupled equations for

the expansion coefficients $B^{D}_{\gamma;JM}$.

$$\left[E^{J}(\rho) - \frac{\hbar l(l+1)}{2\mu\rho^2} - \frac{\hbar j_A(j_A+1)}{2\mu_A q_o^A(\rho)^2} - \frac{\hbar j_B(j_B+1)}{2\mu_B q_o^B(\rho)^2}\right] B^{D}_{\gamma;JM}(q_o^A(\rho),q_o^B(\rho),\rho) = \sum_{\gamma'} V_{\gamma',\gamma}(q_o^A(\rho),q_o^B(\rho),\rho)\, B^{D}_{\gamma';JM}(q_o^A(\rho),q_o^B(\rho),\rho), \tag{4.12}$$

where the potential coupling matrix elements are given by

$$V_{\gamma',\gamma}(q_o^A(\rho),q_o^B(\rho),\rho) = \int d\Theta\, Y^{*}_{j_{A'}\, m_{A'}}(\theta_A,\phi_A)\, Y^{*}_{j_{B'}\, m_{B'}}(\theta_B,\phi_B)\, Y^{*}_{l'\, m_{l'}}(\theta,\phi)\, V(q_o^A(\rho),q_o^B(\rho),\rho,\Theta)\, Y_{j_A\, m_A}(\theta_A,\phi_A)\, Y_{j_B\, m_B}(\theta_B,\phi_B)\, Y_{l\, m_l}(\theta,\phi) \tag{4.13}$$

Given the potential in the form of Eq. (4.10), the potential coupling matrix elements can be reduced using standard angular momentum coupling techniques[86,87,90-93] to yield

$$V_{\gamma',\gamma}(q_o^A(\rho),q_o^B(\rho),\rho) = \sum_{\lambda_1\lambda_2\lambda} (4\pi)^{-3/2}\, (-1)^{j_{A'}+j_{B'}+j_{AB}+J}\, A_{\lambda_1\lambda_2\lambda}(q_o^A(\rho),q_o^B(\rho),\rho)([\lambda]^2[\lambda_1][\lambda_2][j_A'][j_B'][l'][j_{AB}'][j_A][j_B][l][j_{AB}])^{1/2} \begin{pmatrix} \lambda & l & l' \\ 0 & 0 & 0 \end{pmatrix} \begin{pmatrix} \lambda_1 & j_A & j_A' \\ 0 & 0 & 0 \end{pmatrix} \begin{pmatrix} \lambda_2 & j_B & j_B' \\ 0 & 0 & 0 \end{pmatrix} \begin{Bmatrix} l & l' & \lambda \\ j_{AB}' & j_{AB} & J \end{Bmatrix} \begin{Bmatrix} j_{AB} & j_B & j_A \\ j_{AB}' & j_B' & j_A' \\ \lambda & \lambda_2 & \lambda_1 \end{Bmatrix} \tag{4.14}$$

where $[j]\equiv 2j+1$ and $(:::)$, $\{:::\}$, and $\left\{\begin{smallmatrix}:&:&:\\:&:&:\end{smallmatrix}\right\}$ are the well-known 3-j, 6-j, and 9-j coefficients.[86,87]

The expansion vector $B^{D}_{\gamma;JM}$ and energies $E^{J}(\rho)$ can be obtained from Eq. (4.12) using standard eigenvalue problem routines.[97] In practice the number of coupled equations is determined by size of the basis set expansion in Eq. (4.7), which is generally truncated to certain cutoff values (e.g., j_A^*, j_B^*, and l^*, which are maximum values of the summation variables in Eq. (4.7)) chosen to satisfy

a convergence criterion. In the limit $\rho \rightarrow \infty$ the potential becomes zero, and the eigenvectors become the asymptotic states (see Eq. (4.6)). The asymptotic states can be labeled by j_A, j_B, and l, which are good quantum numbers in this region. The expansion coefficients asymptotically satisfy the relationship,

$$B^{D}_{\gamma,JM}(\infty) = \delta_{j_A j_A'} \delta_{j_B j_B'} \delta_{j_{AB} j_{AB}'} \delta_{ll'}. \tag{4.15}$$

We see that the form of the wave function in Eq. (4.7) has the flexibility to describe the D state in both the FC and asymptotic regions.

We note here that a modification to the D state nuclear wave function describing the relative motion of the separating photofragments is necessary. Here $\phi_{rel}(\rho)$ is obtained by solving

$$\left[-\frac{1}{2\mu} \frac{\partial^2}{\partial \rho^2} + U_{eff}(\rho) \right] \phi_{rel}(\rho) = E \, \phi_{rel}(\rho) \tag{4.16}$$

which is similar to Eqs. (3.17-3.18), but inclusion of rotational motion gives an effective potential of the form

$$U_{eff}(\rho) = U(q_o^A(\rho), q_o^B(\rho), \rho) + E_{vib}(\rho) + E^J(\rho). \tag{4.17}$$

We emphasize that in this limit, as observed in chapter 3, the fragment vibrational frequencies and equilibrium bond lengths (and hence, $E_{vib}(\rho)$) may show a strong ρ dependence in the FC region and can differ considerably from their asymptotic values. We find in this limit a similar dependence of the rotational energy $E^J(\rho)$. This dependence is seen through both the potential coupling matrix elements and the equilibrium geometries which affect the moments of inertia (or the rotational contants) of the fragments along the minimum energy

path.

3. Intermediate Cases, $\alpha_r \approx 1$

The general D state wave function for arbitrary α_r can be constructed from the two limiting cases discussed above. We note that the wave functions in the two limiting cases have a similar form and differ only in their dependence on ρ; see Eqs. (4.6) and (4.7). One choice of generating the solution is to employ an interpolation scheme which allows a smooth continuous change in the wave functional form from $\alpha_r << 1$ to $\alpha_r >> 1$. As the expansion of $\phi^{JM}(\Theta,\rho)$ may contain a large number of terms, there is difficulty in trying to interpolate the expansion coefficients as was done for the vibrational problem.

We note that for $\alpha_r << 1$, the ρ-dependence originates from the interfragment potential, $V(q_o^A(\rho),q_o^B(\rho),\rho,\Theta)$. Whereas for $\alpha_r >> 1$, the sudden limit is equivalent to neglecting the D state potential, i.e., $V(q_o^A(\rho),q_o^B(\rho),\rho,\Theta) = 0$. We introduce an interpolating factor $e^{-\alpha_r^2}$ which serves as a multiplicative factor to the interfragment potential. That is, the general form of ϕ^{JM} is obtained from solving the Schrödinger equation Eq. (4.11) with a modified interfragment potential given by

$$\bar{V}(q_o^A(\rho),q_o^B(\rho),\rho,\Theta) = V(q_o^A(\rho),q_o^B(\rho),\rho,\Theta) \cdot e^{-\alpha_r^2} \qquad (4.18)$$

which reduces to the proper potential form for each limit of α_r. The rotational wave function will have a form similar to Eq. (4.7) but with expansion coefficients, $\bar{B}^D_{\gamma,JM}(q_o^A(\rho),q_o^B(\rho),\rho)$ and energy levels $\bar{E}^J(\rho)$ determined the solution of the eigenvalue equation (Eq. (4.12)) using $\bar{V}(q_o^A(\rho),q_o^B(\rho),\rho,\Theta)$.

C. Evaluation of Franck-Condon Overlap Integrals

Relative rovibrational distributions can be obtained by evaluating a multidimensional FC integral of the form,

$$H'_{D\leftarrow Q} \sim \int \phi_D^*(\vec{R})\, \phi_Q(\vec{R})\, d\vec{R} \tag{4.19}$$

Eq. (4.19) involves complicated integrals of normal mode harmonic oscillator functions with spherical harmonic functions. Hoewever, using an approach introduced by Beswick and Gelbart,[96] the bending and rotational motion of the Q state can be expressed in a similar free rotor basis set expansion. In general, bending vibrational motion in polyatomic molecules is slower than the stretching motion, and in an adiabatic approximation these two motions can be separated. Also in the harmonic approximation there is no coupling between normal modes. The analysis is exactly the same as was done for the $\alpha_r \ll 1$ limiting case for the D state. The bending potential can similarly be expanded in terms of SF spherical harmonics (c.f. Eq. (4.10)). The result is that the Q state nuclear wave function can be expressed as

$$\phi_Q(\vec{R}) = \phi_Q^{str}(Q_i)\, \phi_Q^{bend-rot}(\Theta) \tag{4.20}$$

where from a similar analysis as that described above for ϕ_D^{rot}, the bending-rotor wave function of the Q state is given by,

$$\phi_Q^{bend-rot}(\Theta) \equiv \phi_Q^{JM}(\Theta) = \sum_\gamma B^Q_{\gamma;JM} \sum_{\substack{m_A m_B \\ m_{AB} m_l}} \langle j_A m_A j_B m_B \mid j_{AB} m_{AB} \rangle$$
$$\langle j_{AB} m_{AB} l m_l \mid JM \rangle\, Y_{j_A m_A}(\theta_A,\phi_A)\, Y_{j_B m_B}(\theta_B,\phi_B)\, Y_{l\, m_l}(\theta,\phi), \tag{4.21}$$

where the $B^Q_{\gamma;JM}$ are constants determined from solving an eigenvalue equation

similar to Eq. (4.12). Note that the rotational motion of the molelcule is included in the basis set expansion and that the quantum numbers γ have no physical significance for a bound state. The main advantage of using the free rotor representation of the bound Q state is the simplification of the FC integrals.

The FC integral to be evaluated can be rewritten as

$$H'_{D\leftarrow Q} = \int d\rho' \left[\phi_{vib}(\rho') \, \phi_{rot}(\rho') \, \phi_{rel}(\rho') \right], \tag{4.22}$$

where $\rho' = \rho - \rho_0$ is defined in chapter 3 (c.f. Eq. (3.27)). The wave function $\phi_{vib}(\rho')$ is the effective oscillator, which was described in chapter 3, and is obtained from integration over the stretching coordinates (see Eqs. (3.30-3.32)). The wave function $\phi_{rot}(\rho')$ is an effective rotational wave function which results from the integral

$$\phi_{rot}(\rho') = \int d\Theta \; \phi_D^{JM*}(\Theta,\rho') \, \phi_Q^{JM}(\Theta), \tag{4.23}$$

which upon substitution of Eq. (4.7) and employing the orthogonal properties of the spherical harmonic functions yields,

$$\phi_{rot}(\rho') = \sum_{\gamma} \bar{B}^{D}_{\gamma;JM}(q_o^A(\rho),q_o^B(\rho),\rho) \, B^{Q}_{\gamma;JM}. \tag{4.24}$$

The final integration over ρ' can be carried out using standard numerical methods.

It is important to note, that despite the neglect of rotational-vibrational coupling, there exist indirect coupling between these motions from several factors. In Eq. (4.17) we see that the effective potential contains contributions

from both vibrational and rotational energy terms. Both types of motion are coupled to the relative motion of the fragments through the interfragment potential. In addition, comparison of Eq. (4.21) and Eq. (3.31) indicates the former contains the factor $\phi_{rot}(\rho')$, which can serve to modify the vibrational distributions. Finally, the final density of states ρ_E is also a factor in determining the transition probabilities (c.f. Eq. (3.1)). This term is proportional to the square root of the asymptotic translational energy, $\rho_E \sim \epsilon_{rel}^{1/2} = (\epsilon_{avl}-\epsilon_{vib}-\epsilon_{rot})^{1/2}$.

The effective rotational wave function, $\phi_{rot}(\rho')$, is unlike either $\phi_{vib}(\rho')$ or $\phi_{rel}(\rho')$ in that it is nonzero throughout both the FC and asymptotic regions. However, the important region of the FC integral is bounded by the range of the effective oscillator and relative motion wave functions. $\phi_{vib}(\rho')$, will be nonzero only for a small region near the equilibrium geometry of the bound Q state and decreases exponentially as ρ increases. Similarly, $\phi_{rel}(\rho')$ is exponentially small in the classically forbidden region and gains appreciable amplitude only outside the classical turning point of the D state PES. In general, the main contributions to the FC overlap integral will come from a small region which will encompass the crossing point between the Q and D state PES's. Thus, $\phi_{rot}(\rho')$ may need to be evaluated only over a relatively small region.

The above approach is similar to that which is followed in formal scattering theory (i.e., using an asymptotic basis set and the required solution of a similar set of coupled equations). As such, it eventually will encounter similar

problems to those that arise with larger systems or for increasing energy, in which the number of coupled equations becomes prohibitively large. Perhaps future work should be directed towards obtaining a more compact functional form for the description of rotational motion in the D state. One possibility is the use of normal modes in the FC region and the free rotor expansion for the asymptotic region. Some matching function in the intermediate regions could be employed to connect smoothly the two wave function forms. Such an approach is common to many dynamical methods[98–100] and has also been used in fitting potential functions[101] that display different character in various regions of space.

III. Application to $C_2N_2(\tilde{C}\ ^1\Pi_u) \rightarrow CN(X\ ^2\Sigma^+) + CN(A\ ^2\Pi)$

In section II, we presented the theory for two Σ (Λ=0) state diatomics. However, the predissociation of $C_2N_2(\tilde{C}\ ^1\Pi_u, \Lambda=1)$ results in the formation of one $^2\Pi$ state CN radical that has nonzero electronic angular momentum (Λ=1). As the photodissociation process is constrained by conservation of angular momentum, inclusion of electronic angular momentum is important to describe properly possible angular momentum coupling effects.

We employ a generalization,[102–103] appropriate for the presence of electronic angular momentum, of the basis set expansion of the nuclear wave functions used to describe the rotational motion (c.f. Eq. (4.6)). This basis is given by

$$\phi_\gamma^{JM}(\Theta) = \sqrt{\frac{[j_A]\,[j_B]}{16\,\pi^2}} \sum_{\substack{m_A m_B \\ m_{AB} m_l}} \langle j_A m_A j_B m_B \mid j_{AB} m_{AB} \rangle$$

$$\langle j_{AB} m_{AB} l m_l \mid JM \rangle\, D^{j_A^*}_{m_A \Lambda_A}(\phi_A,\theta_A,\eta_A)\, D^{j_B^*}_{m_B \Lambda_B}(\phi_B,\theta_B,\eta_B)\, Y_{l\, m_l}(\theta,\phi). \tag{4.25}$$

The interfragment potential is still expressed as in Eq. (4.10). Following the identical procedure as outlined above yields a similar set of coupled equations as Eq. (4.12); however, the potential coupling matrix elements after manipulation with angular momentum algebra[86,87] reduce in this case to

$$V_{\gamma',\gamma}(q_o^A(\rho),q_o^B(\rho),\rho) = \sum_{\lambda_1\lambda_2\lambda} (4\pi)^{-3/2}\,(-1)^{j_A+j_B+j_{AB}+J+\lambda_1+\lambda_2-\Lambda_A-\Lambda_B}$$
$$A_{\lambda_1\lambda_2\lambda}(q_o^A(\rho),q_o^B(\rho),\rho)([\lambda]^2[\lambda_1][\lambda_2][j_A'][j_B'][l'][j_{AB}'][j_A][j_B][l][j_{AB}])^{1/2}$$
$$\begin{pmatrix} \lambda & l & l' \\ 0 & 0 & 0 \end{pmatrix} \begin{pmatrix} \lambda_1 & j_A & j_A' \\ 0 & -\Lambda_A & \Lambda_A \end{pmatrix} \begin{pmatrix} \lambda_2 & j_B & j_B' \\ 0 & -\Lambda_B & \Lambda_B \end{pmatrix} \begin{Bmatrix} l & l' & \lambda \\ j_{AB}' & j_{AB} & J \end{Bmatrix} \begin{Bmatrix} j_{AB} & j_B & j_A \\ j_{AB}' & j_B' & j_A' \\ \lambda & \lambda_2 & \lambda_1 \end{Bmatrix}. \tag{4.26}$$

Note that Eq. (4.26) reduces to Eq. (4.14) when $\Lambda_A=\Lambda_B=0$. The rotational quantum numbers are restricted to $j_A \geq \Lambda_A$ and $j_B \geq \Lambda_B$.[23,63]

As discussed in chapter 2, $C_2N_2(\tilde{C}\ ^1\Pi_u)$ displays Renner-Teller (RT) character which complicates the bending vibrational analysis. The RT effect is well-known for linear molecules in Π and other electronic states of nonzero electronic angular momentum.[104,105] The RT effect results from nonadiabatic coupling between the bending vibrational and electronic angular momentum. Several studies[105,106] have shown RT effects to be important in chemical reactions in which the reactants pass through a linear transition state with nonzero electronic angular momentum. Exact inclusion of the RT effect would entail

the explicit dynamical coupling of the two electronic PES's (for both the Q and D state PES's) involved which split as the linear molecule becomes non-linear.

In this study we present preliminary results for the rovibrational analysis in which we treat the rotational motion in the sudden limit ($\alpha_r << 1$). Treatment of the general case requires additional information concerning the D state PES which is necessary to describe the bending modes that become rotations along the dissociative coordinate. Presently, this information is not available, but can be obtained from further ab initio analysis. In the present study therefore, we will neglect RT vibrational-electronic angular momentum coupling and consider only the linear $C_2N_2(\tilde{C}\ ^1\Pi_u, {}^1A'')$ component in our analysis (see chapter 2). In this sudden limit only information about the Q state PES is needed. It is difficult to determine apriori the effects of the above approximations. Although our preliminary data are presented here, the size of corrections introduced by proper account of these couplings needs further investigation.

A. The Quasidiscrete State Bending Potential

For $C_2N_2(\tilde{C}\ ^1\Pi_u)$, a harmonic analysis from the ab initio MCHF wave function described in chapter 2 yields a quadratic potential of the form

$$V(x_i,y_i,z_i) = \frac{1}{2} \sum_{i=1}^{4} \sum_{j=1}^{4} f_{ij}^x \Delta x_i \Delta x_j + f_{ij}^y \Delta y_i \Delta y_j + f_{ij}^z \Delta z_i \Delta z_j \quad (4.27)$$

where the molecular axis is chosen to lie along the z coordinate and indices i

and j refer to atoms of C_2N_2 as labeled in Figure 4.1. In this SF frame, x,y and z are completely decoupled in the harmonic approximation. Furthermore, the normal mode analysis indicates that the stretching modes involve motion solely along the molecular z-axis and the bending vibrations can be described as motion orthogonal to the molecular axis in the xz- and yz-planes. The x and y directions are equivalent due to the symmetry of the system, and the bending potential can be expressed as

$$V_{bend}(x_i,y_i) = \frac{1}{2} \sum_{i=1}^{4} \sum_{j=1}^{4} f_{ij} \, (\Delta x_i \, \Delta x_j + \Delta y_i \, \Delta y_j) \qquad (4.28)$$

which we need to express in terms of the SF spherical harmonics (c.f. Eq. (4.10)).

The transformation from cartesian coordinates to the desired set of internal coordinates is given in Table 4.1. The potential can be expressed in the form of Eq. (4.10) by algebraic manipulation and employing relationships between transcendental functions and spherical harmonics.[86,87] The resulting potential coefficients, $A_{\lambda_1\lambda_2\lambda}$, expressed in terms of the cartesian force constant matrix elements are given in Table 4.2. Numerical values of the force constants in each coordinate system are tabulated in Table 4.3. Due to symmetry of the linear $C_2N_2(\tilde{C}\ ^1\Pi_u)$ only two terms in the spherical harmonic expansion are nonzero for the quadratic function (4.27). The implications of this will be discussed below.

B. CN(X $^2\Sigma^+$) and CN(A $^2\Pi$) PRVD's in the Sudden Limit ($\alpha_r >> 1$)

In the sudden limit, $\phi_{rot}(\rho')$ (c.f. Eq. (4.23)) is obtained from projecting the Q state rotational wave function $\phi_Q^{bend-rot}(\Theta)$ onto the final asymptotic free rotor states (Eq. (4.25)). The result is given by

$$\phi_{rot}(\rho') = B^{Q}_{\gamma;JM}. \tag{4.29}$$

In this limit, the effective rotational wave function for the transition to a particular final rotational state (j_A,j_B,(j_{AB}),l) is given by the expansion coefficient of the Q state rotational wave function for that state (Eq.(4.29)). Since for the Q state, these coefficients are constants independent of ρ, the transition matrix elements can be rewritten

$$H'_{D\leftarrow Q} = B^{Q}_{\gamma;JM} \int \left[\phi_{vib}(\rho') \, \phi_{rel}(\rho') \right] d\rho', \tag{4.30}$$

where the integral on the right is the vibrational transition matrix element which was evaluated in chapter 3 (c.f. Eqs. (3.30,3.31)).

As noted above, the Q state bending potential can be expressed in the form of Eq. (4.10). The potential consists of only two nonzero terms in the expansion, A_{000} and A_{110}. This is primarily the result of the quadratic form in the cartesian coordinates of the harmonic potential. Table 4.2 shows that the coefficient A_{000} consists of quadratic terms in q^A, q^B, and ρ, and A_{110} contains a coupling term proportional to $q^A q^B$. From the properties of the 3-j, 6-j, and 9-j coefficients,[86,87] the potential coupling matrix elements (c.f. Eq. (4.26)) reduce to

$$V_{\gamma',\gamma} = \sum_{\lambda_1=0}^{1} (4\pi)^{-3/2} (-1)^{j_A+j_B-\Lambda_A-\Lambda_B} A_{\lambda_1\lambda_1 0} ([\lambda_1]^2[j_A'][j_B'][j_A][j_B][j_{AB}])^{1/2}$$
$$\begin{pmatrix} \lambda_1 & j_A & j_A' \\ 0 & -\Lambda_A & \Lambda_A \end{pmatrix} \begin{pmatrix} \lambda_1 & j_B & j_B' \\ 0 & -\Lambda_B & \Lambda_B \end{pmatrix} \begin{Bmatrix} j_{AB} & j_B & j_A \\ j_{AB} & j_B' & j_A' \\ 0 & \lambda_1 & \lambda_1 \end{Bmatrix}, \tag{4.31}$$

where there is no ρ-dependence in the Q state.

Because the potential consists only of these two terms, the potential coupling matrix and the expansion coefficients of the Q state bending-rotation wave function possess certain properties. It is seen that the $V_{\gamma',\gamma}$ is block diagonal in j_{AB} and l. This property enables the eigenvalue problem to be decomposed based on j_{AB} and l, reducing significantly the number of coupled equations that need to be considered at one time. Furthermore, $V_{\gamma,\gamma'}$ is seen to be independent of l and total J. This results in the following relation for the bending-rotation wave function expansion coefficients

$$B^{Q}_{j_A j_B(j_{AB})l;JM} = B^{Q}_{j_A j_B(j_{AB})l';J'M}. \tag{4.32}$$

The solution of the eigenvalue problem (i.e., the coupled equations of Eq. (4.12)) for the Q state bending potential results in a complete rovibrational spectrum for the given basis set expansion. We found the ground state energy to be well converged using $j_A^*=j_B^*=40$ as maximum values in the basis set expansion Eq. (4.21). However, larger basis set expansions are required to converge excited states. The eigenvectors can be labeled by the quantum numbers j_{AB} and l, which do not have a direct physical meaning for a bound state. However, a correspondence with the good quantum numbers, n_{trans}, n_{cis},

J, and k+Λ can be made by matching up the eigenvalue spectrum. For example, the ground state, which from eigenvalue analysis is the j_{AB}=1, l=0 state, must correspond to the ground rovibrational state of $C_2N_2(\tilde{C}\ ^1\Pi_u)$. The $B^Q_{\gamma,JM}$ for the ground bending state of $C_2N_2(\tilde{C}\ ^1\Pi_u)$ (n_{trans}=0, n_{cis}=0,l_{trans}=0, l_{cis}=0) are given in Table 4.4.

Recall that the state-to-state transition probability for a given D←Q transition is given by Eq. (3.1). Rovibrational distributions for the individual CN(X $^2\Sigma^+$) and CN(A $^2\Pi$) photofragments are obtained from the appropriate summations of the state-to-state transitions probabilities. We label the latter by $P^Q(n_X,j_X,n_A,j_A)$. Then the CN(X $^2\Sigma^+$) and CN(A $^2\Pi$) rovibrational distributions are obtained from

$$\begin{aligned} P^Q(n_X,j_X) &= \sum_{n_Aj_A} P^Q(n_X,j_X,n_A,j_A) \\ P^Q(n_A,j_A) &= \sum_{n_Xj_X} P^Q(n_X,j_X,n_A,j_A). \end{aligned} \tag{4.33}$$

Tables 4.5 through 4.12 and Figures 4.2 and 4.3 give the results for photon energies 164, 158.7, and 153.6 nm corresponding to experiments by Jackson.[49] We note here, that in the sudden limit and with the other approximations imposed in the present treatment, the vibrational distributions obtained in chapter 3 are unchanged from inclusion of the bending modes and rotations. In general, as discussed above in section II.B.1, there will be indirect coupling of rotational and vibrational motion which could significantly alter the PVD's obtained in a 1-D treatment.

The experimental data reported do not give the actual rovibrational distributions, but rather rotational temperatures for each vibrational level of the CN($X\ ^2\Sigma^+$) and CN($A\ ^2\Pi$) fragments. However, we can fit our calculated rotational distributions to a Boltzmann distribution. Plotting -ln(P(n,j)/(2j+1)) versus Bj(j+1)/k, one can obtain a least-squares fit to a linear curve with slope 1/T. Here k is Boltzmann's constant and B is the rotational constant of the diatom fragment. Additional comparisons can be made with results from a simple statistical model based on the final density of states. The final density of states is approximately proportional to the square root of the translational energy times a degeneracy factor,[21]

$$P(n_X,j_X,n_A,ja) \sim (2j_X + 1)\,(2j_A + 1)\,(\epsilon_{avl} - \epsilon_{vib} - \epsilon_{rot})^{1/2}. \qquad (4.34)$$

Note that this simple model does not take into account any angular momentum coupling considerations and only considers energy constraints.

1. CN($X\ ^2\Sigma^+$) PRVD's

Tables 4.5 through 4.7 give the calculated rovibrational distributions for the CN($X\ ^2\Sigma^+$) fragment at energies corresponding to the three experimental photon energies. The distributions were obtained assuming the initially prepared state of $C_2N_2(\tilde{C}\ ^1\Pi_u)$ is the ground bending vibrational state and with zero, one, and two quanta in the symmetric CN stretches for the three experimental energies (as discussed in chapter 3). As discussed above, the distributions are independent of J and l. Since the ground bending vibrational state is j_{AB}=1, any initial rotational angular momentum of the molecule ends

up as relative angular momentum of the fragments. Figure 4.2 and Table 4.8 compare the calculated rotational temperatures with those obtained from experiment and the crude statistical model. The statistical model distributions follow physically reasonable trends. One would expect that the more energy there is available to be released into rotational motion, the higher the rotational temperature, because higher rotational states become accessible. If the fragments are vibrationally excited, less energy is available for rotation. The statistical distributions are broader, peaked at higher j values, and rotationally hotter for the lower vibrational levels.

The experimental data for the CN(X $^2\Sigma^+$) fragment generally follows the trends described above; however, the rotational temperatures are much lower than those of the statistical model. Temperatures fitted to the distributions obtained from the adiabatic sudden limit are much lower than those of either the statistical model or experiment. At all three photon energies, the rotational distributions for each vibrational level ν=0,1,2 are nearly identical. There is actually a slight increase in rotational temperature for higher vibrational levels at 164 and 158.7 nm. However, this is apparently due to the reduction of the number of accessible rotational levels for higher vibrational levels. For example, at 164 nm, the ν=0 vibrational level energetically can reach j=43, ν=1 up to j=36, and ν=2 up to j=27. The distributions are quite similar up to the maximum j value where there is an abrupt drop to zero probability when there is no longer enough available energy. When fitted to a

Boltzmann distribution, this results in higher rotational temperatures.

The calculated distributions are also much narrower than those from the statistical model. However, this can be explained from angular momentum coupling constraints. Angular momentum coupling require that $|j_A - j_B| < j_{AB} < j_A + j_B$. As noted above, the quantum numbers j_{AB} and l label the Q state wave functions as a result of the quadratic bending potential, but the expansion coefficients, $B^{Q}_{\gamma,JM}$, are independent of total J and l. The lowest energy ground bending vibrational state corresponds to $j_{AB} = 1$. For example, if j_A=60, then j_B is restricted to lie between 59 and 61. However, this state may not be energetically possible. The effect of angular momentum coupling combined with conservation of energy, restricts the the maximum rotational quantum numbers to be about half those of the unrestricted statistical model. The quadratic form of the bending potential may be too restrictive. There could be a large contribution from cubic or higher-order terms in the potential which would allow larger coupling values of j_{AB}. However, the existence of angular momentum coupling constraints is one factor which contributes to the experimental temperatures being lower than those of the statistical model.

2. CN(A $^2\Pi$) PRVD's

The CN(A $^2\Pi$) rovibrational distributions are given in Fig. 4.3 and Tables 4.9 through 4.11. Table 4.12 reports the corresponding rotational temperaures resulting from the calculated and statitical model distributions. Again, the statistical distributions show decreasing rotational temperatures with increas-

ing vibrational excitations. The CN(A $^2\Pi$) statistical temperatures are slightly hotter than the corresponding CN(X $^2\Sigma^+$) temperatures due to the smaller vibrational frequency and rotational constant, both of which allow for higher accessible rotational quantum numbers for the CN(A $^2\Pi$) fragments. There are no reported experimental rotational distributions or temperatures for the CN(A $^2\Pi$) state fragment.

Comparing the results obtained from the adiabatic sudden limit, we observe the distributions are similar to those of the CN(X $^2\Sigma^+$) fragment. This is not surprising -- the final asymptotic rotational states of each fragment differ slightly due to different rotational constants (bond lengths), and in the Q state the fragments are indistinguishible. Again, the rotational temperatures are fairly constant and much smaller than those of the statistical model. Only at the 164 nm photon energy does the cutoff effect due to energy constraints appear, resulting in a higher rotational temperature for ν=2 than those of the lower vibrational levels. We also observe that the CN(A $^2\Pi$) rotational temperatures are somewhat lower than the corresponding CN(X $^2\Sigma^+$) temperatures, unlike what is expected from the statistical analysis.

The PRVD's obtained in the adiabatic sudden limit described above do not adequately explain the limited experimental data. In this preliminary study, which only treats the limiting case $\alpha_r >> 1$ of the general adiabatic method presented, several approximations have been made. These include the neglect of the RT character of the quasidiscrete state, rotational-vibrational

coupling, and anharmonicity. In this limit, the final state interactions, that is the rotational-translational coupling of the fragments on the dissociative state PES, have also been completely neglected. These factors could be crucial for the correct description of the $C_2N_2(\tilde{C}\ ^1\Pi_u)$ predissociation to $CN(X\ ^2\Sigma^+)$ and $CN(A\ ^2\Pi)$ fragments, and their effects need to be investigated. However, this preliminary study does suggest that the effects of angular momentum coupling are important.

IV. Conclusions

In this chapter we have described an extension of the photodissociation theory of Kresin and Lester to obtain product rovibrational distributions. Indirect photodissociation is treated as a quantum transition between diabatic states. An adiabatic method is employed to describe the coupling between internal and relative motions of the dissociative state fragments. The treatment of the rotational-translational coupling is similar to that of the vibrational-translational coupling presented in chapter 3. A general form of the D state nuclear wave function describing the internal and relative motions is obtained from interpolating between two adiabatic limits.

The effective rotational wave function is expressed in terms of an asymptotic free rotator basis set in all regions. The rotational-translational coupling is explicitly treated within the ρ-dependence of the expansion coefficients. This choice of wave function satisfies the criteria of correlating to the asymptotic rovibrational states of the products. However, due to similarities with the

coupled-equation formalism in scattering theory, this approach will become cumbersome for high rovibrational energies and for larger systems.

Preliminary application to the indirect photodissociation of $C_2N_2(\tilde{C}\ ^1\Pi_u)$ were presented. PRVD's for the $CN(X\ ^2\Sigma^+)$ and $CN(A\ ^2\Pi)$ were obtained for the adiabatic sudden limit. The treatment neglects several possibly important aspects such as the Renner-Teller effect for linear molecules with nonzero electronic angular momentum, anharmonicities, and the rotational-vibrational coupling due to final state interactions. Further ab initio calculations are needed to obtain the information to treat adequately the photodissociation dynamics. These include (1) characterization of the RT effect for both the Q and D state PES's, (2) higher terms (cubic, quartic, etc.) for the Q and D state potentials to include anharmonicity, (3) D state bending-rotor potential to include rotational translational couplings (final state interactions).

Table 4.1 Transformation from Cartesian to Center of Mass Space-Fixed Internal Coordinates

$$N_3 \text{ —— } C_1 \text{ —— } C_2 \text{ —— } N_4$$

$$x_1 = \frac{m_N\, q^A \sin(\theta_A)\cos(\phi_A)}{m_N+m_C} - \frac{\rho \sin(\theta)\cos(\phi)}{2}$$

$$x_2 = \frac{m_N\, q^B \sin(\theta_B)\cos(\phi_B)}{m_N+m_C} + \frac{\rho \sin(\theta)\cos(\phi)}{2}$$

$$x_3 = -\frac{m_C\, q^A \sin(\theta_A)\cos(\phi_A)}{m_N+m_C} - \frac{\rho \sin(\theta)\cos(\phi)}{2}$$

$$x_4 = -\frac{m_C\, q^B \sin(\theta_B)\cos(\phi_B)}{m_N+m_C} + \frac{\rho \sin(\theta)\cos(\phi)}{2}$$

$$y_1 = \frac{m_N\, q^A \sin(\theta_A)\sin(\phi_A)}{m_N+m_C} - \frac{\rho \sin(\theta)\sin(\phi)}{2}$$

$$y_2 = \frac{m_N\, q^B \sin(\theta_B)\sin(\phi_B)}{m_N+m_C} + \frac{\rho \sin(\theta)\sin(\phi)}{2}$$

$$y_3 = -\frac{m_C\, q^A \sin(\theta_A)\sin(\phi_A)}{m_N+m_C} - \frac{\rho \sin(\theta)\sin(\phi)}{2}$$

$$y_4 = -\frac{m_C\, q^B \sin(\theta_B)\sin(\phi_B)}{m_N+m_C} + \frac{\rho \sin(\theta)\sin(\phi)}{2}$$

$$z_1 = \frac{m_N\, q^A \cos(\theta_A)}{m_N+m_C} - \frac{\rho \cos(\theta)}{2}$$

$$z_2 = -\frac{m_N\, q^B \cos(\theta_B)}{m_N+m_C} + \frac{\rho \cos(\theta)}{2}$$

$$z_3 = -\frac{m_C\, q^A \cos(\theta_A)}{m_N+m_C} - \frac{\rho \cos(\theta)}{2}$$

$$z_4 = \frac{m_C\, q^B \cos(\theta_B)}{m_N+m_C} + \frac{\rho \cos(\theta)}{2}$$

Table 4.2 Coefficients for Bending Potential in Expansion of Space Fixed Spherical Harmonics

$$V_{bend} = \frac{1}{2} \sum_{ij} f_{ij} \, (\Delta x_i \, \Delta x_j + \Delta y_i \, \Delta y_j)$$

$$= \sum_{\lambda_1 \lambda_2 \lambda} \sum_{\mu_1 \mu_2 \mu} A_{\lambda_1 \lambda_2 \lambda} \, <\lambda_1 \mu_1 \lambda_2 \mu_2 \mid \lambda \mu> \, Y_{\lambda_1 \mu_1}(\theta_A, \phi_A) \, Y_{\lambda_2 \mu_2}(\theta_B, \phi_B) \, Y^*_{\lambda \mu}(\theta, \phi)$$

$$A_{000} = \frac{8\pi^{3/2}}{3} \left[\frac{(f_{44} \, m_C^2 - 2 \, f_{24} \, m_C \, m_N + f_{22} \, m_N^2)}{(m_C + m_N)^2} \, q^{B^2} \right.$$

$$+ \frac{(f_{33} \, m_C^2 - 2 \, f_{13} \, m_C \, m_N + f_{11} \, m_N^{2)}}{(m_C + m_N)^2} \, q^{A^2}$$

$$\left. + \, (f_{44} - 2 \, f_{34} + f_{33} + 2 \, f_{24} - 2 \, f_{23} + f_{22} - f_{14} + 2 \, f_{13} - 2 \, f_{12} + f_{11}) \, \frac{\rho^2}{4} \right]$$

$$A_{110} = \frac{32 \, \pi^{3/2}}{3 \sqrt{3}} \left[\frac{f_{34} \, m_C^2 - (f_{23} + f_{14}) \, m_C \, m_N + f_{12} \, m_N^2}{(m_C + m_N)^2} \right] q^A \, q^B$$

Table 4.3 $C_2N_2(\tilde{C}\ ^1\Pi_u)$ Bending Potenial Parameters

$$N_3 \text{ —— } C_1 \text{ —— } C_2 \text{ —— } N_4$$

Center of mass Space-Fixed Cartesian Coordinates

$$V_{bend} = \frac{1}{2} \sum_{ij} f_{ij} \, (\Delta x_i \, \Delta x_j + \Delta y_i \, \Delta y_j)$$

$$f_{11} = f_{22} = 0.10152 \text{ hartree/bohr}^2$$
$$f_{12} = -0.09975 \text{ hartree/bohr}^2$$
$$f_{13} = f_{24} = -0.03543 \text{ hartree/bohr}^2$$
$$f_{14} = f_{23} = 0.03366 \text{ hartree/bohr}^2$$
$$f_{33} = f_{44} = 0.01277 \text{ hartree/bohr}^2$$
$$f_{24} = -0.01100 \text{ hartree/bohr}^2$$

Space-Fixed Internal Coordinates

$$V_{bend} = \sum_{\lambda_1\lambda_2\lambda} \sum_{\mu_1\mu_2\mu} A_{\lambda_1\lambda_2\lambda} \, <\lambda_1\mu_1\lambda_2\mu_2 \mid \lambda\mu> \, Y_{\lambda_1\,\mu_1}(\theta_A,\phi_A) \, Y_{\lambda_2\,\mu_2}(\theta_B,\phi_B) \, Y^*_{\lambda\,\mu}(\theta,\phi)$$

$$A_{000} = 24.525 \text{ hartree}$$
$$A_{110} = 9.216 \text{ hartree}$$

Table 4.4 $B^{Q}_{j_A j_B(j_{AB})l;J}$ for $C_2N_2(\tilde{C}\ ^1\Pi_u, n_{trans}=0, n_{cis}=0; j_{AB}=1, l, J)$

j_A	j_B	$B^{Q}_{j_A j_B(j_{AB})l;J}$	j_A	j_B	$B^{Q}_{j_A j_B(j_{AB})l;J}$	j_A	j_B	$B^{Q}_{j_A j_B(j_{AB})l;J}$
0	1	-0.95723396E-01	17	17	0.98288831E-01	33	34	0.19767750E-02
1	1	0.11669714E+00	17	18	0.66666400E-01	34	33	-0.19187701E-02
1	2	0.11562788E+00	18	17	-0.63047924E-01	34	34	-0.23741683E-02
2	1	-0.66756344E-01	18	18	-0.85627025E-01	34	35	-0.14607391E-02
2	2	-0.14790400E+00	18	19	-0.57689015E-01	35	34	0.14190546E-02
2	3	-0.13047537E+00	19	18	0.54717463E-01	35	35	0.17467715E-02
3	2	0.92257029E-01	19	19	0.73806452E-01	35	36	0.10692260E-02
3	3	0.17023042E+00	19	20	0.49402482E-01	36	35	-0.10395283E-02
3	4	0.14124663E+00	20	19	-0.46981067E-01	36	36	-0.12730303E-02
4	3	-0.10940446E+00	20	20	-0.62953490E-01	36	37	-0.77528160E-03
4	4	-0.18603764E+00	20	21	-0.41872228E-01	37	36	0.75430672E-03
4	5	-0.14844367E+00	21	20	0.39914628E-01	37	37	0.91903418E-03
5	4	0.12119722E+00	21	21	0.53142680E-01	37	38	0.55686989E-03
5	5	0.19641100E+00	21	22	0.35129395E-01	38	37	-0.54218411E-03
5	6	0.15241464E+00	22	21	-0.33559392E-01	38	38	-0.65724360E-03
6	5	-0.12880555E+00	22	22	-0.44403170E-01	38	39	-0.39624424E-03
6	6	-0.20203653E+00	22	23	-0.29175778E-01	39	38	0.38605109E-03
6	7	-0.15346641E+00	23	22	0.27926803E-01	39	39	0.46562270E-03
7	6	0.13289580E+00	23	23	0.36726043E-01	39	40	0.27931709E-03
7	7	0.20346613E+00	23	24	0.23989257E-01	40	39	-0.27230362E-03
7	8	0.15190782E+00	24	23	-0.23003780E-01	40	40	-0.32678740E-03
8	7	-0.13395857E+00	24	24	-0.30071965E-01	40	41	-0.19505956E-03
8	8	-0.20121446E+00	24	25	-0.19529247E-01	41	40	0.19027578E-03
8	9	-0.14806406E+00	25	24	0.18758080E-01	41	41	0.22721123E-03
9	8	0.13241971E+00	25	25	0.24378696E-01	41	42	0.13495257E-03
9	9	0.19579450E+00	25	26	0.15741891E-01	42	41	-0.13171807E-03
9	10	0.14227805E+00	26	25	-0.15143433E-01	42	42	-0.15650833E-03
10	9	-0.12868151E+00	26	26	-0.19568157E-01	42	43	-0.92501485E-04
10	10	-0.18772572E+00	26	27	-0.12564822E-01	43	42	0.90333528E-04
10	11	-0.13490438E+00	27	26	0.12104275E-01	43	43	0.10680643E-03
11	10	0.12313572E+00	27	27	0.15552756E-01	43	44	0.62817160E-04
11	11	0.17752960E+00	27	28	0.99313243E-02	44	43	-0.61376734E-04
11	12	0.12630009E+00	28	27	-0.95798822E-02	44	44	-0.72213562E-04
12	11	-0.11616420E+00	28	28	-0.12240715E-01	44	45	-0.42264778E-04
12	12	-0.16571920E+00	28	29	-0.77737432E-02	45	44	0.41316065E-04
12	13	-0.11681438E+00	29	28	0.75078252E-02	45	45	0.48373776E-04
13	12	0.10813400E+00	29	29	0.95404906E-02	45	46	0.28174583E-04
13	13	0.15278646E+00	29	30	0.60262197E-02	46	45	-0.27555183E-04
13	14	0.10677831E+00	30	29	-0.58267187E-02	46	46	-0.32105506E-04
14	13	-0.99390246E-01	30	30	-0.73640927E-02	46	47	-0.18609004E-04
14	14	-0.13918987E+00	30	31	-0.46266748E-02	47	46	0.18208133E-04
14	15	-0.96495790E-01	31	30	0.44782784E-02	47	47	0.21112299E-04
15	14	0.90249019E-01	31	31	0.56295159E-02	47	48	0.12178204E-04
15	15	0.12534347E+00	31	32	0.35181878E-02	48	47	-0.11921026E-04
15	16	0.86236494E-01	32	31	-0.34087478E-02	48	48	-0.13755800E-04
16	15	-0.80991182E-01	32	32	-0.42622935E-02	48	49	-0.78966955E-05
16	16	-0.11160866E+00	32	33	-0.26497839E-02	49	48	0.77331442E-05
16	17	-0.76230673E-01	33	32	0.25697645E-02			
17	16	0.71857861E-01	33	33	0.31963322E-02			

Table 4.5. Calculated CN($X\ ^2\Sigma^+$) Rovibrational Distributions at 164 nm

j	ν_X=0	ν_X=1	ν_X=2
0	0.00006706	0.00006912	0.00007584
1	0.00078774	0.00081181	0.00089007
2	0.00294571	0.00303427	0.00332281
3	0.00723292	0.00744517	0.00813875
4	0.01392448	0.01431976	0.01561651
5	0.02285280	0.02347392	0.02552217
6	0.03343960	0.03429937	0.03715365
7	0.04479848	0.04587238	0.04946825
8	0.05588450	0.05711105	0.06126370
9	0.06566051	0.06694901	0.07137519
10	0.07324893	0.07449270	0.07885061
11	0.07804418	0.07913639	0.08307479
12	0.07977127	0.08062020	0.08382697
13	0.07848772	0.07902858	0.08127010
14	0.07453683	0.07473854	0.07588384
15	0.06846744	0.06833361	0.06836120
16	0.06093884	0.06050369	0.05949212
17	0.05262807	0.05194860	0.05005479
18	0.04415329	0.04329964	0.04073024
19	0.03602093	0.03506664	0.03204801
20	0.02859875	0.02761246	0.02436385
21	0.02211240	0.02115188	0.01786482
22	0.01665978	0.01576861	0.01259379
23	0.01223637	0.01144306	0.00848428
24	0.00876508	0.00808416	0.00539721
25	0.00612511	0.00555952	0.00315129
26	0.00417668	0.00372073	0.00152712
27	0.00277960	0.00242200	0.00019802
28	0.00180555	0.00153210	0.00000000
29	0.00114477	0.00094048	0.00000000
30	0.00070841	0.00055898	0.00000000
31	0.00042780	0.00032049	0.00000000
32	0.00025203	0.00017614	0.00000000
33	0.00014479	0.00009165	0.00000000
34	0.00008106	0.00004386	0.00000000
35	0.00004418	0.00001743	0.00000000
36	0.00002341	0.00000197	0.00000000
37	0.00001203	0.00000000	0.00000000
38	0.00000598	0.00000000	0.00000000
39	0.00000285	0.00000000	0.00000000
40	0.00000129	0.00000000	0.00000000
41	0.00000055	0.00000000	0.00000000
42	0.00000020	0.00000000	0.00000000
43	0.00000003	0.00000000	0.00000000
T(°K)	368.8	399.6	515.0

Table 4.6. Calculated CN(X $^2\Sigma^+$) Rovibrational Distributions at 158.7 nm

j	ν_X=0	ν_X=1	ν_X=2
0	0.00006592	0.00006681	0.00006856
1	0.00077455	0.00078484	0.00080527
2	0.00289719	0.00293504	0.00301019
3	0.00711673	0.00720734	0.00738744
4	0.01370843	0.01387690	0.01421216
5	0.02251399	0.02277814	0.02330469
6	0.03297180	0.03333645	0.03406484
7	0.04421604	0.04466994	0.04557898
8	0.05522199	0.05573813	0.05677527
9	0.06496827	0.06550735	0.06659536
10	0.07258559	0.07310188	0.07415011
11	0.07746785	0.07791605	0.07883398
12	0.07933119	0.07967297	0.08038313
13	0.07821783	0.07842682	0.07887483
14	0.07445227	0.07451676	0.07467699
15	0.06856426	0.06848746	0.06836377
16	0.06119650	0.06099453	0.06061670
17	0.05301396	0.05271233	0.05212933
18	0.04462817	0.04425753	0.04352926
19	0.03654432	0.03613624	0.03532524
20	0.02913343	0.02871690	0.02788133
21	0.02262760	0.02222656	0.02141516
22	0.01713280	0.01676487	0.01601418
23	0.01265294	0.01232917	0.01166288
24	0.00911856	0.00884405	0.00827396
25	0.00641508	0.00619009	0.00571821
26	0.00440722	0.00422851	0.00384962
27	0.00295760	0.00281976	0.00252396
28	0.00193922	0.00183583	0.00161086
29	0.00124256	0.00116702	0.00100005
30	0.00077818	0.00072437	0.00060321
31	0.00047639	0.00043898	0.00035287
32	0.00028511	0.00025969	0.00019963
33	0.00016681	0.00014993	0.00010870
34	0.00009541	0.00008444	0.00005648
35	0.00005335	0.00004636	0.00002750
36	0.00002916	0.00002479	0.00001195
37	0.00001557	0.00001290	0.00000338
38	0.00000813	0.00000651	0.00000000
39	0.00000414	0.00000318	0.00000000
40	0.00000206	0.00000150	0.00000000
41	0.00000100	0.00000067	0.00000000
42	0.00000047	0.00000028	0.00000000
43	0.00000022	0.00000011	0.00000000
44	0.00000010	0.00000003	0.00000000
45	0.00000004	0.00000000	0.00000000
46	0.00000002	0.00000000	0.00000000
T(°K)	372.3	368.2	405.5

Table 4.7. Calculated CN($X\ ^2\Sigma^+$) Rovibrational Distributions at 153.6 nm

j	ν_X=0	ν_X=1	ν_X=2
0	0.00006545	0.00006605	0.00006706
1	0.00076900	0.00077597	0.00078781
2	0.00287680	0.00290242	0.00294597
3	0.00706793	0.00712925	0.00723353
4	0.01361775	0.01373169	0.01392562
5	0.02237190	0.02255043	0.02285460
6	0.03277583	0.03302207	0.03344209
7	0.04397240	0.04427855	0.04480158
8	0.05494537	0.05529299	0.05588803
9	0.06467992	0.06504230	0.06566421
10	0.07231016	0.07265633	0.07325248
11	0.07722966	0.07752907	0.07804727
12	0.07915073	0.07937763	0.07977365
13	0.07810904	0.07824590	0.07848920
14	0.07442115	0.07446041	0.07453732
15	0.06860878	0.06855297	0.06846696
16	0.06130772	0.06116807	0.06093750
17	0.05317796	0.05297195	0.05262604
18	0.04482834	0.04457684	0.04415078
19	0.03676367	0.03648803	0.03601815
20	0.02935645	0.02907616	0.02859590
21	0.02284154	0.02257262	0.02210965
22	0.01732839	0.01708251	0.01665724
23	0.01282445	0.01260882	0.01223413
24	0.00926343	0.00908127	0.00876317
25	0.00653336	0.00638462	0.00612354
26	0.00450078	0.00438311	0.00417543
27	0.00302943	0.00293908	0.00277863
28	0.00199285	0.00192539	0.00180481
29	0.00128153	0.00123251	0.00114423
30	0.00080578	0.00077106	0.00070803
31	0.00049546	0.00047147	0.00042753
32	0.00029796	0.00028179	0.00025185
33	0.00017528	0.00016462	0.00014467
34	0.00010087	0.00009400	0.00008098
35	0.00005679	0.00005246	0.00004412
36	0.00003128	0.00002861	0.00002337
37	0.00001686	0.00001524	0.00001201
38	0.00000889	0.00000793	0.00000596
39	0.00000458	0.00000403	0.00000284
40	0.00000231	0.00000200	0.00000129
41	0.00000114	0.00000096	0.00000054
42	0.00000055	0.00000045	0.00000019
43	0.00000026	0.00000021	0.00000003
44	0.00000012	0.00000009	0.00000000
45	0.00000005	0.00000004	0.00000000
46	0.00000002	0.00000002	0.00000000
47	0.00000001	0.00000001	0.00000000
T(°K)	372.4	370.7	368.0

Table 4.8 Rotational Temperatures (°K) for CN(X $^2\Sigma^+$) Fragments

Energy	ν	Calc.	Stat.	Expt.[a]
164.0 nm	0	368	2191	1020±45
	1	400	1660	825±85
	2	515	974	
158.7 nm	0	372	2838	1710±65
	1	368	2229	1170±80
	2	405	1790	
153.6 nm	0	372	3247	1685±40
	1	370	2341	1110±85
	2	368	2176	

[a]Reference 49.

Table 4.9. Calculated CN(A $^2\Pi$) Rovibrational Distributions at 164 nm

j	ν_A=0	ν_A=1	ν_A=2
0	0.00000000	0.00000000	0.00000000
1	0.00053341	0.00054365	0.00057611
2	0.00256771	0.00261625	0.00277034
3	0.00679163	0.00691702	0.00731584
4	0.01348929	0.01373040	0.01449908
5	0.02249067	0.02287589	0.02410803
6	0.03320462	0.03374323	0.03547313
7	0.04472428	0.04540162	0.04758867
8	0.05598072	0.05675833	0.05928636
9	0.06591341	0.06673392	0.06942543
10	0.07362575	0.07442126	0.07706281
11	0.07849994	0.07920214	0.08157550
12	0.08025652	0.08080642	0.08271922
13	0.07895586	0.07931147	0.08062166
14	0.07494981	0.07509045	0.07572120
15	0.06879917	0.06872626	0.06866968
16	0.06117629	0.06091084	0.06022143
17	0.05277029	0.05234797	0.05112850
18	0.04420894	0.04367393	0.04205726
19	0.03600509	0.03540390	0.03353401
20	0.02852966	0.02790588	0.02592078
21	0.02200860	0.02139904	0.01941837
22	0.01653798	0.01597053	0.01408794
23	0.01211021	0.01160320	0.00988353
24	0.00864451	0.00820740	0.00668771
25	0.00601655	0.00565135	0.00434464
26	0.00408344	0.00378651	0.00268666
27	0.00270257	0.00246620	0.00155281
28	0.00174419	0.00155660	0.00079736
29	0.00109738	0.00095638	0.00026593
30	0.00067274	0.00057430	0.00000000
31	0.00040154	0.00033395	0.00000000
32	0.00023305	0.00018735	0.00000000
33	0.00013124	0.00010075	0.00000000
34	0.00007141	0.00005128	0.00000000
35	0.00003711	0.00002398	0.00000000
36	0.00001768	0.00000924	0.00000000
37	0.00000877	0.00000111	0.00000000
38	0.00000436	0.00000000	0.00000000
39	0.00000208	0.00000000	0.00000000
40	0.00000095	0.00000000	0.00000000
41	0.00000040	0.00000000	0.00000000
42	0.00000014	0.00000000	0.00000000
43	0.00000002	0.00000000	0.00000000
T(°K)	317.8	341.7	426.8

Table 4.10. Calculated CN(A $^2\Pi$) Rovibrational Distributions at 158.7nm

j	ν_A=0	ν_A=1	ν_A=2
0	0.00000000	0.00000000	0.00000000
1	0.00052479	0.00052633	0.00053623
2	0.00252688	0.00253414	0.00258105
3	0.00668622	0.00670494	0.00682603
4	0.01328685	0.01332272	0.01355534
5	0.02216769	0.02222476	0.02259597
6	0.03275389	0.03283324	0.03335144
7	0.04415882	0.04425791	0.04490827
8	0.05533354	0.05544628	0.05619099
9	0.06523329	0.06535086	0.06613396
10	0.07296998	0.07308215	0.07383783
11	0.07792572	0.07802242	0.07868488
12	0.07981277	0.07988556	0.08039845
13	0.07867681	0.07871999	0.07904376
14	0.07485144	0.07486265	0.07497864
15	0.06887882	0.06885901	0.06877003
16	0.06141493	0.06136792	0.06109560
17	0.05313684	0.05306850	0.05264838
18	0.04466555	0.04458279	0.04405831
19	0.03651233	0.03642220	0.03583867
20	0.02905104	0.02895991	0.02835938
21	0.02251366	0.02242673	0.02184435
22	0.01700403	0.01692504	0.01638709
23	0.01252269	0.01245387	0.01197729
24	0.00899634	0.00893864	0.00853175
25	0.00630678	0.00626007	0.00592413
26	0.00431563	0.00427905	0.00401011
27	0.00288317	0.00285541	0.00264618
28	0.00188083	0.00186041	0.00170194
29	0.00119816	0.00118360	0.00106656
30	0.00074541	0.00073529	0.00065088
31	0.00045285	0.00044603	0.00038647
32	0.00026860	0.00026416	0.00022300
33	0.00015548	0.00015270	0.00012480
34	0.00008778	0.00008612	0.00006753
35	0.00004828	0.00004735	0.00003514
36	0.00002581	0.00002536	0.00001742
37	0.00001328	0.00001321	0.00000806
38	0.00000662	0.00000666	0.00000327
39	0.00000334	0.00000326	0.00000081
40	0.00000164	0.00000156	0.00000000
41	0.00000078	0.00000071	0.00000000
42	0.00000036	0.00000031	0.00000000
43	0.00000016	0.00000013	0.00000000
44	0.00000006	0.00000004	0.00000000
45	0.00000002	0.00000001	0.00000000
46	0.00000001	0.00000000	0.00000000
T(°K)	321.7	329.0	342.3

Table 4.11. Calculated CN(A $^2\Pi$) Rovibrational Distributions at 153.6 nm

j	ν_A=0	ν_A=1	ν_A=2
0	0.00000000	0.00000000	0.00000000
1	0.00051872	0.00052026	0.00052652
2	0.00249810	0.00250539	0.00253503
3	0.00661193	0.00663074	0.00670723
4	0.01314425	0.01318031	0.01332711
5	0.02194032	0.02199774	0.02223174
6	0.03243685	0.03251677	0.03284294
7	0.04376148	0.04386143	0.04427002
8	0.05487938	0.05499331	0.05546005
9	0.06475681	0.06487591	0.06536521
10	0.07251161	0.07262563	0.07309582
11	0.07752570	0.07762450	0.07803418
12	0.07950533	0.07958037	0.07989438
13	0.07848574	0.07853119	0.07872518
14	0.07478761	0.07480094	0.07486392
15	0.06893991	0.06892193	0.06885649
16	0.06158715	0.06154156	0.06136209
17	0.05339798	0.05333055	0.05306006
18	0.04498875	0.04490636	0.04457261
19	0.03686981	0.03677950	0.03641114
20	0.02941714	0.02932535	0.02894876
21	0.02286713	0.02277911	0.02241611
22	0.01732914	0.01724873	0.01691540
23	0.01280947	0.01273902	0.01244550
24	0.00924008	0.00918064	0.00893164
25	0.00650707	0.00645860	0.00625442
26	0.00447517	0.00443689	0.00427465
27	0.00300661	0.00297727	0.00285209
28	0.00197378	0.00195192	0.00185799
29	0.00126638	0.00125053	0.00118189
30	0.00079424	0.00078305	0.00073413
31	0.00048699	0.00047928	0.00044526
32	0.00029195	0.00028677	0.00026366
33	0.00017114	0.00016774	0.00015239
34	0.00009810	0.00009592	0.00008593
35	0.00005498	0.00005362	0.00004726
36	0.00003013	0.00002929	0.00002532
37	0.00001614	0.00001564	0.00001320
38	0.00000845	0.00000816	0.00000669
39	0.00000432	0.00000416	0.00000328
40	0.00000216	0.00000207	0.00000156
41	0.00000105	0.00000100	0.00000071
42	0.00000050	0.00000047	0.00000030
43	0.00000023	0.00000022	0.00000012
44	0.00000010	0.00000010	0.00000003
45	0.00000005	0.00000004	0.00000000
46	0.00000002	0.00000002	0.00000000
T(°K)	334.5	329.8	327.7

Table 4.12 Rotational Temperatures (°K) for CN(A $^2\Pi$) Fragments

Energy	ν	Calc.	Stat.
164.0 nm	0	318	2269
	1	341	1769
	2	427	1263
158.7 nm	0	322	2770
	1	329	2441
	2	342	1783
153.6 nm	0	332	3920
	1	330	2852
	2	327	2458

Figure Captions

Fig. 4.1 SF and BF Coordinates for Two Diatoms

Fig. 4.2 Rovibrational Distributions for CN($X\ ^2\Sigma^+$) at 164, 158.7, 153.6 nm
a - calculated distributions for ν=0–2,
b - statistical distributions for ν=0,
c - statistical distributions for ν=1,
d - statistical distributions for ν=2

Fig. 4.3 Rovibrational Distributions for CN($A\ ^2\Pi$) at 164, 158.7, 153.6 nm
a-d - same as Fig 4.2.

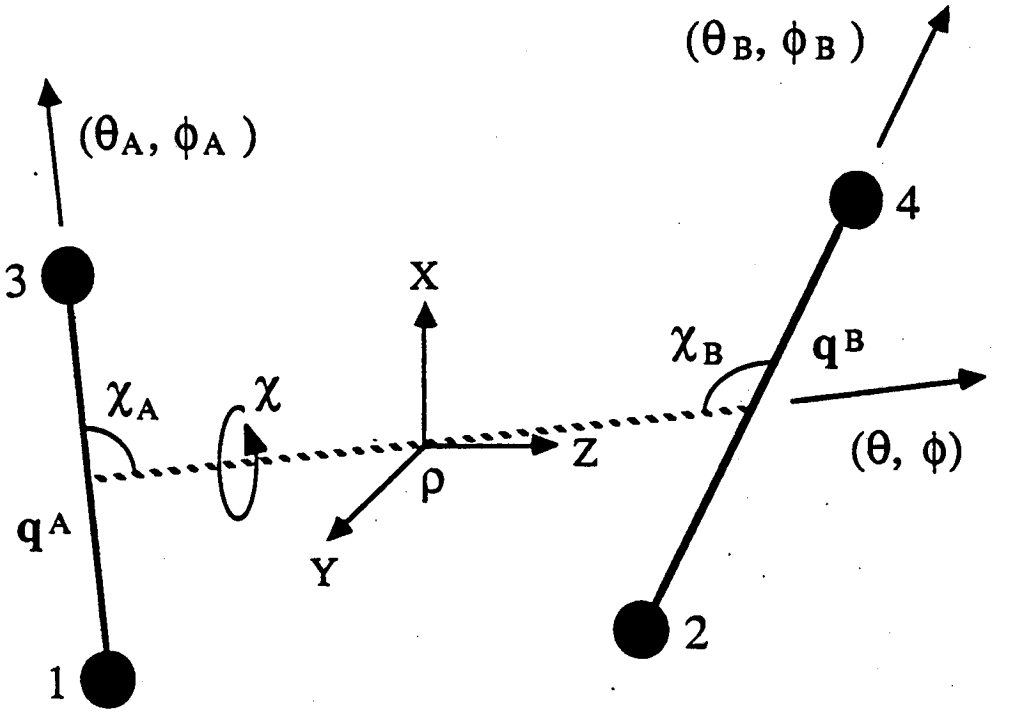

$$\cos\chi_A = \mathbf{q}^A \cdot \rho$$

$$\cos\chi_B = \mathbf{q}^B \cdot \rho$$

$$\cos\chi = \mathbf{q}^A \cdot \mathbf{q}^B$$

(SF angles in parentheses)

Figure 4.1

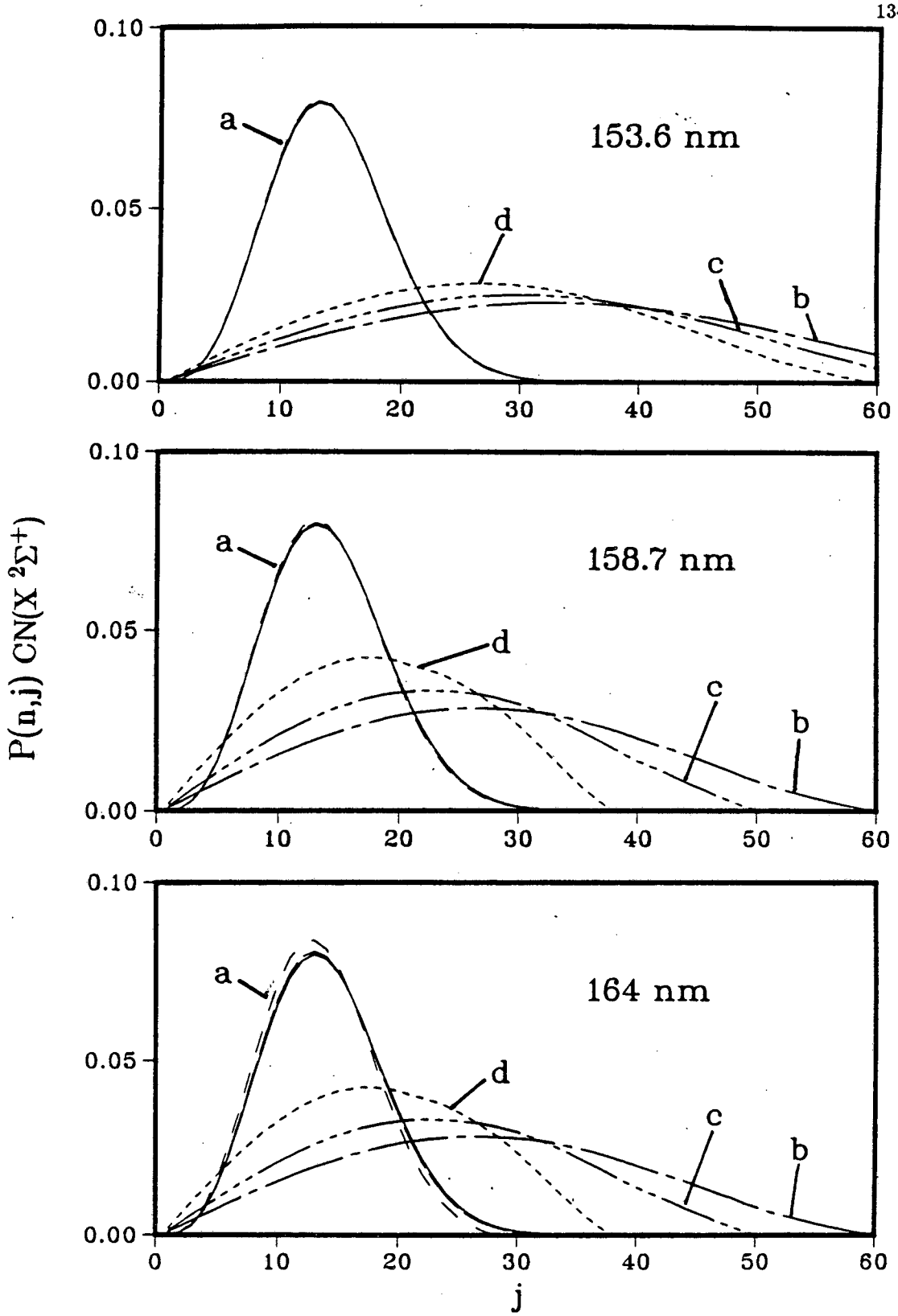
0.10
0.05
0.00
153.6 nm
158.7 nm
164 nm
a
b
c
d
0
10
20
30
40
50
60
P(n,j) CN(X $^2\Sigma^+$)
j

Figure 4.2

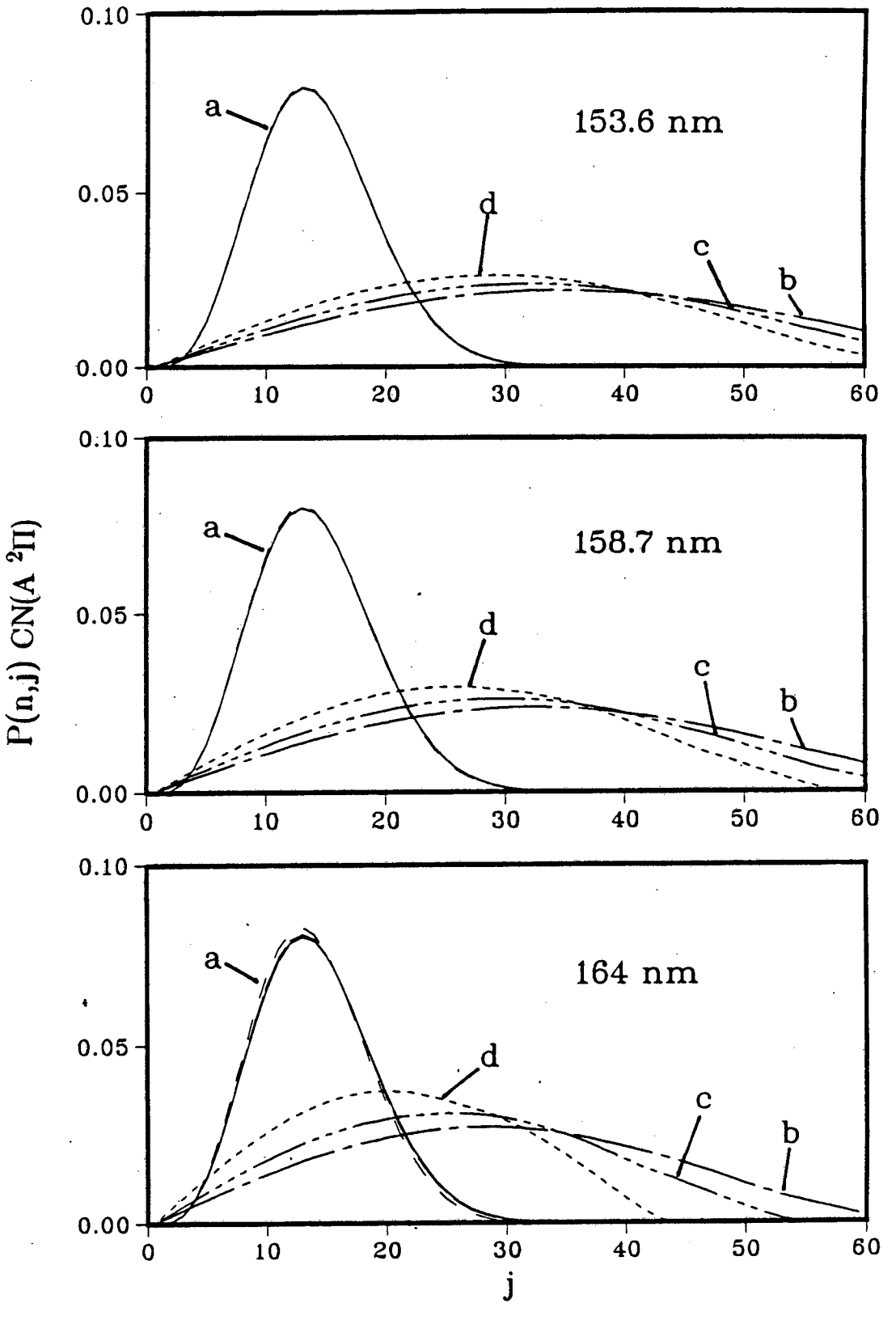
0.10
0.05
0.00
a
153.6 nm
d
c
b
0
10
20
30
40
50
60
158.7 nm
164 nm
P(n,j) CN(A $^2\Pi$)
j

Figure 4.3

Appendix A

General Expression For The Transition Probability

One can write the total Hamiltonian[83]

$$\hat{H} = \hat{H}_o + \hat{V}(t) \,. \tag{A1}$$

The wave function can be expressed in terms of the eigenfuctions, ψ_n, and eigenvalues, E_n, of $\hat{H}_o$

$$\Psi = \sum_n a_n(t)\, \psi_n\, e^{-iE_n t/\hbar} \,. \tag{A2}$$

If the system is initially in a stationary state with energy E_m, the probability of being in a stationary state with energy E_n after the interaction is given by the absolute square of the coefficients $a_{nm}(t)$

$$\omega_{nm}(t) = \left| a_{nm}(t) \right|^2 . \tag{A3}$$

The solution of a_{nm} is an infinite series which can be expressed in terms of transition matrix, $<n \mid \hat{T} \mid m>$, where

$$\begin{aligned} <n \mid \hat{T} \mid m> = <n \mid \hat{V} \mid m> + \sum_f \frac{<n \mid \hat{V} \mid f><f \mid \hat{V} \mid m>}{E_m - E_f + i\eta} \\ + \sum_{f,f'} \frac{<n \mid \hat{V} \mid f><f \mid \hat{V} \mid f'><f' \mid \hat{V} \mid m>}{(E_m - E_f + i\eta)\,(E_m - E_{f'} + i\eta)} + \cdots \,. \end{aligned} \tag{A4}$$

If $\hat{V}(t) = \hat{V}$, then transitions can only occur between states of equal energy. The general expression for the transition probability per unit time from initial state $\mid m>$ to a final state $\mid n>$ can be expressed as

$$W_{nm} = \frac{2\pi}{\hbar}\delta(E_n - E_m) \left| <n \mid \hat{T} \mid m> \right|^2 . \qquad (A5)$$

In first-order $\hat{T} = \hat{V}$ resulting in the well-known golden rule expression of Eq. (3.1). The higher order terms correspond to transitions to virtual electronic states. From Eq. (A4) one can see that these higher-order terms contain products of Franck-Condon factors resulting in additional orders of smallness and serve as a check of the applicability of Eq. (3.1). Based on Eq. (A4) one can calculate higher-order terms to obtain a desired accuracy. We note here that our approach differs from those based on scattering theory[79,81] which lead only to a single Franck-Condon factor.

Appendix B

Wave Functions in the Adiabatic Limits

In this appendix we report the solutions for the nuclear Schrödinger equation in the two adiabatic limits following a similar analysis presented earlier.[28,44]

Case (i): Fast Translational Motion, $\alpha_v \equiv \frac{\epsilon_{rel}}{\epsilon_{vib}} >> 1$

In this limit we can use the clamped translational function approximation[44] and obtain for the D state nuclear wave function the product function,

$$\tilde{\phi}_D(\rho, q^A, q^B) = \phi_{rel}(\rho, q_o^{A'}, q_o^{B'})\, \phi_{int}(q^A, q^B). \tag{B1}$$

The wave function describing relative motion, ϕ_{rel}, is the solution of

$$\left[-\frac{1}{2\mu}\frac{\partial^2}{\partial\rho^2} + U(\rho, q_o^{A'}, q_o^{B'})\right] \phi_{rel}(\rho, q_o^{A'}, q_o^{B'}) = E(q_o^{A'}, q_o^{B'})\, \phi_{rel}(\rho, q_o^{A'}, q_o^{B'}). \tag{B2}$$

In the harmonic approximation, ϕ_{int} is given by

$$\phi_{int}(q_A, q^B) = \phi_{n_A}^A(Q_A(\tau_A^i, \tau_B^i))\, \phi_{n_B}^B(Q_B(\tau_A^i, \tau_B^i)), \tag{B3}$$

where

$$\phi_{n_Z}^{Z}(Q_Z(\tau_A^i, \tau_B^i)) = \left(\frac{\omega_Z^i}{\pi\,\hbar}\right)^{1/4} \frac{1}{\sqrt{2^{n_Z}\, n_Z!}} \exp\left(-\frac{\omega_Z^i\, Q_Z^2(\tau_A^i, \tau_B^i)}{2\,\hbar}\right) \cdot H_Z\left(Q_Z(\tau_A^i, \tau_B^i)\sqrt{\frac{\omega_Z^i}{\hbar}}\right). \tag{B4}$$

Here, Q_z are normal coordinates, which in this limit are the asymptotic bond stretches of the product fragments. The ω_Z^i are vibrational frequencies, $Z \equiv \{A,B\}$ refers to product fragments, and τ_Z^i are given by

$$\tau_Z^i = q^Z - q_o^{Z'}. \tag{B5}$$

It can be shown[44] that in this limit the vibrational frequencies and equilibrium bond lengths are constants and can be well approximated by their asymptotic noninteracting-fragment values, ω_{asy} and q_{asy}.

Case (ii): Slow Translational Motion, $\alpha_v \ll 1$

In this limit the wave function is also separable into two functions of the form

$$\tilde{\phi}_D(\rho, q^A, q^B) = \phi_{rel}(\rho)\, \phi_{int}(q^A, q^B; \rho). \tag{B6}$$

Here the wave function describing the internal motion depends parametrically on the interfragment separation ρ and can be written

$$\phi_{int}(q^A, q^B; \rho) = \phi_{n_A}^{A}(Q_A(\tau_A^{ii}(\rho), \tau_B^{ii}(\rho); \rho))\, \phi_{n_B}^{B}(Q_B(\tau_A^{ii}(\rho), \tau_B^{ii}(\rho); \rho)). \tag{B7}$$

Again in the harmonic approximation,

$$\phi_{n_Z}^{Z}(Q_Z(\tau_A^{ii}(\rho),\, \tau_B^{ii}(\rho);\, \rho)) = \left(\frac{\omega_Z^{ii}(\rho)}{\pi\,\hbar}\right)^{1/4} \frac{1}{\sqrt{2^{n_Z}\, n_Z!}}$$

$$\cdot \exp\left(-\frac{\omega_Z^{ii}(\rho)\, Q_Z^2(\tau_A^{ii}(\rho),\, \tau_B^{ii}(\rho);\, \rho)}{2\,\hbar}\right) H_Z\left(Q_Z(\tau_A^{ii}(\rho),\, \tau_B^{ii}(\rho);\, \rho)\, \sqrt{\frac{\omega_Z^{ii}(\rho)}{\hbar}}\right). \tag{B8}$$

As above, Q_Z are normal coordinates, which asymptotically become the individual bond stretches of each product fragment (see Section III). The $\omega_Z^{ii}(\rho)$ are vibrational frequencies of the fragments, and $\tau_Z^{ii}(\rho)$ are given by

$$\tau_Z^{ii}(\rho) = q^Z - q_o^{Z^u}(\rho). \tag{B9}$$

The wave function ϕ_{rel} is obtained by solving

$$\left[-\frac{1}{2\,\mu}\,\frac{\partial^2}{\partial\rho^2} + U_{eff}(\rho)\right]\phi_{rel}(\rho) = E\,\phi_{rel}(\rho), \tag{B10}$$

where the effective potential U_{eff} is

$$\begin{aligned} U_{eff}(\rho) = U(\rho,\, q_o^{A^u}(\rho),\, q_o^{B^u}(\rho)) + (n_A + 1/2)\,\hbar\,\omega_A^{ii}(\rho) \\ + (n + 1/2)\,\hbar\,\omega_B^{ii}(\rho). \end{aligned} \tag{B11}$$

One notes that in this limit, the vibrational frequencies and equilibrium bond lengths are functions of ρ and differ quite significantly from their asymptotic values (see Figure 3.2).

Intermediate Cases , $\alpha_v \approx 1$

The general form of $\tilde{\phi}_D$ for arbitrary α_v given by Eqs. (3.14,3.17-3.22) results from comparison of the solutions for the two limiting cases given above.

In both limits the total nuclear wave function is expressed as a product of two functions (see Eqs. (B1) and (B6)). Moreover, the structure of the corresponding functions for each case is very similar (cf. (B3) and (B7), (B4) and (B8), (B2) and (B10), (B5) and (B9)). One notes that the limiting cases differ only in the explicit form of the vibrational frequencies and equilibrium bond lengths. For $\alpha_v >> 1$, the frequencies and bond lengths are functions of ρ (see (B8) and (B9)); whereas, the case $\alpha_v << 1$ is characterized by constant values of these quantities. Therefore, it appears reasonable to conclude that a continuous change occurs from the limit $\alpha_v << 1$ to the opposite case, accompanied by a change in the ρ-dependence of the vibrational frequencies and equilibrium bond lengths. This transition is describable by the interpolation expression of Eq. (3.22).

Appendix C

Optimization On The Minimum Energy Path

We seek the minimum energy molecular geometry for a fixed interfragment distance ρ. Employing the method of Lagrange multipliers, we introduce the function $G \equiv U + \lambda\rho$ for which we want to satisfy

$$dG = dU + \lambda d\rho = 0, \tag{C1}$$

where U is the electronic potential depending on the nuclear positions and λ is a constant. For a linear tetra-atomic, choosing the molecular axis to be along the Z axis,

$$\rho = \frac{m_3Z_3 + m_4Z_4}{m_3 + m_4} - \frac{m_1Z_1 + m_2Z_2}{m_1 + m_2}. \tag{C2}$$

Here Z_i is the Z-coordinate of the ith atom. For C_2N_2, $m_1{=}m_4{\equiv}m_N$, and $m_2{=}m_3{\equiv}m_C$. Substituting (C2) in (C1) results in the following condition for the gradients of the atoms on the minimum energy path

$$\frac{\partial U}{\partial Z_1} : \frac{\partial U}{\partial Z_2} : \frac{\partial U}{\partial Z_3} : \frac{\partial U}{\partial Z_4} = m_N : m_C : -m_C : -m_N. \tag{C3}$$

Geometries and force constants (i.e., second derivatives of the energy with respect to nuclear coordinate) along the reaction path were calculated using the minimum basis MC10 wave function for the dissociative state (see Sec. III). Because these geometries are not stationary points of the potential energy

surface, the usual procedure of diagonalizing the force constant matrix to obtain 3N-5 (linear molecule) normal modes and frequencies is not valid. The variable ρ corresponds to unbounded relative motion of the photofragments. We can employ the reaction path Hamiltonian method of Miller, Handy, and Adams[13] to obtain the frequencies of the normal coordinates orthogonal to the reaction path. In this procedure one projects out the reaction path from the matrix of second derivatives of the energy w.r.t. nuclear coordinates to obtain the projected force constant matrix

$$K^P = (1-P)\cdot K\cdot(1-P), \tag{C4}$$

where K and P have dimensions 3N×3N and are given by

$$\begin{aligned} K_{i,j} &= \frac{\partial^2 U}{\partial Z_i \partial Z_j} \\ P_{i,j} &= \hat{L}_i \cdot \hat{L}_j. \end{aligned} \tag{C5}$$

Here $\hat{L}$ is a 3N-dimensional unit vector which defines the direction of the reaction path, and the subscripts i and j label nuclei. Diagonalization of K^P results in 3N-6 nonzero eigenvalues corresponding to the frequencies of the normal coordinates orthogonal to the reaction path. The 6 null eigenvalues correspond to the infinitesimal translations(3) and rotations(2) of an N-atom linear molecule, and motion along the reaction path. For C_2N_2 constrained to be linear, the gradients obey the simple relationship given by Eq. (C3); the unit vector $\hat{L}$ is constant for all values of ρ and is given by

$$\hat{L}_1 = \frac{m_N}{M} \hat{Z}_1$$
$$\hat{L}_2 = \frac{m_C}{M} \hat{Z}_2$$
$$\hat{L}_3 = -\frac{m_C}{M} \hat{Z}_3 \qquad \text{(C6)}$$
$$\hat{L}_4 = -\frac{m_N}{M} \hat{Z}_4$$

where $M = \sqrt{2(m_N^2 + m_C^2)}$.

Appendix D

The Effective Vibrational Wave Function

The transition matrix element, Eq. (3.30), can be rewritten

$$H_{D\leftarrow Q} = \int \left[\int \prod_{i=1}^{5} \phi_{n_i}(Q_i)\, d\tau_A\, d\tau_B \right] \phi_{rel}(\rho')\, d\rho'. \qquad (D1)$$

Here, i=$\{1,2,3\}$ refers to the symmetric CN, CC, and asymmetric CN stretching modes of the quasidiscrete state and i=$\{4,5\}$ refers to the dissociative state symmetric CN and asymmetric CN stretches which asymptotically correlate to CN(X $^2\Sigma^+$) and CN(A $^2\Pi$) localized bond stretches. The normal coordinates can also be expressed in terms of internal coordinates similar to Eqs. (3.26-3.29)

$$Q_i = a_i(\tau_A - \delta q_i^A) + b_i(\tau_B - \delta q_i^B) + c_i\rho' \qquad (D2)$$

The harmonic oscillator functions have the usual form

$$\phi_{n_i}(Q_i) = \left(\frac{\omega_i}{\pi\hbar}\right)^{1/4} \left[2^{n_i}\, n_i!\right]^{-1/2} \exp\left(\frac{\omega_i Q_i^2}{2\hbar}\right) H_{n_i}\left(Q_i\sqrt{\frac{\omega_i}{\hbar}}\right). \qquad (D3)$$

For the quasidiscrete state i=$\{1,2,3\}$ the transformation coefficients (a_i, b_i, c_i), vibrational frequencies (ω_i), and changes in equilibrium bond lengths ($\delta q_i = 0$) are constants. However, for the dissociative state i=$\{4,5\}$, they depend on both ρ and α_v as given by Eqs. (3.22,3.28,3.29).

The effective vibrational wave function is the term enclosed by brackets in Eq. (D1). Substituting Eqs. (D2) and (D3) in Eq. (D1) and employing the generating function for Hermite polynomials

$$H_{n_i}(x_i) = \left(\frac{\partial}{\partial t_i}\right)^{n_i} \exp\left(-t_i^2 + 2\, x_i\, t_i\right) \Big|_{t_i = 0}, \tag{D4}$$

one can integrate over the internal coordinates analytically resulting in the following expression

$$\phi_{vib}(\rho') = \left(\frac{\prod_{i=1}^{5}\omega_i}{\pi^5\hbar^5}\right)^{1/4} \left[2^{(n_1+n_2+n_3+n_4+n_5)} \cdot \prod_{i=1}^{5} n_i!\right]^{-1/2} \frac{\pi^2}{A\cdot B^1} \prod_{i=1}^{5}\left(\frac{\partial}{\partial t_i}\right)^{n_i} \tag{D5}$$

$$\cdot \exp\left[\frac{G^2}{4\,A} + \frac{H_1^2}{4\,B_1} + \frac{J_1^2}{4\,C_1} - K\right] \exp\left[-C_1\left(\rho' + \frac{J_1}{2C_1}\right)^2\right] \Big|_{\text{all } t_i\text{'s} = 0}$$

where

$$A = \sum_{i=1}^{5} \frac{a_i^2\,\omega_i}{2\,\hbar}$$

$$B = \sum_{i=1}^{5} \frac{b_i^2\,\omega_i}{2\,\hbar}$$

$$C = \sum_{i=1}^{5} \frac{c_i^2\,\omega_i}{2\,\hbar}$$

$$D = \sum_{i=1}^{5} \frac{a_i\,b_i\,\omega_i}{\hbar}$$

$$E = \sum_{i=1}^{5} \frac{a_i\,c_i\,\omega_i}{\hbar}$$

$$F = \sum_{i=1}^{5} \frac{b_i\, c_i\, \omega_i}{\hbar}$$

$$G = -\left[2 \sum_{i=1}^{5} a_i \sqrt{\frac{\omega_i}{\hbar}}\, t_i + \sum_{i=1}^{5} \frac{\omega_i}{\hbar} \left(a_i^2\, \delta q_i^A + a_i\, b_i\, \delta q_i^B \right) \right]$$

$$H = -\left[2 \sum_{i=1}^{5} b_i \sqrt{\frac{\omega_i}{\hbar}}\, t_i + \sum_{i=1}^{5} \frac{\omega_i}{\hbar} \left(a_i\, b_i\, \delta q_i^A + b_i^2\, \delta q_i^B \right) \right]$$

$$J = -\left[2 \sum_{i=1}^{5} c_i \sqrt{\frac{\omega_i}{\hbar}}\, t_i + \sum_{i=1}^{5} \frac{\omega_i}{\hbar} \left(a_i\, c_i\, \delta q_i^A + a_i\, b_i\, \delta q_i^B \right) \right]$$

$$K = \sum_{i=1}^{5} t_i^2 + \sum_{i=1}^{5} \frac{\omega_i}{2\hbar} \left(a_i^2\, \delta q_i^{A^2} + b_i^2\, \delta q_i^{B^2} \right)$$

$$+ 2 \sum_{i=1}^{5} \sqrt{\frac{\omega_i}{\hbar}} \left(a_i\, \delta q_i^A + b_i\, \delta q_i^B \right) t_i + \sum_{i=1}^{5} \frac{\omega_i}{\hbar} \left(a_i\, b_i\, \delta q_i^A\, \delta q_i^B \right)$$

$$B_1 = B - \frac{D^2}{4A}$$

$$H_1 = H - \frac{D\,G}{2A}$$

$$F_1 = F - \frac{D\,E}{2A}$$

$$C_1 = C - \frac{E^2}{4A} - \frac{F_1^2}{4B_1}$$

$$J_1 = J - \frac{G\,E}{2A} - \frac{F_1\,H_1}{2B_1}$$

Note that G, H_1, J_1, and K all are functions of the dummy variables t_i which arise from the generating function of Eq. (D4) of the Hermite polynomials. The effective vibrational wave function for a particular vibrational transition $(n_1, n_2, n_3) \rightarrow (n_4, n_5)$ can be obtained from differentiating Eq. (D5) w.r.t. t_i.

The resulting expression has the form of Eq. (3.32).

Appendix E

Computer Source Codes

This appendix contains the major portions of the source codes generated to obtain vibrational and rovibrational distributions reported in chapters 3 and 4. The potential energy surface data was obtained from ab initio MCHF calculations using the computer code HONDO (M. Dupuis, D. Sprangler, and J.J. Wendoloski, HONDO, NRCC Software Catalogue, Vol. 1, Program No. QG01 (1981)). Exponential spline fits of dissociative state potential energy surface parameters were obtained using the code SPLINE, written by Kurt Kaiser, Chemistry Division, Argonne National Laboratory. In FCINT, subroutine TDELAY is taken from program of that name given by reference 85. The matrix diagonalization routine GIVENS is that given by reference 97. Sample input and output follow the source code for each program.

```
0001        program fcint
0002   c
0003   c
0004   c       Program  FCINT  calculates franck-condon integrals within
0005   c       theory of polyatomic photodissociation developed by
0006   c       V.Z. Kresin and W.A. Lester, Jr.
0007   c       this program written explicitly for  collinear
0008   c       c2n2 (C) --> cn(x) + cn(a) to obtain vibrational distributions.
0009   c
0010   c   INPUT --
0011   c
0012   c       n1,n2,n3,npts,pstart,xstep,div  (4i8,3d20.8)
0013   c
0014   c               n1,n2,n3,- vibrational quantum no.s for Q state
0015   c               sym. CN, asym. CN, and CC stretches
0016   c
0017   c               npts -  number of points in TDELAY (points in numerov method for
0018   c               solving translational wave function
0019   c
0020   c               pstart -  where integration for TDELAY starts
0021   c
0022   c               step size is determined by larger of xstep or size of asymptotic
0023   c               spacing of nodes of trans. w.f divided by div
0024   c
0025   c               ipr,ntest,nflag (3i5)
0026   c
0027   c               ipr .gt. 1 debug printing
0028   c
0029   c               ntest -- nothing
0030   c
0031   c               nflag  refers to limiting cases
0032   c                       =0  general case
0033   c                       =1  alpha << 1  slow trans. motion
0034   c                       =2  alpha >> 1  fast  "      "
0035   c                       =4  alpha =  value of alpha asymptotically
0036   c
0037   c       etot,vinf,rmass   (3f15.8)
0038   c
0039   c               etot =  total energy
0040   c
0041   c               vinf  = value of potential asymptotically, such that
0042   c               etot - vinf  is the available energy to go
0043   c                       into vibration and translation.
0044   c
0045   c               rmass = reduced mass of system
0046   c
0047   c       qao,qbo,po,qaa,qba (5f15.8)
0048   c               a- ground state (X)   b-excited state (A)
0049   c
0050   c               qao,qbo  equilibrium CN bond lengths in Q state
0051   c
0052   c               po  = distance between center of masses of each CN in Q State
0053   c
0054   c               qaa,qba = asymptotic bond lengths of fragments
0055   c
0056   c       w,a,b,c (5f15.8)
0057   c
0058   c               1 - Q state sym. CN str.
0059   c               2 - Q state asym. CN. str.
0060   c               3 - Q state  CC str.
0061   c               4 - D state sym. CN str.  ->  CN(X) fragment
```

```
0062   c                5 - D state asym. CN str. ->  CN(A) fragment
0063   c
0064   c                input here refer to Q state and asymptotic values of D state
0065   c
0066   c                w -  vibrational frequencies
0067   c
0068   c                a,b,c, -  normal mode coeeficients  ,i.e.,
0069   c
0070   c                Q(i) = a(i)*ta(i) + b(i)*tb(i) + c(i)*p'(i)
0071   c
0072   c                where ta(i) = qa -qao(i), etc.
0073   c
0074   c       vo,aaax,gammax,nal,xal,naaa,daaa  (3d20.10,i5,d20.10,i5,d20.10)
0075   c
0076   c                v = vo + A*exp(-gamma*p')
0077   c
0078   c                vo - shift in zero of potential
0079   c
0080   c                aaax -  initial value of A
0081   c
0082   c                gammax - initial value of gamma
0083   c
0084   c                nal -  number of A values to test
0085   c
0086   c                xal -   delta value of alpha
0087   c
0088   c                naaa -  number of gamma values to test
0089   c
0090   c                daaa -  delta value of gamma
0091   c
0092   c
0093   c       nxpts (i5)
0094   c
0095   c                nxpts -   number of data points used in exponential spline
0096   c                          along p for D state fit of parameters.
0097   c
0098   c                   following are all (5f20,10) are data points of
0099   c                        parameters along minimum energy path D state pes.
0100   c
0101   c       qqa(i)
0102   c       qqb(i)
0103   c       wwa(i)
0104   c       wwb(i)
0105   c       aa4(i)
0106   c       aa5(i)                (i)  = 1,nxpts
0107   c       bb4(i)
0108   c       bb5(i)
0109   c       cc4(i)
0110   c       cc5(i)
0111   c
0112   c            next read in are parameters to exponential spline routine
0113   c      (SPLINE)of Kurt Kaiser, Chemistry Division, Argonne National Laboratory.
0114   c
0115   c       xpts(i),qqaa(i),qqab(i),qqac(i),qqad(i),qqap(i),i=1,nxpts
0116   c       xpts(i),qqba(i),qqbb(i),qqbc(i),qqbd(i),qqbp(i),i=1,nxpts
0117   c       xpts(i),wwaa(i),wwab(i),wwac(i),wwad(i),wwap(i),i=1,nxpts
0118   c       xpts(i),wwba(i),wwbb(i),wwbc(i),wwbd(i),wwbp(i),i=1,nxpts
0119   c       xpts(i),aa4a(i),aa4b(i),aa4c(i),aa4d(i),aa4p(i),i=1,npxts
0120   c       xpts(i),aa5a(i),aa5b(i),aa5c(i),aa5d(i),aa5p(i),i=1,npxts
0121   c       xpts(i),bb4a(i),bb4b(i),bb4c(i),bb4d(i),bb4p(i),i=1,npxts
0122   c       xpts(i),bb5a(i),bb5b(i),bb5c(i),bb5d(i),bb5p(i),i=1,npxts
```

```
0123  c       xpts(i),cc4a(i),cc4b(i),cc4c(i),cc4d(i),cc4p(i),i=1,npxts
0124  c       xpts(i),cc5a(i),cc5b(i),cc5c(i),cc5d(i),cc5p(i),i=1,npxts
0125  c
0126  c
0127        implicit real*8 (a-h,o-z)
0128  c
0129        common /io/ ir,iw,ip,itt
0130       .      /number/ n1,n2,n3,n4,n5,nflag,ntest,ipr
0131       .      /const/ hb,clt,pi,chb,csp,rmass
0132       .      /energy/ etot,vinf,eviba
0133       .      /zzz/ z0,z1,z2
0134       .      /bonds/ qao,qbo,po,qaa,qba,qa,qb
0135       .      /www/ w,waa,wba
0136       .      /trnsfm/ a,b,c
0137       .      /int1/effosc,ibeg,iend
0138       .      /answ/dwdq
0139       .      /spln/ nxpts,xpts
0140       .      /freq1/ wwa,wwb,wwaa,wwab,wwac,wwad,wwap,
0141       .       wwba,wwbb,wwbc,wwbd,wwbp
0142  c
0143        dimension a(5),b(5),c(5),w(5),
0144       .aa4(25),aa5(25),bb4(25),bb5(25),
0145       .cc4(25),cc5(25),qqa(25),qqb(25),
0146       .wwa(25),wwb(25),
0147       .aa4a(25),aa5a(25),bb4a(25),bb5a(25),
0148       .cc4a(25),cc5a(25),qqaa(25),qqba(25),
0149       .wwaa(25),wwba(25),
0150       .aa4b(25),aa5b(25),bb4b(25),bb5b(25),
0151       .cc4b(25),cc5b(25),qqab(25),qqbb(25),
0152       .wwab(25),wwbb(25),
0153       .aa4c(25),aa5c(25),bb4c(25),bb5c(25),
0154       .cc4c(25),cc5c(25),qqac(25),qqbc(25),
0155       .wwac(25),wwbc(25),
0156       .aa4d(25),aa5d(25),bb4d(25),bb5d(25),
0157       .cc4d(25),cc5d(25),qqad(25),qqbd(25),
0158       .wwad(25),wwbd(25),
0159       .aa4p(25),aa5p(25),bb4p(25),bb5p(25),
0160       .cc4p(25),cc5p(25),qqap(25),qqbp(25),
0161       .wwap(25),wwbp(25),
0162       .v(20000),effosc(20000),dwdq(0:6,0:6),xpts(25)
0163  c
0164        data ir,iw,ip,itt /5,6,7,10/
0165        data hb,pi,clt /6.35076d-4,3.14159265359d+00,2.99776d+10/
0166        data z0,z1,z2 /0.00d+00,1.00d+00,2.00d+00/
0167  c     open (unit = 6,type = 'new')
0168        chb = z2*pi*clt/hb
0169        csp = z2*pi*clt*hb
0170        ierr = 0
0171  c
0172  c     read in input
0173  c
0174        read (ir,1000) n1,n2,n3,npts,pstart,xstep,div
0175        read (ir,1010) ipr,ntest,nflag
0176        read (ir,1020) etot,vinf,rmass
0177        read (ir,1030) qao,qbo,po,qaa,qba
0178        read (ir,1030) w,a,b,c
0179        read (ir,1060) vo,aaax,gammax,nal,xal,naaa,daaa
0180        read (ir,1070) nxpts
0181        read (ir,1030) (qqa(i),i = 1,nxpts)
0182        read (ir,1030) (qqb(i),i = 1,nxpts)
0183        read (ir,1030) (wwa(i),i = 1,nxpts)
```

```
0184        read (ir,1030) (wwb(i),i = 1,nxpts)
0185        read (ir,1030) (aa4(i),i = 1,nxpts)
0186        read (ir,1030) (aa5(i),i = 1,nxpts)
0187        read (ir,1030) (bb4(i),i = 1,nxpts)
0188        read (ir,1030) (bb5(i),i = 1,nxpts)
0189        read (ir,1030) (cc4(i),i = 1,nxpts)
0190        read (ir,1030) (cc5(i),i = 1,nxpts)
0191        read (ir,1040) (xpts(i),qqaa(i),qqab(i),qqac(i),qqad(i),qqap(i),i
0192       . = 1,nxpts)
0193        read (ir,1040) (xpts(i),qqba(i),qqbb(i),qqbc(i),qqbd(i),qqbp(i),i
0194       . = 1,nxpts)
0195        read (ir,1040) (xpts(i),wwaa(i),wwab(i),wwac(i),wwad(i),wwap(i),i
0196       . = 1,nxpts)
0197        read (ir,1040) (xpts(i),wwba(i),wwbb(i),wwbc(i),wwbd(i),wwbp(i),i
0198       . = 1,nxpts)
0199        read (ir,1040) (xpts(i),aa4a(i),aa4b(i),aa4c(i),aa4d(i),aa4p(i),i
0200       . = 1,nxpts)
0201        read (ir,1040) (xpts(i),aa5a(i),aa5b(i),aa5c(i),aa5d(i),aa5p(i),i
0202       . = 1,nxpts)
0203        read (ir,1040) (xpts(i),bb4a(i),bb4b(i),bb4c(i),bb4d(i),bb4p(i),i
0204       . = 1,nxpts)
0205        read (ir,1040) (xpts(i),bb5a(i),bb5b(i),bb5c(i),bb5d(i),bb5p(i),i
0206       . = 1,nxpts)
0207        read (ir,1040) (xpts(i),cc4a(i),cc4b(i),cc4c(i),cc4d(i),cc4p(i),i
0208       . = 1,nxpts)
0209        read (ir,1040) (xpts(i),cc5a(i),cc5b(i),cc5c(i),cc5d(i),cc5p(i),i
0210       . = 1,nxpts)
0211    c
0212        waa = w(4)
0213        wba = w(5)
0214        a4a = a(4)
0215        a5a = a(5)
0216        b4a = b(4)
0217        b5a = b(5)
0218        c4a = c(4)
0219        c5a = c(5)
0220        nnpts = npts
0221    c
0222        write (iw,1260)
0223        write (iw,1080) n1,n2,n3,npts,pstart,xstep,div
0224        if (nflag .eq. 1) write (iw,1090)
0225        if (nflag .eq. 2) write (iw,1100)
0226        if (nflag .eq. 3) write (iw,1110)
0227        if (nflag .eq. 4) write (iw,1120)
0228        write (iw,1130) etot,vinf,rmass
0229        write (iw,1140) qao,qbo,po,qaa,qba
0230        write (iw,1150) w
0231        write (iw,1160)
0232        write (iw,1170) a,b,c
0233        write (iw,1180) vo,aaax,gammax,xal,nal,naaa,daaa
0234        write (iw,1200)
0235        write (iw,1190) (xpts(i),qqa(i),qqb(i),wwa(i),wwb(i),aa4(i),aa5(i)
0236       . ,bb4(i),bb5(i),cc4(i),cc5(i),i = 1,nxpts)
0237        write (iw,1210)
0238        write (iw,*) ' spline coefficients from exp-spline program'
0239        write (iw,*)
0240        write (iw,*)
0241        write (iw,*) ' qa'
0242        write (iw,1050) (xpts(i),qqaa(i),qqab(i),qqac(i),qqad(i),qqap(i),
0243       . i = 1,nxpts)
0244        write (iw,*) ' qb'
```

```
      write (iw,1050) (xpts(i),qqba(i),qqbb(i),qqbc(i),qqbd(i),qqbp(i),
     . i = 1,nxpts)
      write (iw,*) ' wa'
      write (iw,1050) (xpts(i),wwaa(i),wwab(i),wwac(i),wwad(i),wwap(i),
     . i = 1,nxpts)
      write (iw,*) ' wb'
      write (iw,1050) (xpts(i),wwba(i),wwbb(i),wwbc(i),wwbd(i),wwbp(i),
     . i = 1,nxpts)
      write (iw,*) ' a4'
      write (iw,1050) (xpts(i),aa4a(i),aa4b(i),aa4c(i),aa4d(i),aa4p(i),
     . i = 1,nxpts)
      write (iw,*) ' a5'
      write (iw,1050) (xpts(i),aa5a(i),aa5b(i),aa5c(i),aa5d(i),aa5p(i),
     . i = 1,nxpts)
      write (iw,*) ' b4'
      write (iw,1050) (xpts(i),bb4a(i),bb4b(i),bb4c(i),bb4d(i),bb4p(i),
     . i = 1,nxpts)
      write (iw,*) ' b5'
      write (iw,1050) (xpts(i),bb5a(i),bb5b(i),bb5c(i),bb5d(i),bb5p(i),
     . i = 1,nxpts)
      write (iw,*) ' c4 '
      write (iw,1050) (xpts(i),cc4a(i),cc4b(i),cc4c(i),cc4d(i),cc4p(i),
     . i = 1,nxpts)
      write (iw,*) ' c5'
      write (iw,1050) (xpts(i),cc5a(i),cc5b(i),cc5c(i),cc5d(i),cc5p(i),
     . i = 1,nxpts)
      write (iw,1210)
      do 70 nv = 1,naaa
       aaa = aaax - (nv - 1)*daaa
       do 60 na = 1,nal
        gamma = gammax+xal*(na-1)
        write (iw,1270) vo,aaa,gamma
        do 10 i = 0,6
         do 10 j = 0,6
   10    dwdq(i,j) = 0.0d0
        do 50 n4 = 0,6
         do 40 n5 = 0,6
          call second(time1)
          ipts = 0
          ibeg = 0
          iend = 0
          eviba = (n4+.5d+00)*waa + (n5+.5d+00)*wba
          eneed = vinf + eviba
          if (eneed .gt. etot) go to 40
          if (ntest .ne. 0) write (9,1220) n4,n5
          if (ipr .eq. 4) write (7,1220) n4,n5
          eavla = etot-eneed
          eavl = etot-vinf
          pminf = dsqrt(z2*rmass*eavla*csp)
          step = pi*hb*1.0d+8/pminf
          write (iw,1230) step
          step = step/div
          if (step .lt. xstep) step = xstep
          write (iw,1240) step
c
   20     continue
c
          ipts = ipts+1
          if (ipts .gt. nnpts) go to 30
          p = pstart+(ipts-1)*step
          v(ipts) = vo+aaa*dexpf(-gamma*p)
```

```
0306   c
0307           call freq(p,v(ipts),bet,alp,0)
0308           call xvl(nflag,qqa,qqaa,qqab,qqac,qqad,qqap,qa,p,qaa,bet,alp)
0309           call xvl(nflag,qqb,qqba,qqbb,qqbc,qqbd,qqbp,qb,p,qba,bet,alp)
0310           call xvl(nflag,aa4,aa4a,aa4b,aa4c,aa4d,aa4p,a(4),p,a4a,bet,
0311        .   alp)
0312           call xvl(nflag,aa5,aa5a,aa5b,aa5c,aa5d,aa5p,a(5),p,a5a,bet,
0313        .   alp)
0314           call xvl(nflag,bb4,bb4a,bb4b,bb4c,bb4d,bb4p,b(4),p,b4a,bet,
0315        .   alp)
0316           call xvl(nflag,bb5,bb5a,bb5b,bb5c,bb5d,bb5p,b(5),p,b5a,bet,
0317        .   alp)
0318           call xvl(nflag,cc4,cc4a,cc4b,cc4c,cc4d,cc4p,c(4),p,c4a,bet,
0319        .   alp)
0320           call xvl(nflag,cc5,cc5a,cc5b,cc5c,cc5d,cc5p,c(5),p,c5a,bet,
0321        .   alp)
0322   c
0323           call setup(p)
0324   c
0325           call tmat(n1,n2,n3,n4,n5)
0326   c
0327           if (ipr .ne. 0 ) write(itt,1300)ipts,p,v(ipts),
0328        .                    qa,w(4),a(4),b(4),c(4),
0329        .                    qb,w(5),a(5),b(5),c(5)
0330   c
0331           call prob(n1,n2,n3,n4,n5,wdq)
0332   c
0333           effosc(ipts) = wdq
0334           if (wdq .ne. 0.0 .and. ibeg .eq. 0) ibeg = ipts
0335           if (wdq .eq. 0.0 .and. ibeg .ne. 0 .and. iend .eq. 0) iend =
0336        .   ipts
0337           if (wdq .ne. 0.0 .and. iend .ne. 0) iend = 0
0338           go to 20
0339   c
0340     30    continue
0341   c
0342           if (ipr .eq. 1) call print(v,pstart,step,npts,1)
0343           if (ipr .eq. 2) call print(effosc,pstart,step,npts,2)
0344           call second(time2)
0345   c
0346           call tdelay(rmass,pstart,nnpts,step,vo,aaa,gamma,eavla,v,ierr)
0347   c
0348           call second(time3)
0349           tt1 = time2-time1
0350           tt2 = time3-time2
0351           write (iw,1250) tt1,tt2
0352     40    continue
0353     50   continue
0354   c
0355          call stat(dwdq,vo,aaa,gamma)
0356   c
0357     60  continue
0358     70 continue
0359          call second(timeall)
0360          write (iw,1280) timeall
0361          close (unit = 6)
0362   c
0363    1000 format(4i8,3d20.8)
0364    1010 format(3i5)
0365    1020 format(3f15.8)
0366    1030 format(5f15.8)
```

```
0367     1040 format(4d20.13/2d20.13)
0368     1050 format(6d15.8)
0369     1060 format(3d20.10,i5,d20.10,i5,d20.10)
0370     1070 format(i5)
0371     1080 format(' initial state of quasidiscrete state',/,
0372        .' symmetric cn stretch  n1= ',i5,/,
0373        .' asymmetric cn stretch n2= ',i5,/,
0374        .' cc stretch            n3= ',i5,//,
0375        .' npts =',i6,' pstart= ',f10.4,' step size = ',f10.4,/,
0376        .' number of step per node asymp = ',f6.2)
0377     1090 format(' nflag = 1     alpha = 1')
0378     1100 format(' nflag = 2     alpha << 1')
0379     1110 format(' nflag = 3     alpha >> 1')
0380     1120 format(' nflag = 4     alpha = alpha(infinity)')
0381     1130 format(' total energy (cm-1) is ',f14.4,/,
0382        .' vinf (cm-1) is ',f14.4,/,
0383        .' reduced mass  (rmass) is ',f14.8,/)
0384     1140 format(' internal coordinates of quasidiscrete state',/,
0385        .' qao (a) = ',f10.4,' qbo =',f10.4,' po =',f10.4,/,
0386        .' asymptotic values of fragments ',/,
0387        .' qcn(x) = ',f10.4,' qcn(a) = ',f10.4,/)
0388     1150 format(' frequencies',/,' symetric cn stretch (cm-1) =',f10.2,/,
0389        .' asymmetric stretch  = ',f10.5,/,
0390        .' cc stretch = ',f10.5,/,
0391        .' cn(x)    = ',f10.5,/,
0392        .' cn(a)    = ',f10.5,/)
0393     1160 format(' q = a(i)*(ta-da)+b(i)*(tb-db)+c(i)*(p-dp) ')
0394     1170 format(' a(i) = ',5f15.8,/,
0395        .' b(i) = ',5f15.8,/,' c(i) = ',5f15.8)
0396     1180 format(/,' electronic potential fit to form
0397        . v = vo + aexp(-gamma*p)',/,' vo = ',f12.6,' a = ',d12.6,
0398        .' gamma = ',f12.6,/,' xal = ',f12.6, ' nal = ',i5,
0399        .' naaa = ',i5,' daaa = ',d12.6)
0400     1190 format(3f8.4,2f8.2,6f10.6)
0401     1200 format(/,5x,1hp,5x,4hq(x),4x,4hq(a),4x,4hw(4),4x,4hw(5),5x,4ha(4),
0402        .6x,4ha(5),6x,4hb(4),6x,4hb(5),6x,4hc(4),6x,4hc(5))
0403     1210 format('1')
0404     1220 format(' "alp',2i3,'"')
0405     1230 format(/,110(1h:),//,' asymptotic spacing of nodes of trans.
0406        .wf = ',f12.6)
0407     1240 format(' integration step size = ',f16.8)
0408     1250 format(' time for evaluation of eff osc = ',f12.4,/,
0409        .' time for evaluation of tr wf and integral = ',f12.4)
0410     1260 format(110(1h%),//)
0411     1270 format(110(1h^),/,' vo = ',f12.6,' a = ',d12.6,'gamma = ',
0412        .f10.5)
0413     1280 format(' total time of this run = ',f12.4)
0414     1300 format(i4,2x,2d14.5,/,6x,5d14.5,/,6x,5d14.5)
0415          end

0001          subroutine xvl(nfl,co1,co2,co3,co4,co5,co6,vnew,pos,vasy,bet,alp)
0002     c
0003     c     this subroutine evaluates parameter along D state reaction path
0004     c          calls qeval which evaluates exponetial spline
0005     c
0006          implicit real*8 (a-h,o-z)
0007          common /spln/ nxpts,xpts
0008          dimension co1(25),co2(25),co3(25),co4(25),co5(25),co6(25),xpts(25)
0009          vnew = 0.0d+00
0010          if (nfl .ne. 3) go to 10
0011          vnew = vasy
```

```
0012        return
0013      10 if (pos .gt. xpts(1) .and. pos .lt. xpts(nxpts)) go to 30
0014        if (pos .le. xpts(1)) go to 20
0015        vnew = co1(nxpts)
0016        go to 40
0017      20 vnew = co1(1)
0018        go to 40
0019      30 vnew = qeval(pos,xpts,co1,co2,co3,co4,co5,co6,nxpts)
0020      40 continue
0021        if (nfl .ne. 2) go to 50
0022        return
0023      50 if (vasy .eq. 0.0d+00) go to 60
0024        vnew = vasy*(abs(vnew/vasy))**bet
0025        return
0026      60 vnew = vnew*dexpf(-(alp*alp))
0027        return
0028        end

0001        subroutine freq(pos,val,bet,alp,ioff)
0002  c
0003  c     this subroutine evaluates freqencies along D state pes and effective
0004  c        potential
0005  c
0006        implicit real*8 (a-h,o-z)
0007        external yy
0008        dimension wwa(25),wwb(25),w(5),wwaa(25),wwab(25),xpts(25)
0009        dimension wwac(25),wwad(25),wwap(25),wwba(25),wwbb(25)
0010        dimension wwbc(25),wwbd(25),wwbp(25)
0011        common /energy/ etot,vinf,eviba
0012        common /number/ n1,n2,n3,n4,n5,nflag,ntest,ipr
0013        common /zzz/ z0,z1,z2
0014        common /freq1/ wwa,wwb,wwaa,wwab,wwac,wwad,wwap,wwba,wwbb,
0015       . wwbc,wwbd,wwbp
0016        common /www/ w,waa,wba
0017        common /spln/ nxpts,xpts
0018        common /fun/ wap,wbp,eav
0019        data z10,tol,zm10 /10.0d0,1.0d-10,-10.0d0/
0020        wap = z0
0021        wbp = z0
0022        if (nflag .ne. 4) go to 10
0023        etrana = etot-vinf-eviba
0024        alp = etrana/eviba
0025        go to 40
0026      10 if (nflag .ne. 3) go to 40
0027        bet = z0
0028        alp = 1.0d+25
0029      20 evib = (n4+.5d+00)*w(4)+(n5+.5d+00)*w(5)
0030        etran = etot-vinf-val-evib
0031        alpx = etran/evib
0032        val = val+evib-eviba
0033        if (ioff .ne. 0) go to 30
0034        if (ntest .ne. 0) write (9,1010) pos,alp,etran,evib
0035        if (ipr .eq. 4) write (7,1000) pos,alp
0036      30 return
0037      40 if (pos .gt. xpts(1) .and. pos .lt. xpts(nxpts)) go to 60
0038        if (pos .le. xpts(1)) go to 50
0039        wap = wwa(nxpts)
0040        wbp = wwb(nxpts)
0041        go to 70
0042      50 wap = wwa(1)
0043        wbp = wwb(1)
```

```
0044        go to 70
0045      60 wap = qeval(pos,xpts,wwa,wwaa,wwab,wwac,wwad,wwap,nxpts)
0046        wbp = qeval(pos,xpts,wwb,wwba,wwbb,wwbc,wwbd,wwbp,nxpts)
0047      70 w(4) = wap
0048        w(5) = wbp
0049        if (nflag .eq. 4) go to 90
0050        if (nflag .ne. 2) go to 80
0051        bet = z1
0052        alp = z0
0053        go to 20
0054      80 eav = etot-vinf-val
0055        evib = (n4+.5d0)*w(4)+(n5+.5d0)*w(5)
0056        etran = eav-evib
0057        alp = zeroin(zm10,z10,yy,tol)
0058      90 bet = z1/(z1+alp*alp)
0059        w(4) = waa*(wap/waa)**bet
0060        w(5) = wba*(wbp/wba)**bet
0061        go to 20
0062     1000 format(f14.6,d20.10)
0063     1010 format(4d15.5)
0064        end

0001        subroutine setup(p)
0002    c
0003    c     this subroutine sets up constants of transition probability matrix
0004    c
0005        implicit real*8(a-h,o-z)
0006        dimension a(5),b(5),c(5),w(5)
0007        dimension g(5),h(5),h1(5),j(5),j1(5),j2(5)
0008        dimension da(5),db(5),dp(5),kk(5),xm(5),xn(5,5)
0009        real*8 j,j1,j2,jp,j1p,j2p,kk,kp
0010        common /number/ n1,n2,n3,n4,n5,nflag,ntest,ipr
0011        common /const/ hb,clt,pi,chb,csp,rmass
0012        common /energy/ etot,vinf,eviba
0013        common /zzz/ z0,z1,z2
0014        common /bonds/ qao,qbo,po,qaa,qba,qa,qb
0015        common /www/ w,waa,wba
0016        common /trnsfm/ a,b,c
0017        common /set/ xn,xm
0018        common /set2/ aa,b1,c2,q,pp
0019        angs = 1.0d-8
0020        aa = 0.0d+00
0021        bb = 0.0d+00
0022        cc = 0.0d+00
0023        dd = 0.0d+00
0024        ee = 0.0d+00
0025        ff = 0.0d+00
0026        b1 = 0.0d+00
0027        c1 = 0.0d+00
0028        f1 = 0.0d+00
0029        c2 = 0.0d+00
0030        gp = 0.0d+00
0031        hp = 0.0d+00
0032        jp = 0.0d+00
0033        h1p = 0.0d+00
0034        j1p = 0.0d+00
0035        j2p = 0.0d+00
0036        kp = 0.0d+00
0037        q = 0.0d+00
0038        do 20 i = 1,5
0039         do 10 jj = 1,5
```

```
0040          xn(i,jj) = 0.d+00
0041       10 continue
0042          xm(i) = 0.0d+00
0043          da(i) = 0.0d+00
0044          db(i) = 0.0d+00
0045          dp(i) = 0.0d+00
0046       20 continue
0047          da(4) = (qa-qao)*angs
0048          da(5) = da(4)
0049          db(4) = (qb-qbo)*angs
0050          db(5) = db(4)
0051          dp(4) = (p-po)*angs
0052          dp(5) = dp(4)
0053          pp = (p-po)*angs
0054          do 30 i = 1,5
0055           aa = aa + .5d+00*a(i)*a(i)*w(i)*chb
0056           bb = bb + .5d+00*b(i)*b(i)*w(i)*chb
0057           cc = cc + .5d+00*c(i)*c(i)*w(i)*chb
0058           dd = dd + a(i)*b(i)*w(i)*chb
0059           ee = ee + a(i)*c(i)*w(i)*chb
0060           ff = ff + b(i)*c(i)*w(i)*chb
0061           gp = gp-w(i)*chb*(a(i)**2*da(i)+a(i)*b(i)*db(i)+a(i)*c(i)*dp(i))
0062           hp = hp-w(i)*chb*(a(i)*b(i)*da(i)+b(i)**2*db(i)+b(i)*c(i)*dp(i))
0063           jp = jp-w(i)*chb*(a(i)*c(i)*da(i)+b(i)*c(i)*db(i)+c(i)**2*dp(i))
0064           kp = kp+w(i)*chb*(a(i)**2*da(i)**2+b(i)**2*db(i)**2++c(i)**2*dp
0065         . (i)**2)*.5d+00+ w(i)*chb*(a(i)*b(i)*da(i)*db(i)++a(i)*c(i)*da(i)
0066         . *dp(i)+b(i)*c(i)*db(i)*dp(i))
0067       30 continue
0068          b1 = bb - dd/(4*aa)*dd
0069          c1 = cc - ee/(4*aa)*ee
0070          f1 = ff - ee/(2*aa)*dd
0071          c2 = c1 - f1/(4*b1)*f1
0072          h1p = hp-gp/(2*aa)*dd
0073          j1p = jp-gp/(2*aa)*ee
0074          j2p = j1p-h1p/(2*b1)*f1
0075          q = gp/(4*aa)*gp+ h1p/(4*b1)*hp -kp - j2p*pp
0076          do 40 i = 1,5
0077           g(i) = -2*a(i)*((w(i)*chb)**.5d+00)
0078           h(i) = -2*b(i)*((w(i)*chb)**.5d+00)
0079           j(i) = -2*c(i)*((w(i)*chb)**.5d+00)
0080           h1(i) = h(i)-g(i)/(2*aa)*dd
0081           j1(i) = j(i)-g(i)/(2*aa)*ee
0082           j2(i) = j1(i)-h1(i)/(2*b1)*f1
0083           kk(i) = 2.d+00*(w(i)*chb)**.5d+00 *( a(i)*da(i)+b(i)*db(i)+c(i)*
0084         . dp(i))
0085       40 continue
0086          do 60 i = 1,5
0087           do 50 k = 1,5
0088            xn(i,k) = xn(i,k)+g(i)*g(k)/(4*aa)
0089            xn(i,k) = xn(i,k)+h1(i)*h1(k)/(4*b1)
0090            if (i .ne. k) go to 50
0091            xn(i,k) = xn(i,k)-1.d+00
0092       50  continue
0093          xm(i) = gp*g(i)/(2*aa)+h1p*h1(i)/(2*b1)-j2(i)*pp-kk(i)
0094       60 continue
0095          return
0096          end

0001          subroutine tmat(n1,n2,n3,n4,n5)
0002     c
0003     c    this subroutine calculates differentiation with respect to dummy t
```

```
0004   c       variables
0005   c
0006          implicit real*8(a-h,o-z)
0007          dimension t(-1:6,-1:6,-1:6,-1:6,-1:6)
0008          dimension xn(5,5),xm(5)
0009          common /set/ xn,xm
0010          common /ttt/ t
0011          t(0,0,0,0,0) = 1.0d+00
0012          t(-1,0,0,0,0) = 0.0d+00
0013          do 10 i = 1,n1
0014           t(i,0,0,0,0) = xm(1)*t(i-1,0,0,0,0) + (i-1)*2*xn(1,1)*t(i-2,0,0,
0015         . 0,0)
0016       10 continue
0017          do 30 i = 0,n1
0018           do 20 jj = 1,n2
0019            t(i,jj,0,0,0) = xm(2)*t(i,jj-1,0,0,0)+(jj-1)*2*xn(2,2)*t(i,jj-2,
0020         .  0,0,0)+i*(xn(2,1)+xn(1,2))*t(i-1,jj-1,0,0,0)
0021       20  continue
0022       30 continue
0023          do 60 i = 0,n1
0024           do 50 jj = 0,n2
0025            do 40 k = 1,n3
0026             t(i,jj,k,0,0) = xm(3)*t(i,jj,k-1,0,0)+(k-1)*2*xn(3,3)*t(i,jj,k-
0027         .    2,0,0)+jj*(xn(3,2)+xn(2,3))*t(i,jj-1,k-1,0,0)+i*(xn(3,1)+xn(1,
0028         .    3))*t(i-1,jj,k-1,0,0)
0029       40   continue
0030       50  continue
0031       60 continue
0032          do 100 i = 0,n1
0033           do 90 jj = 0,n2
0034            do 80 k = 0,n3
0035             do 70 l = 1,n4
0036              t(i,jj,k,l,0) = xm(4)*t(i,jj,k,l-1,0)+(l-1)*2*xn(4,4)*t(i,jj,
0037         .     k,l-2,0)+k*(xn(4,3)+xn(3,4))*t(i,jj,k-1,l-1,0)+jj*(xn(4,2)+
0038         .     xn(2,4))*t(i,jj-1,k,l-1,0)+i*(xn(4,1)+xn(1,4))*t(i-1,jj,k,l-
0039         .     1,0)
0040       70    continue
0041       80   continue
0042       90  continue
0043      100 continue
0044          do 150 i = 0,n1
0045           do 140 jj = 0,n2
0046            do 130 k = 0,n3
0047             do 120 l = 0,n4
0048              do 110 i1 = 1,n5
0049               t(i,jj,k,l,i1) = xm(5)*t(i,jj,k,l,i1-1)+(i1-1)*2*xn(5,5)*t(i,
0050         .      jj,k,l,i1-2)+l*(xn(5,4)+xn(4,5))*t(i,jj,k,l-1,i1-1)+k*(xn(5,
0051         .      3)+xn(3,5))*t(i,jj,k-1,l,i1-1)+jj*(xn(5,2)+xn(2,5))*t(i,jj-
0052         .      1,k,l,i1-1)+i*(xn(5,1)+xn(1,5))*t(i-1,jj,k,l,i1-1)
0053      110     continue
0054      120    continue
0055      130   continue
0056      140  continue
0057      150 continue
0058          return
0059          end

0001          subroutine prob(n1,n2,n3,n4,n5,wdq)
0002   c
0003   c     this subroutine calculates transition probability
0004   c
```

```
0005        implicit real*8 (a-h,o-z)
0006        dimension t(-1:6,-1:6,-1:6,-1:6,-1:6)
0007        dimension w(5)
0008        common /ttt/ t
0009        common /const/ hb,clt,pi,chb,csp,rmass
0010        common /www/ w,waa,wba
0011        common /energy/ etot,vinf,eviba
0012        common /set2/ aa,b1,c2,q,pp
0013        wdq = 0.0d+00
0014        xfac1 = w(1)*w(2)*w(3)*w(4)*w(5)/pi/pi/pi/pi/pi
0015        xfac2 = dsqrt(dsqrt(xfac1))*chb**1.25d+00
0016        xfac3 = xfac2*f(n1)*f(n2)*f(n3)*f(n4)*f(n5)
0017  c     xfac4 = dexpf(q-c2*pp*pp)
0018        xfac5 = dsqrt(aa)*dsqrt(b1)/pi
0019  c     xfac = xfac3/xfac5*xfac4
0020        xfac = dlog(xfac3) - dlog(xfac5) + (q-c2*pp*pp)
0021        xfac = dexpf(xfac)
0022        hdq = t(n1,n2,n3,n4,n5)*xfac
0023        pmom = (etot-vinf-(n4+.5d+00)*waa-(n5+.5d+00)*wba)*csp*2.d+00*
0024       . rmass
0025        if (pmom .lt. 0) pmom = 0.0d+00
0026        pmom = dsqrt(pmom)
0027        if (pmom .ne. 0) wdq = hdq/dsqrt(pmom)
0028        if (pmom .eq. 0) wdq = -1.0d+00
0029        return
0030        end

0001        real*8 function f(no)
0002        implicit real*8 (a-h,o-z)
0003        j = 1
0004        do 10 i = 1,no
0005       10 j = j*i
0006        x = dfloat(2**no*j)
0007        f = x**(-.5d+00)
0008        return
0009        end

0001        subroutine intgrl(xm2)
0002        implicit real*8 (a-h,o-z)
0003        dimension effosc(20000),wfs(20000),xm2(1)
0004        dimension y(20000)
0005        dimension dwdq(0:6,0:6)
0006        common /number/n1,n2,n3,n4,n5,nflag,ntest,ipr
0007        common /int1/ effosc,ibeg,iend
0008        common /bwf/ wfs
0009        common /answ/ dwdq
0010        common /io/ ir,iw,ip
0011        data ifail /0/
0012        data ans /0.0d+00/
0013        ix = 0
0014        do 10 i = ibeg,iend
0015        ix = ix+1
0016        y(ix) = effosc(i)*wfs(i)
0017        xm2(ix) = xm2(i)
0018       10 continue
0019        num = iend-ibeg+1
0020        call d01gaf(xm2,y,num,ans,er,ifail)
0021        dwdq(n4,n5) = ans*ans
0022        write (iw,1000) n4,n5,dwdq(n4,n5)
0023        return
0024     1000 format(' dwdq(',2i2,') = ',d20.10)
```

```
0025        end

0001        subroutine d01gaf(x,y,npts,ans,er,ifail)
0002        implicit real*8 (a-h,o-z)
0003        dimension x(1),y(1)
0004        ans = 0.0d+00
0005        do 10 i = 1,npts-1
0006        ans = ans+.5d+00*(x(i+1)-x(i))*(y(i)+y(i+1))
0007       10 continue
0008        return
0009        end

0001        subroutine ptlscl(n,rsc,esc,xh,xmin,bz,v,xm2)
0002        implicit real*8 (a-h,o-z)
0003        dimension v(1),xm2(1)
0004        do 10 i = 1,n
0005        xm2(i) = xmin+(i-1)*xh
0006       10 v(i) = bz/esc*v(i)
0007        return
0008        end

0001        subroutine ptlgen(n,rsc,esc,bz,v,rm2,vo,a,gamma)
0002        implicit real*8 (a-h,o-z)
0003        dimension v(1),rm2(1)
0004        do 10 i = 1,n
0005        v(i) = vo+a*dexpf(-gamma*rm2(i))
0006        call freq(rm2(i),v(i),bet,alp,1)
0007        v(i) = bz/esc*v(i)
0008       10 continue
0009        return
0010        end

0001        subroutine stat(dwdq,vo,aaa,gamma)
0002        implicit real*8 (a-h,o-z)
0003        dimension dwdq(0:6,0:6)
0004        dimension xx(0:6),xa(0:6)
0005        common /io/ ir,iw,ip
0006        common /number/ n1,n2,n3,n4,n5,nflag,ntest,ipr
0007        data istat /8/
0008        xtot = 0.0d+00
0009        do 10 i = 0,6
0010        xx(i) = 0.0d+00
0011       10 xa(i) = 0.0d+00
0012        do 30 i = 0,6
0013         do 20 j = 0,6
0014          xx(i) = xx(i)+dwdq(i,j)
0015          xa(i) = xa(i)+dwdq(j,i)
0016          xtot = xtot+dwdq(i,j)
0017       20  continue
0018       30 continue
0019        if (xtot .eq. 0.0d+00) go to 40
0020        do 40 i = 0,6
0021         xx(i) = xx(i)/xtot
0022         xa(i) = xa(i)/xtot
0023       40 continue
0024        write (iw,1020)
0025        write (iw,1030) xx
0026        write (iw,1040) xa
0027        write (iw,1050)
0028        write (istat,1000) n1,n2,n3,nflag,vo,aaa,gamma
0029        write (istat,1010) ((dwdq(j,i),j = 0,6),i = 0,6)
```

```
0030        write (istat,1020)
0031        write (istat,1030) xx
0032        write (istat,1040) xa
0033        write (istat,1050)
0034        do 60 i = 0,6
0035         do 50 j = 0,6
0036          dwdq(i,j) = 0.0d+00
0037       50  continue
0038       60 continue
0039          return
0040     1000 format(' initial state = (',3i2,')  nflag = ',i2,/,
0041        .' vo = ',f10.5,' a = ',d16.8,' gamma  = ',f16.8,//)
0042     1010 format(7d12.5)
0043     1020 format(//,110(1h*),/,13x,'v=0',9x,'v=1',9x,'v=2',9x,'v=3',9x,
0044        .'v=4',9x,'v=5',9x,'v=6',/,110(1h*))
0045     1030 format(' cn(x) ',7f12.8)
0046     1040 format(' cn(a) ',7f12.8,/)
0047     1050 format(110(1h*),//)
0048        end

0001        subroutine print(array,xstart,step,npts,in)
0002        implicit real*8 (a-h,o-z)
0003        dimension array(1)
0004        common /number/n1,n2,n3,n4,n5,nflag,ntest,ipr
0005        common /io/ ir,iw,ip
0006        if (in .eq. 1) write (ip,1000) n4,n5
0007        if (in .eq. 2) write (ip,1010) n4,n5
0008        if (in .eq. 3) write (ip,1020) n4,n5
0009        do 10 i = 1,npts
0010         x = xstart+(i-1)*step
0011         write (ip,1030) x,array(i)
0012       10 continue
0013          return
0014     1000 format('"pot ',2i2,'"')
0015     1010 format('"osc ',2i2,'"')
0016     1020 format('"twf ',2i2,'"')
0017     1030 format(1x,f10.5,2x,d20.10)
0018        end

0001        real*8 function yy(alp)
0002        implicit real*8 (a-h,o-z)
0003        dimension w(5)
0004        common /fun/ wap,wbp,eav
0005        common /www/ w,waa,wba
0006        common /number/ n1,n2,n3,n4,n5,nflag,ntest,ipr
0007        data z0,z1,z2/0.0d0,1.0d0,2.0d0/
0008        alpb = alp*alp
0009        yy = alp + z1 - eav/( (n4+z1/z2)*waa*(wap/waa)**(z1/(z1+alpb))+
0010       . (n5+z1/z2)*wba*(wbp/wba)**(z1/(z1+alpb)) )
0011        return
0012        end

0001        subroutine second(tim)
0002        implicit real*8 (a-h,o-z)
0003        call lib$stat_timer(2,itim)
0004        tim = itim/100
0005        return
0006        end

0001        real*8 function qeval(t,x,y,a,b,c,d,p,n)
0002        implicit real*8 (a-h,o-z)
```

```
0003   c
0004   c       this subroutine evaluates f(t),f'(t),f''(t) where f is
0005   c          the spline function
0006   c
0007         common /silly/ lasti
0008         dimension x(25),y(25),a(25),b(25),c(25),d(25),p(25)
0009         logical*1 print,debug,prnt2,tensn
0010   c
0011   c       quick check to find the section which contains t
0012   c
0013         data lasti /1/
0014         print = .false.
0015         debug = .false.
0016         prnt2 = .false.
0017         tensn = .true.
0018         i = lasti
0019         if (t .lt. x(i)) go to 10
0020         if (t .lt. x(i+1)) go to 60
0021         i = i+1
0022         if (i .ge. n) go to 20
0023         if (t .lt. x(i+1)) go to 60
0024         go to 20
0025      10 continue
0026         i = i-1
0027         if (i .le. 0) go to 20
0028         if (t .ge. x(i)) go to 60
0029   c
0030   c       quick check has failed--use binary search to find the
0031   c                  section which contains t
0032   c
0033      20 continue
0034         ilow = 0
0035         ihigh = n
0036      30 continue
0037         if (ihigh .le. ilow+1) go to 50
0038         i = (ilow+ihigh)/2
0039         if (t .lt. x(i)) go to 40
0040         if (t .lt. x(i+1)) go to 60
0041         ilow = i
0042         go to 30
0043      40 continue
0044         ihigh = i
0045         go to 30
0046      50 continue
0047   c
0048   c       ...and here's another fine kludge you've gotten me into...
0049   c
0050         if (dabs((t-x(n))/(dabs(t)+dabs(x(n)))) .lt. 1d-5) t = x(n)
0051         if (dabs((t-x(1))/(dabs(t)+dabs(x(1)))) .lt. 1d-5) t = x(1)
0052         if (t .gt. x(n)  .or.  t .lt. x(1)) go to 130
0053         if (t .eq. x(1)) i = 1
0054         if (t .eq. x(n)) i = nm1
0055   c
0056   c                     evaluate f,fp,fpp
0057   c
0058      60 continue
0059         dif = t-x(i)
0060         ai = a(i)
0061         bi = b(i)
0062         ci = c(i)
0063         di = d(i)
```

```
0064        pi = p(i)
0065        if (pi .gt. 0.d0) go to 70
0066    c
0067    c       evaluate a cubic spline.
0068    c
0069        temp = di*dif
0070        f = ai+dif*(bi+dif*(ci+temp))
0071        fp = bi+dif*(ci+ci+3.d0*temp)
0072        fpp = ci+ci+6.d0*temp
0073        go to 80
0074    c
0075    c       evaluate an exponential spline.
0076    c
0077      70 continue
0078    c
0079        pidx=pi*dif
0080        if(pidx.gt.85.0d0)goto 75
0081    c
0082        ep=dexpf(pi*dif)
0083        em=di/ep
0084        ep=ci*ep
0085        f = ai+bi*dif+ep+em
0086        fp = bi+pi*(ep-em)
0087        fpp = pi*pi*(ep+em)
0088        goto 80
0089    c
0090      75 continue
0091    c
0092        f = ai*bi*dif
0093        fp = bi
0094        fpp = 0.0d0
0095    c
0096    c       terminate.
0097    c
0098      80 continue
0099        lasti = i
0100        if (print .and. prnt2) write (6,1000) t,f,fp,fpp
0101        qeval = f
0102        return
0103    c
0104    c       error:   t is out of the range of x specified by the knots.
0105    c
0106     130 continue
0107    c
0108        f = 0.0d0
0109        qeval = f
0110        return
0111     1000 format (19x,4(1pd14.7,4x))
0112        end

0001        real*8 function dexpf(arg)
0002        implicit real*8 (a-h,o-z)
0003    c
0004    c     this function eliminates underflow from exponentiation of large
0005    c       negative numbers
0006    c
0007        dexpf=0.0d0
0008        if(arg.lt.-87.0d0) then
0009        return
0010        else
0011        dexpf=dexp(arg)
```

```
0012        endif
0013        return
0014        end
```

TEST INPUT FILE FOR FCINT

```
 1, 0, 0, .3500, 2.250, 0.0050, 20.
0,0,1
60975.61, 52178.36, 13.008925
1.2031, 1.2031, 2.656, 1.1718, 1.2327,
2082.3, 1725.6, 896.0, 2068.7, 1814.0
-1.7054081, -1.79806434, 0.5698546, 2.5428470, 0.0
-1.7054081,  1.79806434, 0.5698546, 0.0      , -2.5428470
 1.1433240,  0.0       , 3.4207968, 0.0      , 0.0
0.0, 2.4e+9, 4.8860, 1, 0.000, 1, 0.00e+9
 14
 1.1397, 1.1635, 1.1704, 1.1801, 1.1865
 1.1842, 1.1748, 1.1672, 1.1669, 1.1702
 1.1717, 1.1716, 1.1718, 1.1718
 1.1397, 1.1635, 1.1704, 1.1801, 1.1865
 1.1933, 1.2052, 1.2148, 1.2287, 1.2312
 1.2322, 1.2321, 1.2327, 1.2327
 2309.4, 2162.7, 2117.4, 2054.2, 2006.8
 1990.7, 1955.2, 1947.6, 2109.3, 2084.9
 2070.6, 2071.2, 2068.7, 2068.7
 1904.0, 1627.0, 1489.0, 1185.0,  674.0
  162.0, 1135.0, 1668.0, 1836.0, 1825.1
 1819.8, 1819.0, 1814.0, 1814.0
 1.79291, 1.79291, 1.79291, 1.79291, 1.79291
 1.80052, 1.82802, 2.05427, 2.53806, 2.53891
 2.53912, 2.53912, 2.54287, 2.54287
 1.79808, 1.79808, 1.79808, 1.79808, 1.79808
 1.79046, 1.76237, 1.49251, 0.07659, 0.03961
 0.02230, 0.02181, 0.00000, 0.00000
 1.79291, 1.79291, 1.79291, 1.79291, 1.79291
 1.79046, 1.76237, 1.48658, 0.06928, 0.03230
 0.01499, 0.01449, 0.00000, 0.00000
-1.79808,-1.79808,-1.79808,-1.79808,-1.79808
-1.80567,-1.83310,-2.05856,-2.53827,-2.53901
-2.53917,-2.53917,-2.54287,-2.54287
-0.27342,-0.27342,-0.27342,-0.27342,-0.27342
-0.27342,-0.27337,-0.26999,-0.19881,-0.19606
-0.19475,-0.19471, 0.00000, 0.00000
 0.00000, 0.00000, 0.00000, 0.00000, 0.00000
 0.00116, 0.00539, 0.04316, 0.18770, 0.19058
 0.19191, 0.19195, 0.00000, 0.00000
 0.2700000000000D+01 0.1139748992622D+01 0.1584427187517D+00-0.1795417529270D-02
 0.1746424907595D-02 0.6882634094530D+01
 0.2888300000000D+01 0.1163500000000D+01 0.1099925229890D+00-0.1440957577311D+00
 0.3365531298870D+00 0.0000000000000D+00
 0.2956100000000D+01 0.1170400000000D+01 0.9509438090944D-01-0.7564085111212D-01
 0.1934333315537D+00 0.0000000000000D+00
 0.3064900000000D+01 0.1180116632095D+01 0.8884870772817D-01-0.5144141197532D-04
 0.3480931704562D-04 0.3877659574468D+02
 0.3158900000000D+01 0.1186500000000D+01 0.1244992813425D-01-0.1479875097662D+01
-0.4492118907624D+01 0.0000000000000D+00
 0.3200000000000D+01 0.1184200000000D+01-0.1319602014334D+00-0.2033753358972D+01
 0.1825914775282D+02 0.0000000000000D+00
 0.3250000000000D+01 0.1174800000000D+01-0.1983919291845D+00 0.7051188039502D+00
 0.4454395594805D+01 0.0000000000000D+00
 0.3300000000000D+01 0.1163186398258D+01 0.1052115846638D-01 0.2356030280587D-09
 0.4013601506628D-02 0.2615935993762D+02
 0.3652700000000D+01 0.1166900000000D+01 0.1057345689187D-01 0.9543249541760D-03
-0.1163201699926D-01 0.0000000000000D+00
 0.4000000000000D+01 0.1177315804053D+01-0.7455747309544D-02 0.5299490835590D-03
```

-0.7645753136364D-02 0.1771470000000D+01
0.4750000000000D+01 0.1171700000000D+01-0.3239544777666D-03-0.3764718353495D-04
0.5002873339350D-03 0.0000000000000D+00
0.5349200000000D+01 0.1171600000000D+01 0.1697995911648D-03 0.8616693279467D-03
-0.9993371942018D-03 0.0000000000000D+00
0.6000000000000D+01 0.1171800217887D+01-0.2200882040430D-06 0.8187448404660D-52
-0.2178873220026D-06 0.1000000000000D+03
0.7000000000000D+01 0.1139700000000D+01 0.1340655132383D+00 0.1171800000000D+01
-0.2646977960170D-22 0.0000000000000D+00
0.2700000000000D+01 0.1139713006490D+01 0.1429841820614D+00-0.4211662918483D-03
0.4081598016767D-03 0.1075411577270D+02
0.2888300000000D+01 0.1163829418749D+01 0.9691442942132D-01 0.3677486583929D-05
-0.3330962354942D-03 0.3318584070796D+02
0.2956100000000D+01 0.1170400558966D+01 0.1085128266158D+00-0.2245384784807D-03
0.2239795122703D-03 0.2068014705882D+02
0.3064900000000D+01 0.1188319668253D+01-0.2311084686576D+00 0.9982137875578D-02
-0.1820180612900D-01 0.1046968085106D+02
0.3158900000000D+01 0.1186500000000D+01 0.1197370790440D+00 0.1090909616023D+01
0.5189747822584D+00 0.0000000000000D+00
0.3200000000000D+01 0.1193300000000D+01 0.2120398216569D+00 0.1154899206675D+01
-0.1271391279626D+02 0.0000000000000D+00
0.3250000000000D+01 0.1205200000000D+01 0.2321753963524D+00-0.7521877127643D+00
-0.1026404285689D+01 0.0000000000000D+00
0.3300000000000D+01 0.1225659882600D+01 0.8971133032511D-02-0.1045801971017D-06
-0.1085977801932D-01 0.1291820243833D+02
0.3652700000000D+01 0.1228700000000D+01 0.1031570827512D-01-0.1034665896683D-01
0.3946979286680D-02 0.0000000000000D+00
0.4000000000000D+01 0.1231200000000D+01 0.4557140792496D-02-0.6234301248043D-02
0.2581188403324D-02 0.0000000000000D+00
0.4750000000000D+01 0.1232200000000D+01-0.4385556489594D-03-0.4266273405640D-03
0.1468640335101D-02 0.0000000000000D+00
0.5349200000000D+01 0.1232100000000D+01 0.6320788436428D-03 0.2213400525814D-02
-0.2716664169201D-02 0.0000000000000D+00
0.6000000000000D+01 0.1232700618123D+01-0.6243665854816D-06 0.2322691134880D-51
-0.6181229196267D-06 0.1000000000000D+03
0.7000000000000D+01 0.1139700000000D+01 0.1340655132383D+00 0.1232700000000D+01
0.1058791184068D-21 0.0000000000000D+00
0.2700000000000D+01 0.2309118520359D+04-0.1198854634312D+04 0.5051333703776D+02
-0.5023185739671D+02 0.3823685608072D+01
0.2888300000000D+01 0.2162700000000D+04-0.7085558668564D+03 0.5798943237117D+03
0.2387376520389D+03 0.0000000000000D+00
0.2956100000000D+01 0.2117400000000D+04-0.6266298801959D+03 0.6284535621364D+03
-0.1911580570269D+04 0.0000000000000D+00
0.3064900000000D+01 0.2054184243858D+04-0.6064940331860D+03 0.1025814248070D+01
-0.1010058105804D+01 0.2393617021277D+02
0.3158900000000D+01 0.2004959725521D+04-0.1951825055326D+03-0.6855102638744D+00
0.2525784743062D+01 0.5474452554745D+02
0.3200000000000D+01 0.1990700000000D+04-0.5658114863765D+03-0.9347115071863D+04
0.1292668959879D+06 0.0000000000000D+00
0.3250000000000D+01 0.1955200000000D+04-0.5310212736539D+03 0.1004291932631D+05
-0.4924987706472D+05 0.0000000000000D+00
0.3300000000000D+01 0.1947600000000D+04 0.1038965809921D+03 0.2655437766606D+04
-0.4678608336489D+04 0.0000000000000D+00
0.3652700000000D+01 0.2150970312204D+04-0.2108390131389D+03 0.2154544125743D+00
-0.4188576661610D+02 0.1049524906421D+02
0.4000000000000D+01 0.2067604561920D+04 0.3962372553863D+01-0.5432160192830D-03
0.1729598129613D+02 0.6750000000000D+01
0.4750000000000D+01 0.2070600000000D+04 0.2644106905510D+01 0.5389739555718D+00
-0.5474937283435D+01 0.0000000000000D+00
0.5349200000000D+01 0.2071200000000D+04-0.2607161664746D+01-0.9302773305132D+01
0.1138020803486D+02 0.0000000000000D+00

0.6000000000000D+01 0.2068697416811D+04 0.2609281790329D-02-0.9706726502872D-48
0.2583188972426D-02 0.1000000000000D+03
0.7000000000000D+01 0.2309400000000D+04-0.8136366842700D+03 0.2068700000000D+04
-0.4336808689942D-18 0.0000000000000D+00
0.2700000000000D+01 0.1904000000000D+04-0.1295240608903D+04-0.1168497849105D+03
-0.4338039822860D+04 0.0000000000000D+00
0.2888300000000D+01 0.1627000000000D+04-0.1800686440345D+04-0.2567408480844D+04
-0.1319199596731D+05 0.0000000000000D+00
0.2956100000000D+01 0.1489000000000D+04-0.2330751514574D+04-0.5250660460595D+04
0.9115630206225D+04 0.0000000000000D+00
0.3064900000000D+01 0.1186936925244D+04-0.3009243764993D+04-0.2416081075647D+01
0.4791558315949D+00 0.4847074468085D+02
0.3158900000000D+01 0.6740000000000D+03-0.1416129939089D+05-0.2702623987004D+06
0.7584411087370D+07 0.0000000000000D+00
0.3200000000000D+01 0.1620000000000D+03 0.2058120594635D+04 0.6648954883724D+06
-0.6337158005302D+07 0.0000000000000D+00
0.3250000000000D+01 0.1135000000000D+04 0.2101898439211D+05-0.2856782124229D+06
0.1569970491615D+07 0.0000000000000D+00
0.3300000000000D+01 0.1849069058392D+04-0.3704424912521D+02 0.1021968554026D-04
-0.1810690686118D+03 0.2354342394386D+02
0.3652700000000D+01 0.1836000000000D+04-0.3501698525616D+02-0.9843479940074D+00
0.3294618497650D+02 0.0000000000000D+00
0.4000000000000D+01 0.1825100000000D+04-0.2377907472968D+02 0.3334228213301D+02
-0.1474542850977D+02 0.0000000000000D+00
0.4750000000000D+01 0.1819800000000D+04 0.1351437859604D+01 0.1650679860352D+00
-0.7758063492430D+01 0.0000000000000D+00
0.5349200000000D+01 0.1819000000000D+04-0.6807124910379D+01-0.1378082694796D+02
0.1910757657988D+02 0.0000000000000D+00
0.6000000000000D+01 0.1813995295039D+04 0.4752485973053D-02-0.1767960889473D-47
0.4704961113322D-02 0.1000000000000D+03
0.7000000000000D+01 0.1904000000000D+04-0.1295240608903D+04 0.1814000000000D+04
0.0000000000000D+00 0.0000000000000D+00
0.2700000000000D+01 0.1792910000000D+01 0.1746289849965D-10-0.1211026520746D-54
0.3288263787485D-13 0.5310674455656D+03
0.2888300000000D+01 0.1792910000000D+01-0.2333851930339D-08 0.5870767744501D-53
-0.4220467808591D-12 0.1474926253687D+04
0.2956100000000D+01 0.1792909999594D+01 0.6039477665158D-06-0.2429325991915D-50
0.4063885776591D-09 0.9191176470588D+03
0.3064900000000D+01 0.1792910048745D+01-0.1112739113266D-03 0.3872972013559D-48
-0.4874520527349D-07 0.1063829787234D+04
0.3158900000000D+01 0.1792910000000D+01 0.1096426061997D-01 0.5891241771968D+01
-0.4021770330290D+02 0.0000000000000D+00
0.3200000000000D+01 0.1800393677935D+01 0.2997000024305D+00 0.2907005349086D-04
0.9725201187458D-04 0.1215000000000D+03
0.3250000000000D+01 0.1828020000000D+01 0.1835566272819D+01 0.9330717743273D+02
-0.7903700577822D+03 0.0000000000000D+00
0.3300000000000D+01 0.2667712184103D+01-0.3379485710295D+00 0.5939764063045D-03
-0.6140361605091D+00 0.9072866458747D+01
0.3652700000000D+01 0.2538537541198D+01 0.1072574122665D-02-0.1814891332203D-13
-0.4775411982805D-03 0.4245781744889D+02
0.4000000000000D+01 0.2538910000000D+01 0.1070628947353D-02-0.4163356931307D-04
-0.1350051147322D-02 0.0000000000000D+00
0.4750000000000D+01 0.2539120000000D+01-0.1270032717722D-02-0.3079248650787D-02
0.8676228154210D-02 0.0000000000000D+00
0.5349200000000D+01 0.2539120000000D+01 0.4385151226996D-02 0.1251713907922D-01
-0.1598233037045D-01 0.0000000000000D+00
0.6000000000000D+01 0.2542873737353D+01-0.3775103583038D-05 0.1404367214625D-50
-0.3737352547208D-05 0.1000000000000D+03
0.7000000000000D+01 0.1792910000000D+01-0.3231174267785D-26 0.2542870000000D+01
0.0000000000000D+00 0.0000000000000D+00
0.2700000000000D+01 0.1798080000000D+01-0.1828354705930D-10 0.1267937300475D-54

-0.3442791911266D-13 0.5310674455656D+03
0.2888300000000D+01 0.1798080000000D+01 0.2443528581389D-08-0.6146657631489D-53
0.4418803773735D-12 0.1474926253687D+04
0.2956100000000D+01 0.1798080000425D+01-0.6323295878213D-06 0.2543489335200D-50
-0.4254863351659D-09 0.9191176470588D+03
0.3064900000000D+01 0.1798079948964D+01 0.1165030990847D-03-0.4054977818869D-48
0.5103592937625D-07 0.1063829787234D+04
0.3158900000000D+01 0.1798080000000D+01-0.1147951326749D-01-0.6168093812011D+01
0.4711475132585D+02 0.0000000000000D+00
0.3200000000000D+01 0.1790508616569D+01-0.2776778923237D+00-0.3278073322747D-04
-0.1583583586377D-04 0.1215000000000D+03
0.3250000000000D+01 0.1762370000000D+01-0.2009617760315D+01-0.1052158845746D+03
0.7492847956188D+03 0.0000000000000D+00
0.3300000000000D+01 0.1492510000000D+01-0.6911570250638D+01 0.7176834768173D+01
0.2940450242684D+01 0.0000000000000D+00
0.3652700000000D+01 0.5159442427623D-01-0.3452115055516D-01 0.1691325075931D-09
0.2499557555464D-01 0.2869138712928D+02
0.4000000000000D+01 0.3961000000000D-01-0.3445172476894D-01 0.1963861576910D-02
0.1759791748668D-01 0.0000000000000D+00
0.4750000000000D+01 0.2230000000000D-01-0.1809446644800D-02 0.4155917592194D-01
-0.6659571623139D-01 0.0000000000000D+00
0.5349200000000D+01 0.2181000000000D-01-0.2373663595087D-01-0.7815328357559D-01
0.9700649511411D-01 0.0000000000000D+00
0.6000000000000D+01-0.2224843949704D-04 0.2247317120913D-04-0.8360190432009D-50
0.2224843949704D-04 0.1000000000000D+03
0.7000000000000D+01 0.1798080000000D+01 0.3231174267785D-26 0.1297019200483D-20
0.3388131789017D-20 0.0000000000000D+00
0.2700000000000D+01 0.1792910000000D+01-0.4710473934997D-11 0.3266644916177D-55
-0.8869822419599D-14 0.5310674455656D+03
0.2888300000000D+01 0.1792910000000D+01 0.6295374554358D-09-0.1583591546354D-53
0.1138436646485D-12 0.1474926253687D+04
0.2956100000000D+01 0.1792910000110D+01-0.1629099666547D-06 0.6552908020826D-51
-0.1096199924990D-09 0.9191176470588D+03
0.3064900000000D+01 0.1792909986851D+01 0.3001522679406D-04-0.1044702500058D-48
0.1314862013894D-07 0.1063829787234D+04
0.3158900000000D+01 0.1792910000000D+01-0.2957519558849D-02-0.1589114247682D+01
0.5126307293029D+01 0.0000000000000D+00
0.3200000000000D+01 0.1790690507604D+01-0.8228089554042D-01-0.2542035223518D-03
0.2369591853166D-04 0.9112500000000D+02
0.3250000000000D+01 0.1762370000000D+01-0.2288140171631D+01-0.1005023969620D+03
0.7189840078925D+03 0.0000000000000D+00
0.3300000000000D+01 0.1486580000000D+01-0.6945999808638D+01 0.7345204221869D+01
0.2708395171554D+01 0.0000000000000D+00
0.3652700000000D+01 0.4384782973421D-01-0.3326590882992D-01 0.2163793554857D-09
0.2543217004941D-01 0.2833717247337D+02
0.4000000000000D+01 0.3230000000000D-01-0.3318898618753D-01 0.2176278951634D-02
0.1506982573120D-01 0.0000000000000D+00
0.4750000000000D+01 0.1499000000000D-01-0.4494236838674D-02 0.3608338684683D-01
-0.5002602069741D-01 0.0000000000000D+00
0.5349200000000D+01 0.1449000000000D-01-0.1513602950499D-01-0.5384338795884D-01
0.6590253453827D-01 0.0000000000000D+00
0.6000000000000D+01-0.1496494409474D-04 0.1511610514620D-04-0.5623305960537D-50
0.1496494409474D-04 0.1000000000000D+03
0.7000000000000D+01 0.1792910000000D+01-0.8077935669463D-27 0.5293955920339D-21
0.0000000000000D+00 0.0000000000000D+00
0.2700000000000D+01-0.1798080000000D+01-0.1740724343820D-10 0.1207166923472D-54
-0.3277783939412D-13 0.5310674455656D+03
0.2888300000000D+01-0.1798080000000D+01 0.2326413836794D-08-0.5852057337427D-53
0.4207016983387D-12 0.1474926253687D+04
0.2956100000000D+01-0.1798079999595D+01-0.6020229571800D-06 0.2421583618140D-50
-0.4050933985532D-09 0.9191176470588D+03

0.3064900000000D+01-0.1798080048590D+01 0.1109192762484D-03-0.3860628673452D-48
0.4858985206020D-07 0.1063829787234D+04
0.3158900000000D+01-0.1798080000000D+01-0.1092931701662D-01-0.5872466113226D+01
0.4002826257451D+02 0.0000000000000D+00
0.3200000000000D+01-0.1805543057110D+01-0.2991814269920D+00-0.2897012912435D-04
-0.9797276071815D-04 0.1215000000000D+03
0.3250000000000D+01-0.1833100000000D+01-0.1829768070579D+01-0.9298646457249D+02
0.7879565196813D+03 0.0000000000000D+00
0.3300000000000D+01-0.2670998311217D+01 0.3492531524528D+00-0.6295017584525D-03
0.6130678129753D+00 0.9072866458747D+01
0.3652700000000D+01-0.2538614447506D+01-0.1139921267387D-02 0.2136880590310D-13
0.3444475058831D-03 0.4776504463000D+02
0.4000000000000D+01-0.2539010000000D+01-0.1123579936066D-02 0.3903212915887D-03
0.1097787793851D-02 0.0000000000000D+00
0.4750000000000D+01-0.2539170000000D+01 0.1314418903441D-02 0.2860343827753D-02
-0.8434524083487D-02 0.0000000000000D+00
0.5349200000000D+01-0.2539170000000D+01-0.4342755828472D-02-0.1230155666472D-01
0.1573237108641D-01 0.0000000000000D+00
0.6000000000000D+01-0.2542873682865D+01 0.3720065584726D-05-0.1383892661096D-50
0.3682864928878D-05 0.1000000000000D+03
0.7000000000000D+01-0.1798080000000D+01 0.0000000000000D+00-0.2542870000000D+01
0.0000000000000D+00 0.0000000000000D+00
0.2700000000000D+01-0.2734200000000D+00-0.1335418046648D-15 0.9260929225498D-60
-0.2514592181839D-18 0.5310674455656D+03
0.2888300000000D+01-0.2734200000000D+00 0.1784736930151D-13-0.4489477616699D-58
0.3227464717270D-17 0.1474926253687D+04
0.2956100000000D+01-0.2734200000000D+00-0.4618493010506D-11 0.1857747596059D-55
-0.3107723729646D-14 0.9191176470588D+03
0.3064900000000D+01-0.2734200000004D+00 0.8509308423775D-09-0.2961728673607D-53
0.3727630141760D-12 0.1063829787234D+04
0.3158900000000D+01-0.2734199999848D+00-0.1208778022549D-06 0.1842500596149D-51
-0.1522023636086D-10 0.2433090024331D+04
0.3200000000000D+01-0.2734205090374D+00 0.1339696414844D-03 0.2691813360913D-09
0.5087682282776D-06 0.2400000000000D+03
0.3250000000000D+01-0.2733700000000D+00 0.1064850142151D-01 0.1261743993660D+01
-0.2454280441802D+01 0.0000000000000D+00
0.3300000000000D+01-0.2699900000000D+00 0.1184157974740D+00 0.8936019273896D+00
-0.1863180652670D+01 0.0000000000000D+00
0.3652700000000D+01-0.1977104195969D+00 0.4752788376174D-02-0.4689522144276D-13
-0.1099580403004D-02 0.4427683198963D+02
0.4000000000000D+01-0.1960600000000D+00 0.4742899375143D-02-0.2193789706667D-03
-0.5034130631958D-02 0.0000000000000D+00
0.4750000000000D+01-0.1947191829141D+00-0.4924863584427D-02 0.2227409763308D-09
-0.3081730861305D-04 0.2737399866489D+02
0.5349200000000D+01-0.1947100000000D+00 0.7610658456516D-01 0.1109077374993D+01
-0.1177475017531D+01 0.0000000000000D+00
0.6000000000000D+01 0.2379649698470D-03-0.2403686564111D-03 0.8941896641034D-49
-0.2379649698470D-03 0.1000000000000D+03
0.7000000000000D+01-0.2734200000000D+00 0.0000000000000D+00 0.2117582368136D-20
-0.2710505431214D-19 0.0000000000000D+00
0.2700000000000D+01-0.5097192616677D-14 0.2706953062495D-11-0.1877232436047D-55
0.5097192616677D-14 0.5310674455656D+03
0.2888300000000D+01 0.6542217639214D-13-0.3617742856586D-09 0.9100375132735D-54
-0.6542217639214D-13 0.1474926253687D+04
0.2956100000000D+01-0.6299497216220D-10 0.9361895198493D-07-0.3765738794017D-51
0.6299497216220D-10 0.9191176470588D+03
0.3064900000000D+01 0.7556075682374D-08-0.1724875484142D-04 0.6003558603555D-49
-0.7556075682374D-08 0.1063829787234D+04
0.3158900000000D+01 0.0000000000000D+00 0.1699588350915D-02 0.9132112264663D+00
-0.6517085191564D+01 0.0000000000000D+00
0.3200000000000D+01 0.1145143914736D-02 0.4441325457264D-01 0.4654874584757D-05

0.1020121067954D-04 0.1215000000000D+03
0.3250000000000D+01 0.5390000000000D-02 0.2903470468239D+00 0.1494082418947D+02
-0.1127953025190D+03 0.0000000000000D+00
0.3300000000000D+01 0.4316000000000D-01 0.9384646968785D+00-0.1978471188383D+01
0.1359773417272D+01 0.0000000000000D+00
0.3652700000000D+01 0.1898531555280D+00 0.2098665091787D-02-0.4693206350641D-09
-0.2153155058652D-02 0.2238986467031D+02
0.4000000000000D+01 0.1905800000000D+00 0.2093860013816D-02-0.5067989381346D-03
0.1059067077661D-03 0.0000000000000D+00
0.4750000000000D+01 0.1919101944060D+00 0.1502161570657D-02-0.1809236841658D-16
-0.1944059945040D-06 0.5255807743658D+02
0.5349200000000D+01 0.1919500000000D+00-0.4371300684958D-01-0.1188211161569D+01
0.1232599892498D+01 0.0000000000000D+00
0.6000000000000D+01-0.2436633737087D-03 0.2461246199077D-03-0.9156022856261D-49
0.2436633737087D-03 0.1000000000000D+03
0.7000000000000D+01 0.0000000000000D+00 0.0000000000000D+00 0.2964615315390D-20
0.0000000000000D+00 0.0000000000000D+00
tdelay exponential potential
0, 1, 1, 0, 0, 0, 1
1.0, 1.0, 0.05d-6, 1.0d-5, 1.0d-6
1, 0, 0.0

TEST OUTPUT FOR FCINT

initial state of quasidiscrete state
symmetric cn stretch n1= 1
asymmetric cn stretch n2= 0
cc stretch n3= 0

npts = 3500 pstart= 2.2500 step size = 0.0050
number of step per node asymp = 20.00
nflag = 1 alpha = 1
total energy (cm-1) is 60975.6100
vinf (cm-1) is 52178.3600
reduced mass (rmass) is 13.00892500

internal coordinates of quasidiscrete state
qao (a) = 1.2031 qbo = 1.2031 po = 2.6560
asymptotic values of fragments
qcn(x) = 1.1718 qcn(a) = 1.2327

frequencies
symetric cn stretch (cm-1) = 2082.30
asymmetric stretch = 1725.60000
cc stretch = 896.00000
cn(x) = 2068.70000
cn(a) = 1814.00000

q = a(i)*(ta-da)+b(i)*(tb-db)+c(i)*(p-dp)

a(i) =	-1.70540810	-1.79806434	0.56985460	2.54284700	0.00000000
b(i) =	-1.70540810	1.79806434	0.56985460	0.00000000	-2.54284700
c(i) =	1.14332400	0.00000000	3.42079680	0.00000000	0.00000000

electronic potential fit to form v = vo + aexp(-gamma*p)
vo = 0.000000 a = 0.240000D+10 gamma = 4.886000
xal = 0.000000 nal = 1 naaa = 1 daaa = 0.000000D+00

p	q(x)	q(a)	w(4)	w(5)	a(4)	a(5)	b(4)	b(5)	c(4)	c(5)	
2.7000	1.1397	1.1397	2309.40	1904.00	1.792910	1.798080	1.792910	-1.798080	-0.273420	0.000000	
2.8883	1.1635	1.1635	2162.70	1627.00	1.792910	1.798080	1.792910	-1.798080	-0.273420	0.000000	
2.9561	1.1704	1.1704	2117.40	1489.00	1.792910	1.798080	1.792910	-1.798080	-0.273420	0.000000	
3.0649	1.1801	1.1801	2054.20	1185.00	1.792910	1.798080	1.792910	-1.798080	-0.273420	0.000000	
3.1589	1.1865	1.1865	2006.80	674.00	1.792910	1.798080	1.792910	-1.798080	-0.273420	0.000000	
3.2000	1.1842	1.1933	1990.70	162.00	1.800520	1.790460	1.790460	-1.805670	-0.273420	0.001160	
3.2500	1.1748	1.2052	1955.20	1135.00	1.828020	1.762370	1.762370	-1.833100	-0.273370	0.005390	
3.3000	1.1672	1.2148	1947.60	1668.00	2.054270	1.492510	1.486580	-2.058560	-0.269990	0.043160	
3.6527	1.1669	1.2287	2109.30	1836.00	2.538060	0.076590	0.069280	-2.538270	-0.198810	0.187700	
4.0000	1.1702	1.2312	2084.90	1825.10	2.538910	0.039610	0.032300	-2.539010	-0.196060	0.190580	
4.7500	1.1717	1.2322	2070.60	1819.80	2.539120	0.022300	0.014990	-2.539170	-0.194750	0.191910	
5.3492	1.1716	1.2321	2071.20	1819.00	2.539120	0.021810	0.014490	-2.539170	-0.194710	0.191950	
6.0000	1.1718	1.2327	2068.70	1814.00	2.542870	0.000000	0.000000	-2.542870	0.000000	0.000000	
7.0000	1.1718	1.2327	2068.70	1814.00	2.542870	0.000000	0.000000	-2.542870	0.000000	0.000000	

1
spline coefficients from exp-spline program

qa
0.27000000D+01 0.11397490D+01 0.15844272D+00-0.17954175D-02 0.17464249D-02 0.68826341D+01
0.28883000D+01 0.11635000D+01 0.10999252D+00-0.14409576D+00 0.33655313D+00 0.00000000D+00
0.29561000D+01 0.11704000D+01 0.95094381D-01-0.75640851D-01 0.19343333D+00 0.00000000D+00
0.30649000D+01 0.11801166D+01 0.88848708D-01-0.51441412D-04 0.34809317D-04 0.38776596D+02
0.31589000D+01 0.11865000D+01 0.12449928D-01-0.14798751D+01-0.44921189D+01 0.00000000D+00
0.32000000D+01 0.11842000D+01-0.13196020D+00-0.20337534D+01 0.18259148D+02 0.00000000D+00

0.32500000D+01 0.11748000D+01-0.19839193D+00 0.70511880D+00 0.44543956D+01 0.00000000D+00
0.33000000D+01 0.11631864D+01 0.10521158D-01 0.23560303D-09 0.40136015D-02 0.26159360D+02
0.36527000D+01 0.11669000D+01 0.10573457D-01 0.95432495D-03-0.11632017D-01 0.00000000D+00
0.40000000D+01 0.11773158D+01-0.74557473D-02 0.52994908D-03-0.76457531D-02 0.17714700D+01
0.47500000D+01 0.11717000D+01-0.32395448D-03-0.37647184D-04 0.50028733D-03 0.00000000D+00
0.53492000D+01 0.11716000D+01 0.16979959D-03 0.86166933D-03-0.99933719D-03 0.00000000D+00
0.60000000D+01 0.11718002D+01-0.22008820D-06 0.00000000D+00-0.21788732D-06 0.10000000D+03
0.70000000D+01 0.11397000D+01 0.13406551D+00 0.11718000D+01-0.26469780D-22 0.00000000D+00
qb
0.27000000D+01 0.11397130D+01 0.14298418D+00-0.42116629D-03 0.40815980D-03 0.10754116D+02
0.28883000D+01 0.11638294D+01 0.96914429D-01 0.36774866D-05-0.33309624D-03 0.33185841D+02
0.29561000D+01 0.11704006D+01 0.10851283D+00-0.22453848D-03 0.22397951D-03 0.20680147D+02
0.30649000D+01 0.11883197D+01-0.23110847D+00 0.99821379D-02-0.18201806D-01 0.10469681D+02
0.31589000D+01 0.11865000D+01 0.11973708D+00 0.10909096D+01 0.51897478D+00 0.00000000D+00
0.32000000D+01 0.11933000D+01 0.21203982D+00 0.11548992D+01-0.12713913D+02 0.00000000D+00
0.32500000D+01 0.12052000D+01 0.23217540D+00-0.75218771D+00-0.10264043D+01 0.00000000D+00
0.33000000D+01 0.12256599D+01 0.89711330D-02-0.10458020D-06-0.10859778D-01 0.12918202D+02
0.36527000D+01 0.12287000D+01 0.10315708D-01-0.10346659D-01 0.39469793D-02 0.00000000D+00
0.40000000D+01 0.12312000D+01 0.45571408D-02-0.62343012D-02 0.25811884D-02 0.00000000D+00
0.47500000D+01 0.12322000D+01-0.43855565D-03-0.42662734D-03 0.14686403D-02 0.00000000D+00
0.53492000D+01 0.12321000D+01 0.63207884D-03 0.22134005D-02-0.27166642D-02 0.00000000D+00
0.60000000D+01 0.12327006D+01-0.62436659D-06 0.00000000D+00-0.61812292D-06 0.10000000D+03
0.70000000D+01 0.11397000D+01 0.13406551D+00 0.12327000D+01 0.10587912D-21 0.00000000D+00
wa
0.27000000D+01 0.23091185D+04-0.11988546D+04 0.50513337D+02-0.50231857D+02 0.38236856D+01
0.28883000D+01 0.21627000D+04-0.70855587D+03 0.57989432D+03 0.23873765D+03 0.00000000D+00
0.29561000D+01 0.21174000D+04-0.62662988D+03 0.62845356D+03-0.19115806D+04 0.00000000D+00
0.30649000D+01 0.20541842D+04-0.60649403D+03 0.10258142D+01-0.10100581D+01 0.23936170D+02
0.31589000D+01 0.20049597D+04-0.19518251D+03-0.68551026D+00 0.25257847D+01 0.54744526D+02
0.32000000D+01 0.19907000D+04-0.56581149D+03-0.93471151D+04 0.12926690D+06 0.00000000D+00
0.32500000D+01 0.19552000D+04-0.53102127D+03 0.10042919D+05-0.49249877D+05 0.00000000D+00
0.33000000D+01 0.19476000D+04 0.10389658D+03 0.26554378D+04-0.46786083D+04 0.00000000D+00
0.36527000D+01 0.21509703D+04-0.21083901D+03 0.21545441D+00-0.41885767D+02 0.10495249D+02
0.40000000D+01 0.20676046D+04 0.39623726D+01-0.54321602D-03 0.17295981D+02 0.67500000D+01
0.47500000D+01 0.20706000D+04 0.26441069D+01 0.53897396D+00-0.54749373D+01 0.00000000D+00
0.53492000D+01 0.20712000D+04-0.26071617D+01-0.93027733D+01 0.11380208D+02 0.00000000D+00
0.60000000D+01 0.20686974D+04 0.26092818D-02 0.00000000D+00 0.25831890D-02 0.10000000D+03
0.70000000D+01 0.23094000D+04-0.81363668D+03 0.20687000D+04-0.43368087D-18 0.00000000D+00
wb
0.27000000D+01 0.19040000D+04-0.12952406D+04-0.11684978D+03-0.43380398D+04 0.00000000D+00
0.28883000D+01 0.16270000D+04-0.18006864D+04-0.25674085D+04-0.13191996D+05 0.00000000D+00
0.29561000D+01 0.14890000D+04-0.23307515D+04-0.52506605D+04 0.91156302D+04 0.00000000D+00
0.30649000D+01 0.11869369D+04-0.30092438D+04-0.24160811D+01 0.47915583D+00 0.48470745D+02
0.31589000D+01 0.67400000D+03-0.14161299D+05-0.27026240D+06 0.75844111D+07 0.00000000D+00
0.32000000D+01 0.16200000D+03 0.20581206D+04 0.66489549D+06-0.63371580D+07 0.00000000D+00
0.32500000D+01 0.11350000D+04 0.21018984D+05-0.28567821D+06 0.15699705D+07 0.00000000D+00
0.33000000D+01 0.18490691D+04-0.37044249D+02 0.10219686D-04-0.18106907D+03 0.23543424D+02
0.36527000D+01 0.18360000D+04-0.35016985D+02-0.98434799D+00 0.32946185D+02 0.00000000D+00
0.40000000D+01 0.18251000D+04-0.23779075D+02 0.33342282D+02-0.14745429D+02 0.00000000D+00
0.47500000D+01 0.18198000D+04 0.13514379D+01 0.16506799D+00-0.77580635D+01 0.00000000D+00
0.53492000D+01 0.18190000D+04-0.68071249D+01-0.13780827D+02 0.19107577D+02 0.00000000D+00
0.60000000D+01 0.18139953D+04 0.47524860D-02 0.00000000D+00 0.47049611D-02 0.10000000D+03
0.70000000D+01 0.19040000D+04-0.12952406D+04 0.18140000D+04 0.00000000D+00 0.00000000D+00
a4
0.27000000D+01 0.17929100D+01 0.17462898D-10 0.00000000D+00 0.32882638D-13 0.53106745D+03
0.28883000D+01 0.17929100D+01-0.23338519D-08 0.00000000D+00-0.42204678D-12 0.14749263D+04
0.29561000D+01 0.17929100D+01 0.60394777D-06 0.00000000D+00 0.40638858D-09 0.91911765D+03
0.30649000D+01 0.17929100D+01-0.11127391D-03 0.00000000D+00-0.48745205D-07 0.10638298D+04
0.31589000D+01 0.17929100D+01 0.10964261D-01 0.58912418D+01-0.40217703D+02 0.00000000D+00
0.32000000D+01 0.18003937D+01 0.29970000D+00 0.29070053D-04 0.97252012D-04 0.12150000D+03
0.32500000D+01 0.18280200D+01 0.18355663D+01 0.93307177D+02-0.79037006D+03 0.00000000D+00

0.33000000D+01 0.26677122D+01-0.33794857D+00 0.59397641D-03-0.61403616D+00 0.90728665D+01
0.36527000D+01 0.25385375D+01 0.10725741D-02-0.18148913D-13-0.47754120D-03 0.42457817D+02
0.40000000D+01 0.25389100D+01 0.10706289D-02-0.41633569D-04-0.13500511D-02 0.00000000D+00
0.47500000D+01 0.25391200D+01-0.12700327D-02-0.30792487D-02 0.86762282D-02 0.00000000D+00
0.53492000D+01 0.25391200D+01 0.43851512D-02 0.12517139D-01-0.15982330D-01 0.00000000D+00
0.60000000D+01 0.25428737D+01-0.37751036D-05 0.00000000D+00-0.37373525D-05 0.10000000D+03
0.70000000D+01 0.17929100D+01-0.32311743D-26 0.25428700D+01 0.00000000D+00 0.00000000D+00
a5
0.27000000D+01 0.17980800D+01-0.18283547D-10 0.00000000D+00-0.34427919D-13 0.53106745D+03
0.28883000D+01 0.17980800D+01 0.24435286D-08 0.00000000D+00 0.44188038D-12 0.14749263D+04
0.29561000D+01 0.17980800D+01-0.63232959D-06 0.00000000D+00-0.42548634D-09 0.91911765D+03
0.30649000D+01 0.17980799D+01 0.11650310D-03 0.00000000D+00 0.51035929D-07 0.10638298D+04
0.31589000D+01 0.17980800D+01-0.11479513D-01-0.61680938D+01 0.47114751D+02 0.00000000D+00
0.32000000D+01 0.17905086D+01-0.27767789D+00-0.32780733D-04-0.15835836D-04 0.12150000D+03
0.32500000D+01 0.17623700D+01-0.20096178D+01-0.10521588D+03 0.74928480D+03 0.00000000D+00
0.33000000D+01 0.14925100D+01-0.69115703D+01 0.71768348D+01 0.29404502D+01 0.00000000D+00
0.36527000D+01 0.51594424D-01-0.34521151D-01 0.16913251D-09 0.24995576D-01 0.28691387D+02
0.40000000D+01 0.39610000D-01-0.34451725D-01 0.19638616D-02 0.17597917D-01 0.00000000D+00
0.47500000D+01 0.22300000D-01-0.18094466D-02 0.41559176D-01-0.66595716D-01 0.00000000D+00
0.53492000D+01 0.21810000D-01-0.23736636D-01-0.78153284D-01 0.97006495D-01 0.00000000D+00
0.60000000D+01-0.22248439D-04 0.22473171D-04 0.00000000D+00 0.22248439D-04 0.10000000D+03
0.70000000D+01 0.17980800D+01 0.32311743D-26 0.12970192D-20 0.33881318D-20 0.00000000D+00
b4
0.27000000D+01 0.17929100D+01-0.47104739D-11 0.00000000D+00-0.88698224D-14 0.53106745D+03
0.28883000D+01 0.17929100D+01 0.62953746D-09 0.00000000D+00 0.11384366D-12 0.14749263D+04
0.29561000D+01 0.17929100D+01-0.16290997D-06 0.00000000D+00-0.10961999D-09 0.91911765D+03
0.30649000D+01 0.17929100D+01 0.30015227D-04 0.00000000D+00 0.13148620D-07 0.10638298D+04
0.31589000D+01 0.17929100D+01-0.29575196D-02-0.15891142D+01 0.51263073D+01 0.00000000D+00
0.32000000D+01 0.17906905D+01-0.82280896D-01-0.25420352D-03 0.23695919D-04 0.91125000D+02
0.32500000D+01 0.17623700D+01-0.22881402D+01-0.10050240D+03 0.71898401D+03 0.00000000D+00
0.33000000D+01 0.14865800D+01-0.69459998D+01 0.73452042D+01 0.27083952D+01 0.00000000D+00
0.36527000D+01 0.43847830D-01-0.33265909D-01 0.21637936D-09 0.25432170D-01 0.28337172D+02
0.40000000D+01 0.32300000D-01-0.33188986D-01 0.21762790D-02 0.15069826D-01 0.00000000D+00
0.47500000D+01 0.14990000D-01-0.44942368D-02 0.36083387D-01-0.50026021D-01 0.00000000D+00
0.53492000D+01 0.14490000D-01-0.15136030D-01-0.53843388D-01 0.65902535D-01 0.00000000D+00
0.60000000D+01-0.14964944D-04 0.15116105D-04 0.00000000D+00 0.14964944D-04 0.10000000D+03
0.70000000D+01 0.17929100D+01-0.80779357D-27 0.52939559D-21 0.00000000D+00 0.00000000D+00
b5
0.27000000D+01-0.17980800D+01-0.17407243D-10 0.00000000D+00-0.32777839D-13 0.53106745D+03
0.28883000D+01-0.17980800D+01 0.23264138D-08 0.00000000D+00 0.42070170D-12 0.14749263D+04
0.29561000D+01-0.17980800D+01-0.60202296D-06 0.00000000D+00-0.40509340D-09 0.91911765D+03
0.30649000D+01-0.17980800D+01 0.11091928D-03 0.00000000D+00 0.48589852D-07 0.10638298D+04
0.31589000D+01-0.17980800D+01-0.10929317D-01-0.58724661D+01 0.40028263D+02 0.00000000D+00
0.32000000D+01-0.18055431D+01-0.29918143D+00-0.28970129D-04-0.97972761D-04 0.12150000D+03
0.32500000D+01-0.18331000D+01-0.18297681D+01-0.92986465D+02 0.78795652D+03 0.00000000D+00
0.33000000D+01-0.26709983D+01 0.34925315D+00-0.62950176D-03 0.61306781D+00 0.90728665D+01
0.36527000D+01-0.25386144D+01-0.11399213D-02 0.21368806D-13 0.34444751D-03 0.47765045D+02
0.40000000D+01-0.25390100D+01-0.11235799D-02 0.39032129D-03 0.10977878D-02 0.00000000D+00
0.47500000D+01-0.25391700D+01 0.13144189D-02 0.28603438D-02-0.84345241D-02 0.00000000D+00
0.53492000D+01-0.25391700D+01-0.43427558D-02-0.12301557D-01 0.15732371D-01 0.00000000D+00
0.60000000D+01-0.25428737D+01 0.37200656D-05 0.00000000D+00 0.36828649D-05 0.10000000D+03
0.70000000D+01-0.17980800D+01 0.00000000D+00-0.25428700D+01 0.00000000D+00 0.00000000D+00
c4
0.27000000D+01-0.27342000D+00-0.13354180D-15 0.00000000D+00-0.25145922D-18 0.53106745D+03
0.28883000D+01-0.27342000D+00 0.17847369D-13 0.00000000D+00 0.32274647D-17 0.14749263D+04
0.29561000D+01-0.27342000D+00-0.46184930D-11 0.00000000D+00-0.31077237D-14 0.91911765D+03
0.30649000D+01-0.27342000D+00 0.85093084D-09 0.00000000D+00 0.37276301D-12 0.10638298D+04
0.31589000D+01-0.27342000D+00-0.12087780D-06 0.00000000D+00-0.15220236D-10 0.24330900D+04
0.32000000D+01-0.27342051D+00 0.13396964D-03 0.26918134D-09 0.50876823D-06 0.24000000D+03
0.32500000D+01-0.27337000D+00 0.10648501D-01 0.12617440D+01-0.24542804D+01 0.00000000D+00
0.33000000D+01-0.26999000D+00 0.11841580D+00 0.89360193D+00-0.18631807D+01 0.00000000D+00

```
0.36527000D+01-0.19771042D+00 0.47527884D-02-0.46895221D-13-0.10995804D-02 0.44276832D+02
0.40000000D+01-0.19606000D+00 0.47428994D-02-0.21937897D-03-0.50341306D-02 0.00000000D+00
0.47500000D+01-0.19471918D+00-0.49248636D-02 0.22274098D-09-0.30817309D-04 0.27373999D+02
0.53492000D+01-0.19471000D+00 0.76106585D-01 0.11090774D+01-0.11774750D+01 0.00000000D+00
0.60000000D+01 0.23796497D-03-0.24036866D-03 0.00000000D+00-0.23796497D-03 0.10000000D+03
0.70000000D+01-0.27342000D+00 0.00000000D+00 0.21175824D-20-0.27105054D-19 0.00000000D+00
 c5
0.27000000D+01-0.50971926D-14 0.27069531D-11 0.00000000D+00 0.50971926D-14 0.53106745D+03
0.28883000D+01 0.65422176D-13-0.36177429D-09 0.00000000D+00-0.65422176D-13 0.14749263D+04
0.29561000D+01-0.62994972D-10 0.93618952D-07 0.00000000D+00 0.62994972D-10 0.91911765D+03
0.30649000D+01 0.75560757D-08-0.17248755D-04 0.00000000D+00-0.75560757D-08 0.10638298D+04
0.31589000D+01 0.00000000D+00 0.16995884D-02 0.91321123D+00-0.65170852D+01 0.00000000D+00
0.32000000D+01 0.11451439D-02 0.44413255D-01 0.46548746D-05 0.10201211D-04 0.12150000D+03
0.32500000D+01 0.53900000D-02 0.29034705D+00 0.14940824D+02-0.11279530D+03 0.00000000D+00
0.33000000D+01 0.43160000D-01 0.93846470D+00-0.19784712D+01 0.13597734D+01 0.00000000D+00
0.36527000D+01 0.18985316D+00 0.20986651D-02-0.46932064D-09-0.21531551D-02 0.22389865D+02
0.40000000D+01 0.19058000D+00 0.20938600D-02-0.50679894D-03 0.10590671D-03 0.00000000D+00
0.47500000D+01 0.19191019D+00 0.15021616D-02-0.18092368D-16-0.19440599D-06 0.52558077D+02
0.53492000D+01 0.19195000D+00-0.43713007D-01-0.11882112D+01 0.12325999D+01 0.00000000D+00
0.60000000D+01-0.24366337D-03 0.24612462D-03 0.00000000D+00 0.24366337D-03 0.10000000D+03
0.70000000D+01 0.00000000D+00 0.00000000D+00 0.29646153D-20 0.00000000D+00 0.00000000D+00
1
^^^^^^^^^^^^^^^^^^^^^^^^^^^^^^^^^^^^^^^^^^^^^^^^^^^^^^^^^^^^^^^^^^^^^^^^^^^^^^^^
 vo =    0.000000 a = 0.240000D+10gamma =    4.88600

::::::::::::::::::::::::::::::::::::::::::::::::::::::::::::::::::::::::::::::::

 asymptotic spacing of nodes of trans.wf =     0.043192
 integration step size =      0.00500000
0 at  l =  0   e = 6855.9000(1/cm)  nodx =  393  phase shift =,-0.19815194E+03
for  x =19.6984   cor3 = 0.00000000E+00
 dwdq( 0 0) =     0.1050077128D-04
 time for evaluation of eff osc =      0.0000
 time for evaluation of tr wf and integral =      0.0000

::::::::::::::::::::::::::::::::::::::::::::::::::::::::::::::::::::::::::::::::

 asymptotic spacing of nodes of trans.wf =     0.050366
 integration step size =      0.00500000
0 at  l =  0   e = 5041.9000(1/cm)  nodx =  337  phase shift =,-0.17200947E+03
for  x =19.7307   cor3 = 0.00000000E+00
 dwdq( 0 1) =     0.1410955695D-08
 time for evaluation of eff osc =      0.0000
 time for evaluation of tr wf and integral =      0.0000

::::::::::::::::::::::::::::::::::::::::::::::::::::::::::::::::::::::::::::::::

 asymptotic spacing of nodes of trans.wf =     0.062948
 integration step size =      0.00500000
0 at  l =  0   e = 3227.9000(1/cm)  nodx =  269  phase shift =,-0.13716691E+03
for  x =19.6808   cor3 = 0.00000000E+00
 dwdq( 0 2) =     0.2499699629D-09
 time for evaluation of eff osc =      0.0000
 time for evaluation of tr wf and integral =      0.0000

::::::::::::::::::::::::::::::::::::::::::::::::::::::::::::::::::::::::::::::::

 asymptotic spacing of nodes of trans.wf =     0.095111
 integration step size =      0.00500000
0 at  l =  0   e = 1413.9000(1/cm)  nodx =   36  phase shift =,-0.91886565E+02
for  x = 6.2057   cor3 = 0.80703569E-04
```

```
 dwdq( 0 3) =     0.2278760303D-16
 time for evaluation of eff osc =       0.0000
 time for evaluation of tr wf and integral =       0.0000

::::::::::::::::::::::::::::::::::::::::::::::::::::::::::::::::::::::::::::::

 asymptotic spacing of nodes of trans.wf =     0.051689
 integration step size =       0.00500000
0 at  l =  0  e = 4787.2000(1/cm)  nodx =  328  phase shift =,-0.16867542E+03
for  x =19.7287    cor3 = 0.00000000E+00
 dwdq( 1 0) =     0.5130046004D-05
 time for evaluation of eff osc =       0.0000
 time for evaluation of tr wf and integral =       0.0000

::::::::::::::::::::::::::::::::::::::::::::::::::::::::::::::::::::::::::::::

 asymptotic spacing of nodes of trans.wf =     0.065588
 integration step size =       0.00500000
0 at  l =  0  e = 2973.2000(1/cm)  nodx =   64  phase shift =,-0.13314861E+03
for  x = 7.6331    cor3 =-0.11644406E-09
 dwdq( 1 1) =     0.9773303394D-10
 time for evaluation of eff osc =       0.0000
 time for evaluation of tr wf and integral =       0.0000

::::::::::::::::::::::::::::::::::::::::::::::::::::::::::::::::::::::::::::::

 asymptotic spacing of nodes of trans.wf =     0.105041
 integration step size =       0.00525206
0 at  l =  0  e = 1159.2000(1/cm)  nodx =   32  phase shift =,-0.84480058E+02
for  x = 6.1858    cor3 = 0.84494326E-04
 dwdq( 1 2) =     0.4255766595D-14
 time for evaluation of eff osc =       0.0000
 time for evaluation of tr wf and integral =       0.0000

::::::::::::::::::::::::::::::::::::::::::::::::::::::::::::::::::::::::::::::

 asymptotic spacing of nodes of trans.wf =     0.068592
 integration step size =       0.00500000
0 at  l =  0  e = 2718.5000(1/cm)  nodx =   49  phase shift =,-0.13272400E+03
for  x = 6.2587    cor3 = 0.20623985E-04
 dwdq( 2 0) =     0.6858260603D-08
 time for evaluation of eff osc =       0.0000
 time for evaluation of tr wf and integral =       0.0000

::::::::::::::::::::::::::::::::::::::::::::::::::::::::::::::::::::::::::::::

 asymptotic spacing of nodes of trans.wf =     0.118914
 integration step size =       0.00594572
0 at  l =  0  e =  904.5000(1/cm)  nodx =   28  phase shift =,-0.76571157E+02
for  x = 6.2278    cor3 = 0.72967977E-04
 dwdq( 2 1) =     0.1056519934D-13
 time for evaluation of eff osc =       0.0000
 time for evaluation of tr wf and integral =       0.0000

::::::::::::::::::::::::::::::::::::::::::::::::::::::::::::::::::::::::::::::

 asymptotic spacing of nodes of trans.wf =     0.140297
 integration step size =       0.00701486
0 at  l =  0  e =  649.8000(1/cm)  nodx =   23  phase shift =,-0.67871700E+02
for  x = 6.2577    cor3 = 0.65453244E-04
 dwdq( 3 0) =     0.3993720838D-16
```

time for evaluation of eff osc = 0.0000
time for evaluation of tr wf and integral = 0.0000

	v=0	v=1	v=2	v=3	v=4	v=5	v=6
cn(x)	0.67153530	0.32802617	0.00043852	0.00000000	0.00000000	0.00000000	0.00000000
cn(a)	0.99988755	0.00009647	0.00001598	0.00000000	0.00000000	0.00000000	0.00000000

total time of this run = 0.0000

```
0001        program rotbas
0002   c
0003   c    Program ROTBAS calculates bound state wave functions for potential
0004   c    written in terms of SF spherical Harmonics in a rigid rotor basis set
0005   c    for diatom-diatom case. Potential here is read in cartesian coordinates
0006   c    including only quadratic terms. The wave function obtained can be mapped
0007   c    onto final asymptotic states
0008   c
0009   c
0010   c    INPUT -- NAMELIST FORMAT
0011   c
0012   c
0013   c    $CNTRL
0014   c
0015   c     iprint > 0  debug printing
0016   c
0017   c     ipdis = 0    distributions not calculated
0018   c
0019   c          = 1    rotational dist. and temps. calculated
0020   c
0021   c     nrts -   number of roots to be printed out
0022   c
0023   c     nroot -  which root to calculate distributions for
0024   c
0025   c     ltype  = 0   l=0,lmax
0026   c
0027   c          = l   l=l
0028   c
0029   c     jtype  =  0  j12=0,j12max
0030   c
0031   c          =  j12  j12=j12
0032   c
0033   c
0034   c     jpar   should be set to zero presently
0035   c
0036   c
0037   c    $DATA
0038   c
0039   c      jtot = total angular momentum
0040   c
0041   c      j1max,j2max,j12max,lmax  -   self explanatory
0042   c
0043   c       kst  -  electronic angular momentum for diatom 2
0044   c
0045   c       ifdim  - dimension of cartesian force constant matrix
0046   c
0047   c       m1,m2    mass of atoms   m2-m1-m1-m2  for BAAB 4-atom molecule
0048   c              which breaks into 2 BA fragments  in amu's
0049   c
0050   c       r1,r2     BA bond lengths   in au's
0051   c
0052   c         r      interfragment distance between cm of each diatom
0053   c
0054   c
0055   c    $FCM
0056   c
0057   c          cartesian force constant matrix elements
0058   c
0059   c
0060   c     $ENGRY
0061   c
```

```
0062   c          nstate  -  number of photon energies to calculate distributions
0063   c
0064   c          brot1,brot2 --  asymptotic rotational constants of each diatom
0065   c
0066   c          freq1,freq2 --  asymptotic vibrational frequencies
0067   c
0068   c          eav(istate) -- available energy for each photon energy
0069   c
0070   c
0071   c
0072   c       $VIB
0073   c
0074   c            title and then square of transition matrix elements for
0075   c            vibrational problem obtained from FCINT
0076   c
0077   c
0078         implicit real*8 (a-h,o-z)
0079         real*8 m1,m2,mf,ms
0080         character*5 fwd,word
0081         common /io/ ir,iw,ip,it
0082        .      /pflag/ iprint,ipdis,nrts,nroot,ltype,jtype,jpar
0083        .      /amom/jtot,j1max,j2max,lmax,j12max,kst
0084        .      /mass4/ m1,m2,mf,ms,bx,ba,bs
0085        .      /coef4/vsf(0:2,0:2,0:2),v0
0086        .      /junk/pi,wave
0087         dimension ac(0:2,-2:2,0:2,-2:2,0:2,-2:2),
0088        .          fx(4,4),fy(4,4)
0089         namelist /cntrl/ iprint,ipdis,nrts,nroot,ltype,jtype,jpar
0090         namelist /data/ jtot,j1max,j2max,lmax,j12max,kst,ifdim
0091         namelist /mass/ m1,m2,r1,r2,r
0092   c
0093         data fwd /' $fcm'/
0094         logical pflg,all
0095   c
0096         xx(i) = sqrt( ( 2.0e0*float(i) + 1.0e+00 )/4.0e+00/pi )
0097         y(i) = float(2*i+1)
0098         z(i) = float(i)
0099   c
0100         ir = 4
0101         iw = 6
0102         ip = 7
0103         it = 8
0104         iprint = 0
0105         pi = 3.14159265358793e0
0106   c
0107   c
0108         call second(tim)
0109   c
0110         wave = 27.212e0*8065.479e0
0111         rmass = 1822.8873e0
0112         jpar = -2
0113         nroot = 1
0114         rewind ir
0115         read (ir,cntrl)
0116         if (iprint .ne. 0) pflg = .true.
0117         if (iprint .gt. 1) all = .true.
0118   c
0119   c     atom coordinates are read in B1,B2,A3,A4
0120   c
0121   c
0122         rewind ir
```

```
0123        read (ir,data)
0124        rewind ir
0125        read (ir,mass)
0126  c
0127        rewind ir
0128       10 read (ir,1010,end = 120) word
0129        if (word .ne. fwd) go to 10
0130        do 20 i = 1,ifdim
0131       20 read (ir,1050) (fx(i,j),j = 1,ifdim)
0132        do 30 i = 1,ifdim
0133       30 read (ir,1050) (fy(i,j),j = 1,ifdim)
0134  c
0135  c     calculate reduced masses
0136  c
0137        mf = m2*m1/(m2+m1)
0138        ms = (m2+m1)**2/(2*(m2+m1))
0139  c
0140        bx = 0.5e0/mf/r1/r1/rmass*wave
0141        ba = 0.5e0/mf/r2/r2/rmass*wave
0142        bs = 0.5e0/ms/r/r/rmass*wave
0143  c
0144        write (iw,1030) iprint,nrts,nroot,ltype,jtype,jpar
0145        write (iw,1040) jtot,j1max,j2max,lmax,j12max,kst,ifdim
0146        write (iw,1060)
0147        write (iw,1050) ((fx(i,j),j = 1,ifdim),i = 1,ifdim)
0148        write (iw,1070)
0149        write (iw,1050) ((fy(i,j),j = 1,ifdim),i = 1,ifdim)
0150        write (iw,1080) m2,m1,mf,ms
0151        write (iw,1090) r1,r2,r
0152        write (iw,1100) bx,ba,bs
0153  c
0154        if (ipdis.eq.0) then
0155        write (it,1030) iprint,nrts,nroot,ltype,jtype,jpar
0156        write (it,1040) jtot,j1max,j2max,lmax,j12max,kst,ifdim
0157        write (it,1060)
0158        write (it,1050) ((fx(i,j),j = 1,ifdim),i = 1,ifdim)
0159        write (it,1070)
0160        write (it,1050) ((fy(i,j),j = 1,ifdim),i = 1,ifdim)
0161        write (it,1080) m2,m1,mf,ms
0162        write (it,1090) r1,r2,r
0163        write (it,1100) bx,ba,bs
0164        endif
0165  c
0166        m1 = m1*rmass
0167        m2 = m2*rmass
0168        mf = mf*rmass
0169        ms = ms*rmass
0170        bx = bx/wave
0171        ba = ba/wave
0172        bs = bs/wave
0173  c
0174        vx1 = (fx(2,2)*m2**2-2.0e0*fx(2,4)*m1*m2+fx(4,4)*m1**2)*r2**2/(m2+
0175       . m1)**2/2.0e0
0176        vx2 = (fx(1,2)*m2**2-fx(2,3)*m1*m2-fx(1,4)*m1*m2+fx(3,4)*m1**2)*
0177       . r1*r2/(m2+m1)**2
0178        vx3 = (fx(2,4)*m2-fx(2,3)*m2+fx(2,2)*m2-fx(1,2)*m2-fx(4,4)*m1+fx
0179       . (3,4)*m1-fx(2,4)*m1+fx(1,4)*m1)*r*r2/(m2+m1)/2.0e0
0180        vx4 = (fx(1,1)*m2**2-2.0e0*fx(1,3)*m1*m2+fx(3,3)*m1**2)*r1**2/(m2+
0181       . m1)**2/2.0e0
0182        vx5 = (fx(1,4)*m2-fx(1,3)*m2+fx(1,2)*m2-fx(1,1)*m2-fx(3,4)*m1+fx
0183       . (3,3)*m1-fx(2,3)*m1+fx(1,3)*m1)*r*r1/(m2+m1)/2.0e0
```

```
0184        vx6 = (fx(4,4)-2.0e0*fx(3,4)+fx(3,3)+2*fx(2,4)-2*fx(2,3)+fx(2,2)-
0185       . 2.e0*fx(1,4)+2*fx(1,3)-2.e0*fx(1,2)+fx(1,1))*r**2/8.0e0
0186        vy1 = (fy(2,2)*m2**2-2.e0*fy(2,4)*m1*m2+fy(4,4)*m1**2)*r2**2/(m2+
0187       . m1)**2/2.0e0
0188        vy2 = (fy(1,2)*m2**2-fy(2,3)*m1*m2-fy(1,4)*m1*m2+fy(3,4)*m1**2)*
0189       . r1*r2/(m2+m1)**2
0190        vy3 = (fy(2,4)*m2-fy(2,3)*m2+fy(2,2)*m2-fy(1,2)*m2-fy(4,4)*m1+fy
0191       . (3,4)*m1-fy(2,4)*m1+fy(1,4)*m1)*r*r2/(m2+m1)/2.0e0
0192        vy4 = (fy(1,1)*m2**2-2.0e0*fy(1,3)*m1*m2+fy(3,3)*m1**2)*r1**2/(m2+
0193       . m1)**2/2.0e0
0194        vy5 = (fy(1,4)*m2-fy(1,3)*m2+fy(1,2)*m2-fy(1,1)*m2-fy(3,4)*m1+fy
0195       . (3,3)*m1-fy(2,3)*m1+fy(1,3)*m1)*r*r1/(m2+m1)/2.0e0
0196        vy6 = (fy(4,4)-2.e0*fy(3,4)+fy(3,3)+2.e0*fy(2,4)-2*fy(2,3)+fy(2,2)
0197       . -2.e0*fy(1,4)+2*fy(1,3)-2.e0*fy(1,2)+fy(1,1))*r**2/8.0e0
0198    c
0199        const = - 8.0e0 * pi**(3.0e0/2.0e0) / 3.0e0
0200    c
0201        ac(2,0,0,0,0,0) = (-8.0e+00)*pi**(3.0e+00/2.0e+00)*(vy4+vx4)/
0202       . (3.0e+00*sqrt(5.e+00))
0203        ac(2,2,0,0,0,0) = -4*sqrt(2.e+00)*pi**(3.0e+00/2.0e+00)*(vy4-vx4)/
0204       . sqrt(15.e+00)
0205        ac(2,-2,0,0,0,0) = -4*sqrt(2.e+00)*pi**(3.0e+00/2.0e+00)*(vy4-vx4)
0206       . /sqrt(15.e+00)
0207        ac(0,0,2,0,0,0) = (-8.0e+00)*pi**(3.0e+00/2.0e+00)*(vy1+vx1)/
0208       . (3.0e+00*sqrt(5.e+00))
0209        ac(0,0,2,2,0,0) = -4*sqrt(2.e+00)*pi**(3.0e+00/2.0e+00)*(vy1-vx1)/
0210       . sqrt(15.e+00)
0211        ac(0,0,2,-2,0,0) = -4*sqrt(2.e+00)*pi**(3.0e+00/2.0e+00)*(vy1-vx1)
0212       . /sqrt(15.e+00)
0213        ac(0,0,0,0,2,0) = (-8.0e+00)*pi**(3.0e+00/2.0e+00)*(vy6+vx6)/
0214       . (3.0e+00*sqrt(5.e+00))
0215        ac(0,0,0,0,2,2) = -4*sqrt(2.e+00)*pi**(3.0e+00/2.0e+00)*(vy6-vx6)/
0216       . sqrt(15.e+00)
0217        ac(0,0,0,0,2,-2) = -4*sqrt(2.e+00)*pi**(3.0e+00/2.0e+00)*(vy6-vx6)
0218       . /sqrt(15.e+00)
0219        ac(1,1,1,1,0,0) = const* (vy2-vx2)
0220        ac(1,-1,1,-1,0,0) = const* (vy2-vx2)
0221        ac(1,-1,1,1,0,0) = const* (vy2+vx2)
0222        ac(1,1,1,-1,0,0) = const* (vy2+vx2)
0223        ac(1,1,0,0,1,1) = const* (vy5-vx5)
0224        ac(1,-1,0,0,1,-1) = const* (vy5-vx5)
0225        ac(1,-1,0,0,1,1) = const* (vy5+vx5)
0226        ac(1,1,0,0,1,-1) = const* (vy5+vx5)
0227        ac(0,0,1,1,1,1) = const* (vy3-vx3)
0228        ac(0,0,1,-1,1,-1) = const* (vy3-vx3)
0229        ac(0,0,1,-1,1,1) = const* (vy3+vx3)
0230        ac(0,0,1,1,1,-1) = const* (vy3+vx3)
0231        ac(0,0,0,0,0,0) = - const* (vy6+vy4+vy1+vx6+vx4+vx1)
0232    c
0233        do 80 l1 = 0,2
0234         do 70 l2 = 0,2
0235          do 60 l3 = abs(l1-l2),min(2,(l1+l2))
0236          do 50 n1 = -l1,l1
0237           do 40 n2 = -l2,l2
0238    c
0239            n3 = n1+n2
0240            if (abs(n3) .gt. l3) go to 40
0241            vsf(l1,l2,l3) = vsf(l1,l2,l3) +clgdn(l1,n1,l2,n2,l3,n3)*ac(l1,
0242       .     n1,l2,n2,l3,n3)/(2.0e0*l3+1.0e0)
0243    c
0244      40    continue
```

```
0245      50   continue
0246           if (vsf(l1,l2,l3) .ne. 0.0e+00) write (iw,1000) l1,l2,l3,vsf(l1,
0247         .  l2,l3)
0248      60   continue
0249      70  continue
0250      80 continue
0251    c
0252         do 110 l1 = 0,1
0253          do 100 l2 = 0,1
0254           do 90 l3 = abs(l1-l2),min(1,(l1+l2))
0255           v0 = v0 + vsf(l1,l2,l3)*clgdn(l1,0,l2,0,l3,0)*xx(l1)*xx(l2)*xx
0256         .  (l3)
0257      90   continue
0258     100  continue
0259     110 continue
0260         write (iw,1020) v0
0261    c
0262         call driver
0263    c
0264         call second(time)
0265         time = (time-tim)
0266         write (iw,1110) time
0267    c
0268     120 stop
0269    c
0270     1000 format(3i5,d20.10)
0271     1010 format(a5)
0272     1020 format(' *** v0 = ',e16.8,' ***')
0273     1030 format(' iprint = ',i5,' **** NUMBER OF ROOTS PRINTED = ',i5,
0274        . /,' NROOT = ',i5,' LTYPE =',i5,' JTYPE =',i5,' JPAR = ',i5)
0275     1040 format(' jtot =',i5,' j1max =',i5,' j2max =',i5,/,
0276        . ' lmax =',i5,' j12max =',i5,' Electronic Angular
0277        . Momentum of Diatom 2 =',i3,/,' ifdim =',i5)
0278     1050 format(4f12.8)
0279     1060 format(' FORCE CONSTANT MATRIX  X- CARTESIANS')
0280     1070 format(' FORCE CONSTANT MATRIX  Y- CARTESIANS')
0281     1080 format(' mass of atom a of abba = ',f12.5,/,
0282        .        ' mass of atom b of abba = ',f12.5,/,
0283        .        ' reduced mass of fragment ab = ',f12.5,/,
0284        .        ' reduced mass of system      = ',f12.5)
0285     1090 format(' Diatom A bond length in a.u.     = ',f14.8,/,
0286        .        ' Diatom B bond length in a.u.     = ',f14.8,/,
0287        .        ' Interfragment Separation in a.u. = ',f14.8,//)
0288     1100 format(' Rotational constants :    diatom A  = ',f14.8,/,
0289        .        '                              diatom B  = ',f14.8,/,
0290        .        '                         diatom-diatom    = ',f14.8,//)
0291     1110 format(/,' Total Time of This Run = ',f14.3,' Seconds')
0292         end

0001          subroutine driver
0002         implicit real*8 (a-h,o-z)
0003         common /io/ ir,iw,ip,it
0004        .       /pflag/ iprint,ipdis,nrts,nroot,ltype,jtype,jpar
0005        .       /amom/jtot,j1max,j2max,lmax,j12max,kst
0006        .       /junk/pi,wave
0007         common /big/ a(31375),
0008        .         b(1500),
0009        .         root(250),
0010        .         vect(250,250)
0011    c
0012         logical pflg,all
```

```
0013        if (iprint .ne. 0) pflg = .true.
0014        if (iprint .gt. 1) all = .true.
0015    c
0016    c     linear 4-atom
0017    c
0018        if (ltype .eq. 0) then
0019        ll = 0
0020        lm = lmax
0021        else
0022        ll = lmax
0023        lm = lmax
0024        endif
0025        do 160  l = ll,lm
0026        if (jtype .eq. 0) then
0027        j12l = abs(jtot-l)
0028        j12m = min((jtot+l),(j1max+j2max))
0029        else
0030        j12l = j12max
0031        j12m = j12max
0032        endif
0033         do 150 j12 = j12l,j12m
0034         if((j12 .gt. (jtot+l)).or.(j12 .lt. abs(jtot-l))) goto 150
0035         if (jpar .ge. 0) then
0036         npar = 1
0037         ipar = jpar
0038         istep = 2
0039         else
0040         npar = 0
0041         ipar = 0
0042         endif
0043         if (jpar.lt.-1) then
0044         istep = 1
0045         npar = 1
0046         else
0047         istep = 2
0048         endif
0049      40  continue
0050    c
0051        call second(t0)
0052    c
0053        write (iw,1000) jtot,j12,l,ipar,kst
0054        nx = 0
0055        nlen = 0
0056        do 80 j1p = 0,j1max
0057             j2lp = max((abs(j12-j1p)+ipar),abs(kst))
0058             j2mp = min((j12+j1p),j2max)
0059         do 70 j2p = j2lp,j2mp,istep
0060         nx = nx+1
0061         if (nx .gt. 250) go to 170
0062         nxp = 0
0063         do 60 j1 = 0,j1max
0064             j2l = max((abs(j12-j1)+ipar),abs(kst))
0065             j2m = min((j12+j1),j2max)
0066          do 50 j2 = j2l,j2m,istep
0067          nxp = nxp+1
0068          if (nxp .gt. nx) go to 70
0069          nlen = nlen+1
0070          a(nlen) = cupl4(j1p,j2p,j12,l,j1,j2,j12,l)
0071      50   continue
0072      60  continue
0073      70  continue
```

```
0074      80  continue
0075    c
0076          if (all) write (ip,1010) (a(j),j = 1,nlen)
0077          if (pflg) write (iw,1020)
0078          if (pflg) call prtr(a,nx)
0079    c
0080          call second(t1)
0081          time0 = (t1-t0)
0082          write (iw,1100) time0,nx
0083    c
0084          njx = 250
0085          if (nx .le. 0) go to 140
0086          call givens(nx,nx,njx,a,b,root,vect)
0087    c
0088          do 90 i = 1,nx
0089           root(i) = root(i)*wave
0090       90  continue
0091    c
0092          iroot = nx-nroot+1
0093          write (iw,1030) nroot,root(iroot)
0094    c
0095          k = 0
0096    c
0097          do 110 j1 = 0,j1max
0098            j2l = max((abs(j12-j1)+ipar),abs(kst))
0099            j2m = min(j12+j1,j2max)
0100           do 100 j2 = j2l,j2m,istep
0101           k = k+1
0102           write (iw,1050) j1,j2,j12,l,k,vect(k,iroot)
0103      100   continue
0104      110  continue
0105          write (iw,1090)
0106    c
0107          call second(t2)
0108          time = (t2-t1)
0109    c
0110          irts = nx-nrts+1
0111          write (iw,1110) time
0112          write (iw,1070) nrts
0113          write (iw,1060) (root(k),k = nx,irts,-1)
0114          write (iw,1120)
0115          if(ipdis.eq.0)call rotdis(nx,j12,l,ipar,istep)
0116          root0 = root(nx)
0117          do 130 j = nx,irts,-5
0118           jmin = max( (j-4),1 )
0119           do 120 i = j,jmin,-1
0120            root1 = root0
0121            root0 = root(i)
0122            root(i) = root(i) - root1
0123      120   continue
0124          write (iw,1060) (root(k),k = j,jmin,-1)
0125      130  continue
0126      140  npar = npar + 1
0127          ipar = ipar + 1
0128          if (npar .lt. 2) go to 40
0129      150  continue
0130      160 continue
0131    c
0132         return
0133    c
0134      170 write (iw,1080)
```

```
0135        stop
0136     1000 format(/,' JTOT =',i4,'  J12 =',i4,'  L =',i4,'   PARITY =',i4,
0137       . '  KST =',i4)
0138     1010 format(5e16.8)
0139     1020 format(' MATRIX TO BE SOLVED ',/)
0140     1030 format(/,' ROOT NUMBER ',i5,9x,f16.8,
0141       ./,'   j1   j2  j12    l   ',
0142       ./,' ---- ---- ---- -----',8x,'--------------')
0143     1040 format(/,' ROOT NUMBER ',i5,9x,f16.8,/)
0144     1050 format(4i5,3x,i4,3x,e16.8)
0145     1060 format(5f16.3)
0146     1070 format(' LOWEST',i4,' ROOTS OF MATRIX ')
0147     1080 format(' **** STOP **** Order of Matrix Greater Than 250')
0148     1090 format(//)
0149     1100 format(/,' Time Spent Calculating Matrix = ',f14.3,' Seconds',/,
0150       .  '   Order of Matrix is ',i6)
0151     1110 format(/,' Time Spent in Givens Diagonalization = ',
0152       .        f14.3,' Seconds',//)
0153     1120 format(' Root Differences [ root(i+1) - root(i) ] ')
0154        end

0001      real*8 function cupl4(j1p,j2p,j12p,lp,j1,j2,j12,l)
0002        implicit real*8 (a-h,o-z)
0003        real*8 m2,m1,mf,ms
0004        common /io/ ir,iw,ip
0005       .       /pflag/ iprint,ipdis,nrts,nroot,ltype,jtype,jpar
0006       .       /amom/jtot,j1max,j2max,lmax,j12max,kst
0007       .       /coef4/vsf(0:2,0:2,0:2),v0
0008       .       /mass4/ m1,m2,mf,ms,bx,ba,bs
0009       .       /junk/pi,wave
0010        logical pflg,all
0011     c
0012        z(i) = float(i*(i+1))
0013     c
0014        if (iprint .ne. 0) pflg = .true.
0015        if (iprint .gt. 1) all = .true.
0016     c
0017        delts = delt(j1p,j1)*delt(j2p,j2)*delt(lp,l)*delt(j12,j12p)
0018     c
0019        sum = (z(j1p)*bx+z(j2p)*ba+z(lp)*bs-v0)*delts +
0020       .vsf(0,0,0)*roteam(j1p,j2p,j12p,lp,j1,j2,j12,l,0,0,0,jtot,kst)+
0021       .vsf(1,1,0)*roteam(j1p,j2p,j12p,lp,j1,j2,j12,l,1,1,0,jtot,kst)
0022        cupl4 = sum
0023        return
0024        end

0001      real*8 function rotrot(j1,j2,j12,l,j1p,j2p,j12p,lp,lm1,
0002       .lm2,lm,jtot)
0003        implicit real*8 (a-h,o-z)
0004        real*8 ninej
0005     c
0006     c    matrix elements (j1,j2,j12,l,jtot/y(lm1,m1)*y(lm2,m2)*y(lm,m)/
0007     c           j1p,j2p,j12p,lp,jtot)  -  summed over m1,m2,m.
0008     c    reference - g. englot and h. rabitz, phys rev a 10, 2187 (1974).
0009     c    see also, h. klar, z. phys. 228, 59 (1969).
0010     c
0011     c    const is factor (4.*pi)**(-3/2)
0012        data const/2.244839025e-2/
0013        data eps/1.e-10/
0014     c    statement function definition . . .
0015        z(i) = float(2*i+1)
```

```
0016   c
0017         rotrot = 0.e0
0018         a = threej(lm,lp,l)
0019         if (abs(a) .le. eps)  go to 10
0020         b =  threej(lm1,j1p,j1)
0021         if (abs(b) .le. eps)  go to 10
0022         c =  threej(lm2,j2p,j2)
0023         if (abs(c) .le. eps)  go to 10
0024         d =  sixj(lp,l,j12p,j12,lm,jtot)
0025         if (abs(d) .le. eps)  go to 10
0026         e =  ninej(j12p,j2p,j1p,j12,j2,j1,lm,lm2,lm1)
0027         if (abs(e) .le. eps)  go to 10
0028         f = a*b*c*d*e*const*z(lm)*sqrt(z(lm1)*z(lm2)*z(j1)*z(j2)*z(j12)*z
0029        . (l)*z(j1p)*z(j2p)*z(j12p)*z(lp)) * parity(j1+j2+j12p+jtot)
0030         rotrot = f
0031   c
0032      10 return
0033         end

0001         function roteam(j1,j2,j12,l,j1p,j2p,j12p,lp,lm1,
0002        .lm2,lm,jtot,kkk)
0003         implicit real*8 (a-h,o-z)
0004         real*8 ninej
0005   c
0006   c     matrix elements (j1,j2,j12,l,kkk,jtot/y(lm1,m1)*y(lm2,m2)*y(lm,m)/
0007   c           j1p,j2p,j12p,lp,kkk,jtot)  -  summed over m1,m2,m.
0008   c     reference - g. englot and h. rabitz, phys rev a 10, 2187 (1974).
0009   c     see also, h. klar, z. phys. 228, 59 (1969).
0010   c     of one Diatom   ie.,   y(j2,m2) ->> sqrt([j2]/4pi) * D(j2,m2,k)
0011   c           will give same results as ROTROT for k==0....
0012   c
0013   c     const is factor (4.*pi)**(-3/2)
0014         data const/2.244839025e-2/
0015         data eps/1.e-10/
0016   c     statement function definition . . .
0017         z(i) = float(2*i+1)
0018         x(i) = float(i)
0019   c
0020         roteam = 0.e+00
0021         a = threej(lm,lp,l)
0022         if (abs(a) .le. eps)  go to 10
0023         b =  threej(lm1,j1p,j1)
0024         if (abs(b) .le. eps)  go to 10
0025         if (kkk.eq.0) then
0026         c =  threej(lm2,j2p,j2)
0027         else
0028         c =  thrj(x(lm2),x(j2p),x(j2),x(0),x(-kkk),x(kkk))
0029         endif
0030         if (abs(c) .le. eps)  go to 10
0031         d =  sixj(lp,l,j12p,j12,lm,jtot)
0032         if (abs(d) .le. eps)  go to 10
0033         e =  ninej(j12p,j2p,j1p,j12,j2,j1,lm,lm2,lm1)
0034         if (abs(e) .le. eps)  go to 10
0035         f = a*b*c*d*e*const*z(lm)*sqrt(z(lm1)*z(lm2)*z(j1)*z(j2)*z(j12)*
0036        .z(l)*z(j1p)*z(j2p)*z(j12p)*z(lp))*parity(j1+j2p+j12p+jtot+lm2-kkk)
0037         roteam = f
0038   c
0039      10 return
0040         end

0001         subroutine rotdis(nx,j12,l,ipar,istep)
```

```
0002        implicit real*8 (a-h,o-z)
0003        character*5 wvib,word
0004        common /io/ ir,iw,ip,it
0005       .       /pflag/ iprint,ipdis,nrts,nroot,ltype,jtype,jpar
0006       .       /amom/jtot,j1max,j2max,lmax,j12max,kst
0007       .       /junk/pi,wave
0008        common /big/ a(31375),
0009       .          b(1500),
0010       .          root(250),
0011       .          vect(250,250)
0012        dimension xj1(0:6,0:200),xj2(0:6,0:200),
0013       .          eav(5),hvib(0:6,0:6,5),xj1tot(0:6),xj2tot(0:6),
0014       .          temp(0:6),title(5,80),j1high(0:6),j2high(0:6)
0015    c
0016        data wvib /' $vib'/
0017    c
0018        x(i) = float(2*i+1)
0019        z(i) = float(i*(i+1))
0020    c
0021        namelist /engry/ eav,brot1,brot2,freq1,freq2,nstate
0022    c
0023        tol = 1.0e-8
0024        iroot = nx - nroot + 1
0025    c
0026        rewind ir
0027        read (ir,engry)
0028    c
0029        rewind ir
0030      1 read (ir,2000,end=9999) word
0031        if (word .ne. wvib) goto 1
0032        do 5 istate = 1,nstate
0033        read (ir,2020) (title(istate,m),m=1,80)
0034        do 6 j = 0,6
0035      6 read (ir,2010) (hvib(i,j,istate),i=0,6)
0036      5 continue
0037    c
0038        write(it,1500) brot1,freq1,brot2,freq2
0039        write (it,2040) nroot,root(iroot)
0040    c
0041        do 80 istate = 1,nstate
0042         write (it,1000) istate,eav(istate),jtot,j12,l,ipar,kst
0043         write (it,2020) (title(istate,m),m=1,80)
0044    c
0045         n1max=0
0046         n2max=0
0047        totxj1 =0.0e+00
0048        totxj2 =0.0e+00
0049        do 150 n=0,6
0050        xj1tot(n) = 0.0e+00
0051        xj2tot(n) = 0.0e+00
0052        do 150 j = 0,j1max
0053        xj1(n,j) = 0.0e+0
0054      150 xj2(n,j) = 0.0e+0
0055    c
0056         do 70 n1 = 0,6
0057          do 70 n2 = 0,6
0058           evib = (n1 + 0.5e+00)*freq1 + (n2 + 0.5e+00)*freq2
0059           if (eav(istate) .lt. evib) go to 70
0060           if (hvib(n1,n2,istate).le.0.0) goto 70
0061           if(n1.gt.n1max)n1max=n1
0062           if(n2.gt.n2max)n2max=n2
```

```
0063          k = 0
0064          do 10 j1 = 0,j1max
0065               j2l = max((abs(j12-j1)+ipar),abs(kst))
0066               j2m = min((j12+j1),j2max)
0067           do 10 j2 = j2l,j2m,istep
0068           k = k + 1
0069           dstate = 0.0e+00
0070           erot = z(j1)*brot1 + z(j2)*brot2
0071           etran = eav(istate) - evib - erot
0072           if (etran .gt. 0.0e+00) dstate = x(j1)*x(j2)*sqrt(etran)
0073           xj1(n1,j1) = xj1(n1,j1)
0074          .              + vect(k,iroot)**2 * dstate * hvib(n1,n2,istate)
0075           xj2(n2,j2) = xj2(n2,j2)
0076          .              + vect(k,iroot)**2 * dstate * hvib(n1,n2,istate)
0077       10 continue
0078       70  continue
0079          do 120 n=0,6
0080          do 121 j=0,j1max
0081          xj1tot(n) = xj1tot(n) + xj1(n,j)
0082      121 xj2tot(n) = xj2tot(n) + xj2(n,j)
0083      120 continue
0084          do 130 n=0,6
0085          totxj1 = totxj1 + xj1tot(n)
0086          totxj2 = totxj2 + xj2tot(n)
0087          do 131 j=0,j1max
0088          if(xj1tot(n).gt.0.0)xj1(n,j)=xj1(n,j)/xj1tot(n)
0089      131 if(xj2tot(n).gt.0.0)xj2(n,j)=xj2(n,j)/xj2tot(n)
0090      130 continue
0091          do 135 n = 0,6
0092          if(totxj1.gt.0.0) xj1tot(n) = xj1tot(n)/totxj1
0093          if(totxj2.gt.0.0) xj2tot(n) = xj2tot(n)/totxj2
0094      135 continue
0095          do 136 n1=0,n1max
0096          do 136 j1=0,j1max
0097      136 if(xj1(n1,j1).gt.tol)j1high(n1)=j1
0098          do 137 n2=0,n2max
0099          do 137 j2=0,j2max
0100      137 if(xj2(n2,j2).gt.tol)j2high(n2)=j2
0101          write(it,1010)
0102          jdum = 0
0103          write(it,1020)jdum,(xj1(n1,jdum),n1=0,n1max)
0104          do 100 j1=1,j1max
0105      100 if(xj1(0,j1).gt.tol)write(it,1020) j1,(xj1(n1,j1),n1=0,n1max)
0106          write(it,1040) (xj1tot(n1),n1=0,n1max)
0107          call ls1(xj1,j1high,temp,n1max,brot1)
0108          write(it,1045) (temp(n1),n1=0,n1max)
0109          write(it,1030)
0110          write(it,1020)jdum,(xj2(n2,jdum),n2=0,n2max)
0111          do 110 j2=1,j2max
0112      110 if(xj2(0,j2).gt.tol)write(it,1020) j2,(xj2(n2,j2),n2=0,n2max)
0113          write(it,1040) (xj2tot(n2),n2=0,n2max)
0114          call ls1(xj2,j2high,temp,n2max,brot2)
0115          write(it,1045) (temp(n2),n2=0,n2max)
0116          write(ip,*)' sequence data.'
0117          do 140 n1=0,n1max
0118          write (ip,*) ' "CN(X, v =',n1,')"'
0119          do 141 j1=0,j1max,5
0120      141 write (ip,3000) (xj1(n1,k1),k1=j1,min(j1+4,j1max))
0121      140 continue
0122          do 142 n2=0,n2max
0123          write (ip,*) ' "CN(A, v =',n2,')"'
```

```
      do 143 j2=0,j2max,5
  143 write (ip,3000) (xj2(n2,k2),k2=j2,min(j2+4,j2max))
  142 continue
      write(ip,*) ' eod. '
   80 continue
      return
 9999 stop
 1000 format(/,' ISTATE =',i3,'   AVAILABLE ENERGY =',f15.8,/,
     .' JTOT =',i4,'  j12 =',i4,'  l =',i4,'  PARITY=',i4,'  KST =',i4)
 1010 format(/,'  CN(X 2 SIGMA +) ROTATIONAL DISTRIBUTIONS ',/,
     .3x,'j1',10x,'v=0',14x,'v=1',14x,'v=2',14x,'v=3',14x,'v=4',14x,
     .'v=5',14x,'v=6',/
     .' ----',2x,'  --------',2x,'  --------',
     .2x,'  --------',2x,'  --------',2x,'  --------',
     .2x,'  --------',2x,'  --------')
 1020 format(i5,3x,f15.8,2x,f15.8,2x,f15.8,2x,f15.8,2x,f15.8,2x,
     . f15.8,2x,f15.8)
 1030 format(/,'  CN(A 2 PI) ROTATIONAL DISTRIBUTIONS ',/,
     .3x,'j2',10x,'v=0',14x,'v=1',14x,'v=2',14x,'v=3',14x,'v=4',14x,
     .'v=5',14x,'v=6',/
     .' ----',2x,'  --------',2x,'  --------',
     .2x,'  --------',2x,'  --------',2x,'  --------',
     .2x,'  --------',2x,'  --------')
 1040 format(8x,'  --------',2x,'  --------',
     .2x,'  --------',2x,'  --------',2x,'  --------',
     .2x,'  --------',/,8x,f15.8,2x,f15.8,2x,f15.8,2x,f15.8,
     .2x,f15.8,2x,f15.8,2x,f15.8)
 1045 format('  T(K)  ',f15.8,2x,f15.8,2x,f15.8,2x,f15.8,2x,f15.8,2x,
     . f15.8,2x,f15.8)
 1500 format(' CN (X 2 SIGMA +) Rotational Constant = ',f10.5,
     .      ' Vibrational Frequency = ',f10.5,/,
     .      ' CN (A 2 PI) Rotational Constant = ',f12.5,
     .      ' Vibrational Frequency = ',f10.5)
 2000 format(a5)
 2010 format(7e12.5)
 2020 format(80a1)
 2040 format(/,' ROOT NUMBER ',i5,9x,f16.8,/)
 3000 format(5f15.8)
      end

      subroutine ls1(xj,jhigh,temp,nmax,brot)
c
c  discrete least-squares fit to simple polynomials.
c
      implicit real*8 (a-h,o-z)
      dimension x(200),y(200),a(10,10),c(10),
     . xj(0:6,0:200),jhigh(0:6),temp(0:6)
c
      ndeg = 1
      boltz = 0.6952e+00
      tol = 1.0d-25
c
      do 1000 nvib = 0,nmax
      n = ndeg + 1
      jl = 1
      if(xj(nvib,0).eq.0.0) then
      jm = jhigh(nvib)
      mpt = jm
      ijump = 0
      else
      jm = jhigh(nvib)+1
```

```
0022        mpt = jm
0023        ijump = -1
0024        endif
0025        do 100 jj=jl,jm
0026        j=jj + ijump
0027        x(jj) = float(j*(j+1))
0028        if( xj(nvib,j).lt.tol) then
0029        dum =tol
0030        else
0031        dum = xj(nvib,j)
0032        endif
0033      100 y(jj) = - log(dum/float(2*j+1)) * boltz/brot
0034        do 2 i=1,n
0035        do 1 j=1,n
0036        a(i,j) = 0.
0037        npower = i+j-2
0038        do 1 k=1,mpt
0039        xk = 1.
0040        if (npower.gt.0) xk=x(k)**(npower)
0041      1 a(i,j) = a(i,j) + xk
0042        a(i,n+1) = 0.
0043        npower = i-1
0044        do 2 k=1,mpt
0045        xk = 1.
0046        if (npower.gt.0) xk=x(k)**(npower)
0047      2 a(i,n+1) = a(i,n+1) + y(k)*xk
0048        do 8 i=1,n-1
0049          j = i
0050      4   if (a(j,i).ne.0) goto 5
0051          j = j + 1
0052          if (j.gt.n) stop ' ***** no unique solution ***** '
0053          goto 4
0054      5   if (j.ne.i) then
0055          do 6 k=1,n+1
0056            t = a(j,k)
0057            a(j,k) = a(i,k)
0058      6     a(i,k) = t
0059          end if
0060          do 7 l=i+1,n
0061            a(l,i) = a(l,i)/a(i,i)
0062            do 7 k=i+1,n+1
0063      7     a(l,k) = a(l,k) - a(l,i)*a(i,k)
0064      8 continue
0065        if (a(n,n).eq.0.) stop ' ***** no unique solution ***** '
0066        c(n) = a(n,n+1)/a(n,n)
0067        do 10 i=n-1,1,-1
0068        sum = 0.
0069        do 9 j=i+1,n
0070      9 sum = sum + a(i,j)*c(j)
0071        c(i) = (a(i,n+1) - sum)/a(i,i)
0072     10 continue
0073    c     write(8,*) (i-1,c(i), i=1,n)
0074          temp(nvib)=1.0/c(2)
0075    c
0076     1000 continue
0077          return
0078      113 stop
0079    c
0080          end

0001          real*8 function binom(n,m)
```

```
0002   c
0003   c *** computation of binomial coefficients ***
0004   c
0005         implicit real*8 (a-h,o-z)
0006         fn = n+1
0007         nm = n-m
0008         mnm = min0(nm,m)
0009         f = 0.e0
0010         b = 1.e0
0011         if (mnm) 30,30,10
0012      10 do 20 i = 1,mnm
0013          f = f+1.e0
0014          c = (fn-f)*b
0015      20 b = c/f
0016      30 binom = b
0017         return
0018         end

0001         real*8 function ninej(ix1,iy1,iz1,ix2,iy2,iz2,ix3,iy3,iz3)
0002   c
0003   c     thaddeus' group 9-j routine modified aug. 74 for integer input.
0004   c     see edmonds, ang. momentum in q. m., p 101, eq (6.4.3)
0005   c
0006         implicit real*8 (a-h,o-z)
0007         dimension ie(3),if(3,3)
0008         equivalence(if(1,1),ia1),(if(1,2),ib1),(if(1,3),ic1),
0009        . (if(2,1),ia2),(if(2,2),ib2),(if(2,3),ic2),
0010        . (if(3,1),ia3),(if(3,2),ib3),(if(3,3),ic3)
0011   c     statement function to interface wig w/ sixj routine in scattering.
0012         wig(i1,i2,i3,i4,i5,i6) = sixj(i1,i2,i5,i4,i3,i6)
0013   c
0014         ifmin = ix1+ix2+ix3+iy1+iy2+iy3+iz1+iz2+iz3
0015         is = ifmin
0016         s = 1.e0
0017         if (1,1) = ix1
0018         if (1,2) = iy1
0019         if (1,3) = iz1
0020         if (2,1) = ix2
0021         if (2,2) = iy2
0022         if (2,3) = iz2
0023         if (3,1) = ix3
0024         if (3,2) = iy3
0025         if (3,3) = iz3
0026   c     find smallest element
0027         do 20 i = 1,3
0028          do 10 j = 1,3
0029           if (ifmin .le. if(i,j)) go to 10
0030           im = i
0031           jm = j
0032           ifmin = if(i,j)
0033      10  continue
0034      20 continue
0035   c     interchange columns if smallest element is on anti-diagonal
0036         if ((im+jm) .ne. 4)  go to 40
0037         km = 1
0038         if (km .eq. jm) km = 2
0039         do 30 i = 1,3
0040          ie(i) = if(i,km)
0041          if (i,km) = if(i,jm)
0042      30 if (i,jm) = ie(i)
0043         s = parity(is)
```

```
0044   c     find range of sum over 6-j symbols.
0045        40 ir1 = iabs(ia1-ic3)
0046           ir2 = iabs(ia2-ib3)
0047           ir3 = iabs(ib1-ic2)
0048           igl = max0(ir1,ir2,ir3)
0049           ir1 = ia1+ic3
0050           ir2 = ia2+ib3
0051           ir3 = ib1+ic2
0052           igu = min0(ir1,ir2,ir3)
0053           sum = 0.e0
0054           if (igu .lt. igl)  go to 60
0055           lim = igu-igl+1
0056           ig = igl
0057           do 50 k = 1,lim
0058            igg = ig+ig
0059            sum = sum+parity(igg)*float(igg+1)*wig(ia1,ia2,ia3,ib3,ic3,ig)*
0060          .  wig(ib1,ib2,ib3,ia2,ig,ic2) * wig(ic1,ic2,ic3,ig,ia1,ib1)
0061        50 ig = ig+1
0062           if (abs(sum) .le. 1.e-12)  sum = 0.e0
0063        60 ninej = s*sum
0064           return
0065           end

0001           real*8 function parity(i)
0002           implicit real(a-h,o-z)
0003           parity = 1.e+00
0004           if ((i-2*(i/2)) .ne. 0)  parity = -parity
0005           return
0006           end
0001           real*8 function pbinom(n,m)
0002   c
0003   c *** computation of elog of binomial coefficients ***
0004   c
0005           implicit real*8 (a-h,o-z)
0006           fn = n+1
0007           nm = n-m
0008           mnm = min0(nm,m)
0009           f = 0.e0
0010           b = 0.e0
0011           if (mnm) 30,30,10
0012        10 do 20 i = 1,mnm
0013            f = f+1.e0
0014            c = log(fn-f)+b
0015        20 b = c-log(f)
0016        30 pbinom  = b
0017           return
0018           end

0001           real*8 function sixj(jp,lp,jn,ln,j,l)
0002   c
0003   c *** computation of 6j coefficient from asymmetric expression of racah
0004   c     in yutsis, p. 50, eq. (16.2) with appropriate sign changes
0005   c                          ( 1 2 5 )
0006   c     sixj(1,2,3,4,5,6)  = -       -
0007   c                          ( 4 3 6 )
0008   c
0009   c     statement function for delta associated w/ racah and sixj symbols
0010   c       see e.g. edmunds p. 99.
0011           implicit real*8 (a-h,o-z)
0012           external pbinom
0013           delta(i,j,k) = (-0.5e0)*(pbinom(i+j+k+1,i+j-k)+pbinom(k+k+1,i-j+k)
```

```
0014        . +log(float(k+j-i+1) ) )
0015    c
0016          k1 = jp+lp-j
0017          k2 = jn+ln-j
0018          k3 = jp+jn-l
0019          k4 = lp+ln-l
0020    c
0021    c *** check triangle inequalities
0022    c
0023          if (k1) 160,10,10
0024       10 if (jp+j-lp) 160,20,20
0025       20 if (lp+j-jp) 160,30,30
0026       30 if (k2) 160,40,40
0027       40 if (jn+j-ln) 160,50,50
0028       50 if (ln+j-jn) 160,60,60
0029       60 if (k3) 160,70,70
0030       70 if (jp+l-jn) 160,80,80
0031       80 if (l+jn-jp) 160,90,90
0032       90 if (k4) 160,100,100
0033      100 if (lp+l-ln) 160,110,110
0034      110 if (l+ln-lp) 160,120,120
0035    c
0036    c *** determine limits for sum
0037    c
0038      120 k5 = jp+ln-j-l
0039          k6 = lp+jn-j-l
0040          lmin = max0(0,k5,k6)
0041          lmax = min0(k1,k2,k3,k4)
0042          if (lmax-lmin) 160,130,130
0043    c
0044    c *** determine sign outside omega sum
0045    c
0046      130 k7 = jp+lp+jn+ln
0047          sign = parity(k7)
0048    c
0049    c *** compute deltas
0050    c
0051          delcof = delta(jp,lp,j)+delta(jn,ln,j)+delta(jp,jn,l)+delta(lp,ln,
0052         . l)
0053    c     if (delcof .eq. 0.0) goto 280
0054          l1 = k7+1
0055          l2 = jn+ln+j+1
0056          l3 = ln-jp+j+l+1
0057          l4 = j+l-lp-jn
0058          l5 = ln-jp+lp+jn+1
0059          l6 = jn-jp+l+1
0060          l7 = l+j-jp-ln
0061          l8 = jn+ln-j+1
0062          xsign = -parity(lmin)
0063          sum = 0.e0
0064          lmin = lmin+1
0065          lmax = lmax + 1
0066          termp = 0.e0
0067          do 150 i = lmin,lmax
0068           iz = i-1
0069           xsign = -xsign
0070           term = pbinom(l1-iz,k1-iz)+pbinom(l2,k3-iz)+pbinom(l3+iz,l4+iz)+
0071          .  pbinom(l5,k4-iz)+pbinom(l6+iz,l7+iz)+pbinom(l8,k2-iz)+pbinom(1+
0072          .  iz,iz)
0073           term = exp(term+delcof)
0074           if (term-termp) 150,150,140
```

```
0075      140  termp = term
0076      150 sum = sum+ term*xsign
0077          ratio = abs(sum)/termp
0078          sixj = sign*sum
0079          if (ratio .gt. 0.01e+00) return
0080          continue
0081    c  22 write (6,23) ratio, sixj
0082    c     write (6,24) jp,lp,jn,ln,j,l
0083          return
0084      160 sixj = 0.e0
0085          return
0086          end

0001          real*8 function threej (j1,j2,j3)
0002    c
0003    c     computation of special wigner 3j coefficient with
0004    c       vanishing projections.  see edmunds, p. 50.
0005    c
0006    c     statement function for delta associated w/ racah and sixj symbols
0007    c       see e.g. edmunds p. 99.
0008          implicit real*8 (a-h,o-z)
0009          delta(i,j,k) = (-0.5e0)*(pbinom(i+j+k+1,i+j-k)+pbinom(k+k+1,i-j+k)
0010         . +log(float(k+j-i+1) ) )
0011    c
0012          i1 = j1+j2+j3
0013          if (parity(i1) .lt. 0.e0)  go to 40
0014          i2 = j1-j2+j3
0015          if (i2) 40,10,10
0016       10 i3 = j1+j2-j3
0017          if (i3)  40,20,20
0018       20 i4 = -j1+j2+j3
0019          if (i4) 40,30,30
0020       30 i5 = i1/2
0021          i6 = i2/2
0022          sign = parity(i5)
0023          temp = delta(j1,j2,j3)+pbinom(i5,j1)+pbinom(j1,i6)
0024          threej = sign*exp(temp)
0025          return
0026       40 threej = 0e0
0027          return
0028          end

0001          real*8 function thrj(f1,f2,f3,g1,g2,g3)
0002          implicit real*8 (a-h,o-z)
0003          dimension x(202),y(202)
0004          data mung/0/
0005          if (mung .eq. 21) go to 20
0006          mung = 21
0007          x(1) = 0.0e+00
0008          do 10 i = 1, 201
0009           a = i
0010          x(i+1) = log(a) +x(i)
0011          y(i+1) = log(a)
0012       10 continue
0013       20 if (f1-abs(g1)) 60,30,30
0014       30 if (f2-abs(g2)) 60,40,40
0015       40 if (f3-abs(g3)) 60,50,50
0016       50 sum = f1+f2+f3
0017          nsum = sum+.01e0
0018          if (sum-nsum) 70,70,60
0019       60 thrj = 0.e+00
```

```
0020        return
0021       70 if (abs(g1+g2+g3)-1.e-08) 80,80,60
0022       80 if (f1+f2-f3) 60,90,90
0023       90 if (f1+f3-f2) 60,100,100
0024      100 if (f2+f3-f1) 60,110,110
0025      110 j1 = 2.e+00*f3+2.001e+00
0026          j2 = f1+f2-f3+1.001e+00
0027          j3 = f1-f2+f3+1.001e+00
0028          j4 = -f1+f2+f3+1.001e+00
0029          j5 = f1+f2+f3+2.001e+00
0030          j6 = f1+g1+1.001e+00
0031          j7 = f1-g1+1.001e+00
0032          j8 = f2+g2+1.001e+00
0033          j9 = f2-g2+1.001e+00
0034          j10 = f3+g3+1.001e+00
0035          j11 = f3-g3+1.001e+00
0036          r = .5e+00*(y(j1)+x(j2)+x(j3)+x(j4)-x(j5)+x(j6)+x(j7)+x(j8)+x(j9)+
0037         . x(j10)+x(j11))
0038          sum = 0.e+00
0039          f = -1
0040          kz = -1
0041      120 kz = kz+1
0042          f = -f
0043          j1 = kz+1
0044          j2 = f1+f2-f3-kz+1.01e+00
0045          if (j2) 180,180,130
0046      130 j3 = f1-g1-kz+1.01e+00
0047          if (j3) 180,180,140
0048      140 j4 = f2+g2-kz+1.01e+00
0049          if (j4) 180,180,150
0050      150 j5 = f3-f2+g1+kz+1.001e+00
0051          if (j5) 120,120,160
0052      160 j6 = f3-f1-g2+kz+1.001e+00
0053          if (j6) 120,120,170
0054      170 s = -(x(j1)+x(j2)+x(j3)+x(j4)+x(j5)+x(j6))
0055          sum = sum+f*exp(r+s)
0056          go to 120
0057      180 int = abs(f1-f2-g3)+0.0001e+00
0058          val = ((-1.0e+00)**int)*sum/sqrt(2.e+00*f3+1.e+00)
0059          if (abs(val) .le. 1.e-6) val = 0.e0
0060          thrj = val
0061          return
0062          end

0001          real*8 function delt(n,m)
0002          implicit real*8 (a-h,o-z)
0003          z = 1.0e+00
0004          if (n .ne. m) z = 0.0e+00
0005          delt = z
0006          return
0007          end

0001          subroutine psq(ndim,x)
0002          implicit real*8 (a-h,o-z)
0003          common /io/ ir,iw,ip
0004         .       /pflag/ iprint,ipdis,nrts,nroot,ltype,jtype,jpar
0005          dimension x(ndim,ndim)
0006          do 10 i = 1,ndim
0007           write (iw,1000) (x(i,j),j = 1,ndim)
0008       10 continue
0009          return
```

```
0010    1000 format(3f12.8)
0011         end

0001         real*8 function clgdn(j1,m1,j2,m2,j,m)
0002         implicit real*8 (a-h,o-z)
0003         xj1 = float(j1)
0004         xm1 = float(m1)
0005         xj2 = float(j2)
0006         xm2 = float(m2)
0007         xj = float(j)
0008         xm = float(-m)
0009         ctem = (-1)**(j2-j1-m)*sqrt(2.0e+00*xj+1.0e+00)*thrj(xj1,xj2,xj,
0010        . xm1,xm2,xm)
0011         clgdn = ctem
0012         return
0013         end

0001         subroutine prsq(v,m,n,ndim)
0002         implicit real*8 (a-h,o-z)
0003    c
0004    c    ---- print out a square matrix ----
0005    c
0006         common /io/ ir,iw,ip
0007    c    common/iofile/ir,iw,ip
0008    c    common/listng/list
0009         dimension v(ndim,1)
0010         list = 2
0011         if (list .eq. 0) max = 10
0012         if (list .eq. 1) max = 7
0013         if (list .eq. 2) max = 7
0014         imax = 0
0015      10 imin = imax+1
0016         imax = imax+max
0017         if (imax .gt. m) imax = m
0018         write (iw,1000)
0019         if (list .eq. 0) write (iw,1010) (i,i = imin,imax)
0020         if (list .eq. 1) write (iw,1030) (i,i = imin,imax)
0021         if (list .eq. 2) write (iw,1050) (i,i = imin,imax)
0022         write (iw,1000)
0023         do 20 j = 1,n
0024          if (list .eq. 0) write (iw,1020) j,(v(j,i),i = imin,imax)
0025          if (list .eq. 1) write (iw,1040) j,(v(j,i),i = imin,imax)
0026          if (list .eq. 2) write (iw,1060) j,(v(j,i),i = imin,imax)
0027      20 continue
0028         if (imax .lt. m) go to 10
0029         return
0030    1000 format(/)
0031    1010 format(6x,10(4x,i3,4x))
0032    1020 format(i5,1x,10f11.5)
0033    1030 format(6x,7(6x,i3,6x))
0034    1040 format(i5,1x,7f15.10)
0035    1050 format(6x,7(6x,i3,6x))
0036    1060 format(i5,1x,7e15.8)
0037         end
```

TEST INPUT FOR ROTBAS

```
$cntrl
  iprint=0, ipdis=0,
  nrts=5, nroot=1,
  ltype=1, jtype=0,
  jpar=-2,
$end
$data
 jtot=15, j1max=75, j2max=75,
 lmax=14, j12max=1, kst=1,
        ifdim=4,
$end
$mass
  m1=12.01115000, m2=14.00670000,
  r1=2.36661768, r2=2.36661768, r=5.01967081,
$end
$fcm
 0.10152000 -0.09975000 -0.03543000  0.03366000
-0.09975000  0.10152000  0.03366000 -0.03543000
-0.03543000  0.03366000  0.01277000 -0.01100000
 0.03660000 -0.03543000 -0.01100000  0.01277000
 0.10152000 -0.09975000 -0.03543000  0.03366000
-0.09975000  0.10152000  0.03366000 -0.03543000
-0.03543000  0.03366000  0.01277000 -0.01100000
 0.03660000 -0.03543000 -0.01100000  0.01277000
$end
$engry
 nstate=3, brot1=1.8996, brot2=1.7165, freq1=2069.0, freq2=1814.0,
 eav= 8797.25, 11273.42, 12925.81,
$end
$vib
Initial Q State  (1,0,0,0,0,0,0)
0.10942e-04 0.52002e-05 0.71921e-08 0.19797e-15 0.00000e+00 0.00000e+00 0.00000e+00
0.13224e-08 0.62792e-10 0.10567e-13 0.00000e+00 0.00000e+00 0.00000e+00 0.00000e+00
0.18534e-09 0.48384e-14 0.00000e+00 0.00000e+00 0.00000e+00 0.00000e+00 0.00000e+00
0.22885e-16 0.00000e+00 0.00000e+00 0.00000e+00 0.00000e+00 0.00000e+00 0.00000e+00
0.00000e+00 0.00000e+00 0.00000e+00 0.00000e+00 0.00000e+00 0.00000e+00 0.00000e+00
0.00000e+00 0.00000e+00 0.00000e+00 0.00000e+00 0.00000e+00 0.00000e+00 0.00000e+00
0.00000e+00 0.00000e+00 0.00000e+00 0.00000e+00 0.00000e+00 0.00000e+00 0.00000e+00
Initial Q State (2,0,0,0,0,0,0)
0.51068e-06 0.29668e-06 0.17355e-06 0.35964e-09 0.39242e-15 0.00000e+00 0.00000e+00
0.75543e-08 0.38143e-09 0.28759e-11 0.45603e-16 0.00000e+00 0.00000e+00 0.00000e+00
0.44122e-08 0.24221e-11 0.18505e-16 0.00000e+00 0.00000e+00 0.00000e+00 0.00000e+00
0.61851e-14 0.12430e-16 0.00000e+00 0.00000e+00 0.00000e+00 0.00000e+00 0.00000e+00
0.60077e-18 0.00000e+00 0.00000e+00 0.00000e+00 0.00000e+00 0.00000e+00 0.00000e+00
0.00000e+00 0.00000e+00 0.00000e+00 0.00000e+00 0.00000e+00 0.00000e+00 0.00000e+00
0.00000e+00 0.00000e+00 0.00000e+00 0.00000e+00 0.00000e+00 0.00000e+00 0.00000e+00
Initial Q State (3,0,0,0,0,0,0)
0.17290e-05 0.14859e-05 0.16983e-06 0.35634e-09 0.82826e-16 0.18736e-19 0.00000e+00
0.24343e-07 0.51069e-11 0.44288e-11 0.12261e-13 0.35406e-18 0.00000e+00 0.00000e+00
0.77661e-09 0.59265e-12 0.40401e-14 0.10165e-17 0.00000e+00 0.00000e+00 0.00000e+00
0.14400e-14 0.10228e-16 0.90833e-20 0.00000e+00 0.00000e+00 0.00000e+00 0.00000e+00
0.13092e-16 0.76947e-19 0.00000e+00 0.00000e+00 0.00000e+00 0.00000e+00 0.00000e+00
0.68404e-19 0.00000e+00 0.00000e+00 0.00000e+00 0.00000e+00 0.00000e+00 0.00000e+00
```

TEST OUTPUT FILE FOR ROTBAS

iprint = 0 **** NUMBER OF ROOTS PRINTED = 5
NROOT = 1 LTYPE = 1 JTYPE = 1 JPAR = -2
jtot = 15 j1max = 75 j2max = 75
lmax = 14 j12max = 1 Electronic Angular Momentum of Diatom 2 = 1
ifdim = 4
FORCE CONSTANT MATRIX X- CARTESIANS
0.10152000 -0.09975000 -0.03543000 0.03366000
-0.09975000 0.10152000 0.03366000 -0.03543000
-0.03543000 0.03366000 0.01277000 -0.01100000
0.03660000 -0.03543000 -0.01100000 0.01277000
FORCE CONSTANT MATRIX Y- CARTESIANS
0.10152000 -0.09975000 -0.03543000 0.03366000
-0.09975000 0.10152000 0.03366000 -0.03543000
-0.03543000 0.03366000 0.01277000 -0.01100000
0.03660000 -0.03543000 -0.01100000 0.01277000
mass of atom a of abba = 14.00670
mass of atom b of abba = 12.01115
reduced mass of fragment ab = 6.46620
reduced mass of system = 13.00892
Diatom A bond length in a.u. = 2.36661768
Diatom B bond length in a.u. = 2.36661768
Interfragment Separation in a.u. = 5.01967081

Rotational constants : diatom A = 1.66224713
diatom B = 1.66224713
diatom-diatom = 0.18365761

0 0 0 0.2452517702d+02
1 1 0 0.9216238997d+01
*** v0 = 0.19220722e+00 ***

JTOT = 15 J12 = 1 L = 14 PARITY = 0 KST = 1

Time Spent Calculating Matrix = 3.319 Seconds
Order of Matrix is 224

ROOT NUMBER 1 762.54241852

j1	j2	j12	l		
0	1	1	14	1	0.95723389e-01
1	1	1	14	2	-0.11669714e+00
1	2	1	14	3	-0.11562786e+00
2	1	1	14	4	0.66756353e-01
2	2	1	14	5	0.14790400e+00
2	3	1	14	6	0.13047534e+00
3	2	1	14	7	-0.92257049e-01
3	3	1	14	8	-0.17023043e+00
3	4	1	14	9	-0.14124661e+00
4	3	1	14	10	0.10940449e+00
4	4	1	14	11	0.18603763e+00
4	5	1	14	12	0.14844362e+00
5	4	1	14	13	-0.12119726e+00
5	5	1	14	14	-0.19641098e+00
5	6	1	14	15	-0.15241458e+00
6	5	1	14	16	0.12880560e+00
6	6	1	14	17	0.20203652e+00
6	7	1	14	18	0.15346638e+00

7	6	1	14	19	-0.13289587e+00
7	7	1	14	20	-0.20346610e+00
7	8	1	14	21	-0.15190776e+00
8	7	1	14	22	0.13395864e+00
8	8	1	14	23	0.20121443e+00
8	9	1	14	24	0.14806401e+00
9	8	1	14	25	-0.13241978e+00
9	9	1	14	26	-0.19579446e+00
9	10	1	14	27	-0.14227799e+00
10	9	1	14	28	0.12868158e+00
10	10	1	14	29	0.18772567e+00
10	11	1	14	30	0.13490430e+00
11	10	1	14	31	-0.12313579e+00
11	11	1	14	32	-0.17752955e+00
11	12	1	14	33	-0.12630001e+00
12	11	1	14	34	0.11616427e+00
12	12	1	14	35	0.16571916e+00
12	13	1	14	36	0.11681430e+00
13	12	1	14	37	-0.10813407e+00
13	13	1	14	38	-0.15278646e+00
13	14	1	14	39	-0.10677824e+00
14	13	1	14	40	0.99390324e-01
14	14	1	14	41	0.13918988e+00
14	15	1	14	42	0.96495758e-01
15	14	1	14	43	-0.90249111e-01
15	15	1	14	44	-0.12534347e+00
15	16	1	14	45	-0.86236472e-01
16	15	1	14	46	0.80991273e-01
16	16	1	14	47	0.11160867e+00
16	17	1	14	48	0.76230641e-01
17	16	1	14	49	-0.71857943e-01
17	17	1	14	50	-0.98288848e-01
17	18	1	14	51	-0.66666373e-01
18	17	1	14	52	0.63048005e-01
18	18	1	14	53	0.85627053e-01
18	19	1	14	54	0.57689014e-01
19	18	1	14	55	-0.54717549e-01
19	19	1	14	56	-0.73806483e-01
19	20	1	14	57	-0.49402487e-01
20	19	1	14	58	0.46981149e-01
20	20	1	14	59	0.62953513e-01
20	21	1	14	60	0.41872236e-01
21	20	1	14	61	-0.39914701e-01
21	21	1	14	62	-0.53142693e-01
21	22	1	14	63	-0.35129397e-01
22	21	1	14	64	0.33559455e-01
22	22	1	14	65	0.44403182e-01
22	23	1	14	66	0.29175782e-01
23	22	1	14	67	-0.27926860e-01
23	23	1	14	68	-0.36726060e-01
23	24	1	14	69	-0.23989269e-01
24	23	1	14	70	0.23003834e-01
24	24	1	14	71	0.30071981e-01
24	25	1	14	72	0.19529261e-01
25	24	1	14	73	-0.18758127e-01
25	25	1	14	74	-0.24378708e-01
25	26	1	14	75	-0.15741901e-01
26	25	1	14	76	0.15143472e-01
26	26	1	14	77	0.19568171e-01
26	27	1	14	78	0.12564832e-01
27	26	1	14	79	-0.12104306e-01

27	27	1	14	80	-0.15552766e-01
27	28	1	14	81	-0.99313302e-02
28	27	1	14	82	0.95799071e-02
28	28	1	14	83	0.12240728e-01
28	29	1	14	84	0.77737487e-02
29	28	1	14	85	-0.75078452e-02
29	29	1	14	86	-0.95405018e-02
29	30	1	14	87	-0.60262234e-02
30	29	1	14	88	0.58267347e-02
30	30	1	14	89	0.73641022e-02
30	31	1	14	90	0.46266793e-02
31	30	1	14	91	-0.44782913e-02
31	31	1	14	92	-0.56295232e-02
31	32	1	14	93	-0.35181913e-02
32	31	1	14	94	0.34087572e-02
32	32	1	14	95	0.42622979e-02
32	33	1	14	96	0.26497851e-02
33	32	1	14	97	-0.25697708e-02
33	33	1	14	98	-0.31963350e-02
33	34	1	14	99	-0.19767751e-02
34	33	1	14	100	0.19187742e-02
34	34	1	14	101	0.23741706e-02
34	35	1	14	102	0.14607391e-02
35	34	1	14	103	-0.14190574e-02
35	35	1	14	104	-0.17467733e-02
35	36	1	14	105	-0.10692256e-02
36	35	1	14	106	0.10395302e-02
36	36	1	14	107	0.12730316e-02
36	37	1	14	108	0.77528115e-03
37	36	1	14	109	-0.75430802e-03
37	37	1	14	110	-0.91903509e-03
37	38	1	14	111	-0.55686959e-03
38	37	1	14	112	0.54218511e-03
38	38	1	14	113	0.65724441e-03
38	39	1	14	114	0.39624416e-03
39	38	1	14	115	-0.38605189e-03
39	39	1	14	116	-0.46562321e-03
39	40	1	14	117	-0.27931710e-03
40	39	1	14	118	0.27230423e-03
40	40	1	14	119	0.32678775e-03
40	41	1	14	120	0.19505955e-03
41	40	1	14	121	-0.19027623e-03
41	41	1	14	122	-0.22721153e-03
41	42	1	14	123	-0.13495261e-03
42	41	1	14	124	0.13171841e-03
42	42	1	14	125	0.15650855e-03
42	43	1	14	126	0.92501507e-04
43	42	1	14	127	-0.90333762e-04
43	43	1	14	128	-0.10680661e-03
43	44	1	14	129	-0.62817182e-04
44	43	1	14	130	0.61376895e-04
44	44	1	14	131	0.72213674e-04
44	45	1	14	132	0.42264784e-04
45	44	1	14	133	-0.41316173e-04
45	45	1	14	134	-0.48373854e-04
45	46	1	14	135	-0.28174591e-04
46	45	1	14	136	0.27555258e-04
46	46	1	14	137	0.32105559e-04
46	47	1	14	138	0.18609011e-04
47	46	1	14	139	-0.18208185e-04
47	47	1	14	140	-0.21112333e-04

47	48	1	14	141	-0.12178210e-04
48	47	1	14	142	0.11921062e-04
48	48	1	14	143	0.13755823e-04
48	49	1	14	144	0.78967008e-05
49	48	1	14	145	-0.77331677e-05
49	49	1	14	146	-0.88805336e-05
49	50	1	14	147	-0.50736139e-05
50	49	1	14	148	0.49705225e-05
50	50	1	14	149	0.56806918e-05
50	51	1	14	150	0.32300254e-05
51	50	1	14	151	-0.31656034e-05
51	51	1	14	152	-0.36006467e-05
51	52	1	14	153	-0.20375976e-05
52	51	1	14	154	0.19976913e-05
52	52	1	14	155	0.22614355e-05
52	53	1	14	156	0.12736847e-05
53	52	1	14	157	-0.12491802e-05
53	53	1	14	158	-0.14074063e-05
53	54	1	14	159	-0.78893893e-06
54	53	1	14	160	0.77402308e-06
54	54	1	14	161	0.86794743e-06
54	55	1	14	162	0.48425005e-06
55	54	1	14	163	-0.47524993e-06
55	55	1	14	164	-0.53041155e-06
55	56	1	14	165	-0.29454223e-06
56	55	1	14	166	0.28915893e-06
56	56	1	14	167	0.32120702e-06
56	57	1	14	168	0.17753493e-06
57	56	1	14	169	-0.17434301e-06
57	57	1	14	170	-0.19275978e-06
57	58	1	14	171	-0.10604374e-06
58	57	1	14	172	0.10416763e-06
58	58	1	14	173	0.11463411e-06
58	59	1	14	174	0.62770825e-07
59	58	1	14	175	-0.61677695e-07
59	59	1	14	176	-0.67559138e-07
59	60	1	14	177	-0.36822121e-07
60	59	1	14	178	0.36190737e-07
60	60	1	14	179	0.39457878e-07
60	61	1	14	180	0.21406439e-07
61	60	1	14	181	-0.21044925e-07
61	61	1	14	182	-0.22838593e-07
61	62	1	14	183	-0.12333069e-07
62	61	1	14	184	0.12127873e-07
62	62	1	14	185	0.13100791e-07
62	63	1	14	186	0.70419919e-08
63	62	1	14	187	-0.69265317e-08
63	63	1	14	188	-0.74477443e-08
63	64	1	14	189	-0.39849586e-08
64	63	1	14	190	0.39205548e-08
64	64	1	14	191	0.41962130e-08
64	65	1	14	192	0.22349219e-08
65	64	1	14	193	-0.21993084e-08
65	65	1	14	194	-0.23431610e-08
65	66	1	14	195	-0.12422728e-08
66	65	1	14	196	0.12227500e-08
66	66	1	14	197	0.12967750e-08
66	67	1	14	198	0.68437231e-09
67	66	1	14	199	-0.67376294e-09
67	67	1	14	200	-0.71129517e-09
67	68	1	14	201	-0.37367126e-09

68	67	1	14	202	0.36795551e-09
68	68	1	14	203	0.38668661e-09
68	69	1	14	204	0.20220693e-09
69	68	1	14	205	-0.19915424e-09
69	69	1	14	206	-0.20834362e-09
69	70	1	14	207	-0.10843001e-09
70	69	1	14	208	0.10681456e-09
70	70	1	14	209	0.11123901e-09
70	71	1	14	210	0.57586825e-10
71	70	1	14	211	-0.56739350e-10
71	71	1	14	212	-0.58825031e-10
71	72	1	14	213	-0.30231019e-10
72	71	1	14	214	0.29791806e-10
72	72	1	14	215	0.30751422e-10
72	73	1	14	216	0.15571441e-10
73	72	1	14	217	-0.15347590e-10
73	73	1	14	218	-0.15775549e-10
73	74	1	14	219	-0.76416208e-11
74	73	1	14	220	0.75332229e-11
74	74	1	14	221	0.77147043e-11
74	75	1	14	222	0.31099712e-11
75	74	1	14	223	-0.30661482e-11
75	75	1	14	224	-0.31313734e-11

Time Spent in Givens Diagonalization = 9.365 Seconds

LOWEST 5 ROOTS OF MATRIX
762.542 1484.855 2205.496 2205.501 2926.143
Root Differences [root(i+1) - root(i)]
0.000 722.312 720.641 0.005 720.641

Total Time of This Run = 13.613 Seconds
iprint = 0 **** NUMBER OF ROOTS PRINTED = 5
NROOT = 1 LTYPE = 1 JTYPE = 1 JPAR = -2
jtot = 15 j1max = 75 j2max = 75
lmax = 14 j12max = 1 Electronic Angular Momentum of Diatom 2 = 1
ifdim = 4
FORCE CONSTANT MATRIX X- CARTESIANS
0.10152000 -0.09975000 -0.03543000 0.03366000
-0.09975000 0.10152000 0.03366000 -0.03543000
-0.03543000 0.03366000 0.01277000 -0.01100000
0.03660000 -0.03543000 -0.01100000 0.01277000
FORCE CONSTANT MATRIX Y- CARTESIANS
0.10152000 -0.09975000 -0.03543000 0.03366000
-0.09975000 0.10152000 0.03366000 -0.03543000
-0.03543000 0.03366000 0.01277000 -0.01100000
0.03660000 -0.03543000 -0.01100000 0.01277000
mass of atom a of abba = 14.00670
mass of atom b of abba = 12.01115
reduced mass of fragment ab = 6.46620
reduced mass of system = 13.00892
Diatom A bond length in a.u. = 2.36661768
Diatom B bond length in a.u. = 2.36661768
Interfragment Separation in a.u. = 5.01967081

Rotational constants : diatom A = 1.66224713

diatom B = 1.66224713
diatom-diatom = 0.18365761

CN (X 2 SIGMA +) Rotational Constant = 1.89960 Vibrational Frequency = 2069.00000
CN (A 2 PI) Rotational Constant = 1.71650 Vibrational Frequency = 1814.00000

ROOT NUMBER 1 762.54241852

ISTATE = 1 AVAILABLE ENERGY = 8797.25000000
JTOT = 15 j12 = 1 l = 14 PARITY= 0 KST = 1
Initial Q State (1,0,0,0,0,0,0)

CN(X 2 SIGMA +) ROTATIONAL DISTRIBUTIONS

j1	v=0	v=1	v=2	v=3
0	0.00006706	0.00006912	0.00007584	0.00020643
1	0.00078774	0.00081181	0.00089007	0.00241117
2	0.00294571	0.00303427	0.00332281	0.00892006
3	0.00723291	0.00744517	0.00813875	0.02154990
4	0.01392447	0.01431975	0.01561651	0.04056247
5	0.02285279	0.02347391	0.02552216	0.06460832
6	0.03343959	0.03429936	0.03715364	0.09093150
7	0.04479846	0.04587236	0.04946823	0.11584189
8	0.05588447	0.05711103	0.06126368	0.13532978
9	0.06566048	0.06694898	0.07137517	0.14565650
10	0.07324889	0.07449266	0.07885057	0.14371513
11	0.07804413	0.07913634	0.08307475	0.12678251
12	0.07977123	0.08062015	0.08382693	0.08963206
13	0.07848770	0.07902857	0.08127009	0.01385229
14	0.07453683	0.07473854	0.07588385	0.00000000
15	0.06846745	0.06833362	0.06836121	0.00000000
16	0.06093885	0.06050370	0.05949213	0.00000000
17	0.05262808	0.05194862	0.05005481	0.00000000
18	0.04415332	0.04329968	0.04073028	0.00000000
19	0.03602097	0.03506667	0.03204805	0.00000000
20	0.02859878	0.02761249	0.02436388	0.00000000
21	0.02211243	0.02115191	0.01786484	0.00000000
22	0.01665980	0.01576863	0.01259380	0.00000000
23	0.01223639	0.01144308	0.00848429	0.00000000
24	0.00876509	0.00808418	0.00539722	0.00000000
25	0.00612513	0.00555954	0.00315130	0.00000000
26	0.00417669	0.00372074	0.00152712	0.00000000
27	0.00277961	0.00242201	0.00019802	0.00000000
28	0.00180555	0.00153210	0.00000000	0.00000000
29	0.00114478	0.00094049	0.00000000	0.00000000
30	0.00070842	0.00055898	0.00000000	0.00000000
31	0.00042780	0.00032049	0.00000000	0.00000000
32	0.00025203	0.00017614	0.00000000	0.00000000
33	0.00014479	0.00009165	0.00000000	0.00000000
34	0.00008106	0.00004386	0.00000000	0.00000000
35	0.00004418	0.00001743	0.00000000	0.00000000
36	0.00002341	0.00000197	0.00000000	0.00000000
37	0.00001203	0.00000000	0.00000000	0.00000000
38	0.00000598	0.00000000	0.00000000	0.00000000
39	0.00000285	0.00000000	0.00000000	0.00000000
40	0.00000129	0.00000000	0.00000000	0.00000000
41	0.00000055	0.00000000	0.00000000	0.00000000
42	0.00000020	0.00000000	0.00000000	0.00000000
43	0.00000003	0.00000000	0.00000000	0.00000000

T(K)	368.79988448	399.57742320	515.00261552	-967.29395523

CN(A 2 PI) ROTATIONAL DISTRIBUTIONS

j2	v=0	v=1	v=2	v=3
0	0.00000000	0.00000000	0.00000000	0.00000000
1	0.00053341	0.00054365	0.00057611	0.00078653
2	0.00256771	0.00261625	0.00277034	0.00377116
3	0.00679163	0.00691702	0.00731584	0.00991458
4	0.01348929	0.01373039	0.01449908	0.01953018
5	0.02249066	0.02287589	0.02410802	0.03221850
6	0.03320461	0.03374322	0.03547313	0.04694134
7	0.04472427	0.04540160	0.04758865	0.06221388
8	0.05598070	0.05675831	0.05928635	0.07637009
9	0.06591339	0.06673390	0.06942541	0.08784461
10	0.07362572	0.07442123	0.07706277	0.09541620
11	0.07849990	0.07920209	0.08157546	0.09837086
12	0.08025648	0.08080639	0.08271918	0.09656372
13	0.07895585	0.07931145	0.08062165	0.09038063
14	0.07494980	0.07509044	0.07572120	0.08061905
15	0.06879918	0.06872627	0.06866969	0.06831783
16	0.06117630	0.06091085	0.06022145	0.05456479
17	0.05277030	0.05234798	0.05112851	0.04028910
18	0.04420897	0.04367395	0.04205728	0.02592681
19	0.03600512	0.03540393	0.03353404	0.00996012
20	0.02852968	0.02790590	0.02592080	0.00000000
21	0.02200862	0.02139906	0.01941839	0.00000000
22	0.01653800	0.01597054	0.01408796	0.00000000
23	0.01211022	0.01160321	0.00988354	0.00000000
24	0.00864452	0.00820741	0.00668772	0.00000000
25	0.00601656	0.00565136	0.00434465	0.00000000
26	0.00408345	0.00378652	0.00268667	0.00000000
27	0.00270257	0.00246621	0.00155281	0.00000000
28	0.00174420	0.00155661	0.00079736	0.00000000
29	0.00109738	0.00095639	0.00026593	0.00000000
30	0.00067274	0.00057430	0.00000000	0.00000000
31	0.00040154	0.00033396	0.00000000	0.00000000
32	0.00023305	0.00018735	0.00000000	0.00000000
33	0.00013124	0.00010075	0.00000000	0.00000000
34	0.00007141	0.00005128	0.00000000	0.00000000
35	0.00003711	0.00002398	0.00000000	0.00000000
36	0.00001768	0.00000924	0.00000000	0.00000000
37	0.00000877	0.00000111	0.00000000	0.00000000
38	0.00000436	0.00000000	0.00000000	0.00000000
39	0.00000208	0.00000000	0.00000000	0.00000000
40	0.00000095	0.00000000	0.00000000	0.00000000
41	0.00000040	0.00000000	0.00000000	0.00000000
42	0.00000014	0.00000000	0.00000000	0.00000000
43	0.00000002	0.00000000	0.00000000	0.00000000

T(K)	317.84763612	341.78190629	426.84325328	1088.41931680

ISTATE = 2 AVAILABLE ENERGY = 11273.42000000
JTOT = 15 j12 = 1 l = 14 PARITY= 0 KST = 1
Initial Q State (2,0,0,0,0,0,0)

CN(X 2 SIGMA +) ROTATIONAL DISTRIBUTIONS

j1	v=0	v=1	v=2	v=3	v=4
0	0.00006592	0.00006681	0.00006856	0.00007353	0.00012414

1	0.00077455	0.00078484	0.00080527	0.00086322	0.00145358
2	0.00289719	0.00293503	0.00301019	0.00322373	0.00540253
3	0.00711673	0.00720734	0.00738743	0.00790030	0.01314529
4	0.01370843	0.01387689	0.01421216	0.01516995	0.02499439
5	0.02251398	0.02277813	0.02330468	0.02481526	0.04036549
6	0.03297179	0.03333644	0.03406483	0.03616578	0.05788045
7	0.04421602	0.04466992	0.04557896	0.04821922	0.07562092
8	0.05522197	0.05573810	0.05677525	0.05981464	0.09147277
9	0.06496824	0.06550732	0.06659533	0.06982148	0.10348640
10	0.07258554	0.07310183	0.07415006	0.07730864	0.11018035
11	0.07746780	0.07791600	0.07883393	0.08166557	0.11073360
12	0.07933115	0.07967293	0.08038308	0.08265961	0.10503693
13	0.07821781	0.07842680	0.07887481	0.08042823	0.09359688
14	0.07445227	0.07451677	0.07467699	0.07541699	0.07728559
15	0.06856427	0.06848747	0.06836378	0.06828201	0.05681673
16	0.06119651	0.06099454	0.06061671	0.05977899	0.03009213
17	0.05301397	0.05271235	0.05212935	0.05065881	0.00231182
18	0.04462820	0.04425756	0.04352929	0.04158457	0.00000000
19	0.03654436	0.03613627	0.03532527	0.03307788	0.00000000
20	0.02913347	0.02871693	0.02788137	0.02549581	0.00000000
21	0.02262762	0.02222658	0.02141518	0.01903400	0.00000000
22	0.01713282	0.01676488	0.01601420	0.01374888	0.00000000
23	0.01265296	0.01232919	0.01166290	0.00959051	0.00000000
24	0.00911857	0.00884406	0.00827397	0.00643832	0.00000000
25	0.00641509	0.00619010	0.00571822	0.00413408	0.00000000
26	0.00440723	0.00422852	0.00384962	0.00250818	0.00000000
27	0.00295760	0.00281977	0.00252396	0.00139698	0.00000000
28	0.00193923	0.00183583	0.00161086	0.00064445	0.00000000
29	0.00124257	0.00116703	0.00100005	0.00008040	0.00000000
30	0.00077818	0.00072437	0.00060321	0.00000000	0.00000000
31	0.00047639	0.00043898	0.00035287	0.00000000	0.00000000
32	0.00028511	0.00025969	0.00019963	0.00000000	0.00000000
33	0.00016681	0.00014993	0.00010870	0.00000000	0.00000000
34	0.00009541	0.00008444	0.00005648	0.00000000	0.00000000
35	0.00005335	0.00004636	0.00002750	0.00000000	0.00000000
36	0.00002916	0.00002479	0.00001195	0.00000000	0.00000000
37	0.00001557	0.00001290	0.00000338	0.00000000	0.00000000
38	0.00000813	0.00000651	0.00000000	0.00000000	0.00000000
39	0.00000414	0.00000318	0.00000000	0.00000000	0.00000000
40	0.00000206	0.00000150	0.00000000	0.00000000	0.00000000
41	0.00000100	0.00000067	0.00000000	0.00000000	0.00000000
42	0.00000047	0.00000028	0.00000000	0.00000000	0.00000000
43	0.00000022	0.00000011	0.00000000	0.00000000	0.00000000
44	0.00000010	0.00000003	0.00000000	0.00000000	0.00000000
45	0.00000004	0.00000000	0.00000000	0.00000000	0.00000000
46	0.00000002	0.00000000	0.00000000	0.00000000	0.00000000
T(K)	372.27063552	368.18269310	405.55948802	474.20136548	1146.35857987

CN(A 2 PI) ROTATIONAL DISTRIBUTIONS

j2	v=0	v=1	v=2	v=3	v=4
0	0.00000000	0.00000000	0.00000000	0.00000000	0.00000000
1	0.00052479	0.00052633	0.00053623	0.00055912	0.00064942
2	0.00252688	0.00253414	0.00258105	0.00268965	0.00311891
3	0.00668622	0.00670494	0.00682603	0.00710685	0.00822065
4	0.01328684	0.01332272	0.01355533	0.01409587	0.01625005
5	0.02216768	0.02222475	0.02259596	0.02346088	0.02692952
6	0.03275388	0.03283323	0.03335143	0.03456304	0.03946132
7	0.04415880	0.04425790	0.04490826	0.04643562	0.05267405
8	0.05533352	0.05544627	0.05619097	0.05794990	0.06522870

9	0.06523327	0.06535084	0.06613394	0.06799745	0.07584074
10	0.07296994	0.07308211	0.07383780	0.07565453	0.08347589
11	0.07792568	0.07802238	0.07868484	0.08030137	0.08748635
12	0.07981273	0.07988552	0.08039841	0.08168098	0.08767023
13	0.07867679	0.07871997	0.07904374	0.07989545	0.08425364
14	0.07485144	0.07486264	0.07497863	0.07534959	0.07780978
15	0.06887883	0.06885901	0.06877003	0.06865948	0.06913848
16	0.06141494	0.06136793	0.06109561	0.06054676	0.05913285
17	0.05313686	0.05306851	0.05264839	0.05173789	0.04865673
18	0.04466557	0.04458281	0.04405833	0.04288292	0.03844998
19	0.03651237	0.03642223	0.03583870	0.03450153	0.02906950
20	0.02905106	0.02895994	0.02835941	0.02695814	0.02086524
21	0.02251368	0.02242675	0.02184437	0.02046218	0.01398111
22	0.01700405	0.01692505	0.01638711	0.01508650	0.00835037
23	0.01252270	0.01245389	0.01197731	0.01080759	0.00328650
24	0.00899635	0.00893865	0.00853177	0.00751718	0.00000000
25	0.00630679	0.00626008	0.00592414	0.00507080	0.00000000
26	0.00431564	0.00427906	0.00401011	0.00331168	0.00000000
27	0.00288318	0.00285542	0.00264618	0.00208801	0.00000000
28	0.00188084	0.00186042	0.00170194	0.00126473	0.00000000
29	0.00119816	0.00118360	0.00106656	0.00072926	0.00000000
30	0.00074542	0.00073529	0.00065089	0.00039257	0.00000000
31	0.00045285	0.00044603	0.00038648	0.00018661	0.00000000
32	0.00026860	0.00026416	0.00022300	0.00005588	0.00000000
33	0.00015548	0.00015270	0.00012480	0.00000000	0.00000000
34	0.00008778	0.00008612	0.00006753	0.00000000	0.00000000
35	0.00004828	0.00004735	0.00003514	0.00000000	0.00000000
36	0.00002581	0.00002536	0.00001742	0.00000000	0.00000000
37	0.00001328	0.00001321	0.00000806	0.00000000	0.00000000
38	0.00000662	0.00000666	0.00000327	0.00000000	0.00000000
39	0.00000334	0.00000326	0.00000081	0.00000000	0.00000000
40	0.00000164	0.00000156	0.00000000	0.00000000	0.00000000
41	0.00000078	0.00000071	0.00000000	0.00000000	0.00000000
42	0.00000036	0.00000031	0.00000000	0.00000000	0.00000000
43	0.00000016	0.00000013	0.00000000	0.00000000	0.00000000
44	0.00000006	0.00000004	0.00000000	0.00000000	0.00000000
45	0.00000002	0.00000001	0.00000000	0.00000000	0.00000000
46	0.00000001	0.00000000	0.00000000	0.00000000	0.00000000
T(K)	321.78098721	329.01020876	342.30787864	388.38020195	613.28402180

ISTATE = 3 AVAILABLE ENERGY = 12925.81000000
JTOT = 15 j12 = 1 l = 14 PARITY= 0 KST = 1
Initial Q State (3,0,0,0,0,0,0)

CN(X 2 SIGMA +) ROTATIONAL DISTRIBUTIONS

j1	v=0	v=1	v=2	v=3	v=4	v=5
0	0.00006545	0.00006605	0.00006706	0.00006914	0.00007599	0.00020939
1	0.00076900	0.00077597	0.00078781	0.00081198	0.00089184	0.00244560
2	0.00287679	0.00290242	0.00294597	0.00303489	0.00332934	0.00904578
3	0.00706793	0.00712924	0.00723353	0.00744666	0.00815446	0.02184753
4	0.01361774	0.01373168	0.01392562	0.01432253	0.01564591	0.04110607
5	0.02237189	0.02255042	0.02285459	0.02347828	0.02556863	0.06543710
6	0.03277582	0.03302206	0.03344208	0.03430542	0.03721842	0.09202520
7	0.04397238	0.04427853	0.04480156	0.04587994	0.04954978	0.11710395
8	0.05494535	0.05529296	0.05588801	0.05711971	0.06135761	0.13657901
9	0.06467989	0.06504227	0.06566418	0.06695814	0.07147466	0.14662210
10	0.07231011	0.07265629	0.07325244	0.07450154	0.07894715	0.14401631
11	0.07722961	0.07752902	0.07804722	0.07914420	0.08315934	0.12581670
12	0.07915068	0.07937759	0.07977360	0.08062633	0.08389079	0.08563284

13	0.07810902	0.07824588	0.07848918	0.07903260	0.08130526	0.01211242
14	0.07442115	0.07446041	0.07453732	0.07474019	0.07588238	0.00000000
15	0.06860879	0.06855298	0.06846697	0.06833291	0.06830685	0.00000000
16	0.06130773	0.06116808	0.06093751	0.06050084	0.05940662	0.00000000
17	0.05317797	0.05297197	0.05262605	0.05194400	0.04997245	0.00000000
18	0.04482838	0.04457687	0.04415081	0.04329378	0.04065275	0.00000000
19	0.03676371	0.03648806	0.03601819	0.03506001	0.03197658	0.00000000
20	0.02935648	0.02907620	0.02859593	0.02760554	0.02429921	0.00000000
21	0.02284156	0.02257265	0.02210967	0.02114509	0.01780720	0.00000000
22	0.01732841	0.01708253	0.01665726	0.01576225	0.01254297	0.00000000
23	0.01282447	0.01260884	0.01223415	0.01143736	0.00843962	0.00000000
24	0.00926345	0.00908128	0.00876319	0.00807923	0.00535755	0.00000000
25	0.00653337	0.00638463	0.00612355	0.00555538	0.00311453	0.00000000
26	0.00450079	0.00438312	0.00417544	0.00371736	0.00148643	0.00000000
27	0.00302944	0.00293908	0.00277863	0.00241932	0.00018567	0.00000000
28	0.00199286	0.00192540	0.00180482	0.00153001	0.00000000	0.00000000
29	0.00128154	0.00123251	0.00114424	0.00093890	0.00000000	0.00000000
30	0.00080578	0.00077106	0.00070803	0.00055779	0.00000000	0.00000000
31	0.00049546	0.00047147	0.00042753	0.00031962	0.00000000	0.00000000
32	0.00029796	0.00028179	0.00025185	0.00017549	0.00000000	0.00000000
33	0.00017528	0.00016462	0.00014467	0.00009117	0.00000000	0.00000000
34	0.00010087	0.00009401	0.00008098	0.00004349	0.00000000	0.00000000
35	0.00005679	0.00005246	0.00004413	0.00001709	0.00000000	0.00000000
36	0.00003128	0.00002861	0.00002337	0.00000187	0.00000000	0.00000000
37	0.00001686	0.00001525	0.00001201	0.00000000	0.00000000	0.00000000
38	0.00000889	0.00000793	0.00000596	0.00000000	0.00000000	0.00000000
39	0.00000458	0.00000403	0.00000284	0.00000000	0.00000000	0.00000000
40	0.00000231	0.00000200	0.00000129	0.00000000	0.00000000	0.00000000
41	0.00000114	0.00000096	0.00000054	0.00000000	0.00000000	0.00000000
42	0.00000055	0.00000045	0.00000019	0.00000000	0.00000000	0.00000000
43	0.00000026	0.00000021	0.00000003	0.00000000	0.00000000	0.00000000
44	0.00000012	0.00000009	0.00000000	0.00000000	0.00000000	0.00000000
45	0.00000005	0.00000004	0.00000000	0.00000000	0.00000000	0.00000000
46	0.00000002	0.00000002	0.00000000	0.00000000	0.00000000	0.00000000
47	0.00000001	0.00000001	0.00000000	0.00000000	0.00000000	0.00000000

T(K)	372.37430250	370.69927727	368.00489048	398.82915616	511.24786180	-1187.00208087

CN(A 2 PI) ROTATIONAL DISTRIBUTIONS

j2	v=0	v=1	v=2	v=3	v=4	v=5
0	0.00000000	0.00000000	0.00000000	0.00000000	0.00000000	0.00000000
1	0.00051872	0.00052026	0.00052652	0.00053769	0.00056289	0.00067081
2	0.00249810	0.00250539	0.00253503	0.00258800	0.00270755	0.00322071
3	0.00661193	0.00663074	0.00670723	0.00684399	0.00715320	0.00848511
4	0.01314424	0.01318030	0.01332710	0.01358987	0.01418527	0.01676238
5	0.02194032	0.02199773	0.02223173	0.02265114	0.02360429	0.02775620
6	0.03243684	0.03251676	0.03284293	0.03342858	0.03476459	0.04063175
7	0.04376147	0.04386142	0.04427001	0.04500526	0.04669075	0.05416934
8	0.05487936	0.05499329	0.05546004	0.05630233	0.05824528	0.06697972
9	0.06475679	0.06487589	0.06536519	0.06625143	0.06831257	0.07773550
10	0.07251157	0.07262559	0.07309578	0.07395168	0.07596461	0.08537435
11	0.07752565	0.07762446	0.07803414	0.07878534	0.08058098	0.08923939
12	0.07950529	0.07958033	0.07989434	0.08047707	0.08190755	0.08913904
13	0.07848572	0.07853117	0.07872517	0.07909454	0.08005214	0.08532615
14	0.07478761	0.07480093	0.07486391	0.07499861	0.07542704	0.07841146
15	0.06893992	0.06892194	0.06885649	0.06875941	0.06865626	0.06923646
16	0.06158716	0.06154157	0.06136209	0.06105740	0.06046867	0.05873329
17	0.05339800	0.05333057	0.05306008	0.05258771	0.05159632	0.04779652
18	0.04498878	0.04490639	0.04457263	0.04398152	0.04269269	0.03718389
19	0.03686984	0.03677953	0.03641117	0.03575243	0.03427850	0.02745308

20	0.02941717	0.02932537	0.02894878	0.02826995	0.02671632	0.01892907
21	0.02286715	0.02277913	0.02241613	0.02175704	0.02020875	0.01166832
22	0.01732916	0.01724874	0.01691542	0.01630589	0.01485621	0.00479546
23	0.01280949	0.01273904	0.01244552	0.01190485	0.01060437	0.00030199
24	0.00924010	0.00918065	0.00893165	0.00846943	0.00734143	0.00000000
25	0.00650708	0.00645861	0.00625443	0.00587223	0.00492239	0.00000000
26	0.00447518	0.00443690	0.00427466	0.00396814	0.00318880	0.00000000
27	0.00300662	0.00297728	0.00285210	0.00261314	0.00198772	0.00000000
28	0.00197378	0.00195192	0.00185799	0.00167653	0.00118342	0.00000000
29	0.00126638	0.00125054	0.00118189	0.00104742	0.00066287	0.00000000
30	0.00079424	0.00078305	0.00073414	0.00063654	0.00033618	0.00000000
31	0.00048699	0.00047928	0.00044526	0.00037600	0.00012837	0.00000000
32	0.00029195	0.00028677	0.00026366	0.00021587	0.00001202	0.00000000
33	0.00017114	0.00016774	0.00015239	0.00012001	0.00000000	0.00000000
34	0.00009810	0.00009592	0.00008593	0.00006433	0.00000000	0.00000000
35	0.00005498	0.00005362	0.00004726	0.00003300	0.00000000	0.00000000
36	0.00003013	0.00002929	0.00002532	0.00001597	0.00000000	0.00000000
37	0.00001614	0.00001564	0.00001320	0.00000703	0.00000000	0.00000000
38	0.00000845	0.00000816	0.00000669	0.00000240	0.00000000	0.00000000
39	0.00000432	0.00000416	0.00000328	0.00000022	0.00000000	0.00000000
40	0.00000216	0.00000207	0.00000156	0.00000000	0.00000000	0.00000000
41	0.00000105	0.00000100	0.00000071	0.00000000	0.00000000	0.00000000
42	0.00000050	0.00000047	0.00000030	0.00000000	0.00000000	0.00000000
43	0.00000023	0.00000022	0.00000012	0.00000000	0.00000000	0.00000000
44	0.00000010	0.00000010	0.00000003	0.00000000	0.00000000	0.00000000
45	0.00000005	0.00000004	0.00000000	0.00000000	0.00000000	0.00000000
46	0.00000002	0.00000002	0.00000000	0.00000000	0.00000000	0.00000000
T(K)	331.50970249	329.85827607	327.72133432	332.16054112	362.51723843	430.18584298

References

1. H. Okabe, Photochemistry of Small Polyatomic Molecules, John Wiley and Sons, New York, 1978.

2. R. Leone, in Advances in Chemical Physics, (K.P. Lawley, Ed.), **vol. L**, John Wiley and Sons, Ltd., New York, 1982, p. 255.

3. J.P. Simons, in Gas Kinetics and Energy Transfer, (P.G. Ashmore and R.J. Donovan, Eds.), The Chemical Society, London, 1977, p.58.

4. R. Zare, Mol. Photochem. **4**, 1 (1972).

5. S. Yang and R. Bersohn, J. Chem. Phys. **61**, 4400 (1974).

6. S. Mukamel and J. Jortner, J. Chem. Phys. **61**, 5348 (1974).

7. W.H. Miller, Adv. Chem. Phys. **25**, 63 (1974).

8. S.J. Singer, K.F. Freed, and Y.B. Band, Chem. Phys. Lett. **91**, 12 (1982).

9. E.F. van Dishoeck, M.C. van Hemert, A.C. Allison, and A. Dalgarno, J. Chem. Phys. **81**, 5709 (1984).

10. S.A. Safron, N.D. Weinstein, D.R. Hershbach, and J.C. Tully, Chem. Phys. Lett. **12**, 564 (1972).

11. D.C. Truhlar and B.C. Garrett, Acc. Chem. Res. **13**, 440 (1980).

12. K. Fukui, Acc. Chem. Res. **14**, 363 (1981).

13. W. H. Miller, N. C. Handy, and J. E. Adams, J. Chem. Phys. **72**, 99 (1980).

14. E. Segev and M. Shapiro, J. Chem. Phys. **77**, 5604 (1982).

15. (a) R. W. Heather and J. C. Light, J. Chem. Phys. **78**, 5513 (1983); (b) **79**, 147 (1983).

16. (a) M. Shapiro, J. Chem. Phys. **56**, 2582 (1972); (b) Israel J. Chem. **11**, 691 (1973); (c) G.G. Balint-Kurti and M. Shapiro, Chem. Phys. **61**, 137 (1981).

17. K. Takatsuka and M. Gordon, J. Chem. Phys. **74**, 5718 (1981).

18. R. W. Numrich and K. G. Kay, J. Chem. Phys. **70**, 4343 (1979).

19. Y. Band, K. Freed, and D. Kouri, J. Chem. Phys. **74**, 4380 (1981).

20. D. C. Clary, J. Chem. Phys. **84**, 4288 (1986).

21. See for example, L. Landau and E. Lifshitz, Quantum Mechanics, Pergamon Press, New York, 1976.

22. G. Miller, W. M. Jackson, and J. Halpern, J. Chem. Phys. **71**, 4025 (1979).

23. G. Herzberg, Molecular Spectra and Molecular Structure I. Spectra of Diatomic Molecules, Van Nostrand Reinhold Co., New York, 1950.

24. S. A. Rice, in Excited States, (E. C. Lim, Ed.), **vol. 2**, Academic Press, New York, 1975, p. 111;

25. K. F. Freed and Y. B. Band, in Excited States, (E. C. Lim, Ed.), **vol. 3**, Academic Press, New York, 1977, p. 109;

26. W. F. Gelbart, Ann. Rev. Phys. Chem. **28**, 323 (1977);

27. M. Shapiro and R. Bersohn, Ann. Rev. Phys. Chem. **33**, 409 (1982);

28. V. Z. Kresin and W. A. Lester, Jr., in Advances in Photochemistry, (Volman, Gollnick, and Hammond, Eds.), **vol. 13**, John Wiley and Sons, Inc., New York, 1986, p. 95.

29. P. Brumer and M. Shapiro, in Advances in Chemical Physics, (I. Prigogine and S. Rice, Eds.), **vol. LX**, John Wiley and Sons, New York, 1985, p.371.

30. G.G. Balint-Kurti and M. Shapiro, in Advances in Chemical Physics, (I. Prigogine and S. Rice, Eds.), **vol. LX**, John Wiley and Sons, New York, 1985, p.403.

31. K. Holdy, L. Klotz, and K. Wilson, J. Chem. Phys. **52**, 4588 (1970).

32. M. Shapiro and R. Levine, Chem. Phys. Lett. **5**, 499 (1970).

33. H. Gebelein and J. Jortner, Theor. Chim. Acta. **25**, 143 (1972).

34. (a) J.P. Simons and P.W. Tasker, Mol. Phys. **26**, 1267 (1973); (b) **27**, 1691 (1974).

35. M. Berry, Chem. Phys. Lett. **29**, 329 (1974).

36. (a) O. Atabeck, J. A. Beswick, R. Lefebvre, S. Mukamel, and J. Jortner, Mol. Phys. **31**, 1 (1976); (b) J. Chem. Phys. **65**, 4035 (1976); (c) S. Miret-Artes, G. Delgado-Barrio, O. Atabek, and J. A. Beswick, Chem. Phys. Lett. **98**, 554 (1983).

37. Y. B. Band and K. F. Freed, Chem. Phys. Lett. **28**, 328 (1974).

38. U. Halvee and M. Shapiro, J. Chem. Phys. **64**, 2836 (1976).

39. (a) S. Mukamel and J. Jortner, J. Chem. Phys.**60**, 4760 (1974); (b) **65**, 3735 (1976).

40. J.A. Beswick and J. Jortner, Chem. Phys. **24**,1 (1977).

41. (a) Y. B. Band and K. F. Freed, J. Chem. Phys. **63**, 3382 (1975); (b) **67**, 1462 (1977); (c) **68**, 1292 (1978).

42. V. Z. Kresin and W. A. Lester, Jr., Int. J. Quantum Chem., Symp. **15**, 703 (1981).

43. V. Z. Kresin and W. A. Lester, Jr., Chem. Phys. Lett. **87**, 392 (1982).

44. V. Z. Kresin and W. A. Lester, Jr., J. Phys. Chem. **86**, 2182 (1982).

45. J. B. Halpern and W. M. Jackson, J. Phys. Chem. **86**, 973 (1982).

46. D. Eros, M. Gurnick, and J. D. McDonald, J. Chem. Phys. **81**, 5552 (1984).

47. R. J. Cody, M. J. Sabety-Dzvonik, and W. M. Jackson, J. Chem. Phys. **66**, 2145 (1977).

48. W. M. Jackson, J. Photochem. **17**, 509 (1981).

49. W. M. Jackson and H. Okabe, in Advances in Photochemistry, (Volman, Gollnick, and Hammond, Eds.), **vol. 13**, John Wiley and Sons, Inc., New York, 1986, p. 1.

50. M. Taherian and T. Slanger, J. Chem. Phys. **81**, 3814 (1984).

51. J. H. Callomon and A. B. Davey, Proc. Phys. Soc. (London) **82**, 335 (1963).

52. G. J. Cartwright, D. O. O'Hare, A. D. Walsh, and P. A. Warsop, J. Mol. Spectrosc. **39**, 393 (1971).

53. G. B. Fish G. J. Cartwright, A. D. Walsh, and P. A. Warsop, J. Mol. Spectrosc. **41**, 20 (1972).

54. S. Bell, G. J. Cartwright, G. B. Fish, D. O. O'Hare, R. K. Ritchie, A. D. Walsh, and P. A. Warsop, J. Mol. Spectrosc. **30**, 162 (1969).

55. R. E. Connors, J. L. Roebber, and K. Weiss, J. Chem. Phys. **60**, 5011 (1974).

56. S. Bell, Chem. Phys. Lett. **67**, 498 (1974)

57. H. F. Schaefer III and T. G. Heil, J. Chem. Phys. **54**, 2580 (1971).

58. A. D. McLean and M. Yoshimine, IBM J. Res. Develop. Suppl. (1967).

59. L. Engelbrecht and B. Liu, J. Chem. Phys. **78**, 3097 (1983).

60. W. J. Hehre, R. R. Stewart, and J. A. Pople, J. Chem. Phys. **51**, 2657 (1969).

61. T. H. Dunning, Jr. and P. J. Hay, in Modern Theoretical Chemistry, (H. F. Schaefer III, Ed.), **vol. 2**, Plenum Press, New York, 1976, p. 1.

62. E. B. Wilson, J. C. Decius, and P. C. Cross, Molecular Vibrations, McGraw-Hill Co., New York, 1955.

63. G. Herzberg, Molecular Spectra and Molecular Structure III. Electronic Spectra of Polyatomic Molecules, Van Nostrand Reinhold Co., New York, 1966.

64. (a) K. Kulander and J. C. Light, J. Chem. Phys. **85**, 1938 (1986); (b) **73**, 4337 (1980).

65. C. E. Caplan and M. S. Child, Mol. Phys. **23**, 249 (1972).

66. R. T. Pack, J. Chem. Phys. **65**, 4765 (1976).

67. S. Lee and E. Heller, J. Chem. Phys. **76**, 3035 (1982).

68. J. A. Beswick, M. Shapiro, and R. Sharon, J. Chem. Phys. **67**, 4045 (1977).

69. Y. B. Band and K. F. Freed, J. Chem. Phys. **64**, 4329 (1976).

70. J. A. Beswick and M. Horani, Chem. Phys. Lett. **78**, 4 (1981).

71. K. C. Kulander, Chem. Phys. Lett. **103**, 373 (1984).

72. T. O'Malley, Phys. Rev. **152**, 98 (1967).

73. F. T. Smith, Phys. Rev. **179**, 111 (1969).

74. S. Mukamel and J. Ross, J. Chem. Phys. **66**, 3759 (1977).

75. (a) B. C. Garrett, and D. G. Truhlar, in Theoretical Chemistry: Advances and Perspectives, (D. Henderson, ed.), **vol. 6a**, Academic Press, Inc., New York, 1981, p. 1; (b) C. A. Mead and D. G. Truhlar, J. Chem. Phys. **77**, 6090 (1982).

76. F. Rebentrost, in Theoretical Chemistry: Advances and Perspectives, (D. Henderson, ed.), **vol. 6b**, Academic Press, Inc., New York, 1981, p. 1.

77. V. Z. Kresin, W. A. Lester, Jr., M. Dupuis, and C. E. Dateo, Int. J. Quantum Chem., Symp. **18**, 691 (1984).

78. V. Z. Kresin and W. A. Lester, Jr., Chem. Phys. **90**, 335 (1984).

79. (a) G. Schatz and J. Ross, J. Chem. Phys. **66**, 1021 (1977); (b) **66**, 1037 (1977); (c) **66**, 2943 (1977).

80. K. Fung and K. Freed, Chem. Phys. **30**, 249, (1978).

81. (a) C. Vila, D. Zvijac, and J. Ross, J. Chem. Phys. **70**, 2414 (1979); (b) **70**, 5362 (1979).

82. J. Bardeen, Phys. Rev. Lett. **6**, 57 (1961).

83. See for example, A. Davydov, Quantum Mechanics, Pergamon Press, Oxford, 1976.

84. C. E. Dateo, M. Dupuis, and W. A. Lester, Jr., J. Chem. Phys. **83**, 265 (1985).

85. The translational wave functions were calculated using the computer code TDELAY, written by R. J. LeRoy, University of Waterloo Chem. Phys. Res. Reports, CP-107 (1978).

86. M.E. Rose, Elementary Theory of Angular Momentum, John Wiley and Sons, Inc., New York, 1957.

87. A.R. Edmonds, Angular Momentum in Quantum Mechanics, Princeton University Press, Princeton, New Jersey, 1960.

88. R.T. Pack, J. Chem. Phys. **60**, 633 (1974).

89. K.H. Kramer and R.B. Bernstein, J. Chem. Phys. **47**, 4417 (1967).

90. H. Rabitz, in Modern Theoretical Chemistry: Dynamics of Molecular Collisions, Part A, (W.H. Miller, Ed.), **vol. 1**, Plenum Press, New York,

1976, p.33.

91. G.F. Englot and H. Rabitz, Phys. Rev. A **10**, 2187 (1974).

92. H. Klar, Z. Physik **228**, 59 (1969).

93. S. Green, J. Chem. Phys. **62**, 2271 (1975).

94. (a) R. Schinke and V. Engel, J. Chem. Phys. **83**, 5068 (1985); (b) V. Engel, R. Schinke, and V. Staemmler, Chem. Phys. Lett. **130**, 413 (1986); (c) Z. Bacic, R. Schinke, G.H.F. Diercksen, J. Chem. Phys. **82**, 236 (1985); (d) **82**, 245 (1985).

95. R. Schinke and P. MgGuire, Chem. Phys. **31**, 391 (1978).

96. J.A. Beswick and W.M. Gelbart, J. Phys. Chem. **84**, 3148 (1980).

97. F. Prosser, NRCC Software Cat., **vol. 1**, Prog. No. ND01 (GIVENS), 1980.

98. R.E. Wyatt, in Atom-Molecule Collision Theory, (R.B. Bernstein, Ed.), Plenum Press, New York, 1979, p.567.

99. A. Kupperman, Chem. Phys. Lett. **32**, 374 (1975).

100. R. Gordon, Methods. Comput. Phys. **10**,81 (1971).

101. J.N. Murrell, S. Carter, J.C. Farontos, P. Huxley, and A.J.C. Varandas, Molecular Potential Energy Functions, John Wiley and Sons, Inc., New York, 1984.

102. M.D Morse, K.F. Freed, and Y.B. Band, J. Chem. Phys. **70**, 3604 (1979).

103. H. Klar, J. Phys. B **10**, 2139 (1973).

104. R. Renner, Z. Physik **92**, 172 (1934).

105. J.M. Brown and F. Jorgenson, Adv. Chem. Phys. **LII**, 117 (1983).

106. A.F. Wagner, J.M. Bowman, L.B. Harding, J. Chem. Phys. **82**, 1866 (1985).

LAWRENCE BERKELEY LABORATORY
TECHNICAL INFORMATION DEPARTMENT
UNIVERSITY OF CALIFORNIA
BERKELEY, CALIFORNIA 94720